PETROGENESIS OF THE WATHAMAN BATHOLITH AND LA RONGE DOMAIN PLUTONS IN THE REINDEER LAKE AREA, TRANS-HUDSON OROGEN, SASKATCHEWAN

CENTRE FOR NEWFOUNDLAND STUDIES

TOTAL OF 10 PAGES ONLY MAY BE XEROXED

(Without Author's Permission)

TREVOR GEORGE MacHATTIE

INFORMATION TO USERS

This manuscript has been reproduced from the microfilm master. UMI films the text directly from the original or copy submitted. Thus, some thesis and dissertation copies are in typewriter face, while others may be from any type of computer printer.

The quality of this reproduction is dependent upon the quality of the copy submitted. Broken or indistinct print, colored or poor quality illustrations and photographs, print bleedthrough, substandard margins, and improper alignment can adversely affect reproduction.

In the unlikely event that the author did not send UMI a complete manuscript and there are missing pages, these will be noted. Also, if unauthorized copyright material had to be removed, a note will indicate the deletion.

Oversize materials (e.g., maps, drawings, charts) are reproduced by sectioning the original, beginning at the upper left-hand corner and continuing from left to right in equal sections with small overlaps.

ProQuest Information and Learning
300 North Zeeb Road, Ann Arbor, MI 48106-1346 USA
800-521-0600

Petrogenesis of the Wathaman Batholith and La Ronge Domain plutons in the Reindeer Lake Area, Trans-Hudson Orogen, Saskatchewan.

Trevor George MacHattie
B.Sc. First Class Honours

A Thesis Submitted to the School of Graduate Studies
in partial fulfilment of the requirements for the degree of Master of Science

Department of Earth Sciences
Memorial University of Newfoundland
2001

St. John's Newfoundland

Memorial
University of Newfoundland

This is to authorize the Dean of Graduate Studies to deposit two copies of my thesis/report entitled

Petrogenesis of the Hathaway, Batholith and LA RONGE DOMAIN PLUTONS IN THE REINDEER LAKE AREA, TRANS-HUDSON OROGEN, SASKATCHEWAN.

in the University Library, on the following conditions. I understand that I may choose only ONE of the Options here listed, and may not afterwards apply for any additional restriction. I further understand that the University will not grant any restriction on the publication of thesis/report abstracts.

(After reading the explanatory notes at the foot of this form, delete TWO of a, b and (c), whichever are inapplicable.)

The conditions of deposit are:

(a) that two copies are to be made available to users at the discretion of their custodians,

OR

(b) that access to, and quotation from, this thesis/report is to be granted only with my written permission for a period of one year from the date on which the thesis/report, after the approval of the award of a degree, is entrusted to the care of the University, namely, Sept. 30 19 02, after which time the two copies are to be made available to users at the discretion of their custodians,

OR

(c) that access to, and quotation from, this thesis/report is to be granted only with my written permission for a period of _____ years from the date on which the thesis/report, after approval for the award of a degree, is entrusted to the care of the University; namely, _____, 19 ___; after which time two copies are to be made available to users at the discretion of their custodians.

Date Sept. 24/01

Dean of Graduate Studies

Signed Ian M. Hatcher

Witnessed by Maureen Moore

NOTES

1. *Restriction (b) will be granted on application, without reason given.*

   However, applications for restriction (c) must be accompanied with a detailed explanation, indicating why the restriction is thought to be necessary, and justifying the length of time requested. Restrictions required on the grounds that the thesis is being prepared for publication, or that patents are awaited, will not be permitted to exceed three years.

   Restriction (c) can be permitted only by a Committee entrusted by the University with the task of examining such applications, and will be granted only in exceptional circumstances.

2. *Thesis writers are reminded that, if they have been engaged in contractual research, they may have already agreed to restrict access to their thesis until the terms of the contract have been fulfilled.*

National Library of Canada
Acquisitions and Bibliographic Services
395 Wellington Street
Ottawa ON K1A 0N4
Canada

Bibliothèque nationale du Canada
Acquisitions et services bibliographiques
395, rue Wellington
Ottawa ON K1A 0N4
Canada

Your file Votre référence

Our file Notre référence

The author has granted a non-exclusive licence allowing the National Library of Canada to reproduce, loan, distribute or sell copies of this thesis in microform, paper or electronic formats.

L'auteur a accordé une licence non exclusive permettant à la Bibliothèque nationale du Canada de reproduire, prêter, distribuer ou vendre des copies de cette thèse sous la forme de microfiche/film, de reproduction sur papier ou sur format électronique.

The author retains ownership of the copyright in this thesis. Neither the thesis nor substantial extracts from it may be printed or otherwise reproduced without the author's permission.

L'auteur conserve la propriété du droit d'auteur qui protège cette thèse. Ni la thèse ni des extraits substantiels de celle-ci ne doivent être imprimés ou autrement reproduits sans son autorisation.

0-612-73655-5

Canada

ABSTRACT

The Paleoproterozoic Wathaman Batholith forms a major part of the Trans Hudson Orogen in northern Saskatchewan and Manitoba. On Reindeer Lake in Saskatchewan the batholith is 125 km wide and may continue for 800-900 km along strike. The size is comparable to Phanerozoic batholiths associated with destructive continental margins. The plutonism took place over a relatively short time interval, between 1865 and 1850 Ma.

The batholith and satellite intrusions have been divided into 3 major zones based on modal, geochemical and Nd isotopic composition, from south to north these are the: La Ronge Domain (LRD); South Central (SCZ); and North East (NEZ). The LRD hosts satellite intrusions that are mainly metaluminous, calc-alkaline tonalites and granodiorites. εNd(t) in this zone ranges from +4.8 to -0.4. The SCZ is composed of two distinct series, a K-feldspar megacrystic granodiorite and a monzogranite series. The granodioritic series range in εNd(t) from -2.3 to -5.4; whilst the monzogranite series are characterized by εNd(t) +0.2 to -0.4. These rocks are all of high-K calc-alkaline affinity. The NEZ is composed of a K-feldspar megacrystic monzogranite and a monzonitic series, both of shoshonitic affinity. The monzogranites rocks have εNd(t) of -1.4 to -6.9, while the monzonites have εNd(t) of -0.3 to -4.

The Wathaman Batholith had been interpreted as the root of a continental arc but was enigmatic in that it lacked co-magmatic mafic phases and was considered too homogeneous, too felsic, and too megacrystic, i.e., more like post-collisional granitoids. This study has resolved many of the uncertainties in the origin of this batholith. There is a greater diversity of rock types than previously described, and good field evidence for mingling of mafic and felsic magmas. Within a series εNd(t) is independent of rock type, and both the SC and NE zones rocks are characterized by high Sr and Ba. The petrogenesis of the batholith can be explained by mixing between 3 end-

members: Archean crust; Proterozoic supra-subduction zone depleted mantle; and a late Archean enriched lithospheric mantle. Relative contributions from end-members change from south to north, with a major role for: depleted, subduction zone affected mantle in the LRD; enriched mantle in the SCZ; and enriched mantle + crust in the NEZ. The batholith is interpreted to have formed in a subduction zone setting where mixing was dominantly occurring in the asthenosphere and at the crust-mantle boundary. Upper level contamination processes can only be clearly seen in the NEZ.

ACKNOWLEDGMENTS

I would first like to acknowledge my research supervisor Dr. George Jenner, and Dr. David Corrigan of the Geological Survey of Canada who came up with a great thesis topic and work for two summers, I am thankful for the opportunity they provided.

Dr. Jenner provided financial support for analytical work, and is thanked for allowing me the independence to develop some of these ideas, and his eagerness to help when asked. He is also thanked for his expeditious reading of the thesis. Dr. Corrigan's expertise in field geology was an invaluable asset when mapping and collecting samples for this study. He is thanked especially for his work in logistical planning, geochronological work, and providing a strong regional geological framework for this study to develop. Sally Pehrsson, Don Wright, Joyia Chackungal, Liza Piper, Birgita Lassen, William Matthews, and Melanie Bathalon contributed to the mapping on Reindeer Lake.

The laboratory technicians at Memorial University are thanked for their help in acquiring the geochemical data. Pat Horan introduced me to the isotope dilution method for Sm and Nd isotopes and the basics of mass spectrometry. Pam King helped with all XRF analyses, and Mike Tubrett and Lakmali Hewa with ICP-MS data.

I would also like to than my fellow 5th floor hard rockers Jason Krauss, Richard Cox, Alana Rawlings, Vanessa Bennett and Lawrence "look-at-buddy" Winter for their friendship and putting up with constant talk of granites. Lastly I would like to thank Nicole for her love and support and for putting up with me not being around much.

TABLE OF CONTENTS

ABSTRACT ii
ACKNOWLEDGMENTS iv
TABLE OF CONTENTS v
LIST OF TABLES ix
LIST OF FIGURES x
LIST OF PLATES xv
LIST OF ABBREVIATIONS A xviii
LIST OF ABBREVIATIONS B xviii

CHAPTER 1: INTRODUCTION 1-1

1.1 INTRODUCTION 1-1

1.2 SETTING OF THIS AREA 1-2

1.3 AIMS OF THE THESIS 1-3

1.4 ORGANIZATION OF THE THESIS 1-5

CHAPTER 2: REGIONAL GEOLOGY 2-1

2.1 INTRODUCTION 2-1

2.2 GEOLOGY OF THE TRANS-HUDSON OROGEN IN NORTHERN SASKATCHEWAN AND MANITOBA 2-1

2.3 GEOLOGY OF THE NORTHWEST REINDEER ZONE 2-2
2.3.1 Geology of the La Ronge Domain 2-3
2.3.2 The Rottenstone Domain and its Relationships 2-4

2.4 THE WATHAMAN BATHOLITH 2-6

2.5 THE CREE LAKE ZONE OF THE SOUTHEASTERN HEARNE DOMAIN 2-7

2.6 U-PB ZIRCON GEOCHRONOLOGY OF IGNEOUS ROCKS OF THE NORTHWEST REINDEER ZONE, THE WATHAMAN BATHOLITH, AND THE CREE LAKE ZONE 2-8

2.7 TECTONIC HISTORY OF THE AREA 2-10

CHAPTER 3: GEOLOGY AND DESCRIPTION OF THE PLUTONIC ROCKS IN THE

REINDEER LAKE AREA 3-1

3.1 INTRODUCTION 3-1

3.2 GEOLOGY OF THE REINDEER LAKE AREA 3-1
3.2.1 Geological overview of the Area 3-2

3.3 EARLY ASSEMBLAGES OF THE LA RONGE DOMAIN
3.3.1 Rottenstone and Kisseynew Domains 3-5
3.3.2 Structural and Metamorphic Framework 3-6

3.4 THE PETER LAKE DOMAIN 3-7
3.4.1 U-Pb geochronology of the Peter Lake Domain 3-9

3.5 GRANITOID ROCKS IN THE REINDEER LAKE AREA 3-9
3.5.1 The Wathaman Batholith 3-10
3.5.1.1 South-Central Zone (SCZ) of the Wathaman Batholith 3-11
3.5.1.2 North-East Zone (NEZ) of the Wathaman Batholith 3-12
3.5.1.3 U-Pb Geochronology of the Wathaman Batholith 3-13
3.5.1.4 Minor Intrusive phases 3-14
3.5.1.5 Xenoliths 3-15
3.5.1.6 Structure and Deformation 3-16
3.5.2 The La Ronge Domain Plutons 3-16
3.5.2.1 U-Pb Geochronology of the La Ronge Domain Plutons 3-17
3.5.2.2 Quartz diorites, tonalites and granodiorites 3-18

3.6 DETAILS OF THE PETROGRAPHY AND OCCURRENCE OF THE WATHAMAN BATHOLITH SERIES 3-19
3.6.1 The SCZ K-feldspar megacrystic granodiorite series 3-19
3.6.1.1 Quartz diorites and quartz monzodiorites 3-19
3.6.1.2 K-feldspar megacrystic granodiorites and monzogranites 3-22
3.6.2 The SCZ monzogranite series 3-25
3.6.3 The NEZ K-feldspar megacrystic monzogranite series 3-25
3.6.3.1 K-feldspar megacrystic granodiorites and monzogranites 3-25
3.6.3.2 Syn-plutonic diorite dykes and microdiorite enclaves 3-27
3.6.4 The NEZ Monzonitic series 3-27

3.7 SUMMARY 3-29

CHAPTER 4: GEOCHEMICAL AND ND ISOTOPIC SIGNATURE OF THE WATHAMAN BATHOLITH AND THE LA RONGE DOMAIN PLUTONS 4-1

4.1 INTRODUCTION 4-1

4.2 GEOCHEMISTRY OF THE WATHAMAN BATHOLITH 4-1

4.2.1 Majors Elements 4-1
4.2.1.1 Magma Series and Alumina Indices 4-3
4.2.3 Trace Elements 4-5
4.2.3.1 SCZ 4-5
4.2.3.2 NEZ 4-6
4.2.4 Rare Earth Elements (REE) 4-7
4.2.5 Extended Element Diagrams 4-10
4.2.6 Sm and Nd Isotopes 4-12

4.3 GEOCHEMISTRY OF THE LA RONGE DOMAIN PLUTONS 4-14
4.3.1 Introduction 4-14
4.3.2 Majors Elements 4-14
4.3.3 Trace Elements 4-15
4.3.4 Rare Earth Elements (REE) 4-16
4.3.5 Extended Element Diagrams 4-17
4.3.6 Sm and Nd Isotopes 4-17

4.4 CHAPTER SUMMARY 4-19

CHAPTER 5: PETROGENESIS OF THE WATHAMAN BATHOLITH AND THE LA RONGE DOMAIN PLUTONS 5-1

5.1 INTRODUCTION 5-1

5.2 PETROGENESIS OF THE WATHAMAN BATHOLITH 5-1
5.2.1 The SCZ K-feldspar megacrystic granodiorite series 5-1
5.2.1.1 Role of Fractional Crystallization 5-2
5.2.2 Origin of the Isotopic Signature 5-5
5.2.2.1 The Nd isotopic composition of Paleoproterozoic and Archean crust 5-6
5.2.2.2 The Nd isotopic composition of ca. 1800-1900 Ma depleted mantle 5-7
5.2.2.3 Crust-Mantle mixing models and the generation of parental magmas 5-8
5.2.3 The NEZ K-feldspar megacrystic monzogranite series 5-14
5.2.4 The NEZ Monzonitic series 5-15
5.2.5 The SCZ monzogranite series 5-17

5.3 PETROGENESIS OF THE LA RONGE DOMAIN PLUTONS 5-19

5.4 TECTONOMAGMATIC SUMMARY OF GRANITOID MAGMATISM ALONG THE REINDEER LAKE TRANSECT 5-21

REFERENCES

APPENDIX A: ANALYTICAL METHODS A-1
A.1 GEOCHEMICAL SAMPLING, PREPARATION AND METHODOLOGY A-1

A.2 X-RAY FLUORESCENCE (XRF) A-2
A.2.1 Major Element Analysis (glass bead) A-2
A.2.2 Trace Element Analysis (pressed pellet) A-3
A.2.3 Test for Precision and accuracy (XRF) A-3
A.3 INDUCTIVELY COUPLED PLASMA MASS SPECTROMETRY (ICP-MS) A-5
A.3.1 Test for Precision and accuracy (ICP-MS) A-6
A.4 ISOTOPE DILUTION PROCEDURE FOR THE ANALYSIS OF SAMARIUM AND NEODYMIUM A-7

APPENDIX B: GEOCHEMICAL AND ISOTOPIC ANALYSES DATABASE B-1
B.1 MAJOR AND TRACE ELEMENT XRF ANALYSES B-1
B.2 ICP-MS TRACE ELEMENT ANALYSES B-18
B.3 SM AND ND ISOTOPIC MEASURMENTS B-28

APPENDIX C: PRIMITIVE MANTLE TRACE ELEMENT NORMALIZING VALUES C-1

APPENDIX D: PARTITION COEFFICIENTS USED D-1

SAMPLE LOCATION MAP

LIST OF TABLES

Table 4.1 Representative major, trace and REE analyses for granitoids of the Southern-Central Zone (SCZ) of the Wathaman Batholith 4-22

Table 4.2 Representative major, trace and REE analyses for granitoids of the Northeast Zone (NEZ) of the Wathaman Batholith 4-23

Table 4.3 Representative major, trace and REE analyses for Monzonitic series rocks of the Northeast Zone (NEZ) of the Wathaman Batholith 4-24

Table 4.4 Sm and Nd isotopic analyses of the Wathaman Batholith 4-25

Table 4.5 Representative major, trace and REE analyses for granitoid plutons of the La Ronge Domain 4-26

Table 4.6 Sm and Nd isotopic analyses of La Ronge Domain plutons 4-27

Table 4.7 Summary of relevant geochemical parameters that identify the magmatic zones and granitoid series in the Reindeer Lake area 4-28

Table 4.8 Geochemical comparison between NEZ and SCZ monzodiorites and quartz diorites with andesites from the CVZ of the Andes and Archean Sanukitoids from the southwest Superior Province 4-29

Table A.1 Summary of XRF precision and accuracy between March 1999 and December 1999 ..... A-10

Table A.2 Summary of ICP-MS test for precision and accuracy between April 1999 and December 1999 ..... A-11

Table A.3 Duplicate Sm and Nd isotopic analyses of two granitoids A-12

LIST OF FIGURES

Figure 2.1 Extent of the Trans-Hudson Orogen in northern Saskatchewan and Manitoba and its lithotectonic subdivisions 2-11

Figure 2.2 Lithotectonic domains of northern Saskatchewan and location of Reindeer Lake within the northwest Reindeer Zone 2-12

Figure 2.3 Summary of U-Pb zircon geochronology of the northwest Reindeer Zone, the Wathaman Batholith and the Cree Lake Zone 2-13

Figure 3.1 Generalized geological map of the Reindeer Lake area comprising parts of NTS 64D and NTS 64E 3-31

Figure 3.2a Schematic cross-section of the La Ronge Domain on Reindeer Lake 3-32

Figure 3.2b Schematic 3-D sketch of the fold geometry of structural levels in the central La Ronge Domain on Reindeer Lake 3-32

Figure 3.3 Generalized geological map of the Wathaman Batholith and Peter Lake Domain on Reindeer Lake 3-33

Figure 3.4a QAP mesonorm diagram for the SCZ of the Wathaman Batholith 3-34

Figure 3.4b QAP mesonorm diagram for the NEZ of the Wathaman Batholith 3-34

Figure 3.5 Generalized geological map of the La Ronge Domain on Reindeer Lake 3-35

Figure 3.6 QAP mesonorm diagram for La Ronge Domain Plutons 3-36

Figure 4.1 Major element Harker variation diagrams for granitoids of the Wathaman Batholith 4-30

Figure 4.2 Major element Harker variation diagrams for granitoids of the Wathaman Batholith 4-30

Figure 4.3a Total alkalies versus silica diagram for SCZ granitoids of the Wathaman Batholith 4-32

Figure 4.3b Total alkalies versus silica diagram for NEZ granitoids of the Wathaman Batholith 4-32

Figure 4.4a Ternary AFM diagram for SCZ granitoids of the Wathaman Batholith 4-33

Figure 4.4b Ternary AFM diagram for NEZ granitoids of the Wathaman Batholith 4-33

Figure 4.5a K_2O versus silica diagram for SCZ granitoids of the Wathaman Batholith 4-34

Figure 4.5b K_2O versus silica diagram for NEZ granitoids of the Wathaman Batholith 4-34

Figure 4.6a Molecular $Al_2O_3/(Na_2O + K_2O)$ versus $Al_2O_3/(CaO + Na_2O + K_2O)$ diagram for SCZ granitoids of the Wathaman Batholith 4-35

Figure 4.6b Molecular $Al_2O_3/(Na_2O + K_2O)$ versus $Al_2O_3/(CaO + Na_2O + K_2O)$ diagram for NEZ granitoids of the Wathaman Batholith 4-35

Figure 4.7 Trace element Harker variation diagrams for granitoids of the Wathaman Batholith 4-36

Figure 4.8 Trace element Harker variation diagrams for granitoids of the Wathaman Batholith 4-37

Figure 4.9a Primitive mantle normalized REE diagram for SCZ and NEZ granitoids in the 61-63 wt % SiO_2 range.....4-38

Figure 4.9b Primitive mantle normalized REE diagram for SCZ and NEZ granitoids in the 64-65 wt % SiO_2 range.....4-38

Figure 4.9c Primitive mantle normalized REE diagram for SCZ and NEZ granitoids in the 67-72 wt % SiO_2 range.....4-38

Figure 4.10a Primitive mantle normalized REE diagram for SCZ quartz diorites containing <60 wt % SiO_2 4-39

Figure 4.10b Primitive mantle normalized REE diagram for NEZ syn-plutonic diorite dykes containing <52 wt % SiO_2.....4-39

Figure 4.10c Primitive mantle normalized REE diagram for NEZ monzonitic series rocks between 51-57 wt % SiO_2.....4-39

Figure 4.11a Primitive mantle normalized extended element diagram for SCZ and NEZ granitoids in the 61-63 wt % SiO_2 range.....4-40

Figure 4.11b Primitive mantle normalized extended element diagram for SCZ and NEZ granitoids in the 64-65 wt % SiO_2 range.....4-40

Figure 4.11c Primitive mantle normalized extended element diagram for SCZ and NEZ granitoids in the 67-72 wt % SiO_2 range.....4-40

Figure 4.12a Primitive mantle normalized extended element diagram for SCZ quartz diorites containing < 60 wt % SiO_2.....4-41

Figure 4.12b Primitive mantle normalized extended element diagram for NEZ syn-plutonic diorite dykes containing <52 wt % SiO_2 4-41

Figure 4.12c Primitive mantle normalized extended element diagram for NEZ monzonitic series rocks between 51-57 wt % SiO_2 4-41

Figure 4.13a εNd(t) versus silica plot for granitoids of the Wathaman Batholith 4-42

Figure 4.13b εNd(t) versus $(La/Sm)_N$ for granitoids of the Wathaman Batholith 4-42

Figure 4.13c εNd(t) versus $(La/Yb)_N$ for granitoids of the Wathaman Batholith 4-42

Figure 4.14 Major element Harker variation diagrams for La Ronge Domain plutons 4-43

Figure 4.15 Major element Harker variation diagrams for La Ronge Domain plutons 4-43

Figure 4.16a Total alkalies versus silica diagram for La Ronge Domain plutons 4-45

Figure 4.16b Ternary AFM diagram for La Ronge Domain plutons 4-45

Figure 4.17a K_2O versus silica diagram for La Ronge Domain plutons 4-46

Figure 4.17b Molecular $Al_2O_3/(Na_2O + K_2O)$ versus $Al_2O_3/(CaO + Na_2O + K_2O)$ diagram for La Ronge Domain plutons 4-46

Figure 4.18 Trace element Harker variation diagrams for La Ronge Domain plutons 4-47

Figure 4.19 Trace element Harker variation diagrams for La Ronge Domain plutons 4-48

Figure 4.20a Primitive mantle normalized REE diagram for tonalitic plutons of the La Ronge Domain containing 58-62 wt % SiO_2 4-49

Figure 4.20b Primitive mantle normalized REE diagram for granodioritic plutons of the La Ronge Domain containing 62-68 wt % SiO_2 4-49

Figure 4.21a Primitive mantle normalized extended element diagram for tonalitic plutons of the La Ronge Domain containing 58-62 wt % SiO_2 4-50

Figure 4.21b Primitive mantle normalized extended element diagram for granodioritic plutons of the La Ronge Domain containing 62-68 wt % SiO_2 4-50

Figure 5.1a Ba versus Sr plot for SCZ K-feldspar megacrystic granodiorite series rocks, with 40 % fractional crystallization vectors for plag, K-spar, bio and hb 5-25

Figure 5.1b Primitive mantle normalized REE-averages (61-63, 64-65 and 68-72 wt % SiO_2) for SCZ K-feldspar megacrystic granodiorite series rocks 5- 25

Figure 5.1c Results of 10 and 20 % hornblende fractionation using the 61-63 wt % SiO_2 REE-

average as the starting composition for the SCZ K-feldspar megacrystic granodiorite series rocks 5-25

Figure 5.1d Molecular A/NK versus A/CNK plot for SCZ K-feldspar megacrystic granodiorite series rocks 5-25

Figure 5.1e $(La/Sm)_N$ versus Th (ppm) plot for SCZ K-feldspar megacrystic granodiorite series rocks 5-25

Figure 5.2a Frequency of εNd values for granitoids of the Wathaman Batholith 5-26

Figure 5.2b εNd(t) versus Age (Ga) diagram for granitoids of the Wathaman Batholith and La Ronge Domain 5-26

Figure 5.3a εNd(t) versus SiO_2 plot of primitive Wathaman Batholith magmas with calculated mixing curves between a depleted mantle and two Archean crustal end members 5-27

Figure 5.3b εNd(t) versus Ba (ppm) plot of primitive Wathaman Batholith magmas with calculated mixing curves between a depleted mantle and three potential Archean crustal end members 5-27

Figure 5.4 εNd(t) versus SiO_2 plot with calculated mixing curves between an enriched mantle end member and two Archean crustal end members 5-28

Figure 5.5 Selected trace element versus SiO_2 plots for the NEZ K-feldspar megacrystic monzogranite series. A field for SCZ granitoids and various crustal contaminants compositions are also plotted 5-29

Figure 5.6a Primitive mantle normalized REE field enclosing the REE-averages (61-63, 64-65 and 68-72 wt % SiO_2) for the NEZ K-feldspar megacrystic monzogranite series samples and the average REE patterns for the SCZ K-feldspar megacrystic granodiorite series for comparison 5-30

Figure 5.6b Ba versus Sr plot for NEZ K-feldspar megacrystic monzogranite series rocks, with 40 % fractional crystallization vectors for plag, K-spar, bio and hbl, and the SCZ K-feldspar megacrystic granodiorite series 5-30

Figure 5.7 Primitive mantle normalized REE patterns of SCZ monzogranite series rocks, and the results of 10-40 % hornblende fractionation using the 61-63 wt % SiO_2 REE-average as the starting composition 5-31

Figure 5.8 Schematic tectonic diagram for the northwest Reindeer Zone and the Hearne craton margin at ca. 1865-1845 Ma during the emplacement of the La Ronge plutons and the Wathaman Batholith 5-32

LIST OF PLATES

Plate 3.1a Intermediate volcaniclastic rock containing angular rhyolitic fragments in an andesitic matrix 3-37

Plate 3.1b Dioritic and granitic orthogneisses of the Crowe Island Complex 3-37

Plate 3.1c Migmatitic metasedimentary gneiss of the Milton Island metasedimentary assemblage 3-37

Plate 3.1d Cross bedding in arkose of the Park Island metasedimentary assemblage 3-37

Plate 3.1e Intensely migmatized arkose of the Park Island metasedimentary assemblage 1.5 km south of the Wathaman Batholith 3-37

Plate 3.2a Migmatitic paragneiss of the Peter Lake Domain 3-38

Plate 3.2b Foliated and recrystallized fine to medium grained biotite granodiorite of the Peter Lake Domain 3-38

Plate 3.2c Bio-hbl-bearing K-feldspar augen monzogranite of the Peter Lake Domain 3-38

Plate 3.3a Olivine-clinopyroxene gabbro of the Swan River Complex 3-39

Plate 3.3b Rhythmic layering in gabbro of the Swan River Complex 3-39

Plate 3.3c Mingling between gabbroic and dioritic magmas of the Swan River Complex .3-39

Plate 3.3d Injection of K-feldspar megacrystic quartz monzodiorite into fine grained gabbro of the Swan River Complex 3-39

Plate 3.3e Pegmatitic gabbro of the Swan River Complex collected for U-Pb zircon analysis 3-39

Plate 3.4a Medium-grained bio-hbl-bearing granodiorite of the Jack Pine Bay Pluton 3-40

Plate 3.4b Medium-grained bio±hbl-bearing tonalite of the McMillian Lake Pluton 3-40

Plate 3.4c Medium- to coarse-grained hbl-bio-bearing quartz diorite of the Butler Island Pluton 3-40

Plate 3.4d Medium-grained hbl-bio-bearing tonalite of the Cowie Bay Pluton 3-40

Plate 3.5a-b Hbl-bio-bearing quartz diorite and quartz monzodiorite 3-41

Plate 3.5c-d Hbl-bio-bearing K-feldspar megacrystic quartz monzodiorite and granodiorite 3-41

Plate 3.5e-f Hbl-bio- to bio-hbl-bearing K-feldspar megacrystic granodiorites 3-41

Plate 3.5g-h Bio±hbl-bearing K-feldspar megacrystic granodiorite and monzogranite 3-41

Plate 3.6a Layered quartz diorite-quartz monzodiorite body containing numerous microdiorite enclaves and scattered K-feldspar megacrysts 3-42

Plate 3.6b Quartz diorite containing a K-feldspar megacryst 3-42

Plate 3.6c K-feldspar megacrystic quartz monzodiorite containing a microdiorite enclave with K-feldspar xenocrysts 3-42

Plate 3.6d Hbl-bio-bearing K-feldspar megacrystic granodiorite overlying the layered quartz diorite-quartz monzodiorite body 3-42

Plate 3.7 Typical Hbl-bio-bearing K-feldspar megacrystic granodiorite containing accessory epidote, titanite and magnetite 3-43

Plate 3.8a Myrmekitic texture, composed of vermicular inclusions of quartz within plagioclase in K-feldspar megacrystic granodiorite 3-44

Plate 3.8b Macroscopically euhedral diamond-shaped crystal of titanite in K-feldspar megacrystic granodiorite 3-44

Plate 3.8c Hornblende-biotite-epidote-rich clot and inclusions of euhedral epidote in biotite in K-feldspar megacrystic granodiorite 3-44

Plate 3.8d Brown metamict allanite overgrown by smaller epidote crystals, note the subhedral apatite crystals at top of photomicrograph in K-feldspar megacrystic granodiorite 3-44

Plate 3.8e Brown metamict allanite crystal with an overgrowth of epidote where both allanite and epidote contain simple twins in K-feldspar megacrystic granodiorite 3-44

Plate 3.9 Typical medium-grained, bio-bearing granodiorite of the SCZ monzogranite series 3-45

Plate 3.10a Hbl-bio-bearing K-feldspar megacrystic quartz monzodiorite 3-46

Plate 3.10b Hbl-bio-bearing K-feldspar megacrystic granodiorite 3-46

Plate 3.10c-d Bio±hbl-bearing K-feldspar megacrystic granodiorite and

monzogranite 3-46

Plate 3.10e-g Bio-bearing K-feldspar megacrystic to coarse-grained monzogranite 3-46

Plate 3.11a Large macroscopically-euhedral K-feldspar megacryst in biotite-bearing monzogranite 3-47

Plate 3.11b Plagioclase-phyric diorite dyke intrusive to the NEZ megacrystic monzogranite series 3-47

Plate 3.11c Large microdiorite enclave containing K-feldspar megacrysts in hbl-bio-bearing K-feldspar megacrystic granodiorite 3-47

Plate 3.11d Mingling zone between diorite and bio-hbl-bearing K-feldspar megacrystic granodiorite 3-47

Plate 3.12a-b Hornblende-rich monzodiorites 3-48

Plate 3.12c-d Hbl-bio-bearing K-feldspar megacrystic to coarse-grained quartz monzodiorites 3-48

Plate 3.12e Hbl-cpx-bio-bearing K-feldspar megacrystic monzonite 3-48

Plate 3.13a Clot of hornblende crystals containing numerous inclusions of quartz, Fe-Ti-oxides and apatite in hornblende-rich monzodiorite 3-49

Plate 3.13b Crystallographic control to the orientation of quartz inclusions in hornblende in hornblende-rich monzodiorite 3-49

Plate 3.13c Relict growth zoning in K-feldspar crystal in hbl-bio-bearing K-feldspar megacrystic quartz monzodiorite 3-49

Plate 3.13d Perthitic-texture of plagioclase exsolutions in K-feldspar in hbl-bio-bearing K-feldspar megacrystic quartz monzodiorite 3-49

Plate 3.13e-f Relict cpx cores rimmed with hornblende in hbl-cpx-bio-bearing K-feldspar megacrystic monzonite 3-49

LIST OF ABBREVIATIONS A:

A/CNK ..... Molecular Al2O3/(CaO + Na2O + K2O)
A/NK ..... Molecular Al2O3/(Na2O + K2O)
AFM ..... Na2O + K2O (A) - FeO* (F) - MgO (M)
Bio ..... Biotite
CHUR ..... Chondritic Uniform Reservoir
Gb ..... Gabbro
Gdr ..... Granodiorite
Hbl ..... Hornblende
HFSE ..... High-field-strength elements
HREE ..... Heavy rare earth elements
Kd ..... Distribution coefficient
LFSE ..... Low-field-strength elements
LREE ..... Light rare earth elements
Md ..... Monzodiorite
Mgn ..... Monzogranite
MREE ..... Middle rare earth elements
Musc ..... Muscovite
Mz ..... Monzonite
QAP ..... Quartz-Alkali Feldspar-Plagioclase
QD ..... Quartz Diorite
Qmd ..... Quartz Monzodiorite
Tn ..... Tonalite
εNd ..... Epsilon Neodymium

LIST OF ABBREVIATIONS B:

CIC ..... Crowe Island Complex
CMB ..... Central Metavolcanic Belt
LRD ..... La Ronge Domain
DLSZ ..... Duck Lake Shear Zone
MIA ..... Milton Island metasedimentary assemblage
NEZ ..... Northeast Zone
PIA ..... Park Island metasedimentary assemblage
PLD ..... Peter Lake Domain
PLSZ ..... Parker Lake Shear Zone
RLSZ ..... Reilly Lake Shear Zone
SCZ ..... Southern-Central Zone
SCZ-KMGS ..... SCZ-K-feldspar megacrystic granodiorite series
SCZ-MS ..... SCZ-monzogranite series
THO ..... Trans-Hudson Orogen
NEZ-KMMS ..... NEZ-K-feldspar megacrystic monzogranite series
NEZ-MS ..... NEZ-monzonitic series

CHAPTER 1: INTRODUCTION

1.1 INTRODUCTION

The upper crust of the Earth is dominantly composed of 'granitoid' plutonic rocks, and its bulk composition is that of granodiorite (Taylor and McLennan, 1985). That granitoid rocks form such a volumetrically important component of the crust naturally leads to the inference that the processes involved in granitoid magma generation are important to the formation and evolution of the continental crust itself.

The sources for this voluminous granitoid plutonism have been variously attributed to sites within the crust, the mantle or combinations of both. Petrogenetic models proposed for the development of calc-alkaline magmatic arcs, and their associated granitoids, often call on a significant contribution from the mantle. However, granitoid plutonism is also linked spatially and temporally to other orogenic processes and the formation of granitoid magmas in such zones (*e.g.*, post-collisional settings) is commonly attributed to thermal/deformation induced disturbances in the lithosphere and asthenosphere. Distinguishing between granitoids formed in active arc settings versus post-collisional settings is an important part of deciphering the magmatic record in any orogenic belt.

Studies of large Phanerozoic granitoid batholiths, which are largely restricted to continental margin arcs or within continental plates, show that they are composed of mixtures of mantle and crustal components in varying proportions (DePaolo, 1981; Bennett and DePaolo, 1987; Liew and McCulloch, 1985; Farmer and DePaolo, 1983; Samson et al., 1991). The crustal material in these batholiths can be derived from subduction of continentally-derived sediments and/or may involve *in situ* "recycling" of the continental crust. The "mantle signature" in these large batholiths may come from the underlying asthenosphere, from subcontinental mantle lithosphere or from remelting

of a basaltic underplate previously added to the crust from the mantle (Gromet and Silver, 1987; Leake, 1990; Atherton, 1993). Isotopic constraints on the origin of the mantle signature often indicate that if this signature originated from melting of a basaltic underplate to the crust, then the recycling of this crust must have been on a rapid basis. Mixing of the crustal and mantle derived material is often hypothesized to occur at or near the crust-mantle boundary. Complex zones of mixing, assimilation, storage and homogenization (MASH) have been proposed as the ultimate source for many large granitoid batholiths (Hildreth and Moorbath, 1988), with subsequent modification of the parental magmas by fractionation and assimilation processes in the mid to upper crust (Boily et al., 1989; Davidson et al., 1991).

1.2 SETTING OF THE THESIS AREA

This thesis presents the results of an integrated field, petrological, geochemical and isotopic (Nd) study of granitoid rocks formed during the Paleoproterozoic Trans-Hudson Orogen (THO) (Hoffman 1988; Lewry and Stauffer 1990) in northern Saskatchewan. The geology of northern Saskatchewan is interpreted to preserve evidence for Paleoproterozoic continental rifting, intraoceanic island arc volcanism and sedimentation, arc accretionary events, continental magmatic arc development and eventual continent-continent collision(s). The purpose of the study is to determine the nature and evolution of granitoid magmatism in northern Saskatchewan in order to better constrain the tectonomagmatic evolution of this part of the THO.

The study area is located on Reindeer Lake which provides a unique ~ 175 km transect across several lithotectonic domains of the northern THO in Saskatchewan. This thesis was part of a regional mapping (1:50,000) project, centred in the Reindeer Lake area, which was conducted by a Geological Survey of Canada field party led by Dr. David Corrigan. Mapping was done the summers of 1998 and 1999, with a total of five months spent, by the author, in the field area.

Geochronology of volcanic, plutonic and metamorphic rocks (conventional U-Pb zircon, monazite and titanite) have, and are, being conducted by Dr. David Corrigan at the Geological Survey of Canada. This thesis draws upon the currently available geochronological data set, both published and unpublished.

Due to the scale of mapping and the size of the major plutonic body, this study was devised as a regional scale geochemical study of granitoid plutonism. The purpose of this type of approach is to try and resolve regional differences in the geochemistry and nature of the source regions for the granitoid magmatism. These differences may be related to the history and evolution of specific lithotectonic domains. One limitation of this type of study is that a detailed evolution of individual plutons, inferred to have been emplaced during the same magmatic event, cannot be adequately addressed.

Reindeer Lake provides a well exposed and an easily accessible transect through the THO. The southern and central portions of Reindeer Lake expose rocks of the Kisseynew, La Ronge and Rottenstone lithotectonic domains. The La Ronge and Rottenstone domains occupy most of this area, with parts of the Kisseynew Domain exposed at the southern end of the lake. These domains are dominantly comprised of juvenile volcano-sedimentary belts of arc-affinity, which are intruded by several later plutons of variable size and composition. The northern portion of the lake exposes portions of the Wathaman Batholith and Archean basement rocks of the Peter Lake Domain.

1.3 AIMS OF THE THESIS

The major aim of the thesis was to examine the nature and evolution of plutonism associated with the Wathaman Batholith and to determine its relationship to the plutonism located within the mainly juvenile arc-related terranes of the La Ronge and Rottestone domains. Although many of the plutons within the confines of these arc-related domains are contemporaneous with the

emplacement of the Wathaman Batholith (and not with volcanism), they have traditionally been thought to have formed in an island arc setting (Bickford et al., 1990). These interpretations are largely based on the interpretation of major and trace element data, with only a limited number of Nd and Pb isotopic measurements from restricted portions of the domains. However, it has also been suggested that the Wathaman Batholith and contemporaneous plutons of the La Ronge and Rottenstone domains represent one large batholithic complex (Lewry et al., 1980).

Studies of the Wathaman Batholith (Fumerton et al., 1984; Meyer et al., 1992) have emphasised that it is a remarkably homogeneous granite-granodiorite pluton and suggest that it is quite different from the Phanerozoic batholiths formed in continental-arc settings, although they interpret it as the root of a continental-arc based on trace element geochemical characteristics. It is now recognised that arc-type geochemical signatures, *e.g.*, calc-alkaline affinity, high low field-strength element (LFSE) to high field strength element (HFSE) ratios, negative Nb (relative to Th and La) on primitive mantle normalised plots, occur in rocks where no evidence for contemporaneous subduction is found (*e.g.*, Morris et al., 2000). The observation that the Wathaman Batholith apparently also lacks comagmatic mafic phases (Fumerton et al., 1984), a common feature of subduction-related granitoids (Pitcher, 1997) is in conflict with an origin for the batholith by subduction-related processes. Fumerton et al. (1984) suggests that the batholith "*may be considered as just one phase of a larger batholithic belt that also includes numerous smaller plutons. Taken as a whole the composite batholithic belt is similar in many aspects to Mesozoic Pacific rim batholitic belts, and like them was probably emplaced during plate collision*". The Wathaman Batholith may indeed be part of this "composite batholithic belt", however this does not explain its remarkably homogeneous nature and felsic character. The interpretation that it may represent a single "phase" of this batholitic complex is difficult to explain considering its size. The

homogeneity of the Wathaman Batholith must be re-evaluated, as it poses the biggest threat to subduction-related models for its formation, and thus for the tectonic development of the northwest Reindeer Zone, as all tectonic models involve a northerly dipping subduction zone beneath the Hearne margin during the emplacement of the batholith.

New mapping in the La Ronge-Rottenstone domains and the Wathaman Batholith, combined with geochronological, geochemical, and isotopic studies have been undertaken to help resolve the apparent dichotomy that the Wathaman Batholith is the root of a continental-arc but is not similar to Phanerozoic equivalents (save for a few geochemical characteristics). These studies will also help clarify the Wathaman Batholiths relationship to contemporaneous plutonism in the northwest Reindeer Zone.

1.4 ORGANIZATION OF THE THESIS

Chapter 2 reviews the previous geological and geochronological information available on the northwest Reindeer Zone, the Wathaman Batholith and the Cree Lake Zone. This information is mainly derived from studies conducted along strike to the southwest of the Reindeer Lake area. This will provide a basis to compare and contrast the regional geological information obtained from mapping in the Reindeer Lake area. Chapter 3 describes the geological information from mapping in the Reindeer Lake area with descriptions of the various lithotectonic domains of interest. The rock types found in these domains as well as their structural, metamorphic and geochronological histories will be discussed. The second half of chapter three will discuss the granitoid rocks, beginning with a brief description of the major subdivisions of the granitoid rocks in the area, and a justification for that subdivision. This will be followed by a detailed description of the composition, textural features, field relationships, structural and metamorphic histories, and available geochronological data for the granitoids. Chapter 4 presents the geochemical and

isotopic data obtained from the Wathaman Batholith and La Ronge Domain plutons. It includes a discussion of the major, trace and rare earth element (REE) data, as well as Sm and Nd isotopic data. Chapter 5 presents the results of geochemical modelling and provides a petrogenetic model for the formation and evolution of the Wathaman Batholith and plutons of the La Ronge Domain. Concluding the thesis, a tectonomagmatic model is proposed for the evolution of the northwest Reindeer Zone between ca. 1865-1850 Ma.

To facilitate the review of the material in this thesis, each chapter presents the text - followed by the tables, figures and plates. Descriptions of the analytical techniques and the data obtained during this study are presented in the appendices.

CHAPTER 2: REGIONAL GEOLOGY

2.1 INTRODUCTION

The Trans-Hudson Orogen (THO) (Hoffman, 1988; Lewry and Stauffer, 1990) extends from South Dakota, through the exposed Canadian Shield in Saskatchewan and Manitoba, across Hudson Bay to northern Quebec. It is part of the larger Paleo- to Meso-proterozoic orogenic system that assembled several Archean cratonic blocks and juvenile Paleoproterozoic terranes during the assembly of the North American continent (Hoffman, 1988). The THO is the most extensively preserved Paleoproterozoic orogenic belt on Earth (Bickford et al., 1990), with remarkable preservation in northern Saskatchewan and Manitoba (Figure 2.1).

Volcanic rocks preserved within the THO provide evidence of extended periods of dominantly mantle-derived (juvenile) arc and oceanic volcanism (Watters and Pearce, 1987; Chauvel et al., 1987; Syme, 1990; Thom et al., 1990). The formation, accretion and preservation of these juvenile intraoceanic terranes clearly represents new additions to the crust from the mantle, whether or not they represent net crustal growth is a matter of speculation. Within northern Saskatchewan the THO is also comprised of extensive tracts of plutonic rocks, whose relationship to volcanism is equivocal. Some of the plutonism is coeval with volcanism, however, much of it is later (Bickford et al., 1986; Van Schmus et al., 1987; Bickford et al., 1992; Heaman et al., 1992). The origin of this later plutonism can shed light on the tectonic and magmatic evolution of the orogen and may preserve evidence of the pre-intrusion history of the underlying crustal section through which they were emplaced.

2.2 GEOLOGY OF THE TRANS-HUDSON OROGEN IN NORTHERN SASKATCHEWAN AND MANITOBA

The THO, as exposed in northern Saskatchewan and Manitoba, is composed of a collage of

juvenile arc-related Paleoproterozoic lithotectonic domains, that were accreted to the Archean Hearne margin during Paleoproterozoic collision(s) (Lewry et al., 1990). Domain subdivisions are based on variations in lithological associations, structural style, metamorphic grade and are largely separated from each other by high strain zones. Within northern Saskatchewan and Manitoba these domains (volcano-plutonic-sedimentary belts) are collectively known as the Reindeer Zone (Stauffer, 1984). The Reindeer Zone occupies the internal portion of the orogen and is bounded by Archean rocks and their reworked margins (Figure 2.1). The Superior Province and its reworked margin (Churchill-Superior Boundary Zone) confines the orogen to the southeast. In the northwest the Reindeer Zone is separated from the Hearne Domain and its reworked margin (Cree Lake Zone) by the Wathaman Batholith. This extremely large batholith has an exposed strike length of over 800 km parallel to the regional trend of the orogen, and varies from less than 15 km to over 150 km in width. Archean basement is exposed as tectonic windows within the Reindeer Zone (Van Schmus et al., 1987; Chiarenzelli, 1989). Seismic studies across the THO have revealed the presence of an Archean microcontinent, known as the Sask Craton (Ansdell et al., 1995) underlying portions of the central Reindeer Zone. This new result places a fundamental constraint on the volume of juvenile material within the Reindeer Zone.

2.3 GEOLOGY OF THE NORTHWEST REINDEER ZONE

The Reindeer Zone in northern Saskatchewan and Manitoba consists of all lithotectonic elements lying between the Wathaman Batholith to the north and west, and the Churchill-Superior Boundary Zone to the southeast. The following discussion will be limited to the northwestern portion of the Reindeer Zone as exposed in northern Saskatchewan. This is not a strictly defined area *per se* and for the purposes of this work describes the northerly dipping volcano-sedimentary belts of the Rottenstone Domain, La Ronge Domain (LRD), and portions of the northwestern

Kisseynew Domain (MacLean Lake Belt) as exposed in northern Saskatchewan (Figure 2.2).

The remaining portions of the Kisseynew, the Glennie and Flin Flon domains to the south and west are important portions of the THO; however, they are not intimately involved with this northern portion and its relationship to the Archean Hearne margin. Interaction between these domains and the northwest Reindeer Zone did not occur until major collisional events late in the evolution of the orogen.

An emphasis will be placed on the Rottenstone and LRDs, and the Archean Peter Lake Domain, since granitoids from this study are found within, or are bounded by these domains.

2.3.1 Geology of the La Ronge Domain

The LRD is bordered by the Rottenstone Domain to the west and the Kisseynew Domain (MacLean Lake Belt) to the east. It is comprised of a series of variably strained northwest- to north-dipping volcano-sedimentary belts and is bounded by a high strain zone with the Kisseynew Domain (McLennan Lake Tectonic Zone) (Thomas, 1993). The domain can be divided into two distinctive belts, the Central Metavolcanic Belt (CMB) underlying the central LRD, and the Crew Lake Belt flanking it to the northwest. The CMB is dominantly comprised of metavolcanic and minor intercalated sedimentary rocks, intruded by late volcanic, to syn- to post-tectonic plutons, plugs and dykes (Thomas, 1993). The Crew Lake Belt is comprised of a monotonously uniform package of pelitic and psammopelitic rocks.

At the McLennan Lake Tectonic Zone, the LRD is structurally emplaced above rocks of the Kisseynew Domain. Occupying the immediate structural footwall are meta-arkoses of the McLennan Group. At the southern portion of this tectonic boundary, arkoses of the McLennan Group have been observed to stratigraphically overlie metavolcanic rocks of the CMB, and are interpreted to be part of a younger molasse basin (Stauffer, 1984). These younger arkoses

structurally overlie a heterogeneous sedimentary package comprised of pelitic, psammopelitic, conglomeratic, calcareous and amphibolitic rocks known as the MacLean Lake Gneisses. The northern boundary of the LRD with the Rottenstone Domain will be discussed in detail in the next section.

In the CMB metavolcanics, subaqueous and subareal volcanics are recognized, mafic compositions dominate and felsic volcanic material comprises less than 10% of the volcanic successions. The proportion of flows versus volcaniclastic material is quite variable, although flows seem to dominate in the southwestern portion of the belt (Thomas, 1993). The rocks range in composition from low-K tholeiitic to calc-alkaline series (Watters and Pearce, 1987). Based on geochemical patterns and field observations the volcanics in the southern part of the CMB are interpreted to have formed in a dominantly oceanic island-arc type tectonic environment (Watters, 1984, 1985, 1986; Watters and Pearce, 1987). Portions of the belt display continental-arc geochemical (Watters and Pearce, 1987) and isotopic affinities (Thom et al., 1990).

The metavolcanic and metasedimentary belts of the LRD are intruded by numerous syn- to post- tectonic, and minor late volcanic plutons. The plutons vary from composite intrusions of gabbro, quartz diorite to granite, homogeneous tonalitic, granodioritic and granitic plutons to late high level porphyritic leuco-granodiorites and granites (Thomas, 1985). A strong calc-alkaline character combined with other major and trace element characteristics are consistent with formation within a volcanic-arc type environment (Watters, 1985,1986; Thomas, 1993; Janser, 1994). It has been noted that plutons located within the CMB are more mafic in composition than those that intrude into areas dominated by sedimentary rocks. All plutons display some degree of deformation and foliation development either at the margins or internally.

2.3.2 The Rottenstone Domain and its Relationships

The Rottenstone Domain has been defined (see Ray and Wanless, 1979) to include deformed and migmatized rocks of plutonic and supracrustal protoliths, as well as the K-feldspar megacrystic granitoids of the Wathaman Batholith. A tonalite-granodiorite suite and a later more acidic phase were identified in the complex zone located between the batholith and earlier supracrustal and intrusive rocks. The acidic phase in this complex zone was interpreted to be related to the Wathaman Batholith (Gilboy, 1975; Lewry, 1976; Ray and Wanless, 1980) and provided the main rationale for including the Wathaman Batholith in the Rottenstone Domain.

More recently, the currently accepted subdivisions of the THO in northern Saskatchewan and Manitoba were established by Stauffer (1984). Stauffer (1984) separated the Wathaman Batholith and the tonalite-migmatite-acidic complex described above, and defined the Reindeer Zone as all lithotectonic elements lying between the Wathaman Batholith and the Churchill Superior Boundary Zone to the southeast.

The boundary between supracrustal rocks of the Rottenstone and LRDs is a transitional one, and varies from about 2-5 km wide in the southwest to approximately 10-15 km wide in the Reindeer Lake area, where it is even less well defined (Lewry et al., 1981). Ray and Wanless (1980) report that supracrustal rocks of the Rottenstone Domain pass gradationally into metamorphosed volcanics, volcaniclastics, and sedimentary rocks of the LRD. They attribute the decrease in migmatization found within the LRD to an overall lowering of the metamorphic grade. The LRD also contains plutonic rocks of similar character to those found within the Rottenstone Domain. Thus the main distinguishing feature between the Rottenstone and the LRDs appears to be that the LRD contains more extensive and less migmatized supracrustal material. Lewry and others (1981) actually grouped the La Ronge and Rottenstone domains together, and termed them the Rottenstone-La Ronge magmatic belt.

The relationship between the Wathaman Batholith and supracrustal rocks of the Rottenstone Domain also appears gradational (Ray and Wanless, 1980; Stauffer et al., 1980; Lewry et al., 1981). The contact zone has been interpreted as a complex zone of injection and metasomatism that varies from several hundred metres to over two kilometres (Lewry et al., 1981), although it has been reported to be over 20 km wide in sections exposed on Reindeer Lake (Fumerton et al., 1984).

2.4 THE WATHAMAN BATHOLITH

The Wathaman Batholith straddles the boundary between and separates the reworked Archean basement rocks of the Cree Lake Zone from the Paleoproterozoic lithotectonic domains of the Reindeer Zone. The batholith has been described as a remarkably homogeneous intrusion, dominated by K-feldspar megacrystic to coarse-grained monzonite, quartz monzonite, granodiorite, and granite, with only minor diorite and aplite (Stauffer et al., 1981; Fumerton et al., 1984; Meyer et al., 1992). It has been interpreted as representing the root of a continental magmatic arc, and is comparable in size and geochemical characteristics to some of the large Phanerozoic arc-related batholiths of the western cordillera of North and South America (Fumerton et al., 1984; Meyer et al., 1992).

The batholith is separated from the rocks of the Cree Lake Zone to the north and west over much of its length by post-emplacement ductile shear zones. The most westerly portion of the batholith is in structural contact with rocks of the Cree Lake Zone along the extensive Needle Falls Shear Zone. The northern portion of this mega-shear splays of into the Parker Lake Shear Zone. The Reilly Lake Shear Zone is an eastern extension of the predominantly northeast trending Parker Lake Shear Zone that cuts across and attenuates the batholith. The Reilly Lake Shear Zone extends at least as far as Reindeer Lake where it separates the batholith from the Rottenstone Domain (see

Figure 2.2).

2.5 THE CREE LAKE ZONE OF THE SOUTHEASTERN HEARNE PROVINCE

The southeastern portion of the Archean Hearne domain to the north and west of the Wathaman Batholith has undergone extensive thermotectonic reworking during the THO and is known as the Cree Lake Zone. The Cree Lake Zone is further subdivided into the Wollaston and Peter Lake domains due to differences in lithological association and structural relationships.

The Wollaston Domain occupies the western portion of the Cree Lake Zone and is composed of two contrasting lithological and chronological entities. The basement to the Wollaston Domain consists of foliated and gneissic plutonic rocks of Archean age (Ray and Wanless, 1980; Krogh and Clarke, 1987), unconformably overlain by and in-folded with Lower Proterozoic supracrustal assemblages of the Wollaston Group. The lowermost sequence of the Wollaston Group records a Lower Proterozoic rifting event of the eastern margin of the Hearne craton at ca. 2100 Ma (MacNeil, 1998; Frossenier et al., 1994) and subsequent development of a passive margin sequence in the upper portions of the Wollaston Group.

The Peter Lake Domain is a sharply defined crustal block that occupies the area between the Wollaston Domain and the Wathaman Batholith in northern Saskatchewan. This domain is dominantly composed of plutonic rocks with only minor supracrustal rocks. Two major plutonic suites are recognized: older gabbroic, dioritic and tonalitic rocks with minor anorthosite and ultramafic plutonic bodies; and younger bodies of syeno- and monzo-granite (Ray and Wanless, 1980). The older mafic suite often preserves well-developed igneous textures and layering (Fumerton et al., 1984). It is separated from the Wollaston Domain by the Needle Falls Shear Zone and from the Wathaman Batholith by the Parker Lake Shear Zone. However, Ray and Wanless (1980) have reported an intrusive relationship between K-feldspar megacrystic rocks of

the Wathaman Batholith and sheared rocks of the southwestern portion of Peter Lake Domain. The relationship between the northeasterly portion of the Peter Lake Domain and the Wathaman Batholith is described as a complex intrusive junction on Reindeer Lake (Lewry et al., 1981).

2.6 U-PB ZIRCON GEOCHRONOLOGY OF IGNEOUS ROCKS OF THE NORTHWEST REINDEER ZONE, THE WATHAMAN BATHOLITH AND THE CREE LAKE ZONE

Igneous activity within the northwest Reindeer Zone and emplacement of the Wathaman Batholith took place between ca. 1915 and 1834 Ma (Figure 2.3). The oldest known rocks in the northwest Reindeer Zone are volcanic rocks. Ages of felsic volcanism within the Lynn Lake Belt (eastern extension of LRD in Manitoba) range from 1915 Ma to 1878 Ma (Baldwin et al., 1987). Volcanism within the LRD is better constrained and ranges in age from 1876 to 1882 Ma (Van Schmus and Bickford, 1984; Bickford et al., 1986). A diabase dyke from the Barlett Lake area of the LRD yielded an age of 1885 ±3 Ma (Heaman et al., 1991), in agreement with the age of volcanism.

Two plutons within the Lynn Lake belt, a quartz diorite and a tonalite yielded ages of 1876 +8/-7 and 1876 +8/-6 Ma (Baldwin et al., 1987), respectively, and overlap with the youngest age of volcanism in the belt (1878 ±3 Ma). Within the LRD plutonism is bracketed between 1874 ±1 and 1834 ±13 Ma (Bickford et al., 1986; Van Schmus et al., 1987; Bickford et al., 1992; Heaman et al., 1991), most group between 1860-1848 Ma, i.e., approximately 15 to 25 Ma after volcanic activity in the domain.

Two gneissic tonalites from the Rottenstone Domain have yielded igneous crystallization ages of 1863 ±12 and 1867 ±8 Ma. One sample yielded ages of 1885 ±14 and 1922 ±24 Ma, which were attributed to inheritance of older zircon cores. The younger 1867 ±8 Ma age was obtained on hand picked core-free zircons.

The Wathaman Batholith has been dated between 1866 ±12 and 1853 ±10 Ma (Ray and Wanless, 1980; Bickford et al., 1986; Meyer et al., 1992). A late undeformed granitic sheet that cross cuts the main foliation of the batholith yielded a 1830 ±6 Ma age, placing a minimum age on the major deformation experienced by the batholith (Meyer et al., 1992).

Plutonic rocks from the Peter Lake Domain yield ages of ca. 2500 ±50 Ma to 2597 ±20 Ma (Ray and Wanless, 1980; Bickford et al., 1987; Bickford et al., 1992; Annesley et al., 1992). However, two samples in this domain obtained from the northwestern shore of Reindeer Lake yield Proterozoic ages. A granitic gneiss gave an age of 1860 ±5 Ma (Bickford et al., 1987), in agreement with the age for the immediately adjacent Wathaman Batholith, and suggests the gneiss is possibly a highly deformed early phase of it. A gabbro pegmatite yielded an age of 1865 ±10 Ma (Bickford et al., 1986), but with further analysis of zircon a revised age of 1908 ±27 Ma was reported (Bickford et al., 1987). The youngest age suggests that the gabbro could be one of the earliest phases of the Wathaman Batholith at 1865 Ma. The revised age of 1908 Ma does not correspond well with other ages in the area and the significance of this result (? inheritance) is unclear.

Basement plutonic rocks of the Wollaston Domain (2494 ±38 Ma to 2733 ±9 Ma) average slightly older ages than those from the Peter Lake Domain (Ray and Wanless, 1980; Krogh and Clarke, 1987). Within the Courtney Lake area of the eastern Wollaston Domain a foliated syenogranite and a mylonitic quartzofeldspathic gneiss have been dated at 2086 +52/-8 Ma and 2076 ±3 Ma respectively. The 2076 ±3 Ma age was obtained by the analysis of three individual zircons, which gave concordant ages of 2074, 2075 and 2079 Ma respectively. It has been argued that the zircons were derived from the syenogranite mentioned above, if so they place a maximum age of rifting in the Courtney Lake area (see Fossenier et al., 1994).

2.7 TECTONIC HISTORY OF THE AREA

The oldest volcanic rocks in the northwest Reindeer Zone are interpreted to be remnants of juvenile intraoceanic arc-terranes formed between 1915 and 1878 Ma (Baldwin et al., 1987; Van Schmus and Bickford, 1984; Van Schmus et al., 1987; Bickford et al., 1986). These juvenile arc-terranes (volcano-sedimentary belts) were accreted to the Hearne margin prior to the emplacement of the Wathaman Batholith at ca. 1865 Ma, interpreted to have formed over a northerly dipping subduction zone beneath the Hearne Craton (Bickford et al., 1990; Meyer et al., 1992). Terminal collision of the Reindeer Zone with the Superior and Sask cratons occurred between 1830 and 1800 Ma (e.g. Bickford et al., 1990). Regional metamorphism, deformation and south-directed thrusting of the Reindeer Zone occurred during this period (Lewry et al., 1990).

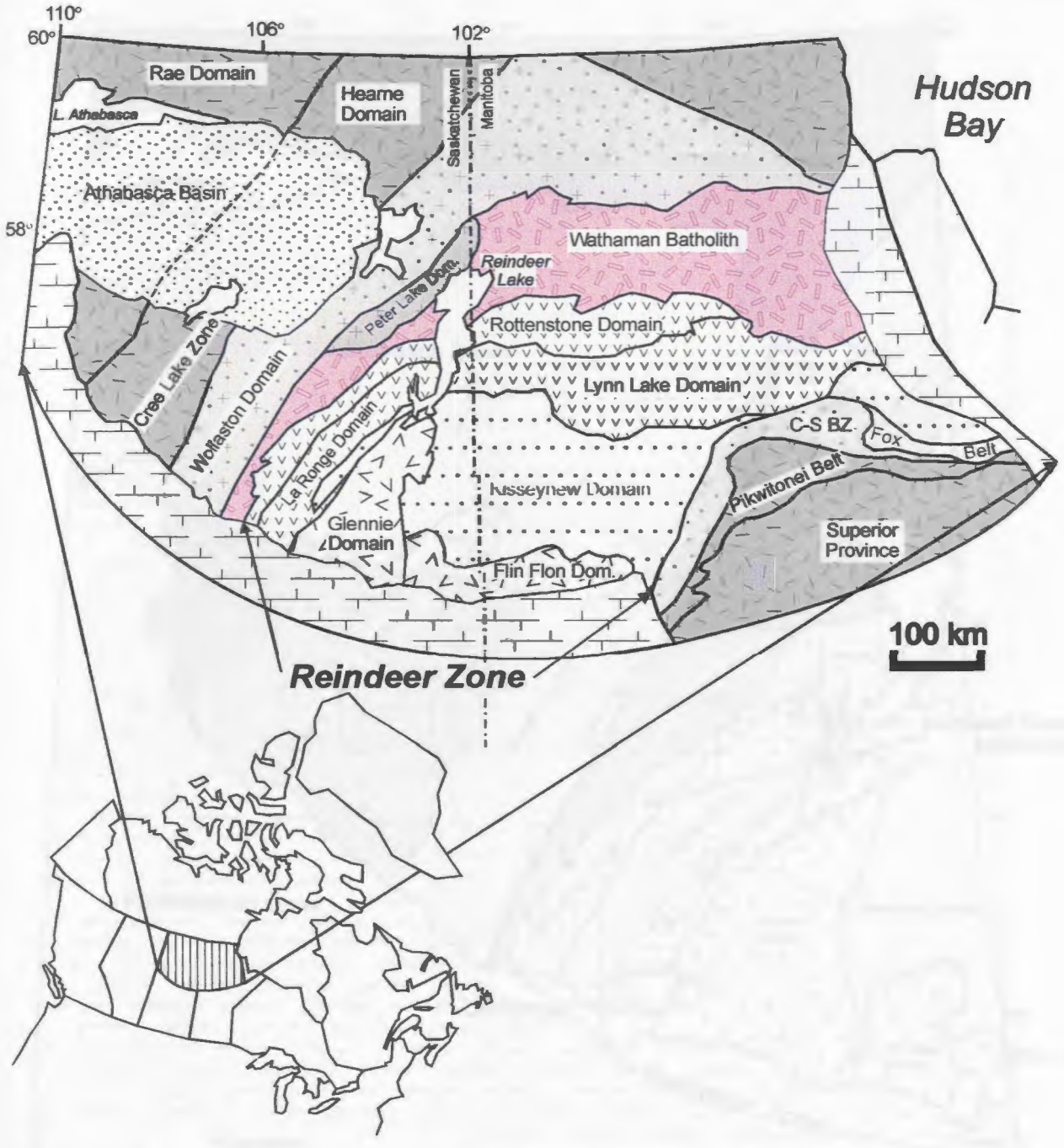

Figure 2.1 Extent of the Trans-Hudson Orogen (THO) in northern Saskatchewan and Manitoba and its lithotectonic subdivisions. Lithotectonic domains (unshaded) are collectively termed the *Reindeer Zone* (Stauffer, 1984). Bounding Archean rocks (dark shading) to the THO are the Rae-Hearne domains to the northwest, and the Superior Province to the southeast. Archean basement and their Paleoproterozoic cover sequences are represented by the light shading. Extensively reworked portions of these Archean domains are know as the Cree Lake Zone (Hearne) and the Churchill-Superior Boundary zone (C-S BZ - Superior). The Wathaman Batholith is shaded light pink. (Modified after Lewry et al., 1990).

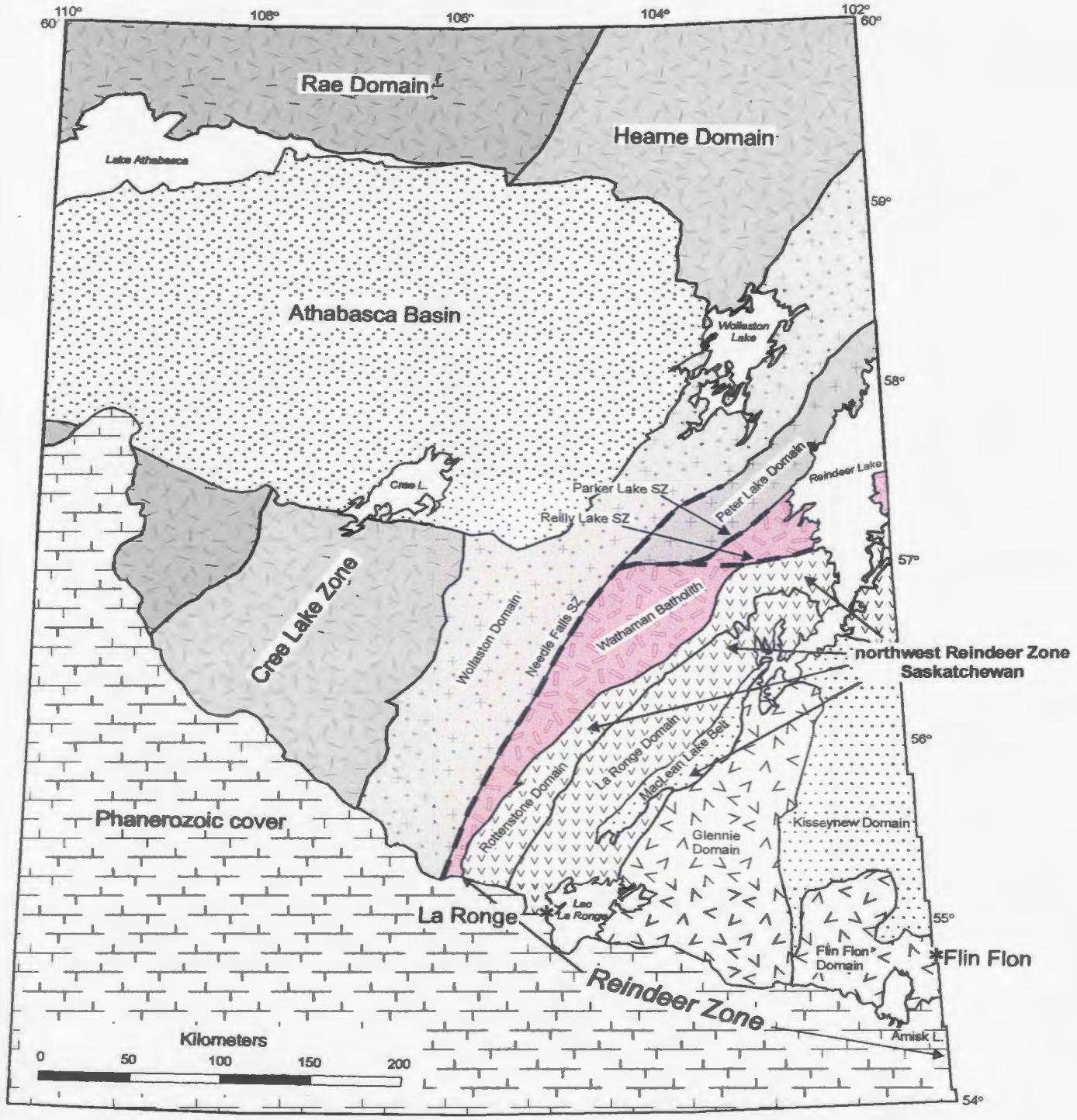

Figure 2.2 Lithotectonic domains of northern Saskatchewan and location of Reindeer Lake within the northwest Reindeer Zone (as discussed in the text). Archean Rocks of the complex Rae-Hearne Domains are located in the northwestern portion of Saskatchewan (grey shading). Modified after Ashton, (1999).

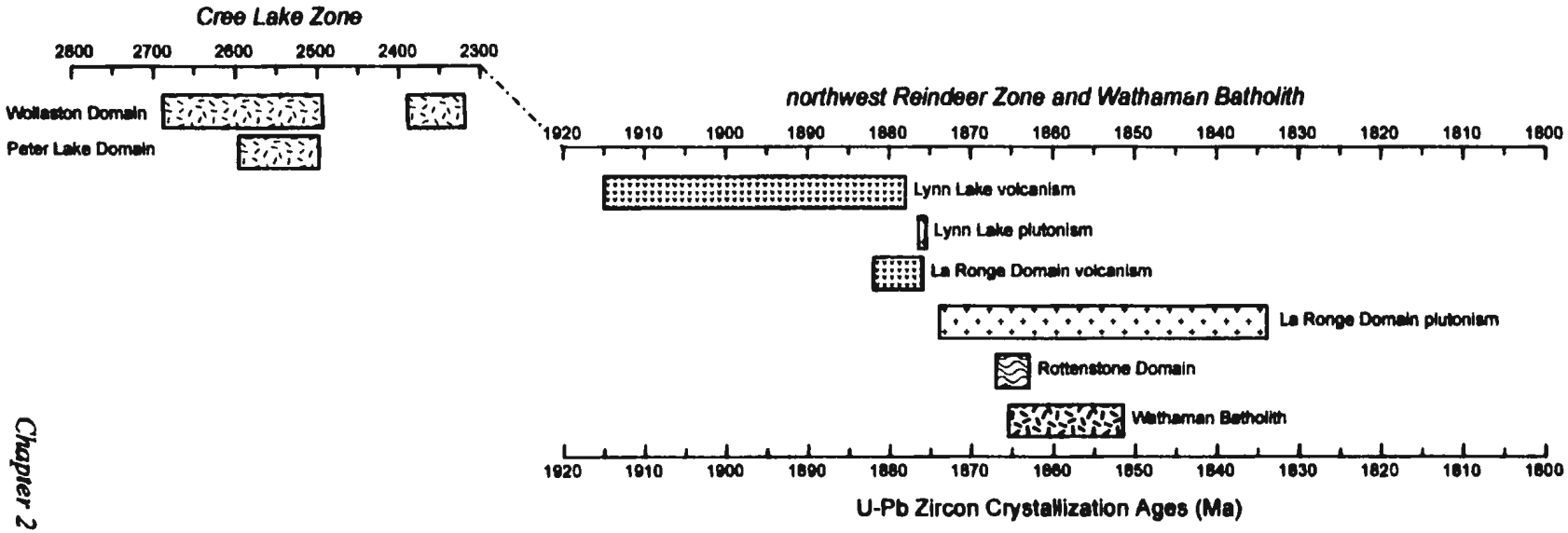

Figure 2.3 Summary of U-Pb zircon geochronology of the northwest Reindeer Zone, the Wathaman Batholith and the Cree Lake Zone. References are cited in the text.

CHAPTER 3: GEOLOGY AND DESCRIPTION OF PLUTONIC ROCKS IN THE REINDEER LAKE AREA

3.1 INTRODUCTION

In this chapter we review the geology of the Reindeer Lake area, including the geochronology, structural and metamorphic history. Most importantly, the division of the plutonic rocks into zones and series will be discussed, and a description of their field characteristics, composition, mineralogy, texture, fabrics, and distribution within the map area will follow. The division of the plutonic rocks is based on field observations, spatial distribution and modal mineralogy. However, as the reader can appreciate, the establishment of the divisions was an iterative process that also involved examination of the geochemical data. For example, mesonorms based on major element data were used in conjunction with the results of staining of rock slabs to classify the rocks. This use of the geochemistry is primarily descriptive, basic and from a practical perspective - unavoidable.

3.2 GEOLOGY OF THE REINDEER LAKE AREA

Reindeer Lake has been mapped at a variety of scales since 1928; Stockwell, 1929; 1:253,440 - Alcock, 1938; 1:63,000 - Cheesman 1959, Pyke 1960, Shklanka 1962, Sibbald 1977, Johnston 1983; 1:100,000 - Stauffer et al. 1979, 1980; Gilboy 1980. The results of this previous mapping were compiled at 1:250,000 for the northern (Macdonald and Thomas, 1983; NTS 64E), and southern (Johnstone and Thomas, 1984; NTS 64 D) portions of the lake. Other mapping investigations of the northern portion of the lake have been conducted by Potter (1979), and MacDougal (1988).

The most recent mapping on Reindeer Lake was conducted by the Geological Survey of Canada (GSC) and details of the preliminary mapping results can be found in Corrigan et al.

(1997; 1998a; 1998b; 1999a; 1999b). The regional mapping by the GSC is part of a collaborative effort with the Saskatchewan Geological Survey (SGS) in and around the Reindeer Lake area. This mapping forms part of the La Ronge - Lynn Lake Bridge Project, initiated in 1996 and focussed on remapping portions of the northern LRD and its exposures in the southern Reindeer Lake area. Preliminary results of 1:20,000 mapping by the SGS can be found in Maxeiner (1996; 1997; 1998; 1999) and Harper (1996; 1997; 1998; 1999).

3.2.1 Geological overview of the area

The geology of Reindeer Lake north of the Kisseynew Domain can be divided into three main components. These include: (1) The LRD - early assemblages consisting of poly-deformed and metamorphosed Paleoproterozoic volcanic, plutonic and sedimentary rocks; (2) a slightly younger series of calc-alkaline plutons, including the Wathaman Batholith; and (3) The PLD - a relatively narrow belt of Archean basement rocks, dominated by metaplutonic rocks. The early assemblages of the LRD underlie most of the southern half of the lake, with the later plutons comprising approximately 40 % of that area. The northern portion of the lake is almost completely underlain by the Wathaman Batholith, and the PLD is exposed along a narrow ~10 km long strip on the northwestern shore of the lake (Figure 3.1).

3.3 EARLY ASSEMBLAGES OF THE LA RONGE DOMAIN

The LRD as defined on Reindeer Lake underlies the area between the DLSZ in the south, and the RLSZ to the north (Figure 3.1). The early assemblages in the domain can be divided into three main lithological units: (1) discrete belts of volcanic, volcaniclastic, epiclastic and intercalated sedimentary rocks, known as volcano-sedimentary belts. These form a collage of west-southwest-striking, northerly dipping Paleoproterozoic volcano-sedimentary belts (referred to as lithotectonic domains); (2) a series of banded dioritic to granitic orthogneiss; and (3) two large

tracts of metasedimentary assemblages. Extensive tracts of later plutons intrude the LRD.

In the southern LRD two discrete belts of volcanogenic rocks were identified and interpreted as eastern extensions of the CMB identified to the southwest (Maxeiner, 1997; Corrigan et al., 1997; 1998a). These two belts contain highly deformed mafic to intermediate volcanic and volcaniclastic rocks, altered volcanogenic and epiclastic rocks, and minor metapelites and ferruginous psammitic rocks (Corrigan et al., 1998a). Both belts contain tabular granodioritic and gabbroic intrusive rocks, and one of them contains tectonically disrupted layered to massive mafic-ultramafic intrusions.

Within the northern and central parts of the domain very similar belts of volcanogenic material have recently been identified (Corrigan et al., 1998b, 1999a) (Figure 3.1). Volcaniclastic rocks dominate these northerly belts (Plate 3.1a), with lesser amounts of mafic volcanic material. Corrigan et al. (1998b) suggested that these belts were northern equivalents of the CMB identified to the south. A preliminary U-Pb zircon age of 1905 +22/-5 Ma has recently been obtained on a rhyolite from Clements Island area in the central LRD (Corrigan et al., unpubl. rept.). This age is similar to ages of felsic volcanism reported from the Lynn Lake Belt in Manitoba between 1915 and 1878 Ma (Baldwin et al., 1987). However, this age is older than the reported age of felsic volcanism from the LRD to the southwest (1882 and 1876 Ma; Van Schmus and Bickford, 1984; Bickford et al., 1986). This result suggests a closer association between these northern volcanogenic belts, and those of the Lynn Lake Belt and further geochronological and geochemical investigations are needed. Regardless of the temporal relationship between these volcanogenic belts, they are all several 10's of Ma older than the plutons investigated during this study.

Spatially associated with the volcanogenic belts is a series of distinctive banded dioritic to granitic orthogneiss named the Crowe Island Complex (CIC) (Corrigan et al., 1997) (Figure 3.1).

On outcrop scale the complex is very heterogeneous, and contains early dioritic and tonalitic phases cut by the later more granitic phases (Plate 3.1b). Original igneous textures are not preserved and the rocks are completely recrystallized, the degree of partial melting ranges from incipient to approximately 40 % (Corrigan et al., 1997). Two U-Pb zircon ages have been obtained from a tonalite and a granite from the CIC, yielding ages of 1892 ± 2 and 1886 ± 4 Ma respectively (Corrigan et al., 1988b). These ages are broadly similar to those determined for volcanic rocks of the LRD and Lynn Lake Belt, and are also significantly older than the major plutons of the LRD (1866-1848 Ma; Bickford et al., 1986; Van Schmus et al., 1986). Corrigan et al. (1998b) interpreted the complex as representing a deformed calc-alkaline intrusive complex, and possibly the plutonic root to some of the La Ronge volcanogenic belts, this is supported by their close spatial and temporal relationship and isotopic data discussed in later sections.

Metasedimentary rocks underlie large portions of the LRD (Figure 3.1). The metasedimentary rocks have been separated into two compositionally and stratigraphically distinct units: the Milton Island metasedimentary assemblage (MIA), and the Park Island metasedimentary assemblage (PIA). The MIA structurally and stratigraphically overlies rocks of the CMB, and CIC (Corrigan et al., 1999a). It consists of variably migmatized, finely graded and layered biotite psammite and psammo-pelite, with muscovite, graphite and fibrolite as common metamorphic minerals. Stromatic leucosomes of quartz and/or granitic composition are separated from the paleosome by thin biotite-rich selvages (Plate 3.1c). This assemblage is remarkably homogeneous over a large geographical area, although it is locally interlayered with thin, metre scale, volcanic and or epiclastic volcanic rocks as well as rare calc-silicate (Corrigan et al., 1999). The PIA forms a distinctive package of siliciclastic rocks lying structurally and stratigraphically on top of the CMB and the MIA. A polymictic conglomerate, containing various clasts of rocks with similarities

to those in the CMB marks the basal section. The conglomerate is overlain by pink to grey arkoses rocks dominated by K-feldspar. Sedimentary structures are locally preserved such as trough crossbeds and laminated beds (Plate 3.1d). Calc-silicate layers and pods are also present in some outcrops. Biotite and magnetite porphyroblasts form the main mafic minerals with hornblende only occurring locally. Migmatization has effected this assemblage to varying degrees, from only minor migmatitic segregations to almost complete remobilization near the Wathaman Batholith (Plate 3.1e). Large rafts of the arkose are also found within the Wathaman Batholith (Figure 3.1) constraining its minimum age of deposition.

3.3.1 Rottenstone and Kisseynew Domains

An important result from the regional mapping conducted on Reindeer Lake was the recognition that LRD lithologies mapped in the southern portion of the lake, continue northward as far as the Wathaman Batholith and are intruded by it. The tonalite-granodiorite-acid migmatite complex (see Chapter 2) that characterizes the Rottenstone Domain to the southwest (e.g. Ray and Wanless, 1980) does not outcrop on Reindeer Lake. The Rottenstone Domain on Reindeer Lake was found to be dominantly underlain by supracrustal rocks, very similar in character to those mapped further south. Compositionally similar plutons are also found, and display similar relationships to the surrounding supracrustals. These observations suggested to Corrigan et al. (1998b, 1999a) that these rocks were actually part of the LRD. Hence for the purposes of this thesis no further reference will be made to the Rottenstone Domain concerning rocks exposed on Reindeer Lake.

The Kisseynew Domain on Reindeer Lake lies south of the DLSZ (Maxeiner, 1997), where rocks of the CMB are thrust over younger arkoses rocks of the McLennan Group (Figure 3.1). The arkoses form a footwall synformal structure below the DLSZ. In this study all granitoid samples

are found within the LRD, and the Wathaman Batholith, and thus a detailed description of the Kisseynew Domain is not warranted. For a more detailed description of the Kisseynew Domain on Reindeer Lake see Corrigan et al. (1999a).

3.3.2 Structural and Metamorphic Framework

From currently available geochronological data and tectonostratigraphic relationships, four distinct structural levels have been identified along the Reindeer Lake transect (Corrigan et al., 1999a) (Figure 3.2a). Rocks of the CMB, and their northern extensions, along with orthogneiss of the CIC are the oldest rocks in the area, and form structural level 1. The MIA stratigraphically overlies the CMB and the CIC and forms Level 2. The PIA lies unconformably on rocks of level 1 and 2, and forms level 3. Level 4 is comprised of rocks of the McLennan Group of the Kisseynew Domain (Figure 3.2a).

Three major episodes of ductile deformation are observed in the area (Sibbald, 1977; Stauffer et al., 1979; Maxeiner, 1997; Corrigan et al., 1998a). The earliest phase of deformation consists of large-scale recumbent folds (F_1) that fold rocks of the CMB, CIC, and MIA (Figure 3.2a). The M_1 metamorphism only produced phyllosilicates (S_1) parallel to bedding planes.

The most pervasive deformational event (D_2) consisted of the formation of south-verging reclined to recumbent folds and south-directed ductile thrust zones, and was coincident with the attainment of peak metamorphic conditions (M_2). The F_2 axial traces strike predominantly west to west-southwest, and peak mineral assemblages are contained in F_2 axial planes and S_2 mylonitic foliations. Shear zones have developed at the structural base of the Wathaman Batholith (RLSZ), and along the structural base of the LRD (DLSZ). These shear zones are very similar and contain consistent down-dip mineral extension lineations. All the major rock units in the Reindeer lake area have been affected by the D_2-M_2 event including a 1830 Ma porphyry dyke (Corrigan et al.,

unpubl. rept.) suggesting that it occurred after that date. Concordant monazite ages of 1822 ± 1 and 1804 ± 1 Ma from the CIC and 1810 ± 1 Ma for the MIA suggest that the D_2-M_2 event occurred during that interval (Corrigan et al., 1998b).

The last major regional deformational event (D_3) involved the formation of large-wavelength upright open folds (F_3) with axial traces oriented approximately to the northeast. The map patterns developed in the rocks are largely due to the interference patterns between F_1 and F_2 orogen-parallel and F_3 orogen-perpendicular folds (Figure 3.2b). The D_3 deformation is only locally associated with the growth of low-grade chlorite and muscovite. The D_3 folding must post-date the intrusion of the 1773 ± 2 Ma Reynolds Island pluton (Figure 3.1) since it has been affected by this phase of deformation (Corrigan et al., 1998b).

3.4 THE PETER LAKE DOMAIN

The PLD is a well delineated, fault-bounded, Archean crustal block (Ray and Wanless, 1980; Bickford et al., 1992; Annesley et al., 1992) lying to the northwest of the Wathaman Batholith. A narrow 8 to 10 km strip of the northeastern part of the PLD is exposed on the shoreline and islands of Reindeer Lake. The Parker Lake Shear Zone (PLSZ) separates the PLD from the Wathaman Batholith southwest of Reindeer Lake, but becomes diffuse and splays off into the batholith on Reindeer Lake (Lafrance and Varga, 1996). On Reindeer Lake, the Wathaman Batholith clearly intrudes rocks of the PLD, and contains large rafts and screens of PLD lithologies (Corrigan et al., 1999b).

Three major rock units of the PLD have been identified on Reindeer Lake. These consist of: migmatitic orthogneiss and subordinate paragneisses; strongly foliated and recrystallized granitic to granodioritic gneiss; and a heterogeneous suite of dyke, sill and pod like gabbroic and dioritic layered intrusives. The Lueaza River Granitoids of Stauffer (1979) include the migmatitic gneisses

and the foliated and recrystallized granodioritic and granitic rocks. Gabbroic and dioritic intrusives are included in Stauffer's Swan River Pluton (1979). The Swan River Pluton has been renamed the Swan River Complex (Corrigan et al., 1999b) due to the great compositional and textural diversity of this rock package.

The orthogneisses of the PLD are banded at centimetre to metre scale, highly to moderately strained and well foliated. Minor amounts of migmatitic paragneiss (Plate 3.2a) are observed within the dominantly migmatitic orthogneiss package. The gneisses are cut by at least two sets of mafic dykes that likely predate the intrusion of the Wathaman Batholith.

Foliated non-migmatitic granitoids underlie large portions of the PLD exposed in the map area, flanking the migmatitic para- and ortho-gneisses (Figure 3.1). This belt is comprised of several cross cutting plutons of mainly tonalite and granodiorite, with lesser granite and syenite. All the plutons are fine to medium grained, biotite-bearing (< 10 %) and completely recrystallized, giving a sugary texture (Plate 3.2b). The tonalitic and granodioritic rocks are cut by later pink granitic phases. Individual plutons do not form continuous mappable bodies and for that reason they have been grouped together. Foliated and K-feldspar augen megacrystic granitoids are also found in the PLD, and from their position and intense deformation (Plate 3.2c) are also considered to be Archean in age.

The Swan River Complex (Corrigan et al., 1999b) is a compositionally heterogeneous group of layered mafic to ultramafic intrusions. Although dominated by gabbro and diorite the complex contains minor peridotite, leuco-gabbro and anorthosite. This unit outcrops in several elongate sills and dykes that intrude the gneissic rocks. Several pods up to a few kilometres in size are also found within the northwestern portion of the Wathaman Batholith adjacent to the PLD (Figure 3.1). A remarkable feature of the Swan River Complex is its general state of preservation when

compared to other gneissic rocks of the PLD. Several igneous features are well preserved, i.e., primary mineralogy, igneous layering, and magma mixing-mingling textures (Plate 3.3a,b and c). The gabbros are in places intruded by K-feldspar megacrystic granitoids of the Wathaman Batholith (Plate 3.3d).

3.4.1 U-Pb geochronology of the Peter Lake Domain

Bickford et al. (1986) dated rocks from exposures of the PLD on Reindeer Lake, producing both Proterozoic and Archean crystallization ages. A grey megacrystic granite and a granitic gneiss gave U-Pb zircon ages of 2582 ± 19 and 2556 ± 22Ma, respectively. Another granitic gneiss gave an age of 1860 ± 5 Ma, apparently contemporaneous with the Wathaman Batholith. These results emphasize the complex nature of the boundary between the PLD and the Wathaman Batholith and that megacrystic granitoids of both Proterozoic and Archean age are present in this complex boundary zone.

A pegmatitic gabbro sample from the Swan River Complex (Plate 3.3e) has yielded a U-Pb zircon crystallization age of 2562 ± 2 Ma (Corrigan et al., unpubl. rept.) with a lower intercept of 1830 Ma. The lower intercept is slightly older than monazite ages from the CIC of 1822 ± 1 Ma, but is consistent with the approximate time period of regional metamorphism. Another pegmatitic gabbro from the PLD on Reindeer Lake has been dated at 1865 ± 10 Ma (Bickford et al., 1986), later revised to 1908 ± 27 Ma (Bickford et al., 1987). It is unclear where exactly this sample was collected, and detailed descriptions of the zircons are lacking. The significance of this result is unclear, although there is the possibility that some Proterozoic gabbroic material exists in the area.

3.5 GRANITOID ROCKS IN THE REINDEER LAKE AREA

All rock names used in the following discussions follow Streckheisen (1976), and are based on mesonorm calculations using the major element geochemistry. Rock slabs were stained to

determine the modal feldspar proportions and the results obtained are in agreement with the normative calculations. Samples collected and described during this study were fresh, and free of any significant alteration and deformation. This did not bias the sampling toward the "undeformed rocks"; since, the majority of the major deformation is related to locally developed, late shear zones. Minor amounts of chloritization of biotite, and sericite growth in feldspars was observed in the samples.

The granitoid rocks are divided into two main groups based on their geographic distribution and positions relative to the Paleoproterozoic volcano-sedimentary assemblages of the LRD. These are plutons found within the confines of the LRD (*i.e.*, LRD plutons) and granitoids of the Wathaman Batholith. Although the Wathaman Batholith is now separated from the LRD by the RLSZ, it has been found to intrude the supracrustal rocks of the LRD, and also contains large rafts of lithologies that lie immediately south of the shear zone. These observations, combined with U-Pb ages, suggest a temporal continuity in plutonism across the RLSZ. If a genetic link between the plutons of the LRD and the Wathaman Batholith is to be established it must explain the fundamental differences observed between the two. For example, the Wathaman Batholith contains an abundance of K-feldspar megacrystic granodiorite and monzogranite, and almost no rocks of tonalitic composition. This is in stark contrast to the majority of the plutons of the LRD, which are tonalitic, and granodioritic (without megacrysts).

3.5.1 The Wathaman Batholith

The Wathaman Batholith is composed dominantly of K-feldspar megacrystic granodiorite-monzogranite intrusions. On Reindeer Lake, the batholith has a strike length of over 70 km and varies in width from 30 to 35 km in the southwest to over 70 km toward the northeast (Figure 3.3). Based on differences in the modal and geochemical compositions, and their distribution within the

batholith, the granitoids have been divided into two main zones in this study. The two zones contain rocks of similar, but distinctive character, and are the Southern-Central Zone (SCZ) and the Northeast Zone (NEZ) (Figure 3.3). The dividing line between these two zones corresponds to major changes in the overall bulk composition of the batholith from dominantly hbl-bio-bearing K-feldspar megacrystic granodiorites in the SCZ, to mainly bio-hbl-bearing K-feldspar megacrystic to coarse-grained monzogranites within the NEZ. This will be discussed further in Chapter 4 when the complete set of geochemical data is evaluated. Within each of the SCZ and NEZ, distinctive series have been identified. These series were identified by distinctive compositions, both modal and geochemical, field relationships and in some cases the relative timing of the various intrusive phases.

3.5.1.1 South-Central Zone (SCZ) of the Wathaman Batholith

The SCZ of the batholith has been divided into two series, the K-feldspar megacrystic granodiorite series, and the monzogranitic series. The K-feldspar megacrystic granodiorite series underlies the majority of the SCZ of the Wathaman Batholith and is composed of a semi-continuous series ranging from quartz diorite, through quartz monzodiorite to granodiorite and minor monzogranite (Figure 3.4a). K-feldspar megacrysts are commonly found in compositions from quartz monzodiorite onwards. Hornblende and biotite are the major ferromagnesisan phases, with hornblende dominating over biotite in the quartz diorites well into the granodiorites. Due to the overwhelming occurrence of K-feldspar megacrysts, combined with the dominance of granodioritic compositions this group of rocks are hereafter referred to as the KMGS.

Throughout the SCZ, and scattered amongst the KMGS rocks are several large- to moderately-sized bodies of coarse-grained, equigranular, biotite-bearing granodiorite and monzogranite (Figure 3.3). These largely non-megacrystic granodiorites and monzogranites are

distinct in that they contain very low mafic mineral contents, exclusively comprised of biotite (5 %), and are restricted to felsic compositions. This distinctive group of rocks will be hereafter referred to as the MS (Figure 3.4A) since their compositions are mainly monzogranitic, and since they rarely contain K-feldspar megacrysts.

Also scattered throughout the SCZ are several small dykes and pods of quartz diorite and tonalite (Figure 3.4a). The relationship between these small bodies and other rocks of the batholith is uncertain. The samples collected during this study were found to cross cut some of the more felsic granitoids of the SCZ. For now they are considered separately from the larger bodies of quartz diorite spatially associated with the KMGS

3.5.1.2 North-East Zone (NEZ) of the Wathaman Batholith

This is a northeasterly trending, wedged-shaped zone that widens considerably toward the northeast (Figure 3.3). The northeast-trending dividing line between the SCZ and NEZ is roughly inline with the northeasterly-trending contact between the PLD and the Wathaman Batholith to the southwest, i.e., the PLSZ. This observation may indicate a genetic link between the SCZ-NEZ transition and the older basement rocks of this domain. Within this zone two series have been identified, with highly contrasting compositions, and geochemical characteristics. The majority of this zone is underlain by biotite-bearing K-feldspar megacrystic to coarse-grained monzogranites, with lesser granodiorites and quartz monzodiorites (Figure 3.4b). This series is similar to the KMGS of the SCZ, however, the abundance of quartz monzodiorite and granodiorite is greatly decreased, as is the hornblende content of the granitoids. This series is referred to as the K-feldspar megacrystic monzogranite series (KMMS).

Associated with the granitoids of the NEZ-KMMS are numerous fine- to medium-grained synplutonic diorite dykes (Figure 3.4b). These dykes also appear to be related to the production of

the locally abundant, microdiorite enclaves found scattered throughout the batholith. These mafic microdiorite enclaves are also found throughout the SCZ of the batholith. The NEZ also contains a very distinctive series of hornblende-rich monzodiorites, K-feldspar megacrystic to coarse-grained quartz monzodiorites and K-feldspar megacrystic monzonites (Figure 3.3). This series of rocks will be referred to as the monzonitic series (MS) (Figure 3.4b). The low modal quartz, and distinctively high modal K-feldspar component to these rocks is also more typical of a monzonitic differentiation trend, or monzonitic series (Pitcher, 1997; see inset on figure 3.4) distinct from the more typical calc-alkaline series trends defined by the other series of the batholith.

3.5.1.3 U-Pb Geochronology of the Wathaman Batholith

A medium-grained, equigranular bio-bearing granodiorite (98-D301) has been dated at ca. 1850 +6/-2 Ma. This sample possesses a weak to moderately developed foliation but retains igneous minerals and textures. The sample was collected from a northeast trending bio-bearing granodiorite-monzogranite lens located in the southern portion of the batholith and is part of the SCZ-MS. Also collected from the southern portion of the batholith, was a completely recrystallized fine-grained bio-bearing granodiorite (98-D246b) possessing a penetrative foliation, this sample yielded an age of 1856 ± 5 Ma. A bio-bearing, coarse-grained to K-feldspar megacrystic monzogranite of the NEZ-KMMS was collected at the extreme northwest margin of the batholith, less than two kilometres from foliated granitoids of the PLD. This sample yielded a preliminary U-Pb age of 1862 +13/-2 Ma. These three ages are all in good agreement with previously published U-Pb zircon ages for the batholith (Ray and Wanless, 1980; Bickford et al., 1986) that currently constrain magmatism within the Wathaman Batholith between ca. 1865 and 1852 Ma. Currently, two other samples from the Wathaman Batholith are being processed for U-Pb zircon analysis and include a hbl-bio-bearing K-feldspar megacrystic granodiorite (98-T223) of

the SCZ -KMGS, and a hbl-cpx-bio-bearing K-feldspar megacrystic monzonite of the NEZ-MS. The latter pluton is found on Patterson Island (Figure 3.3) and is an ovoid intrusion apparently lacking any foliation, suggesting that it may be one of the youngest phases of the Wathaman Batholith.

3.5.1.4 Minor Intrusive phases

Although the batholith is dominated by K-feldspar megacrystic to coarse grained granodiorite and monzogranite plutons, minor amounts of gabbro, tonalite and aplite are also present, and are locally important phases of the batholith (Fumerton et al., 1984). These rocks have not been sampled for detailed petrographic or geochemical analysis. Their characteristics and field relationships to the main phases of the batholith are discussed below.

The aplitic rocks are one of the latest intrusive phases of the batholith and crosscut all other rock types and the main foliation in the batholith. They are themselves seldom foliated. These rocks are most abundant at the northern and southern margins of the batholith, as previously noted by Fumerton et al. (1984). In the NEZ, medium-grained pink aplite to aplite-pegmatite generally containing less than 5 % biotite is locally abundant. The aplite characteristically contains abundant magnetite, titanite, epidote and allanite. The aplite is most abundant northeast of Cummines Island and forms a locally important component of the outcrops in that area.

A moderately sized equigranular hornblende-biotite tonalite-granodiorite pluton was mapped in the NEZ, and is well exposed on the northeastern side of Cummines Island where it forms a large ovoid north-trending pluton. Tonalite can be found at several outcrops in the general area of Cummines Island. A notable feature of this rock type is the ubiquitous amount of titanite and epidote, clearly visible in hand specimen. The tonalite is younger than both the KMMS and the MS of the NEZ and contains xenoliths and large rafts of both. The tonalite does, however, seem to be

more closely related to the MS rocks, and the two are commonly found together. The tonalite almost always contains distinctive xenocrysts of hornblende when in contact with the monzodioritic rocks, and they are likely derived from it.

3.5.1.5 Xenoliths

Xenoliths are exclusively restricted to the northern and southern margins of the batholith respectively, and are not generally found within the batholith at greater distances than ~10 km from its margins. In the SCZ, xenoliths are varied and both igneous and sedimentary xenoliths can be found. The southeastern portion of the batholith contains a rather large (continuous over 10 km) screen of metasedimentary material that contains large sillimanite blades, as well as numerous calc-silicate pods. This xenolith is similar compositionally to arkosic rocks of the PIA, which have been mapped up to the margin of the batholith less than five kilometres south of the xenolith.

Numerous xenoliths of gabbro and diorite are also found near the southern margin of the batholith. Some xenoliths are compositionally banded and gneissic, similar to orthogneisses of the CIC. The origin of these dioritic and gabbroic xenoliths is unclear, they may represent early mafic phases of the batholith incorporated and entrained by later pulses, or entirely unrelated exotic material, possibly related to similar mafic rocks found in the LRD. Resolving relationships between xenoliths and the host rocks of the batholith is also complicated by the locally intense deformation at its southern margin related to movement along the RLSZ.

Along the northern margin of the batholith large gabbroic and dioritic xenoliths and pods are quite common (Figure 3.3) as well as less frequent gneissic granitoid inclusions. The gabbro and diorite pods and xenoliths are for the most part indistinguishable from gabbroic material found within the adjacent PLD and may be derived from the Swan River Complex. The migmatitic and gneissic granitoid xenoliths in the northern zone are also most likely derived from the PLD.

3.5.1.6 Structure and Deformation

The Wathaman Batholith contains at least two tectonic fabrics: (1) an earlier fabric marked by a strong- to moderately-developed mineral foliation observed in the Wathaman Batholith and is part of the regional fabric; and (2) a younger mylonitic foliation, locally well developed, associated with strike-slip shearing along the PL and RLSZ (Corrigan et al., 1999). The first fabric consists of a weak to moderately developed biotite and hornblende foliation and a down-dip mineral and extension lineation defined by elongate strain shadows surrounding K-feldspar megacrysts. The primary magmatic foliation is parallel to this tectonic foliation, indicating that emplacement of the batholith was coincident with regional deformation (Lewry et al., 1981). Since this mineral foliation mostly overprints the magmatic foliation, this suggests that deformation and cooling also continued after the emplacement of the batholith (Corrigan et al., 1999).

The latest deformation event included strike-slip shearing along the PLSZ (Lafrance and Varga, 1996). It is interpreted as a northeasterly splay of the Needle Falls Shear Zone, a major transcurrent structure that separates the Wollaston Domain of the Hearne Province from the Wathaman Batholith (Lewry and Sibbald, 1980; Stauffer and Lewry, 1993; Lafrance and Varga, 1996). To the southwest of Reindeer Lake, the Parker Lake Shear Zone separates the PLD from the Wathaman Batholith. Investigations on Reindeer Lake by Lafrance and Varga (1996) along the Parker Lake Shear Zone concluded that it was dominated by dextral strike-slip movement, but with evidence for sinistral movement as well. They also concluded that on Reindeer Lake the shear zone does not separate the PLD from the Wathaman Batholith but instead cuts into the batholith. Investigations during this study, which extended beyond the area investigated by Lafrance and Varga (1996), found no evidence that the shear zone extends much further into the batholith.

3.5.2 The La Ronge Domain Plutons

The LRD plutons underlie the area between the DLSZ in the south, and the RLSZ to the north (Figure 3.5). The major plutons of this domain have been divided into three broad compositional groups based on field identification. These include: (1) medium- to coarse-grained hbl-bio-bearing dioritic, quartz dioritic and tonalitic plutons; (2) medium- to coarse-grained bio-hbl-bearing tonalitic and granodioritic plutons; and (3) medium- to coarse-grained magnetite-bearing leuco-tonalites and bio-musc-bearing granodiorites and monzogranites (Figure 3.5). The latter group of intrusions, certainly the magnetite-bearing leuco-tonalites, are probably of similar age to the 1773 ± 3 Ma Reynolds Island pluton (Corrigan et al., 1988b). It is unclear, however, if the bio-musc-bearing plutons found throughout the southern and central portions of the domain are related to the younger leuco-tonalites or the older quartz diorites, tonalites and granodiorites. Some of the older plutons display close spatial relationships to some of these more felsic bodies, including the southwestern lobe of the McMillian Lake pluton, and the core of an ovoid quartz dioritic pluton approximately five kilometres north of the Milton Island pluton (Figure 3.5). All the samples collected during this study are from the larger quartz dioritic, tonalitic and granodioritic plutons; these more felsic bodies were not sampled.

3.5.2.1 U-Pb Geochronology of La Ronge Domain Plutons

To date, only the Butler Island pluton (97-A001) has been dated in the LRD from Reindeer Lake. The pluton is composed of hbl-bio-bearing dioritic, quartz dioritic and tonalitic phases. The pluton intrudes the CMB in the southernmost LRD and yielded an age of ca. 1858 +3/-2 Ma (Corrigan et al., 1998b).

A U-Pb monazite age of 1773 ± 2 Ma has been obtained from a magnetite-bearing leuco-tonalite from the southern lobe of the Reynolds Island pluton (97-D223), and is interpreted as an igneous crystallization age (Corrigan et al., 1998b). The pluton intrudes but is not deformed by the

DLSZ, but has been affected by the D_3 deformation in the area. Only a small percentage of the plutons exposed in the Reindeer Lake area posses similar compositions, and field relationships to the Reynolds Island pluton. The overwhelming majority of plutons are similar in structural style and composition to the Butler Island pluton. They are hornblende-bearing, possess penetrative to moderately developed foliations and lineations (both focussed at pluton margins), and the pluton shapes and outcrop patterns are controlled largely by the interference of the D_2 and D_3 folds. Based on these broad compositional similarities, and similar structural features, the overwhelming majority of the major plutons of the LRD investigated and sampled during this study are believed to be of similar age to the Butler Island pluton.

Two of the larger plutons from the LRD are currently being processed for U-Pb zircon analysis. A bio-hbl-bearing tonalite from the McMillian Lake pluton (98-D093) located in the central portion of the domain, and a well foliated bio-hbl-bearing granodiorite from a foliated diorite-granodiorite pluton (98-D108b) located in the northeastern portion of the domain.

3.5.2.2 Quartz diorites, tonalites and granodiorites

The largest plutons found in the LRD are comprised of bio-hbl-bearing tonalites and granodiorites, typically containing between 5 and 20 % combined biotite and hornblende (Plate 3.4a, b). These large bodies are found mainly on the eastern shoreline and islands of Reindeer Lake, with smaller plutons found in the central portion of the domain (Figure 3.5). These large bodies include the McMillian Lake Pluton, the Jack Pine Bay pluton and an unnamed foliated diorite-granodiorite pluton. On a QAP mesonorm diagram the samples collected from these plutons range from tonalite to granodiorite in composition (Figure 3.6). These plutons are remarkably homogeneous in composition. The foliated diorite-granodiorite pluton does, however, have abundant dioritic phases associated with it, unlike the more homogeneous tonalitic-

granodioritic composition of the McMillian Lake pluton. The accessory minerals, magnetite, apatite, titanite, epidote, allanite and zircon are commonly found in these plutons.

Several moderately sized bodies of hbl-bio-bearing diorite, quartz diorite and tonalite are found. These plutons include the Butler Island pluton and Milton Island plutons in the southern portion of the domain and the Cowie Bay pluton at the extreme northwestern portion of the domain (Figure 3.5). Several smaller bodies are also found scattered throughout the central portion of the domain. These plutons generally contain between 10 and 25 % combined hornblende and biotite and range from hbl > bio (Plate 3.4a) to bio-hbl-bearing plutons (Plate 3.4b). On QAP mesonorm diagrams the samples collected from these plutons plot almost exclusively in the tonalite field, however, many cluster about the quartz diorite-tonalite join (Figure 3.6). The accessory minerals magnetite, apatite, titanite, epidote, allanite and zircon are common as in the larger tonalite-granodiorite plutons.

All the LRD plutons exposed on Reindeer Lake have a moderate to strongly developed mineral foliation defined by the planar alignment of hornblende and/or biotite. This foliation is also developed in host rocks, and formed as a result of the regionally pervasive D_2 deformational event, coincident with south verging reclined to recumbent fold development and the initiation of south-directed ductile thrust zones.

3.6 DETAILS OF THE PETROGRAPHY AND OCCURRENCE OF THE WATHAMAN BATHOLITH SERIES

3.6.1 The SCZ-KMGS

3.6.1.1 Quartz diorites and quartz monzodiorites

Quartz diorites (Plate 3.5a) and quartz monzodiorites (Plate 3.5b), without K-feldspar megacrysts are the most mafic compositions identified within the SCZ-KMGS. Based on field

relationships and the smooth variation of modal compositions between these various rock types, they are interpreted to be genetically related to the more voluminous K-feldspar megacrystic quartz monzodiorites (Plate 3.5c) and granodiorites (Plate 3.5d,e and f) and lesser amounts of monzogranite (Plate 3.5g). This is supported by geochemical and isotopic data (Chapter 4).

These quartz diorites and quartz monzodiorites (with or without K-feldspar megacrysts and/or xenocrysts) are coarse grained and dominantly composed of plagioclase (50-60 %), hornblende and biotite (20-40 %), with lesser quartz (5-15 %), and K-feldspar (5-15 %). Commonly, some of the more mafic rocks contain between 30 to 40 % combined hornblende and biotite. Hornblende is usually the dominant mafic mineral in quartz diorites and quartz monzodiorites. Hornblende forms subhedral grains commonly several millimetres in length, sometimes containing numerous blebby inclusions of apatite and quartz, as well as biotite. Biotite commonly forms irregular clots composed of several subhedral grains of variable size, ragged edges are associated with epidote and titanite. Plagioclase usually forms tabular, subhedral to euhedral grains between 2 and 5 mm, although larger grains, and plagioclase megacrysts have been found. Plagioclase crystals are for the most part not visibly zoned. Quartz is always interstitial and anhedral, as is K-feldspar, within the quartz diorites. Within the quartz monzodiorites, however, as indicated above, K-feldspar megacrysts may be present, even in some of the most mafic compositions. Where observed the megacrysts are commonly twinned, and may display faint growth zoning.

The accessory minerals apatite, epidote, titanite, zircon, allanite, minor magnetite and late interstitial calcite have been identified. Titanite, epidote and apatite are particularly abundant in these rocks. Titanite commonly forms small subhedral grains associated with hornblende and biotite, but also forms independent subhedral grains that can reach large sizes of 1 to 2 mm.

Epidote forms both euhedral and subhedral grains as well as anhedral, and interstitial grains associated with the minor amounts of calcite.

Field relationships between the quartz diorites and quartz monzodiorites suggest they were intruded contemporaneously with K-feldspar megacrystic granodiorites and monzogranites. This is supported by the absence of any sharp contacts between these rock types, mingling relationships observed between mafic and felsic magmas and the close spatial association between the rock types. Contacts between quartz dioritic-quartz monzodioritic and K-feldspar megacrystic granitoids are largely gradational, and inter-layering of megacrystic granodiorites and monzogranites with the quartz diorites and monzodiorites (with or without megacrysts) is quite common. In some cases quartz diorites and quartz monzodiorites have been observed to grade progressively (sometimes unnoticeably) into hbl-bio-bearing K-feldspar megacrystic granodiorites. The quartz diorites and quartz monzodiorites are often spectacularly layered (Plate 3.6a), and may contain numerous fine-grained microdiorite enclaves. The enclaves where observed are of highly variable sizes, from metre-sized blobs to small < 10 cm sized fragments. In several cases enclave-rich layers have been traced back to larger bodies/pods and dykes of fine grained diorite near the bases of some of the larger, well exposed sections. Immediately before these dioritic units are found, the abundance of microdiorite enclaves increases, suggesting that the dioritic bodies are the source for the enclaves. It is also common for scattered K-feldspar megacrysts or xenocrysts to be found within these larger bodies of quartz diorite and quartz monzodiorite (Plate 3.6a and b), within the microdiorite enclaves themselves (Plate 3.6c), and across boundaries between the enclaves and host. This relationship suggests that the microdiorite enclaves were introduced as dioritic magma injections (see Vernon, 1983). The disruption of these mafic magmas formed the enclaves and the mingling of the magma with a partially crystallized host facilitated the

incorporation of xenocrysts (K-feldspar megacrysts) into the mafic enclaves. The K-feldspar megacrysts in hornblende-rich rock types were previously interpreted as porphyroblasts, and these rock types were thus interpreted as metasomatized xenoliths of uncertain origin (Fumerton et al., 1984).

The fact that quartz dioritic and quartz monzodioritic bodies are gradational with K-feldspar megacrystic granodiorites, that granodiorites in some cases clearly overlie some of these larger mafic bodies (Plate 3.6d) suggests a co-magmatic relationship. Some larger mafic bodies and more extensive outcrops of quartz dioritic and quartz monzodioritic bodies, as well as hbl-bearing granodiorites are found on South Porcupine Point, Bradley and Beaver Islands, and along the southern half of Hourston Island (Figure 3.3). Smaller mafic bodies are commonly found at many outcrops dominated by megacrystic granodiorite, as are the microdiorite enclaves. It is difficult to place an exact estimate on the actual abundance of these rock types, although it is clear that they are subordinate to the larger volumes of granodiorite. Earlier estimates of the abundance of mafic rock types, not only within the the SCZ but within the entire batholith, have clearly been low.

A somewhat later set of quartz dioritic and tonalitic pods and dykes with no obvious association to the K-feldspar megacrystic granitoids were also sampled from the SCZ. They are a volumetrically minor component of this zone and differ from the larger quartz diorite bodies of the SCZ in their medium-grained size, and absence of any association with K-feldspar megacrystic rocks. They contain both hornblende and biotite as ferromagnesian phases and the accessory minerals titanite, apatite, allanite and zircon. Geochemical similarities between these quartz diorites and tonalites and many of the tonalite plutons of the LRD suggests they are related, and their origin will be discussed in Chapter 4.

3.6.1.2 K-feldspar megacrystic granodiorites and monzogranites

K-feldspar megacrystic hbl-bio- to bio-hbl-bearing granodiorite (Plate 3.5d,e and f) is the most abundant rock type, not only within the SCZ-KMGS, but also within the entire Wathaman Batholith. These granodiorites are gradational into the lesser amounts of more felsic bio-hbl- to bio-bearing granodiorites and monzogranites (Plate 3.5g and h) within the series.

These granitoids are light grey to pink in colour, and contain K-feldspar megacrysts, set in a medium- to coarse-grained matrix of plagioclase, hornblende, biotite and quartz. The samples collected during this study have modal compositions of 10-30 % K-feldspar, 35-50 % plagioclase, 20-30 % quartz and 5-20 % combined hornblende and biotite. Although the amount of mafic minerals is highly variable (5-20 %), they decrease steadily toward the more felsic compositions. Within the more differentiated granodiorites and monzogranites biotite begins to replace hornblende as the dominant mafic mineral.

The K-feldspar megacrysts, where little deformed are tabular, euhedral to subhedral, and average in size from smaller, 1 cm x 2 cm grains to larger 2 cm x 6 cm grains. They are commonly twinned and may display faint growth zoning. Some K-feldspar megacrysts can reach sizes up to 10 cm in the long dimension. Although most of the megacrysts are within the size ranges mentioned above, the size distribution can vary widely, as does their abundance. This point is particularly important to note while sampling for geochemistry. K-feldspar megacryst accumulations have occurred in several areas throughout this zone. In some cases they can make up > 50 % of the rock and have also been observed to concentrate in pods and layers parallel to the main foliation. Within these layers and pods there may be > 90 % K-feldspar megacrysts. Clearly these, and other samples where the modal content of K-feldspar appeared anomalously large were avoided in order to not bias the geochemistry toward the composition of the megacrysts. Textures developed in the feldspars include both perthitic intergrowths of albite in K-feldspar and

myrmekitic intergrowths of quartz and plagioclase around the edges of K-feldspar grains (Plate 3.8a).

Accessory minerals are ubiquitous within the K-feldspar megacrystic granodiorites, and common in the monzogranites of the SCZ. Titanite, epidote, magnetite, apatite, allanite, zircon, and minor carbonate have been identified. Titanite, epidote and magnetite are the most abundant accessory minerals, and are clearly visible in hand specimen (Plate 3.7). Titanite, as found in the quartz diorites and quartz monzodiorites displays two forms: subhedral to rare euhedral (macroscopically) grains that can be larger than a few millimetres in size (Plate 3.8b); to small blades and wedges associated with biotite. A similar relationship between titanite and hornblende is also observed in some samples. Epidote is a very common accessory mineral, particularly within the granodiorites often forming subhedral to euhedral grains, and in some cases epidote-rich clots associated with mafic minerals and other accessories (Plate 3.8c). Allanite is also a common accessory mineral, and although almost always metamict, some grains have preserved zoning and can reach large sizes of several millimetres. A unique feature of allanite is that it is almost always rimmed or overgrown by epidote (Plate 3.8d) and in some instances preserves optical continuity in twins (Plate 3.8e). These relationships with allanite, and the presence of euhedral to subhedral independent crystals of epidote, suggest that they may potentially be magmatic in origin. In general the abundance of accessory minerals decreases within the more felsic compositions, and the abundance of epidote apatite and titanite are noticeably decreased.

As with the more mafic quartz diorites and quartz monzodiorites, microdiorite enclaves are found throughout the SCZ, and within both granodiorites and monzogranites. The presence and abundance of these enclaves is extremely variable and at the scale of mapping no systematic distribution could be observed. They are not found at every outcrop, but when observed can make

up a substantial portion of the rock. The presence of these microdiorite enclaves is interpreted to represent the input of mafic magma into a partially crystallized magma chamber.

3.6.2 The SCZ monzogranite series

Several large- to moderately-sized bodies of medium- to coarse-grained equigranular bio-bearing granodiorite and monzogranite occur within the SCZ (Figure 3.3). These granitoids are almost exclusively bio-bearing, and only rarely are K-feldspar megacrysts found (Plate 3.9). The granodiorites and monzogranites are dominantly composed of quartz (25-40 %), K-feldspar (15-25 %), and plagioclase (30-45 %), and contain ~5 % biotite. On a QAP mesonorm diagram these granitoids are restricted to monzogranitic and felsic granodioritic compositions (Figure 3.4). The accessory minerals titanite, allanite and zircon have been identified in the rocks but are quite low in abundance. Apatite and magnetite were observed in only a few samples and epidote was not observed.

These largely non-megacrystic felsic granitoids are similar in composition to the matrix assemblage of some of the more felsic K-feldspar megacrystic monzogranites of the SCZ-KMGS. Locally these granitoids are inter-layered with K-feldspar megacrystic granodiorites and monzogranites on the metre to kilometre scale. These relationships are best preserved on Kellough and Gibson Islands (Figure 3.3). Unfortunately later deformation in these areas has made original contact relationships difficult to determine. However, where later deformation is less localized non-megacrystic granitoids were observed cutting foliated K-feldspar megacrystic granodiorites, indicating they may be slightly younger. The observed relationships do no preclude or necessitate a genetic relationship between these more felsic non-megacrystic granitoids.

3.6.3 The NEZ K-feldspar megacrystic monzogranite series

3.6.3.1 K-feldspar megacrystic granodiorite and monzogranites

K-feldspar megacrystic granitoids in the NEZ are dominated by bio-hbl- to bio-bearing K-feldspar megacrystic monzogranites (Plate 3.10d, e, f and g). As in the SCZ, hbl-bio-bearing quartz monzodiorites (Plate 3.10a), and granodiorites (Plate 3.10b) are found, but are clearly less abundant (Figure 3.3; Figure 3.4b). The granodiorites and monzogranites of this zone are dominantly composed of quartz (20-35 %), K-feldspar (20-35 %), plagioclase (30-45 %), and 5-10 % combined biotite and hornblende. In thin section and hand specimen the major minerals display textures indistinguishable from those observed in the SCZ-KMGS. Perhaps the only noticeable difference between the two (besides the variation in modal abundances) is that the K-feldspar megacrysts are on average smaller, generally not larger than two centimetres in the NEZ, although some quite large megacrysts are found (Plate 3.11a). Coarse-grained monzogranites are common and interpreted to be related to the megacrystic granitoids.

A major difference between the two series is found in the accessory minerals. Similar to the megacrystic granitoids of the SCZ, the accessory minerals magnetite, titanite, apatite, allanite and zircon are found. Differences in abundance include low contents of apatite and allanite. Epidote is absent and allanite grains are much smaller. Major differences are also observed in the titanites. It is the most abundant accessory mineral, and is commonly zoned and contains highly birefringent cores, dark in plane polarized light. These dark cores are often rimmed by one or more clear titanite overgrowths. The Fe-Ti-oxides are also very abundant. The oxides are always rimmed by highly birefringent titanite. This magnetite-titanite association is characteristic of all the NEZ K-feldspar megacrystic monzogranite series and was not observed in the SCZ-KMGS. The observed differences in the abundance and texture of the accessory minerals are not due to differences in bulk compositions, since they were also observed in the few samples of quartz monzodiorite and granodiorite sampled in this zone. This suggests a dramatic change in magmatic processes and or

sources for the NEZ granitoids versus the SCZ.

3.6.3.2 Syn-plutonic diorite dykes and microdiorite enclaves

The NEZ K-feldspar megacrystic granodiorites and monzogranites are also closely associated with locally abundant syn-plutonic diorite dykes. The diorites are generally medium- to coarse-grained, plagioclase-phyric and hornblende-rich (plate 3.11b). The mafic mineral contents are often very high and some samples contain up to 50 % combined hornblende and biotite. The hornblende within these diorites is generally subhedral to euhedral and some are zoned. Accessory titanite occurs as small blades and wedges associated with biotite and hornblende. Minor allanite and zircon can also be found in these dykes.

Associated with these diorites are numerous microdiorite enclaves, ranging in size from centimetres to several metres. These enclaves are generally fine-grained, and may contain fine-grained mafic rims and K-feldspar megacrysts (Plate 3.11c). Many outcrops where the dioritic rocks are abundant preserve evidence of magma mingling relationships between the dioritic and K-feldspar megacrystic granodioritic and monzogranitic rocks (Plate 3.11d). These relationships are similar to those observed in the SCZ-KMGS. However, the syn-plutonic features are better preserved in the NEZ and the sizes of the dioritic dykes were large with some greater than 10 metres in width. For this reason, samples were collected from these dykes for geochemical and Nd isotopic analysis to better constrain their origin and relationship to the felsic plutonism. This does not suggest that microdiorite enclaves are any more abundant in the NEZ than they are in the SCZ.

3.6.4 The NEZ Monzonitic series

Large areas of this zone are underlain by a very distinctive series of hbl-rich monzodiorites (Plate 3.12a and b), hbl-bio-bearing K-feldspar megacrystic quartz monzodiorites (Plate 3.12c and d), and hbl-cpx-bio-bearing K-feldspar megacrystic monzonites (Plate 3.12e). These monzonitic

series rocks are found exclusively within the NEZ and were, along with the differences noted in the more typical calc-alkaline K-feldspar megacrystic granitoids, important in defining the zone.

The monzodiorites contain 40-50 % plagioclase, 5-10 % K-feldspar, < 5 % quartz, and 30-40 % combined hornblende and biotite (Plate 3.12a and b). The K-feldspar megacrystic quartz monzodiorites contain 50-60 % plagioclase, 10-20 % K-feldspar, 5-10 % quartz, and 10-20 % combined hornblende and biotite (Plate 3.12c and d). The monzonites contain 30-45 % plagioclase, 20-35 % K-feldspar, <5 % quartz, and between 15 and 40 % hornblende, augite and lesser biotite (Plate 3.12e).

Quartz monzodiorite is the most abundant rock type in this series and grades into the lesser volumes of monzodiorite (Figure 3.4b). The two rock types display similar petrographic features. Fe-Ti-oxides, apatite and titanite are common accessory minerals in the monzodiorites and quartz monzodiorites, along with lesser amounts of allanite and zircon. Some samples contain abundant Fe-Ti-oxides and apatite, often associated with large clots of hornblende (Plate 3.13a). The hornblende often contains numerous blebby inclusions of quartz, apatite and Fe-Ti-oxides (Plate 3.13a). The quartz inclusions in hornblende sometimes show a clear crystallographic control to their orientation (Plate 3.13b). In some samples the inclusions are so abundant that the hornblende crystals are almost completely disaggregated. The quartz monzodiorites commonly contain K-feldspar megacrysts. These megacrysts are grey-blue to white in colour, quite distinct form the pink K-feldspar megacrysts found in other granitoid series in the batholith. The megacrysts sometimes display growth zoning (Plate 3.13c), and perthitic intergrowths of albite in K-feldspar (Plate 3.13d).

A large northeast trending body over 25 km long has been outlined in the central portion of the NEZ and is dominantly composed of these K-feldspar megacrystic quartz monzodiorites, with

lesser volumes of diorite and monzodiorite. The diorites and monzodiorites generally occur as dykes and pods within the larger bodies of quartz monzodiorite and are associated with mafic enclaves in adjacent quartz monzodiorite. The intrusive relationships between this large northeasterly trending body and the adjacent granodiorites and monzogranites is unclear due to high strain zones developed along the contacts, and lack of outcrop in these areas. At two locations, small volumes of K-feldspar megacrystic granodiorite were observed to cross-cut foliated quartz monzodiorites. It is suggested that intrusion of both rock types overlapped significantly in time since no conclusively sharp contacts were observed or well preserved.

Approximately 20 to 25 km southwest of the aforementioned large northeast trending body of quartz monzodiorite, are further exposures of similar monzodiorites and quartz monzodiorites, and in this zone associated monzonites (Figure 3.3). An ovoid hbl-cpx-bio-bearing K-feldspar megacrystic monzonite intrusion located on Patterson Island contains only a weak foliation, and randomly oriented, and distributed K-feldspar megacrysts. The monzonitic rocks in this area commonly preserve relict clinopyroxene cores with overgrowths of pargasitic amphibole (Plate 3.13e and f). These southwestern intrusions intrude a heterogeneous series of gabbroic rocks interpreted as part of the Swan River Complex of the PLD. These southwestern bodies cross-cut the dominant southwest striking, northerly dipping foliation in the batholith and are themselves un-foliated: potentially indicating that they are some of the youngest phases of the batholith.

3.7 SUMMARY

Available U-Pb geochronology, both from Reindeer Lake and along strike to the southwest indicate that peak plutonic activity in the LRD was between ca. 1866 and 1848 Ma (Bickford et al., 1986; Corrigan et al., unpubl. rept.; Van Schmus et al., 1986). The emplacement of the Wathaman Batholith occurred between ca. 1865 and 1850 Ma (Bickford et al., 1986; Corrigan et al., unpubl.

rept.; Ray and Wanless, 1980). The close relationship in time between the emplacement of the Wathaman Batholith and plutons of the LRD, combined with the fact that they both intrude the older volcano-sedimentary assemblages suggests continuity in plutonism between the larger intrusive bodies in the LRD and the Wathaman Batholith.

The Wathaman Batholith not only intrudes volcano-sedimentary assemblages of the LRD, but also the granitoids and gabbroic rocks of the Archean PLD. This supports the interpretation that the early assemblages of the LRD were accreted to the Hearne margin prior to the emplacement of the Wathaman Batholith and plutons of the LRD. This ca. 1865 to 1850 Ma magmatism clearly occurred a minimum of 10 to 25 Ma after recorded volcanic activity in the LRD and Lynn Lake Belt and greater than 20 Ma after the crystallization of the dioritic and granitic phases in the CIC. The peak metamorphism and deformation (D_2) in the area post-dated the major plutonic activity in the area by > 30 Ma.

There is a compositional zonation in the 1865-1850 Ma plutonism in the Reindeer Lake area that leads to the establishment of three zones. The southern most zone, within the LRD, is dominated by coarse-grained hbl-bio-bearing quartz diorites and tonalites and bio-hbl-bearing tonalites and granodiorites. North of this zone is the SCZ of the Wathaman Batholith comprised of the SCZ-KMGS, ranging from quartz diorite through quartz monzodiorite to granodiorite and monzogranite. Also scattered throughout this zone are several bodies of medium- to coarse-grained bio-bearing granodiorites and monzogranites of the SCZ-MS. Further north within the NEZ of the batholith, K-feldspar megacrystic bio-hbl- to bio-bearing K-feldspar megacrystic monzogranites of the NEZ-KMMS predominates. The distinctive hbl-rich monzodiorites, hbl-bio-bearing quartz monzodiorites and hbl-cpx-bio-bearing monzonites of the NEZ-MS are also important components of the batholith in the NEZ.

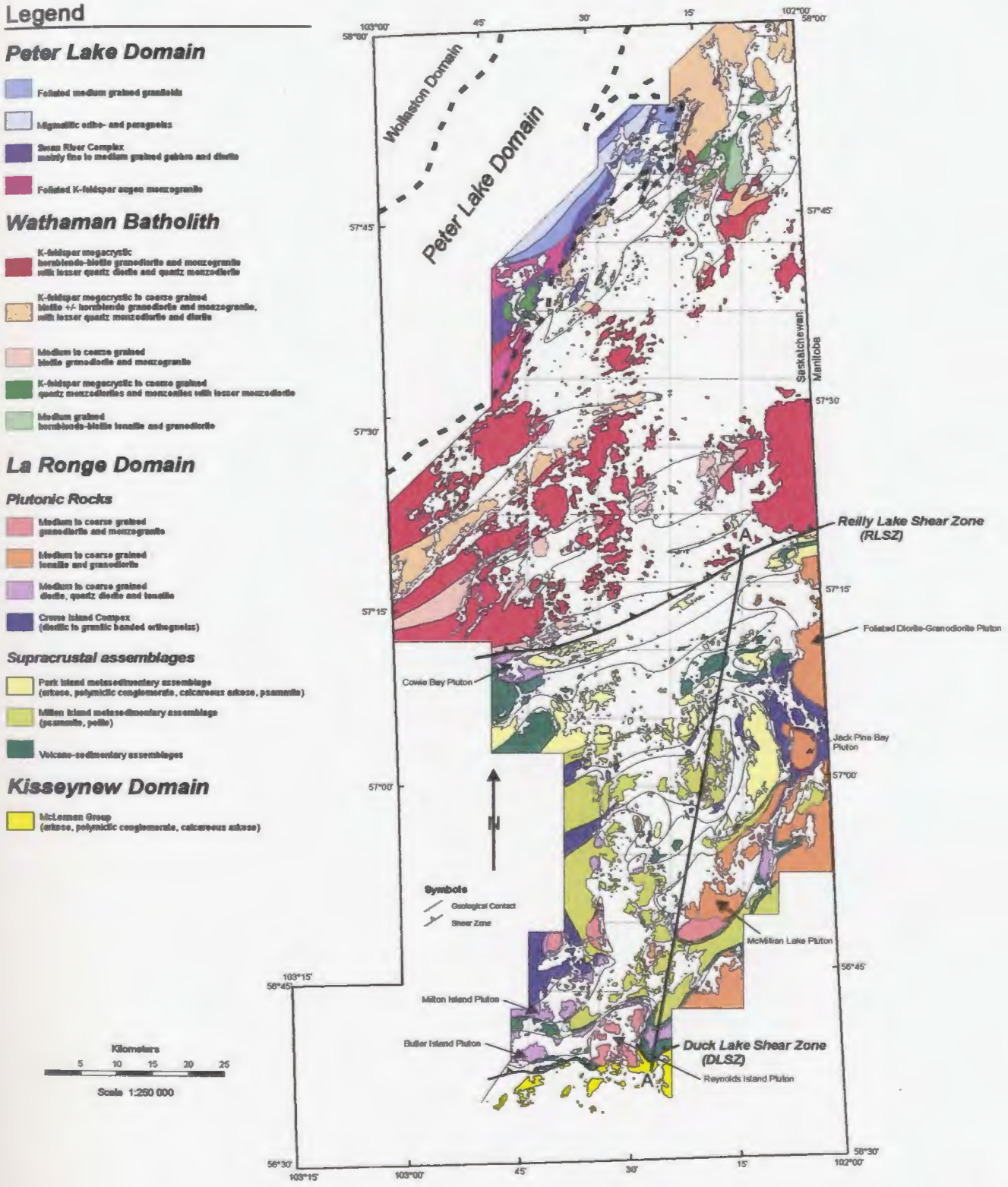

Figure 3.1 Generalized geological map of the Reindeer Lake Area comprising parts of NTS 64D and NTS 64E. A-A' locates the cross section depicted in Figure 3.2.

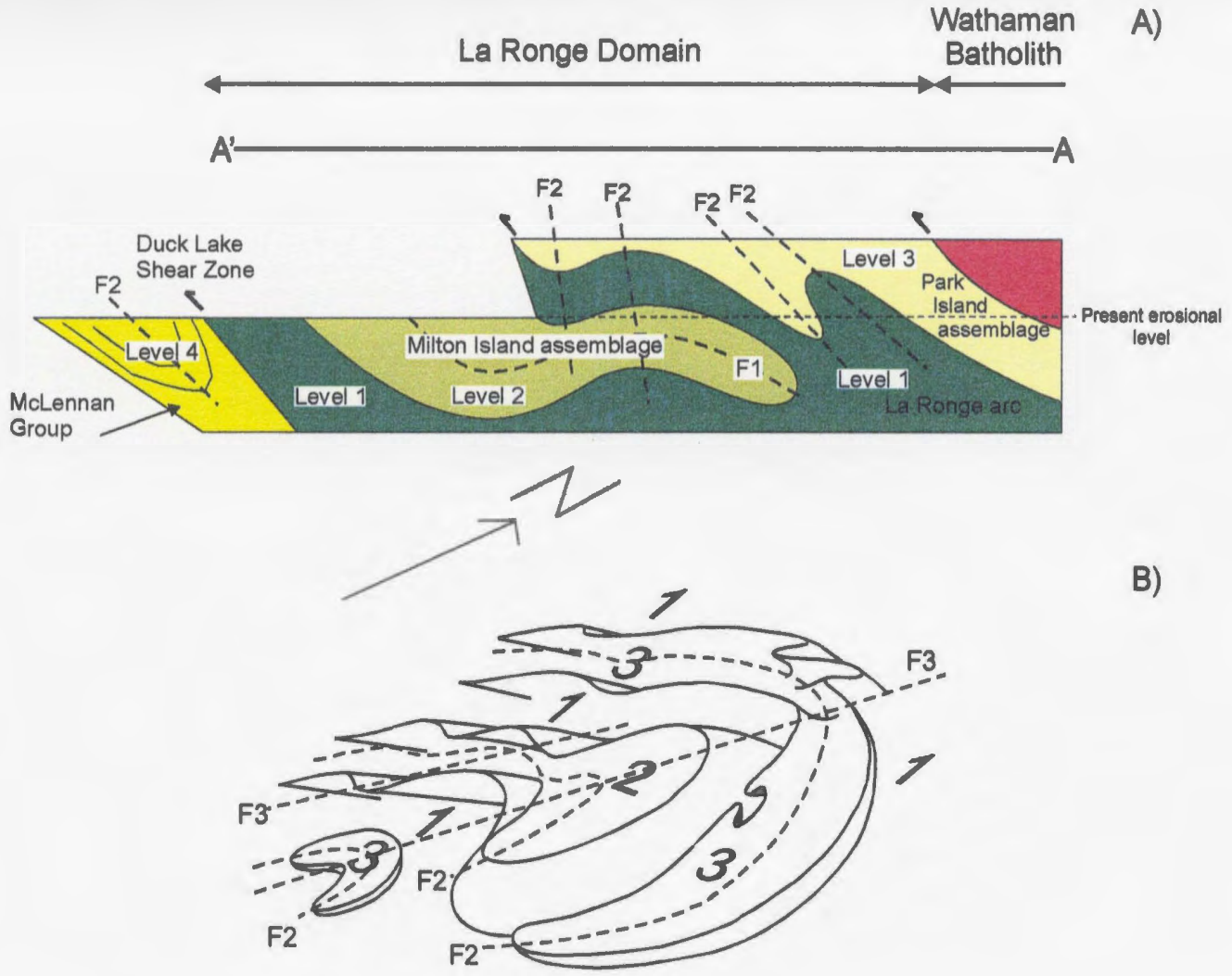

Figure 3.2 A) Schematic cross-section A -A' (see Figure 3.1) through the La Ronge Domain and southern margin of the Wathaman Batholith on Reindeer Lake. B) Schematic 3-D sketch of the fold geometry of the La Ronge Domains structural levels on Reindeer Lake. Modified after Corrigan et al. (1999).

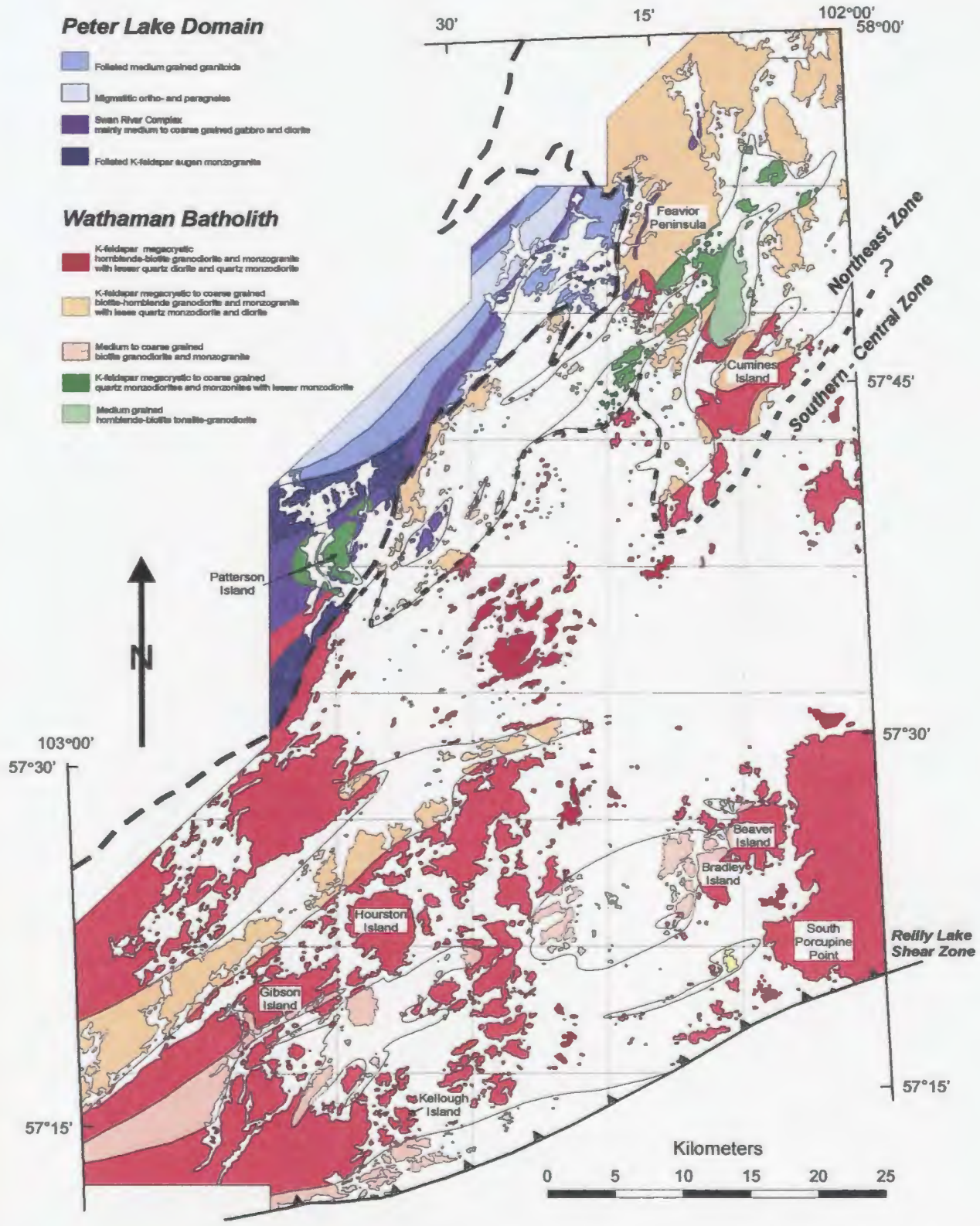

Figure 3.3 Generalized geological map of the Wathaman Batholith and Peter Lake Domain on Reindeer Lake.

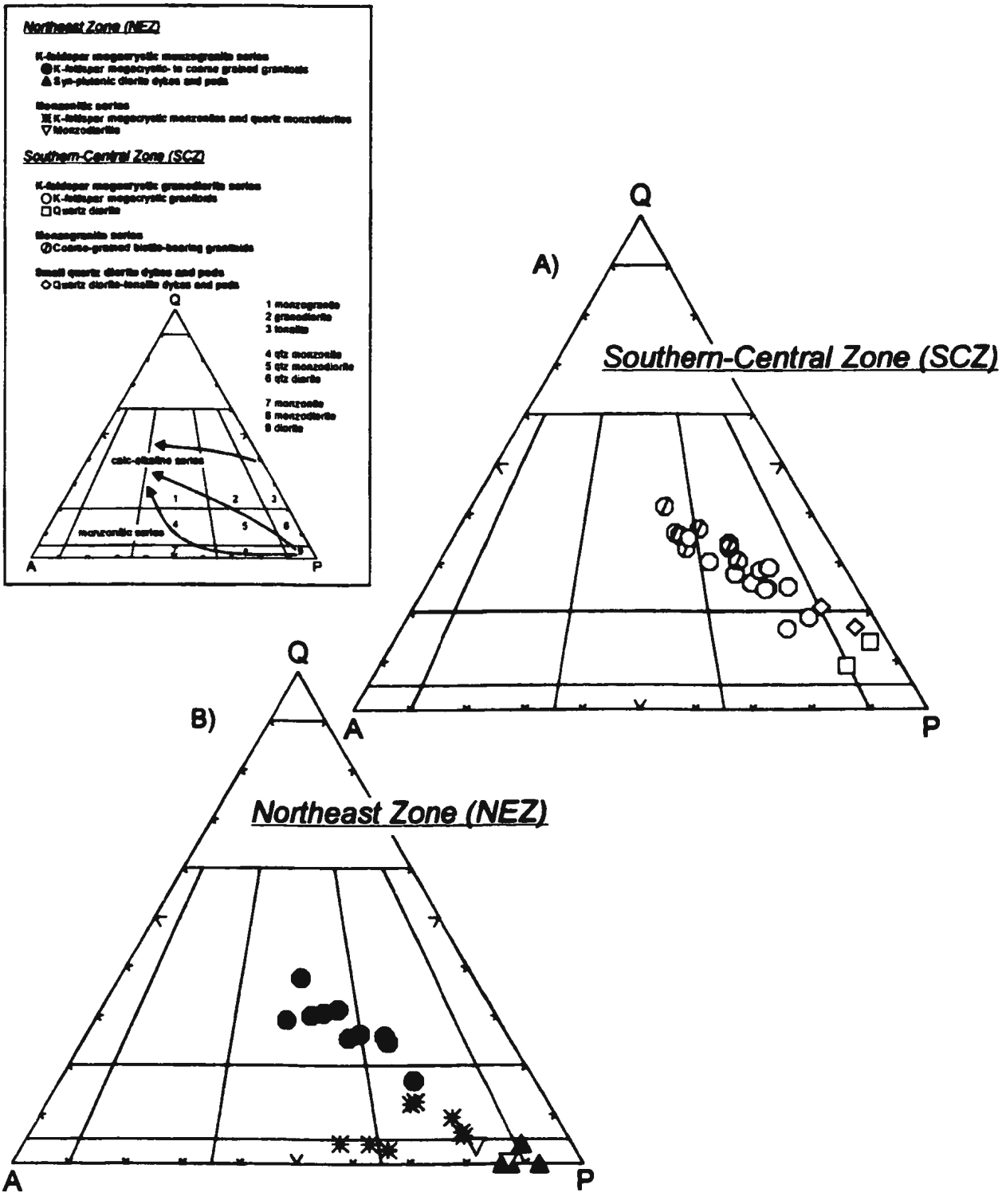

Figure 3.4. Quartz-plagioclase-alkali feldspar (QAP) mesonorm diagrams for rocks of the Wathaman Batholith: A) the Northeast Zone (NEZ) and; B) the Southern-Central Zone (SCZ) as discussed in the text. Rock names follow Streckheisen (1976).

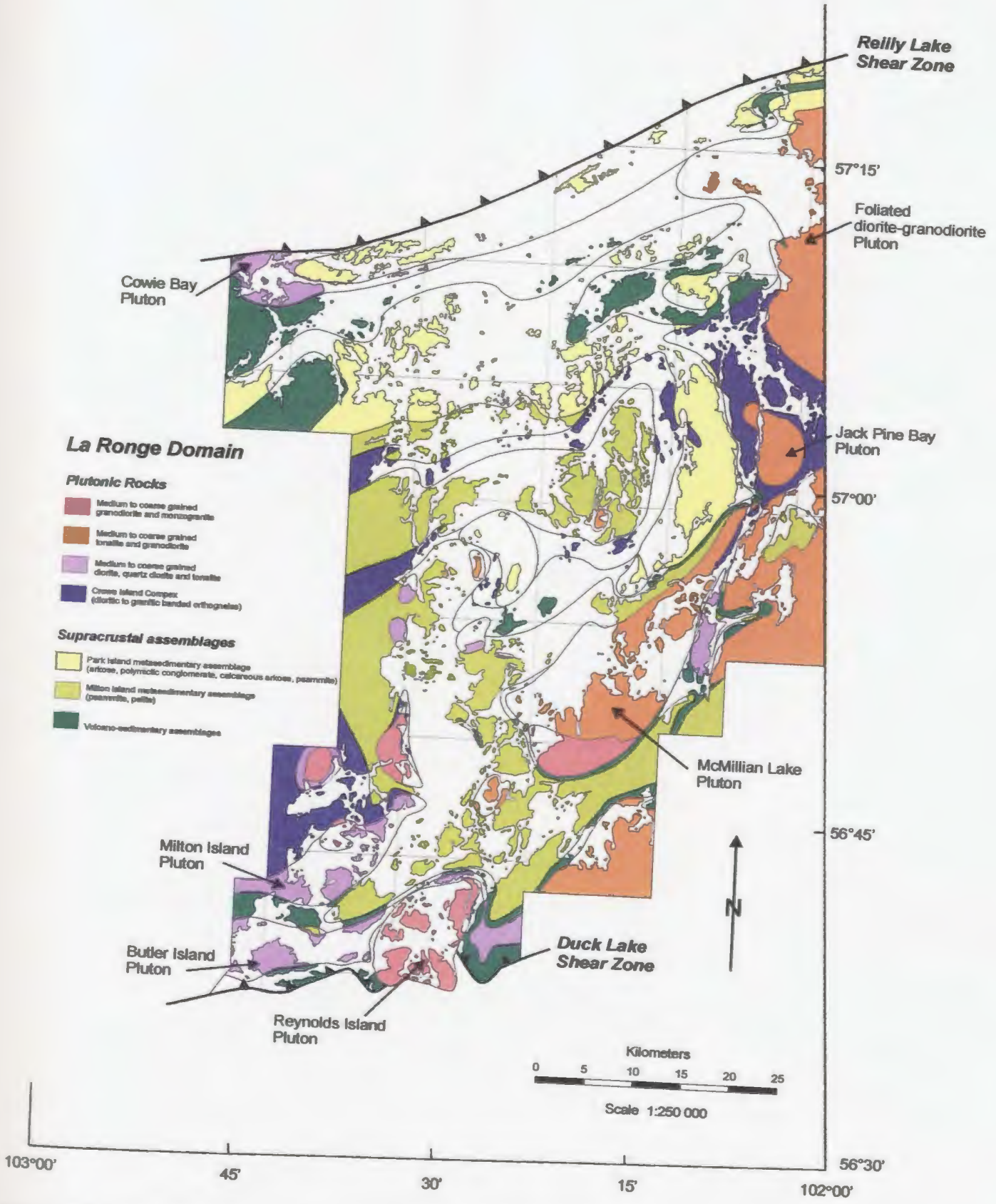

Figure 3.5 Generalized geological map of the La Ronge Domain on Reindeer Lake.

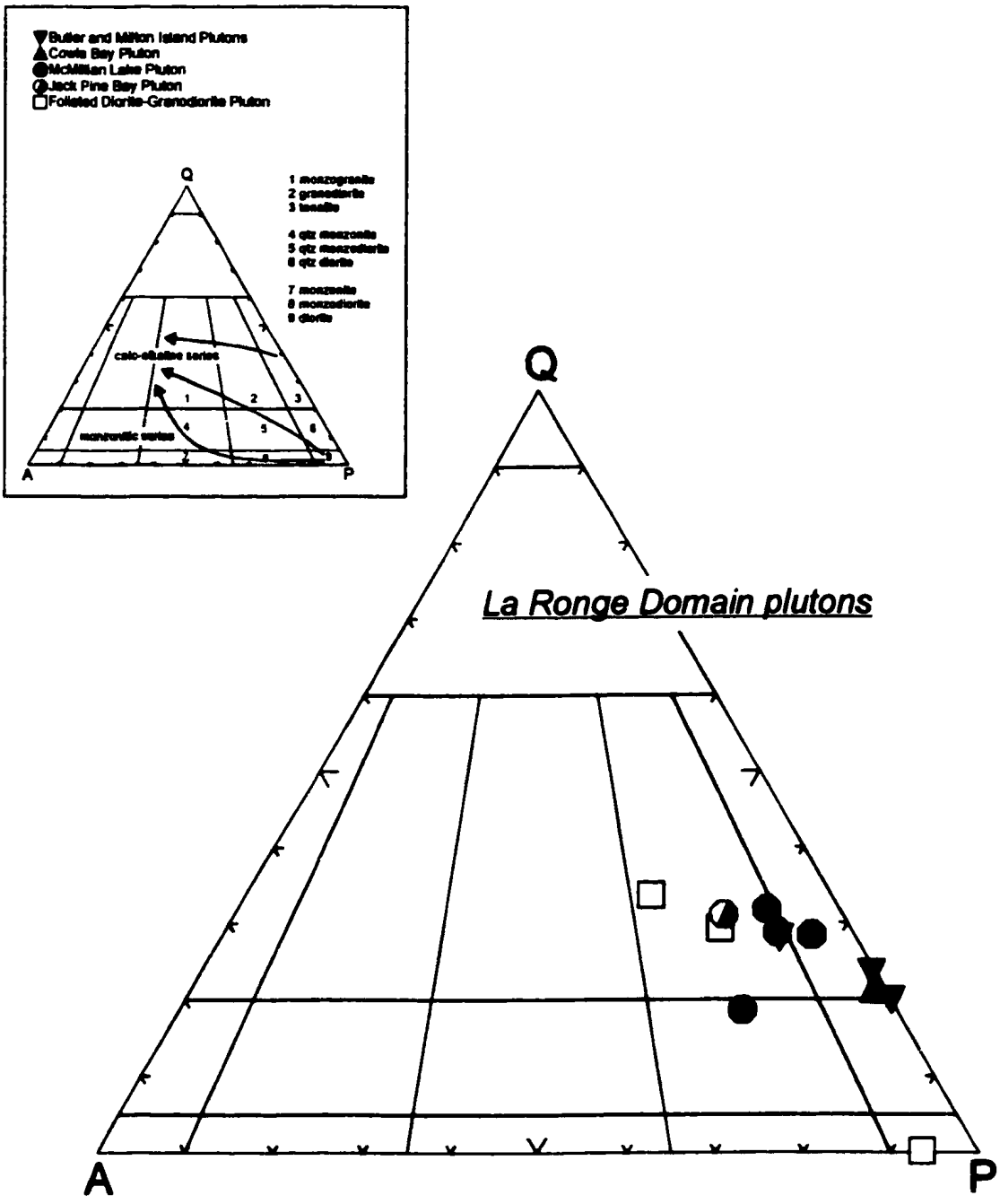

Figure 3.6 Quartz-plagioclase-alkali feldspar (QAP) mesonorm diagram for plutons of the La Ronge Domain. Rock names follow Streckheisen (1976).

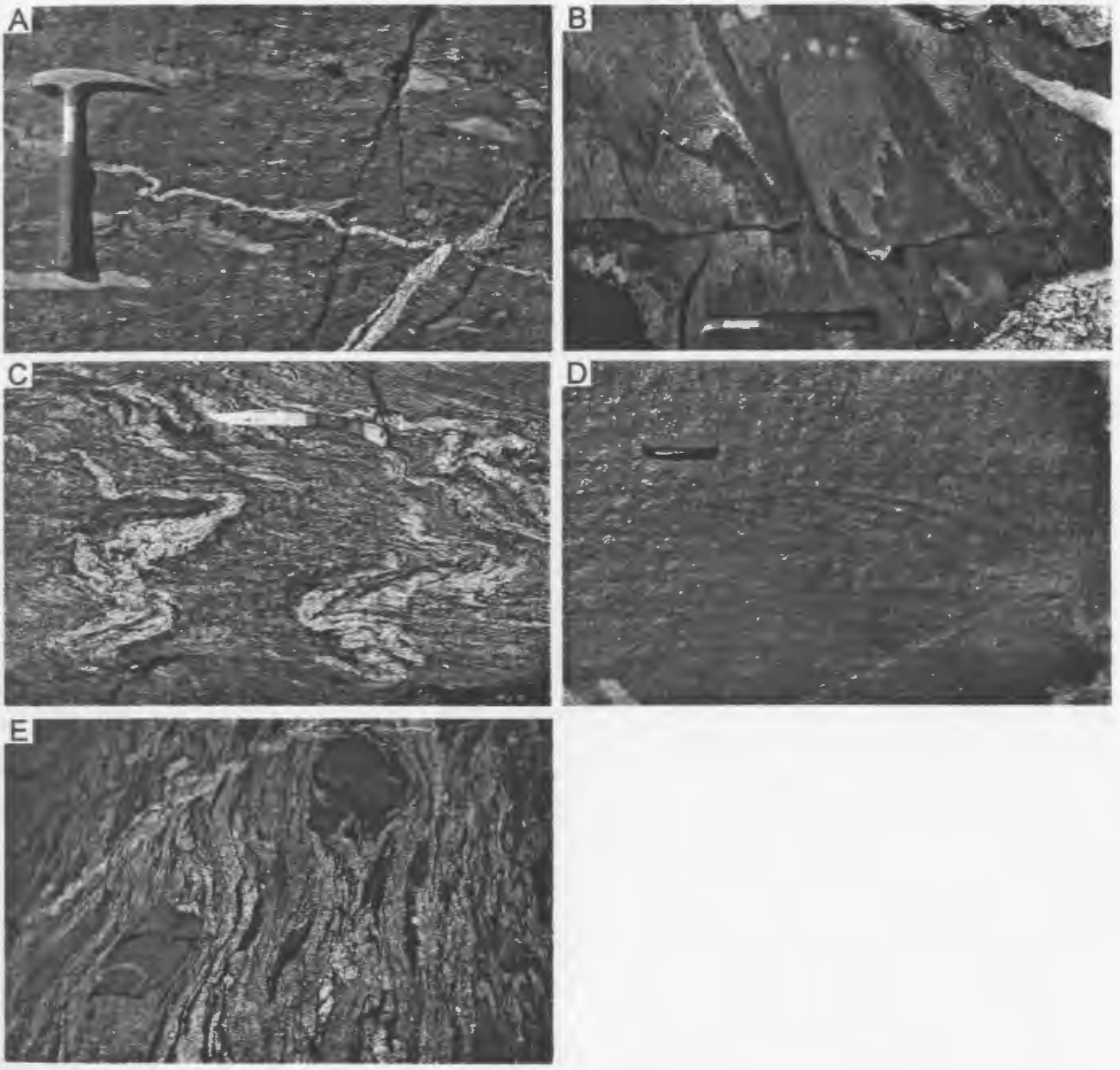

Plate 3.1 A) Intermediate volcaniclastic rock containing angular rhyolitic fragments in an adesitic matrix. B) Dioritic to granitic orthogneisses of the Crowe Island Complex. C) Migmatitic metasedimentary gneiss of the Milton Island metasedimentary assemblage. D) Cross bedding in arkose of the Park Island metasedimentary assemblage. E) Intensely migmatized arkose of the Park Island metasedimentary assemblage 1.5 km south of the Wathaman Batholith.

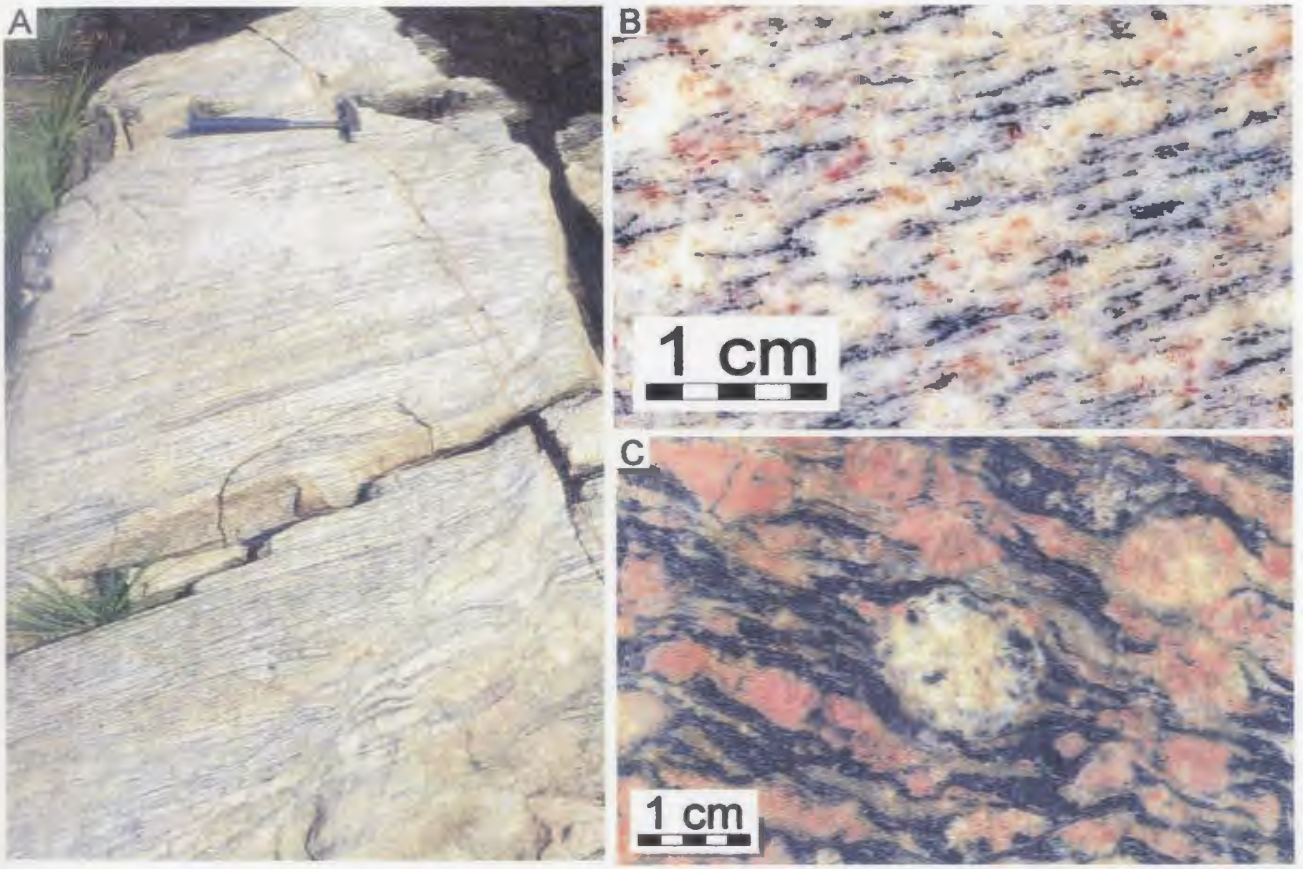

Plate 3.2 A) Migmatitic paragneiss. B) Foliated and recrystallized fine- to medium-grained biotite-bearing granodiorite. C) Bio-hbl-bearing K-feldspar augen monzogranite.

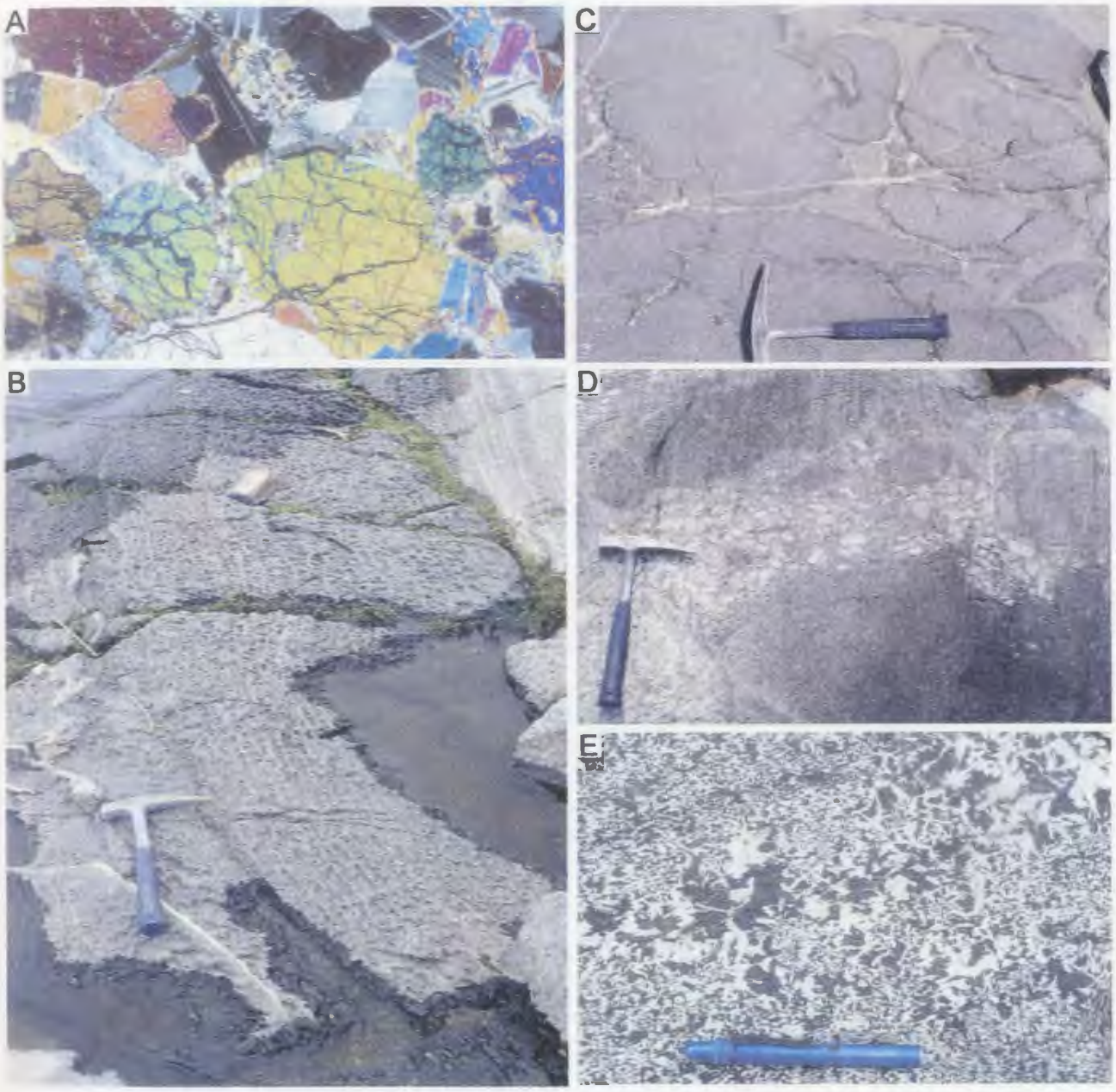

Plate 3.3 A) Olivine-cpx-bearing gabbro. B) Rhythmic layering in gabbro consisting of alternating plagioclase and hornblende-rich layers. C) Mingling between gabbroic and dioritic magmas. D) Intrusion of K-feldspar megacrystic quartz monzodiorite into fine grained gabbro. E) Pegmatitic (hydrated) gabbro of the Swan River Complex dated at ca. 2562 ±4 Ma (Corrigan et al., unpub. rept.).

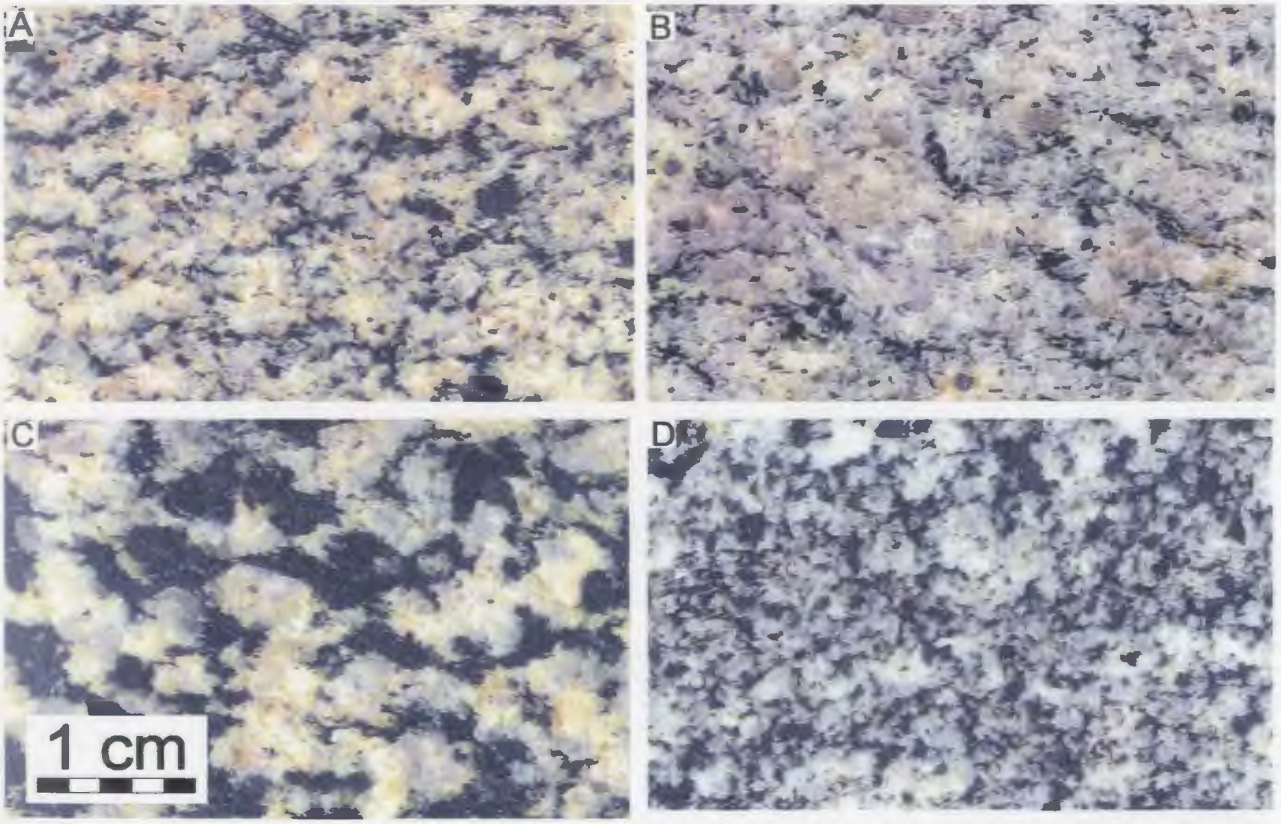

Plate 3.4 Polished rock slabs of selected La Ronge Domain plutons. A) Medium-grained bio-hbl-bearing granodiorite of the Jack Pine Bay Pluton. B) Medium-grained bio±hbl-bearing tonalite of the McMillian Lake Pluton. C) Medium- to coarse grained hbl-bio-bearing quartz diorite of the Butler Island Pluton. D) Medium-grained hbl-bio-bearing tonalite of the Cowie Bay Pluton.

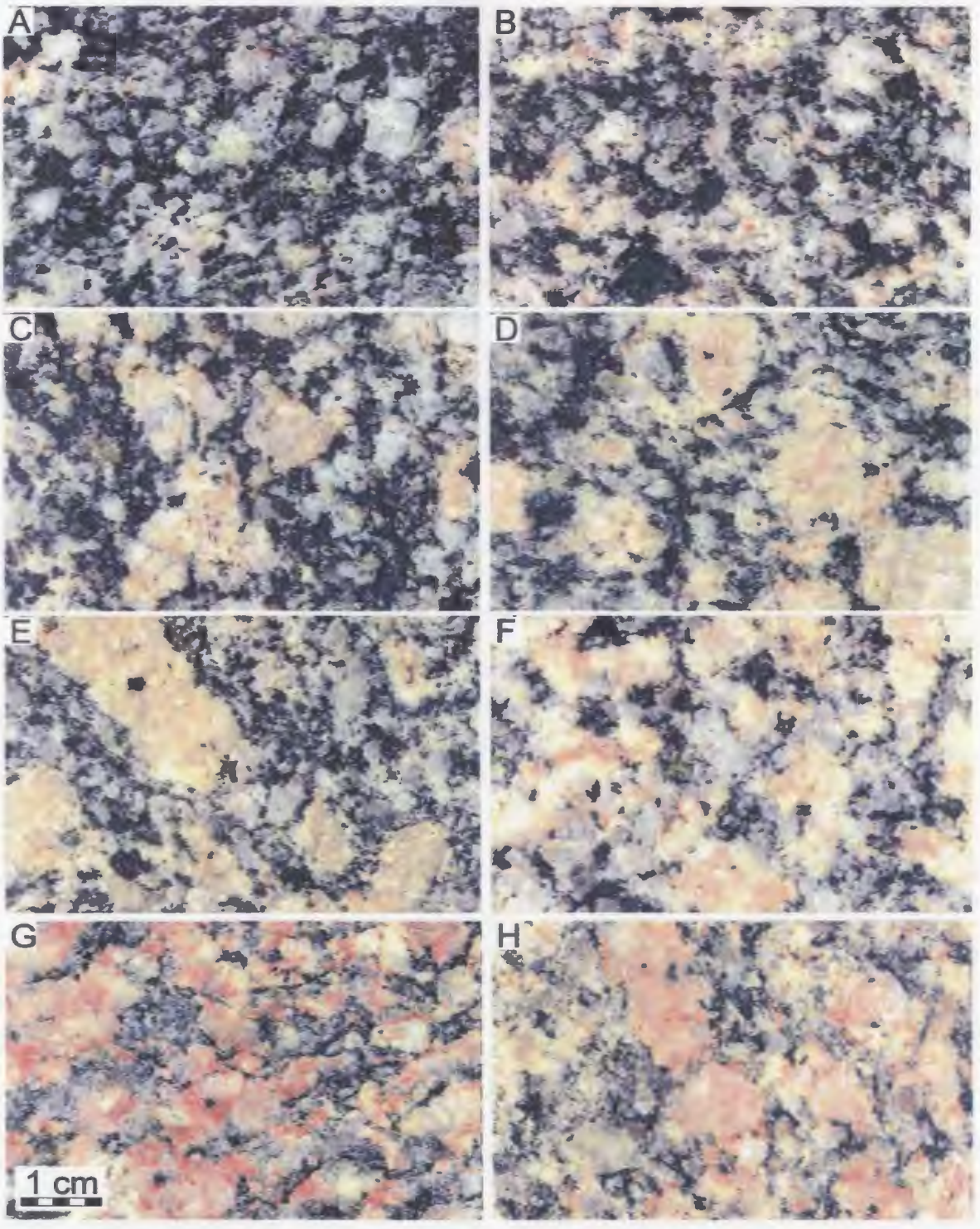

Plate 3.5 Polished rock slabs for K-feldspar megacrystic granodiorite series rocks of the Southern-Central Zone (SCZ) of the Wathaman Batholith. A) and B) Hbl-bio-bearing quartz diorite and quartz monzodiorite. C) and D) Hbl-bio-bearing quartz monzodiorite and granodiorite. E) and F) Hbl-bio- to bio-hbl-bearing K-feldspar megacrystic granodiorites. G) and H) Bio±hbl-bearing K-feldspar megacrystic granodiorite and monzogranite.

Plate 3.6 A) Layered quartz diorite-quartz monzodiorite body containing numerous microdiorite enclaves and scattered K-feldspar meagacrysts. B) Quartz diorite containing a euhedral K-feldspar megacryst. C) K-feldspar megacrystic quartz monzodiorite containing a microdiorite enclave with K-feldspar xenocrysts. D) Hbl-bio-bearing K-feldspar megacrystic granodiorite overlying the layered quartz diorite-quartz monzodiorite body.

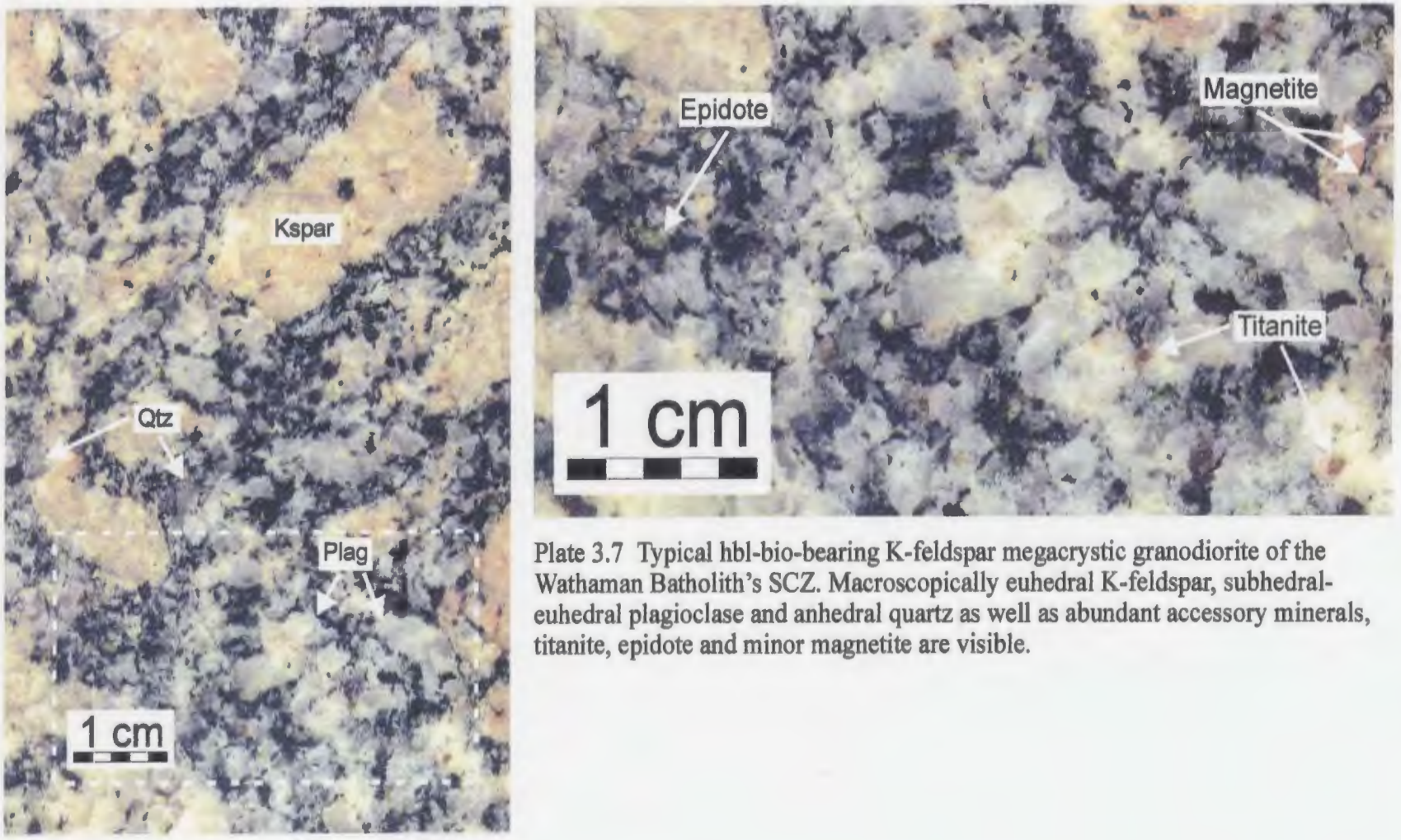

Plate 3.7 Typical hbl-bio-bearing K-feldspar megacrystic granodiorite of the Wathaman Batholith's SCZ. Macroscopically euhedral K-feldspar, subhedral-euhedral plagioclase and anhedral quartz as well as abundant accessory minerals, titanite, epidote and minor magnetite are visible.

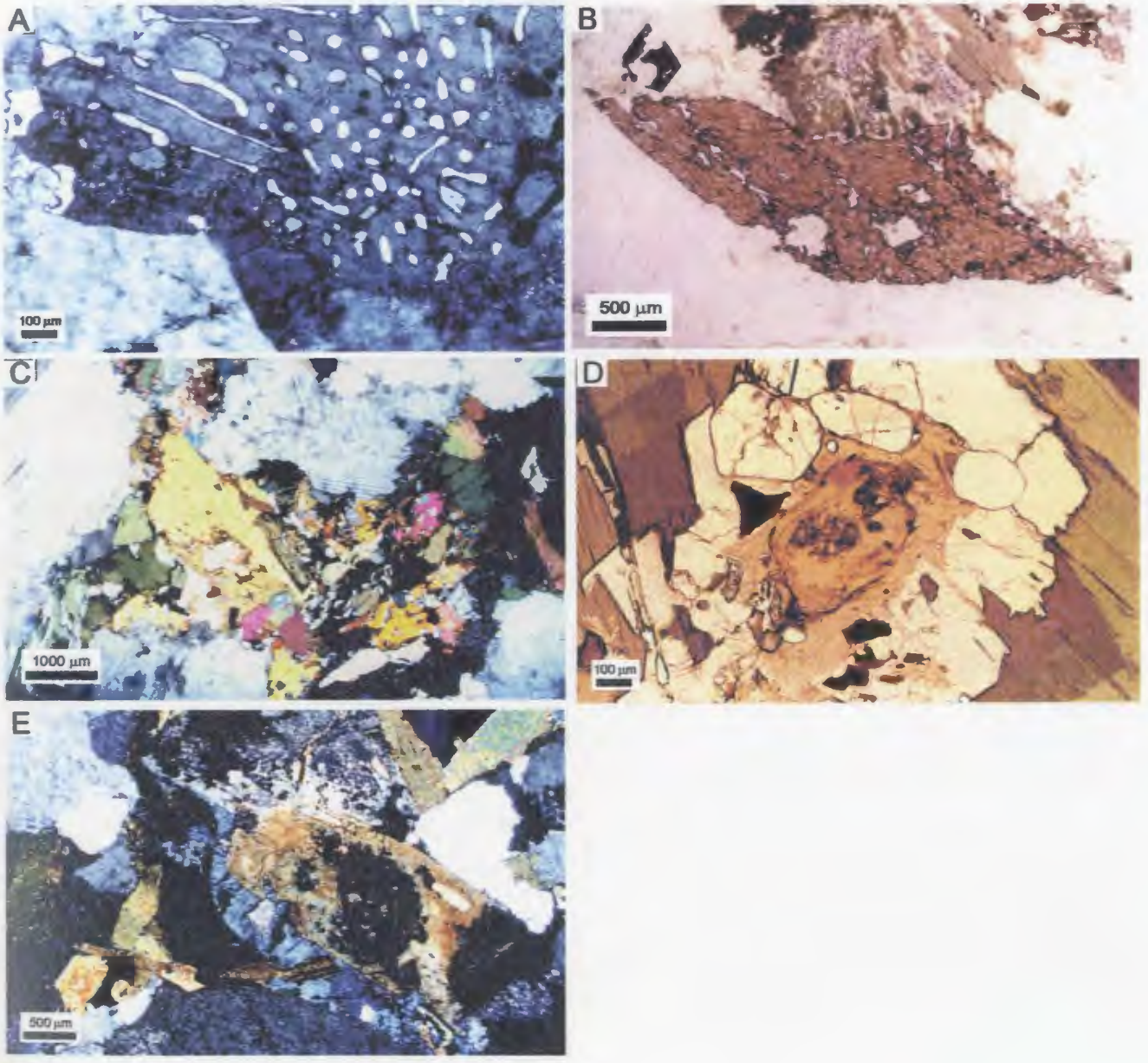

Plate 3.8 Photomicrographs of hbl-bio-bearing K-feldspar megacrystic granodiorites. A) Myrmekitic texture, composed of vermicular inclusions of quartz within plagioclase. B) Macroscopically euhedral diamond-shaped crystal of titanite. C) Hornblende-biotite-epidote rich clot and inclusions of euhedral epidote in biotite. D) Metamict allanite crystal overgrown by smaller epidote crystals, note the subhedral apatite crystal at top of photomicrograph. E) Metamict allanite crystal with an overgrowth of epidote where both crystals contain simple twins.

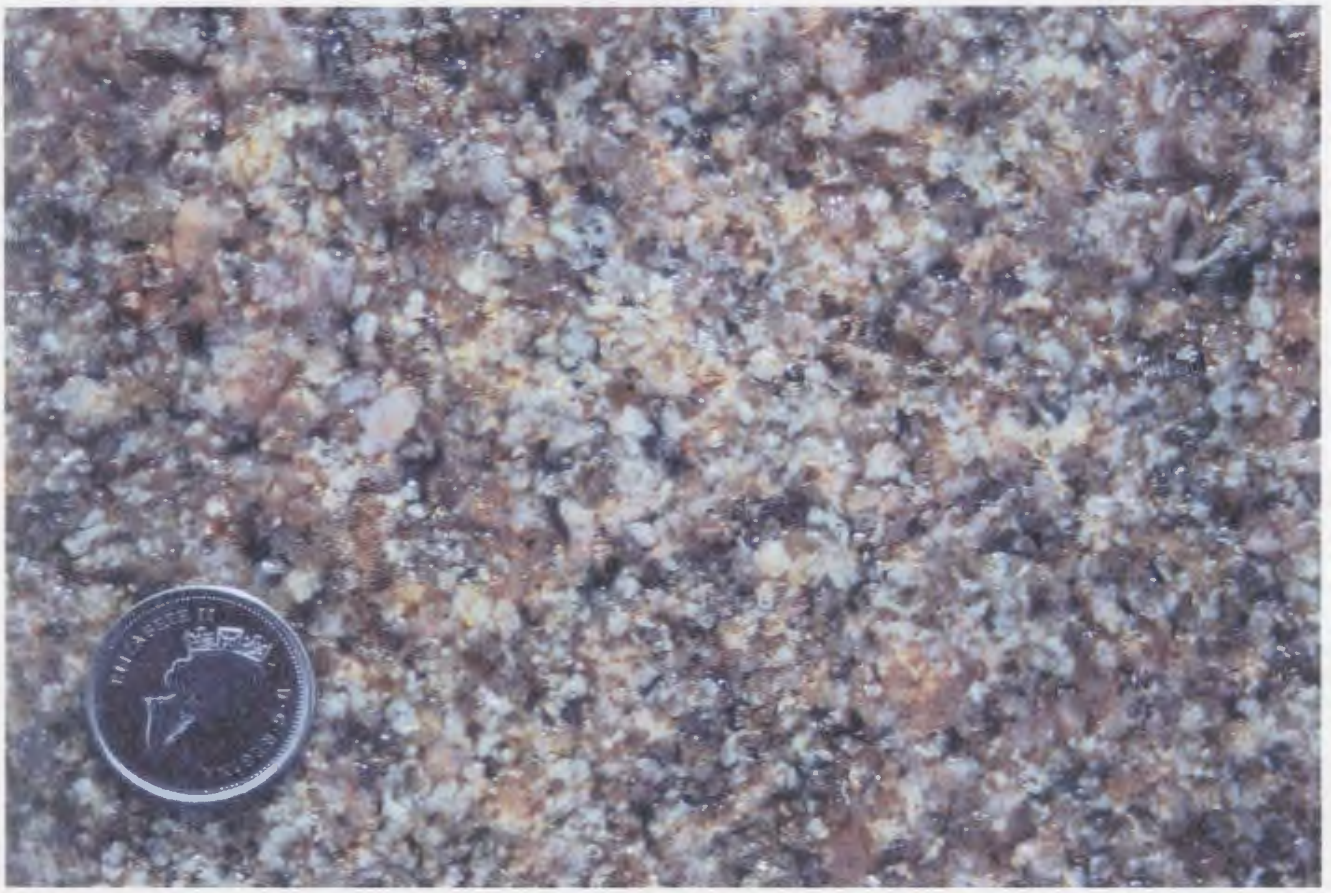

Plate 3.9 Typical medium-grained biotite-bearing granodiorite of the SCZ monzogranite series.

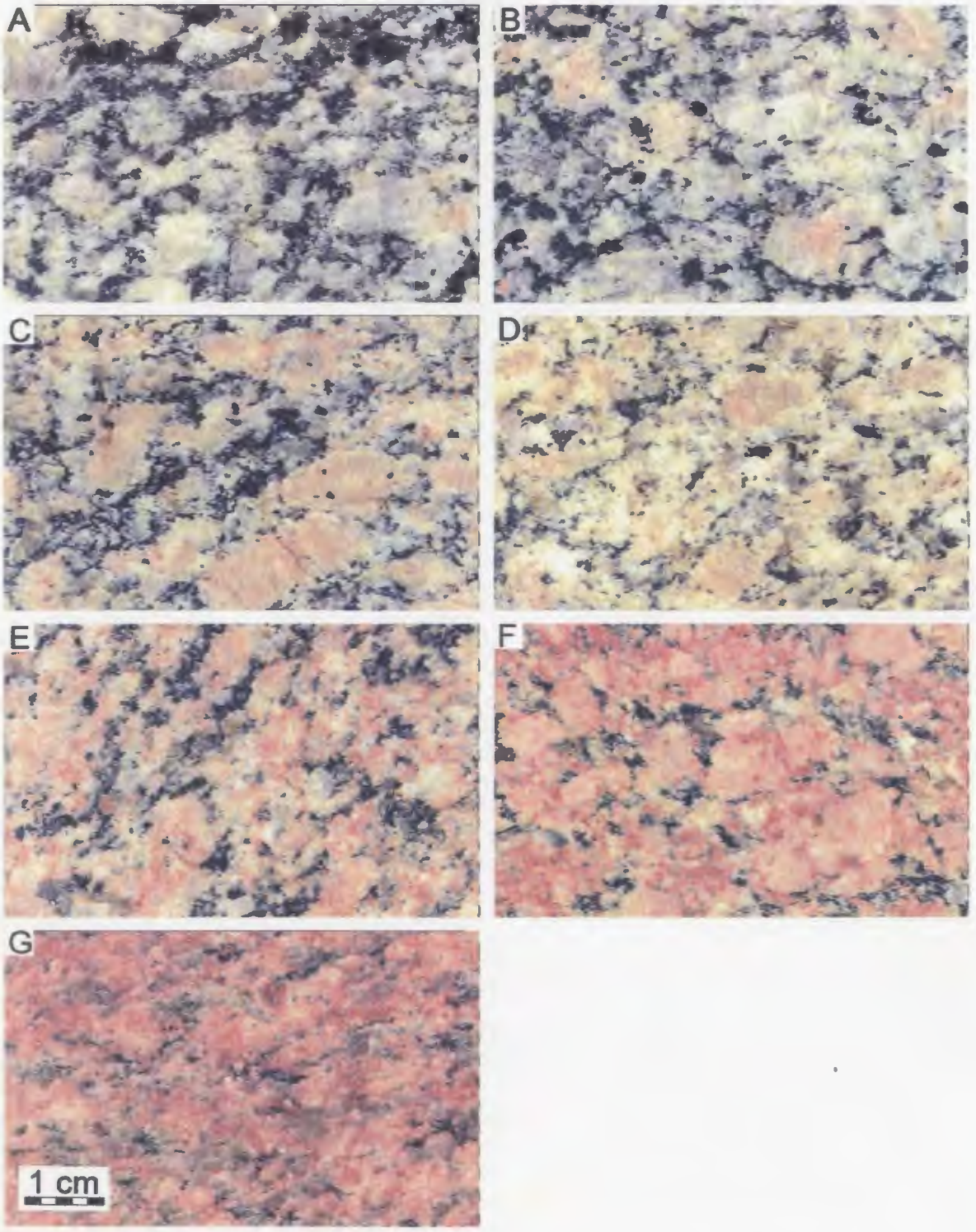

Plate 3.10 Polished rock slabs for K-feldspar megacrystic monzogranite series rocks of the Northeast Zone (NEZ) of the Wathaman Batholith. A) Hbl-bio-bearing K-feldspar megacrystic quartz monzodiorite. B) Hbl-bio-bearing K-feldspar megacrystic granodiorite. C) and D) Bio-hbl K-feldspar megacrystic granodiorite and monzogranite. E), F) and G) Bio-bearing K-feldspar megacrystic to coarse-grained monzogranite.

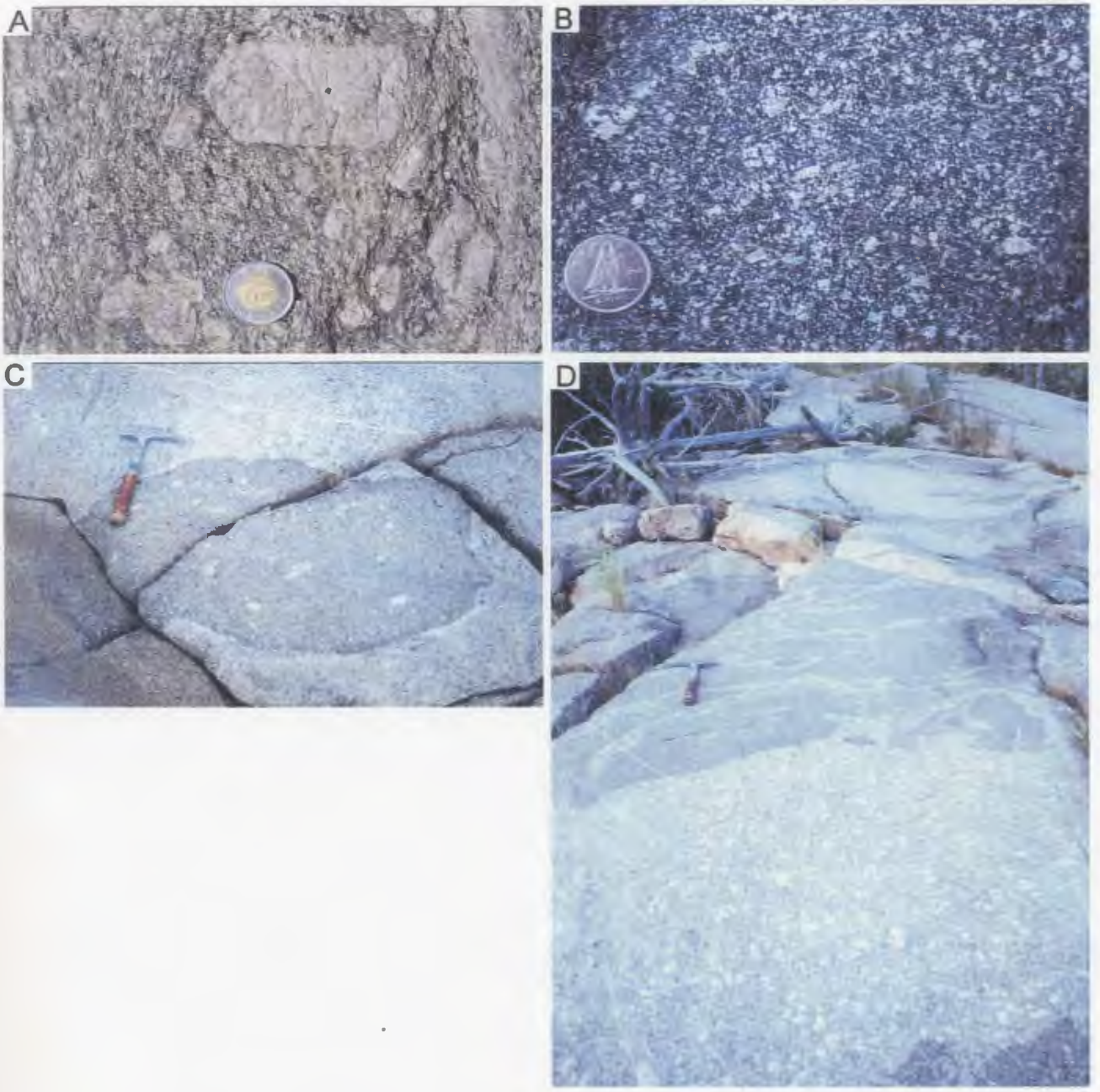

Plate 3.11 A) Large macroscopically-euhedral K-feldspar megacryst in bio-bearing monzogranite. B) Plag-phyric medium-grained syn-plutonic diorite dyke. C) Large microdiorite enclave containing K-feldspar xenocrysts in hbl-bio-bearing K-feldspar megacrystic granodiorite. D) Mingling between diorite and bio-hbl-bearing K-feldspar megacrystic granodiorite.

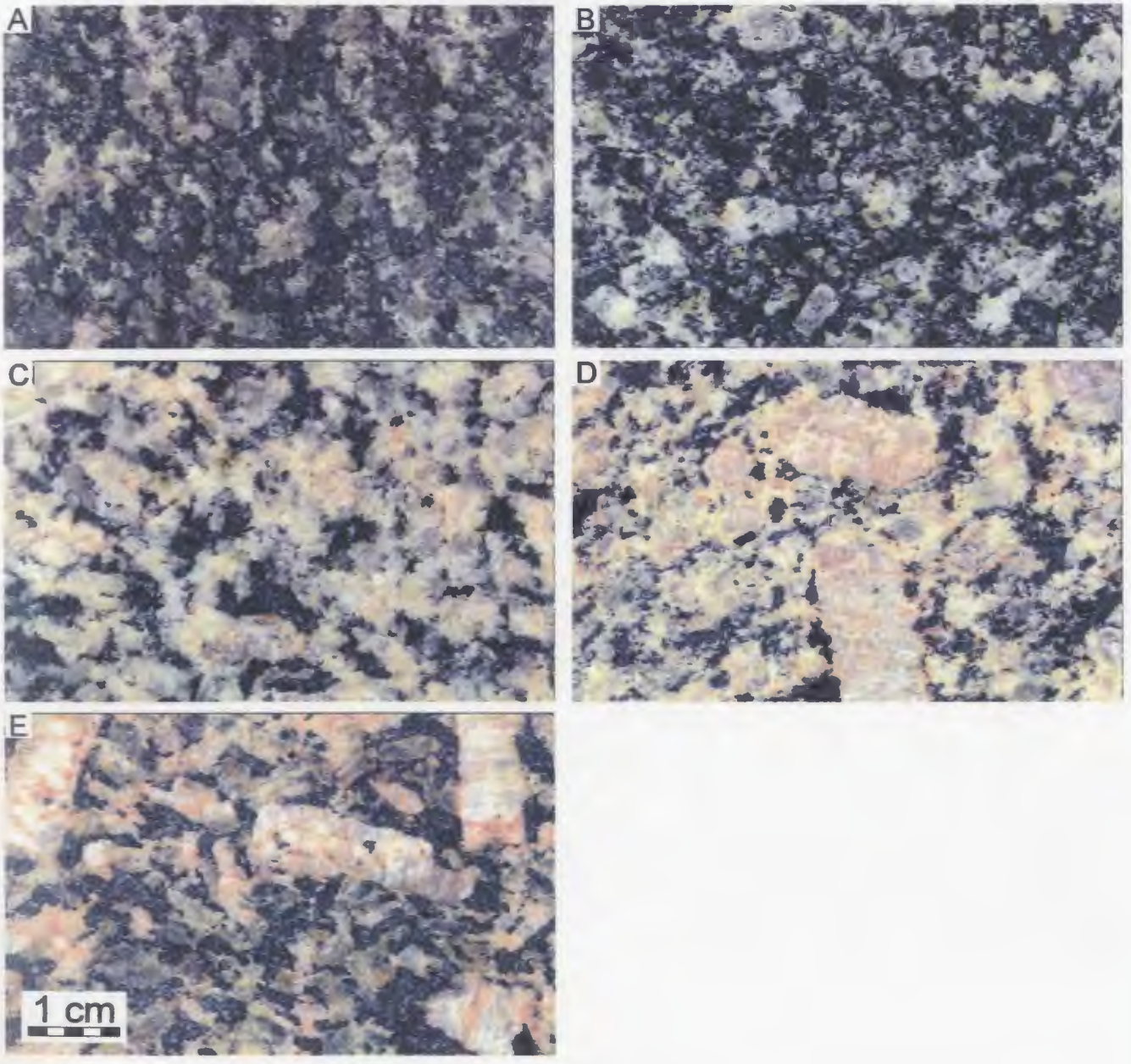

Plate 3.12 A) and (B) Hornblende-rich monzodiorites. C) and (D) Hbl-bio-bearing coarse-grained to K-feldspar megacrystic quartz monzodiorites. E) Hbl-cpx-bio-bearing K-feldspar megacrystic monzonite.

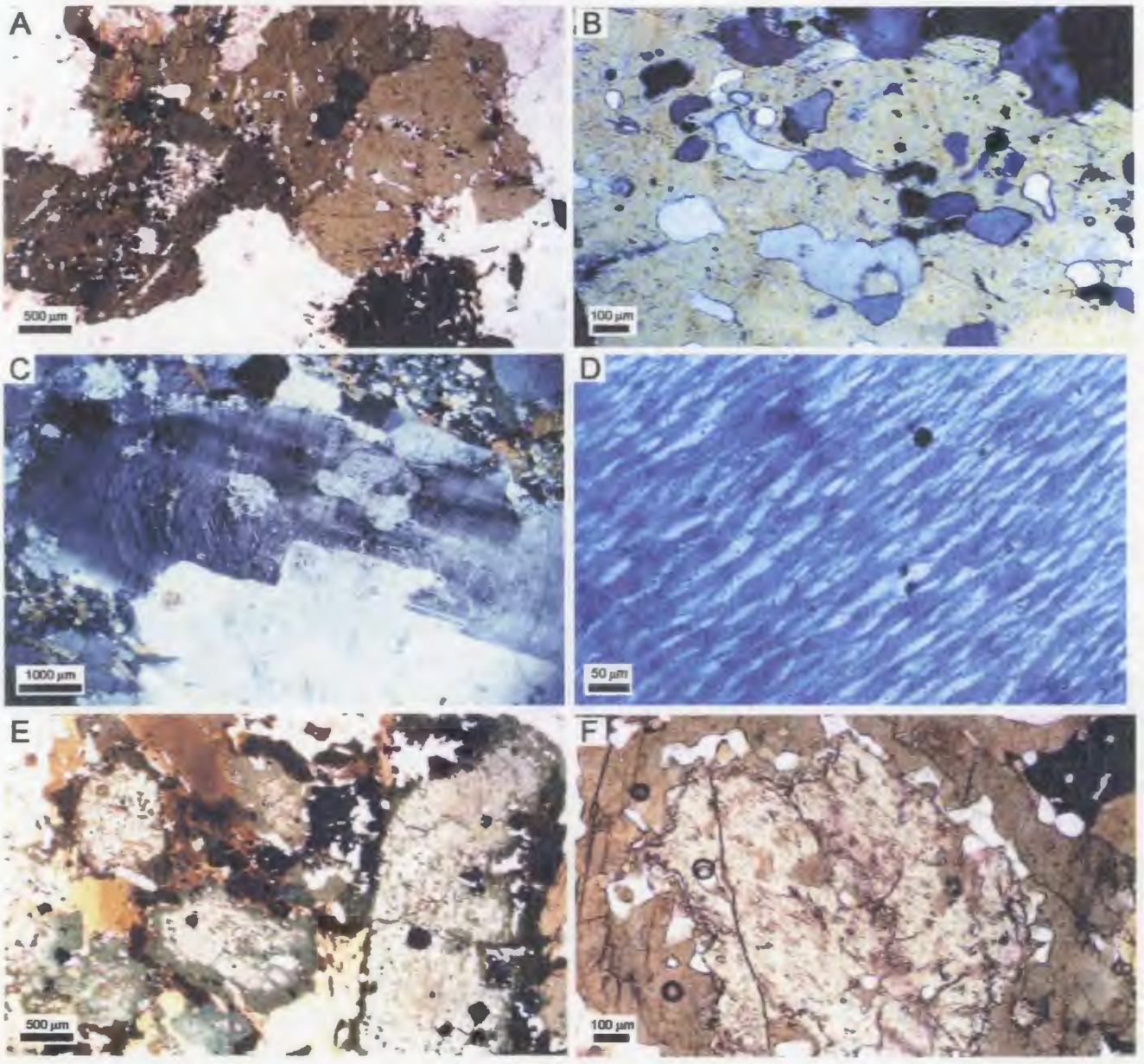

Plate 3.13 Photomicrographs of monzonitic series rocks. A) Clots of hornblende crystals containing numerous inclusions of quartz, Fe-Ti-oxides and apatite in hornblende-rich monzodiorite. B) Crystallographic control to the orientation of some quartz inclusions in hornblende in hornblende-rich monzodiorite. C) Relict growth zoning in K-feldspar crystal in hbl-bio-bearing K-feldspar megacrystic quartz monzodiorite. D) Perthitic-texture of plagioclase exsolutions in K-feldspar in hbl-bio-bearing K-feldspar megacrystic quartz monzodiorite. E) and (F) Relict clinopyroxene cores rimed with hornblende (pargasite) in hbl-cpx-bio-bearing K-feldspar megacrystic monzonite.

CHAPTER 4: GEOCHEMISTRY AND ND ISOTOPIC SIGNATURE OF THE WATHAMAN BATHOLITH AND LRD PLUTONS

4.1 INTRODUCTION

The major emphasis of this study has been the Wathaman Batholith and a more detailed account of its field relationships and characteristics, and consequently sampling for geochemistry and isotopic analyses has been made. This will allow for a more detailed account of its petrogenesis, than is possible for the LRD. Nonetheless important insights into the LRD granitoids, their petrogenesis and comparison with rocks of the Wathaman Batholith can be made.

From the Wathaman Batholith, 47 samples have been analysed for major, and selected trace elements by XRF, 29 of these for their REE concentrations by ICP-MS, and 20 for their Sm and Nd isotopic compositions. From the major plutons of the LRD, 13 samples have been analysed for major, and selected trace elements by XRF, 7 of these for their REE concentrations by ICP-MS, and 5 for their Sm and Nd isotopic compositions.

4.2 GEOCHEMISTRY OF THE WATHAMAN BATHOLITH

4.2.1 Major Elements

Representative whole rock, major, trace and REE analyses of the Wathaman Batholith granitoids are listed in Tables 4.1 to 4.3. The FeO/Fe_2O_3 was calculated using the method of LeMaitre (1976). The SCZ K-feldspar megacrystic granodiorite (SCZ-KMGS), and monzogranite series (SCZ-MS) rocks are listed in Table 4.1, the NEZ K-feldspar megacrystic monzogranite series (NEZ-KMMS) rocks in Table 4.2, and the monzonitic series (NEZ-MS) rocks in Table 4.3.

Major element Harker variation diagrams for granitoids of the Wathaman Batholith are plotted in Figures 4.1 and 4.2. Data for all four series are plotted together for ease of presentation and to facilitate comparisons between series. With increasing SiO_2, the major elements TiO_2, CaO,

Fe_2O_3, MgO and P_2O_5 always decrease, Al_2O_3 and Na_2O initially increase to silica contents between 57-58 wt. %, then decrease, and K_2O steadily increases (Figure 4.1, 4.2). Specific aspects of major element chemistry for individual series will be discussed separately below.

The SCZ-KMGS displays the widest and most continuous range in silica contents, between 53 and 72 wt. %. Only two samples taken for this study have silica contents below 60 wt. %, reflecting a sampling bias. Fortunately, five quartz diorite samples (SiO_2 - 53 to 58 wt. %) were collected in the southern and central portion of the Wathaman Batholith from a previous study by Fumerton et al. (1984). These samples have very similar major and trace element contents to those collected during this study, which suggests they are part of the SCZ-KMGS as defined in this study. In the Al_2O_3 and Na_2O versus SiO_2 plot there is an inflection near 60 wt. % SiO_2. The inflection separates samples that have K-feldspar megacrysts (> 60 wt. %), from samples where K-feldspar is still an interstitial phase (< 60 wt. %). In the granitoids with silica contents > 60 wt. %, smooth curvilinear trends are developed for Al_2O_3, CaO, Fe_2O_3, MgO and P_2O_5, with significant scatter on Na_2O, K_2O and TiO_2 versus SiO_2 plots (Figure 4.1,4.2).

The SCZ-MS rocks have silica contents between 69 and 75 wt. %. These granitoids display similar major element trends, and some similar compositions to the more differentiated end members of the SCZ-KMGS (Figure 4.1,4.2). However, they have slightly higher Al_2O_3 at a given SiO_2 value, and lower TiO_2, Fe_2O_3 and P_2O_5 contents. Two samples also contain distinctly higher Na_2O contents, compared to others in the series (Figure 4.1,4.2).

The NEZ-KMMS is distinctly bi-modal in character. The syn-plutonic diorite dykes have low silica contents between 49 and 53 wt. %, and correspondingly high MgO (5.4-10.1 wt. %) contents. They contain distinctly low P_2O_5 (< 0.3 wt. %) contents when compared to similarly fractionated monzodiorites and quartz diorites from other series. One diorite sample contains

anomalously low Al_2O_3 (13.9 wt. %) and Na_2O (2.7 wt. %), and a very high MgO (10.1 wt. %) content, suggesting that it contains a substantial cumulate hornblende component. The granodiorites and monzogranites of this series have intermediate-felsic compositions, and silica contents between 61-74 wt.%. Almost all the granitoids of this series have silica contents ≥ 65 wt. %, and are thus, on average considerably more felsic than the majority of the SCZ-KMGS, which have silica contents lying mainly between 60-65 wt.% respectively. Compared to the SCZ-KMMS and SCZ-MS, the NEZ-KMMS granitoids define a distinctly higher, increasing K_2O trend, and a lower, decreasing CaO trend (Figure 4.1,4.2). Within this series, smooth trends with silica are exhibited by Al_2O_3 and CaO, although a considerable amount of scatter is found on other major element versus SiO_2 plots.

The NEZ-MS is characterized by mafic-intermediate compositions with silica contents between 49-59 wt. %. This series exhibits increasing Al_2O_3, Na_2O and K_2O, and decreasing TiO_2, CaO, Fe_2O_3, MgO and P_2O_5 with increasing SiO_2 (Figure 4.1), and has notably high Al_2O_3 (16-21 wt. %), Na_2O (3-5 wt. %) and K_2O (2-5 wt. %) contents. The anomalously high Al_2O_3 (21 wt. %) content of one sample suggests a cumulate feldspar component. In contrast to other series, this series displays a large amount of scatter on many major element versus SiO_2 plots, for example TiO_2, Fe_2O_3, MgO and P_2O_5. The low MgO (1.5-4.2 wt. %) contents of the monzonites and quartz monzodiorites of this series are notable when compared to the other series (Figure 4.1,4.2). Note that the monzodiorites of the series do possess moderate to high MgO (4.5-5.3 wt. %) contents. The origin of the variability in this series may suggest that several distinctive magma batches have been sampled, or that the compositions of these samples are highly non-liquid, and contain variable amounts of cumulate minerals, especially Fe-Ti-oxides and apatite.

4.2.1.1 Magma Series and Alumina Indices

An important part of describing igneous rocks is defining which magma series/suites they belong to. In large part, the concept of magma series (spatial, non-genetic association) or magma suites (common lineage or source material) is based on geochemical variations in volcanic rocks, where the assumption that the bulk composition represents the liquid composition is more easily ascertained (Carmichael et al., 1974). However, defining plutonic rocks in terms of their alkalic, tholeiitic or calc-alkalic nature is a common and requisite step in classifying the nature of plutonism (Clarke, 1992).

Figure 4.3 illustrates the total alkali versus silica (TAS) scheme of Irvine and Baragar (1971). The majority of rocks in the Wathaman Batholith are sub-alkaline (i.e., tholeiitic or calc-alkalic), whereas the NEZ-MS is transitionally alkaline. Also illustrated on this plot is a reference line at $Na_2O + K_2O = 8$ wt. %. Note that the subalkaline SCZ plot under this line, while those similar rocks in the NEZ plot above this line. The alkali-lime index of Peacock (1931) arbitrarily divides rocks into 4 groups based on the weight percent of SiO_2 when the amount of $CaO = Na_2O + K_2O$ (*cf.*, Carmichael et al., 1974). Based on this criteria the SCZ plutons are calc-alkalic (~59 wt. % SiO_2); whereas, the NEZ (~53 wt. % SiO2) are alkali-calcic. Thus, there are quite fundamental and important distinctions between the SCZ and NEZ related to the K_2O, CaO and Na_2O contents of the rocks.

To characterize the subalkaline rocks as tholeiitic or calc-alkalic, the ternary AFM plot (Figure 4.4) (after Irvine and Baragar, 1971) has been utilized. All of the subalkaline rocks are calc-alkalic in nature.

Figure 4.5 illustrates the variation in K_2O with SiO_2 with field boundaries modified from Peccerillo and Taylor (1976). This plot clearly indicates that the SCZ and NEZ granitoids belong to two distinct magma series. The SCZ-KMS/MS define a uniquely high-K calc-alkaline trend

(Figure 4.5a), in contrast to the NEZ where both the KMMS and MS define a shoshonitic trend (Figure 4.5b). The most mafic, dioritic and monzodioritic, end-members of each series have lower K_2O contents and plot within the low silica portion of the high-K calc-alkaline field (Figure 4.5b).

Using the molecular A/NK versus A/CNK plot (Figure 4.6) with field boundaries from Maniar and Piccoli (1989) the SCZ-KMGS range from metaluminous to weakly peraluminous compositions (A/CNK ~ 0.8 -> 1.1), while the SCZ-MS cluster at a weakly peraluminous composition (A/CNK ~ 1.1). The small quartz dioritic and tonalitic plugs and dykes of the SCZ are strictly metaluminous (Figure 4.6a). The NEZ-KMGS rocks with ≥ 60 wt. % SiO_2 define a small range of slightly metaluminous to weakly peraluminous compositions (A/CNK 1 - 1.1) (Figure 4.6b). The syn-plutonic diorite dykes of this series are all strongly metaluminous having A/CNK ≤ 0.8 (Figure 4.6b). The NEZ-MS rocks are all metaluminous.

4.2.3 Trace Elements

Trace element contents of the Wathaman Batholith granitoids are highly variable, and significant scatter exists for all trace elements when plotted on Harker variation diagrams. This is the case for rocks of the same zone and those that are considered to be part of the same series. Given the size of the Wathaman Batholith, distance between collected samples, wide compositional range and ubiquitous accessory mineral phases, the scatter is not surprising. Despite the scatter, important trends and distinctions between series can be made. Selected high field strength (HFSE) and low field strength (LFSE) elements are plotted versus SiO_2 in Figure 4.7 and 4.8

4.2.3.1 SCZ

Within The KMGS, Y and Nb decrease with increasing fractionation, Zr, Sr, and Ba initially increase to silica contents of ~ 60 wt. % then decrease, and Th, Rb and Pb show slight

increases. The quartz diorites have moderate amounts of Ni (36-64 ppm), and Cr (147-161 ppm), and high Y (12-25 ppm), Nb (11-12 ppm), Sr (942-1084 ppm), and Ba (1088-1234 ppm) contents. The high Sr and Ba contents are quite remarkable considering the low silica (53-56 wt. %), and primitive ferromagnesian element contents of the quartz diorites. Over the 60-72 wt. % silica range, Y, Zr, Nb, Sr and Ba decrease with increasing differentiation. The quartz monzodiorites and granodiorites between 60-65 wt. % SiO_2 have very high Sr (632-1364 ppm), and Ba (1528-3388 ppm) contents. The entire series has generally low Rb (38-83 ppm), Th (<1-11 ppm), and Pb (5-21 ppm).

The granodiorites and monzogranites of the MS have trace element contents that largely plot as extrapolations to the KMGS trends. They have similarly high Sr (366-818 ppm), and Ba (1417-2768 ppm) contents to the megacrystic rocks, and distinctly lower Y (< 5 ppm) and Nb (< 5 ppm). They have low Zr (88-132 ppm), Th (<1-6 ppm), and Rb (55-77 ppm) contents. The small quartz diorite-tonalite plugs and dykes of the SCZ have broadly similar trace element systematics to the similarly fractionated rocks of this zone. They have moderate Ni (30-41 ppm), and Cr (111-117 ppm) similar to the quartz diorites of the SCZ-KMGS, however they do contain lower Sr (611-737 ppm), and considerably lower Ba (397-602 ppm) contents.

4.2.3.2 NEZ

These KMMS rocks have very distinctive trace element geochemical signatures when compared to similarly fractionated rocks of both the SCZ-KMGS and -MS rocks with > 60 wt. % SiO_2. The NEZ granitoids have higher average contents of Y, Zr, Nb, Th, Rb, and Pb (Figure 4.6). Both NEZ and SCZ granitoids have similarly high contents of Sr (~ 1100-130) and Ba (~ 2600-400). Y, Nb and Sr decrease with increasing differentiation. Considerable scatter exists in Zr, Rb, Th, Ba, and Pb versus SiO_2 and little or no correlation can be made with silica content. The most

notable increases occur in Zr, Nb, Th, Rb, and Pb contents.

The syn-plutonic dioritic rocks have significant contents of Ni (55-134 ppm) and Cr (16-624 ppm), low Th (< 1 ppm), Pb (7-9 ppm), and Rb (22-47 ppm), highly variable Y (11-40 ppm), Zr (33-141 ppm), Nb (8-26 ppm), and Ba (399-1273 ppm) and high Sr (719-1029 ppm).

The most conspicuous feature of the MS rocks are the LFSE contents. These are variable but generally they contain high Rb (40-121 ppm), and very high Sr (828-1350 ppm) and Ba (1042-2919 ppm). Excluded from this range is the sample 98-T311, that contains anomalously high Al_2O_3 (21 wt. %), and Sr (1692 ppm), suggesting a strong cumulate plagioclase component. Although obvious trends are difficult to discern, a fairly consistent ~ 3-fold increase in Ba (1042-2919 ppm), and a strong decrease in Y (27-10 ppm) contents occur with increasing silica. In contrast to the Ba, Sr is generally lower in the more differentiated rocks on this series.

The monzodiorites of the MS contain relatively high Ni (41-53) and Cr (99-113), and high V (155-190 ppm). They contain highly variable contents of Rb (40-75 ppm), Pb (10-18 ppm), Y (16-38 ppm), Zr (78-146 ppm), Nb (9-24 ppm) and Th (1.6-7 ppm), and very high Sr (1036-1057 ppm) and Ba (1264-1390 ppm) contents. The monzonites and quartz monzodiorites are quite depleted in transition metals, Ni is below the detection limit of XRF (< 5 ppm), and Cr is low (< 7-32 ppm), although moderate to high contents of V (52-202 ppm) are found. Y (10-28 ppm), and especially Zr (5-330 ppm) are variable, Nb (7-14 ppm), Th (3-7 ppm) and Pb (10-19) are generally low. The high to very high Sr and Ba contents characterize the monzonites and quartz monzodiorites.

4.2.4 Rare Earth Elements (REE)

All REE data for these samples have been normalized to primitive mantle values obtained from Sun and McDonough (1989) and are plotted in Figures 4.9 and 4.10. REE patterns for the

SCZ-KMGS and MS, and the NEZ-KMMS, containing > 60 wt. % SiO_2 are plotted in Figure 4.9. For each series, groups based on divisions in the silica contents at: 61-63; 64-65; and 67-72 wt. % (Fig. 4.9a, b and c respectively) are presented. Comparing similarly fractionated rocks is important especially considering that there is little overlap, especially at lower silica contents between the SCZ and NEZ megacrystic granitoids.

REE patterns for the SCZ and NEZ granitoids with 61-63 wt. % (Figure 4.9a) show that these rocks have similar patterns and abundances. The quartz monzodiorites and granodiorites of the SCZ are fractionated [$(La/Yb)_N$ = 15-20], contain moderate REE contents [$(Ce)_N$ = 42-59; $(Yb)_N$ = 3-4], and small negative Eu-anomalies (Eu/Eu* ~ 0.8). The quartz monzodiorite of the NEZ contains slightly higher LREE contents [$(Ce)_N$ = 70], more fractionated REE [$(La/Yb)_N$ = 26], but similar HREE [$(Yb)_N$ = 4] and Eu-anomaly (Eu/Eu* ~ 0.8).

REE patterns (Figure 4.9B) in the granodiorites (64-65 wt. %) of the SCZ and NEZ are characterized by different REE patterns and abundances. With the exception of one sample, the SCZ granodiorites are highly fractionated [$(La/Yb)_N$ = 25-49], contain slightly concave upward, depressed MREE and HREE [$(Dy)_N$ = 2-3; $(Yb)_N$ < 2), and small positive Eu-anomalies (Eu/Eu* = 1.1-1.2). The NEZ granodiorites are less fractionated [$(La/Yb)_N$ = 14-19], contain elevated, flat MREE and HREE [$(Dy)_N$ = 4-6; $(Yb)_N$ = 4-5], and small to moderate negative Eu-anomalies (Eu/Eu* = 0.6-0.8). The degree of LREE fractionation is highly variable in the SCZ granodiorites [$(La/Sm)_N$ = 3-7], in contrast to the constant LREE fractionation [$(La/Sm)_N$ ~ 4] of the NEZ granodiorites. One of the five NEZ granodiorites contains elevated MREE and HREE contents, and a small negative Eu-anomaly.

The REE patterns of felsic granitoids (67-72 wt. %) of the SCZ and NEZ are plotted in Figure 4.9c. The granodiorites and monzogranites of the SCZ-MS are also included on this plot.

Major differences, most notably in the REE abundances, are clear between the three series. The granodiorites and monzogranites of the NEZ contain the highest REE contents [$(Ce)_N$ = 81-103; $(Yb)_N$ = 3-4], are highly fractionated [$(La/Yb)_N$ = 25-47], and have small negative Eu-anomalies (Eu/Eu* = 0.8-0.9). The granodiorites and monzogranites of the SCZ-KMGS contain lower REE contents [$(Ce)_N$ = 25-63; $(Yb)_N$ 1-2], are highly fractionated [$(La/Yb)_N$ = 22-67], and have variable Eu-anomalies (Eu/Eu* = 0.7-1.1). The degree of LREE fractionation [$(La/Sm)_N$ = 3-8], as with the 64-65 wt. % silica granodiorites of the SCZ, is highly variable. The granodiorites and monzogranites of the KMGS have very low REE contents [$(Ce)_N$ = 12-23; $(Yb)_N$ < 1], are very highly fractionated [$(La/Yb)_N$ = 69-72], contain distinctive concave upward MREE patterns, and posses small to large positive Eu-anomalies (Eu/Eu* = 1.2-2.0).

The REE patterns of SCZ, and NEZ granitoids containing < 60 wt. % silica are plotted in Figures 4.10a-c. REE patterns of two quartz diorites from the SCZ-KMGS are plotted in Figure 4.10a. These rocks have moderately to highly fractionated [$(La/Yb)_N$ = 21-25], contain moderate to high REE contents [$(Ce)_N$ = 39-92; $(Yb)_N$ = 2-5), and possess small negative Eu-anomalies (Eu/Eu* = 0.8-0.9). The least fractionated quartz diorite (98-T062) contains the highest REE contents in the entire KMS.

The REE patterns of two syn-plutonic diorite dykes from the NEZ-KMMS are plotted in Figure 4.10b. The diorites are moderately fractionated [$(La/Yb)_N$ = 8-12], contain high REE contents, especially the MREE and HREE [$(Ce)_N$ = 49-53; $(Yb)_N$ = 4-6], posses small negative Eu-anomalies (Eu/Eu* = 0.8-0.9). The diorites also have unique, downward curving LREE patterns. The dykes contain high modal abundances of hornblende, and combined with the downward curving LREE pattern, this suggests they may contain a small cumulate hornblende component.

REE data for NEZ-MS rocks are plotted in Figure 4.10c. The monzodiorites and a

monzonite from this series have similar REE patterns, and abundances, and equal to higher REE contents than the more fractionated quartz monzodiorites. The monzodiorites and monzonite are moderately fractionated [$(La/Yb)_N$ ~ 17], contain moderate to very high REE contents [$(Ce)_N$ = 44-102; $(Yb)_N$ = 3-7], and small to moderate negative Eu-anomalies (Eu/Eu* = 0.9-0.6). The quartz monzodiorites of this series have more fractionated REE [$(La/Yb)_N$ = 23-29), generally contain lower REE contents, more pronounced in the MREE and HREE [$(Ce)_N$ = 36-56; $(Yb)_N$ = 2-3), and small to moderate positive Eu-anomalies (Eu/Eu* = 1.1-1.6). The quartz monzodiorite with the more pronounced positive Eu-anomaly also has a very high Al_2O_3 (21 wt. %) content, compared to similarly fractionated rocks of the series, suggesting a cumulate feldspar component.

4.2.5 Extended Element Diagrams

Extended element diagrams, including selected REE, LFSE (Rb, Ba, K and Sr), and HFSE (Th, Nb, Zr, P, Ti and Y) are plotted in Figures 4.11 and 4.12. In general, the element order is based on increasing incompatibility toward the left during melting of a lherzolite (leaving a harzburgite residue). The ordering of the elements follows that used by Whalen et al. (1999). Normalizing values are from Sun and McDonough (1989). The silica groupings used for the REE, have also been employed on the extended element diagrams.

Extended element diagrams for the SCZ, and NEZ granitoids containing > 60 wt. % silica are plotted in Figures 4.11a, b and c. All granitoids, over the 61-72 wt. % silica range, in both the SCZ and NEZ contain elevated Rb, Ba, K and LREE, and low Nb, Zr, P, Ti, Y and HREE contents, with pronounced negative Nb, P and Ti anomalies.

The 61-63 wt. % silica granitoids from the SCZ and NEZ are plotted in Figure 4.11a. The SCZ granitoids contain large, positive Ba anomalies, small positive to negative Sr anomalies, very weak negative Th anomalies, and strongly negative Nb, P and Ti anomalies. The NEZ quartz

monzodiorite has a smaller, positive Ba anomaly, a distinctively strong positive Th anomaly, and strongly negative Nb, P and Ti anomalies. The NEZ quartz monzodiorite clearly contains higher, to much higher contents of Rb, K, Th, Nb, LREE and Zr than the SCZ quartz monzodiorite and granodiorites.

Data for the granodiorites (64-65 wt. %) from the SCZ and NEZ is presented in Figure 4.11b. The SCZ granitoids contain very strong, positive Ba anomalies, variable Sr and Th anomalies, and strong negative Nb, P and Ti anomalies. The NEZ granitoids contain small, to very weakly positive Ba anomalies, strongly positive Th anomalies, negative Sr anomalies, and strongly negative Nb, P and Ti anomalies.

The extended element patterns for granitoids (67-72 wt. %), from the SCZ and NEZ are plotted in Figure 4.11c. The NEZ granitoids have small to moderate, positive Ba anomalies, moderate to strongly negative Sr anomalies, strong positive Th anomalies, and strongly negative Nb, P and Ti anomalies. The SCZ granitoids have: small to moderate, positive Ba anomalies; moderate positive, to strongly negative Sr anomalies; positive to negative Th anomalies; and negative Nb, P and Ti anomalies. The granodiorites and monzogranites of the SCZ-MS have moderate, positive Ba anomalies, weakly positive to negative Th anomalies, strongly positive Sr anomalies, and negative Nb, P and Ti anomalies. The NEZ-KMMS granitoids contain higher to much higher contents of Rb, K, Th, Nb, LREE when compared to any, similarly fractionated granitoids of the SCZ.

Primitive mantle normalized extended element diagrams of SCZ, and NEZ granitoids containing < 60 wt. % silica are plotted in Figure 4.12. The extended element patterns of two quartz diorites from the SCZ-KMGS are given in Figure 4.12a. The quartz diorites have strongly positive Ba anomalies, significant positive and negative Sr anomalies, small to strongly positive Th

anomalies, and moderate to strongly negative Nb, P and Ti anomalies. The two syn-plutonic diorite dykes from the NEZ-KMMS are illustrated in Figure 4.12b. The diorites have moderate positive, to no Ba anomalies, small negative Sr anomalies, and strongly negative Th, P and Ti anomalies. The diorites are the only samples from the entire batholith that do not posses some form of negative Nb anomaly.

Extended element patterns for the NEZ-MS are plotted in Figure 4.12c. The monzodiorites contain strong positive Ba anomalies, negative to weakly positive Sr anomalies, positive and negative Th anomalies, variable Zr, and negative Nb, P and Ti anomalies. The monzonite contains no Ba or Th anomalies, and negative Sr, Zr, Nb, P and Ti anomalies. The quartz monzodiorites contain strongly positive Ba anomalies, strongly positive to no Sr anomalies, positive and negative Th anomalies, and negative Nb, P and Ti anomalies. The sample with the strongly positive Sr anomaly, also contained a very strong positive Eu-anomaly, and very high Al_2O_3 (21 wt. %), further suggesting the sample contains a cumulate plagioclase component.

4.2.6 Sm and Nd Isotopes

Initial $^{143}Nd/^{144}Nd$, and εNd(t) values for the Wathaman Batholith have been calculated using an age of ca. 1855 Ma, and present day CHUR values of $^{143}Nd/^{144}Nd = 0.512638$, and $^{147}Sm/^{144}Nd = 0.1967$. All Sm and Nd isotopic measurements obtained from the Wathaman Batholith are listed in Table 4.4. Errors on calculated εNd values are generally not larger than ±0.5, the respective 2 sigma errors are reported in Table 4.4. εNd(t) versus silica, $(La/Sm)_N$ and $(La/Yb)_N$ are illustrated in Figure 4.13. Including samples collected from all series, the Wathaman Batholith has a range in εNd(t) values between +0.2 and -6.9 (Table 4.4). No relationship is apparent between εNd(t) and silica (Figure 4.13a), or any degree of REE fractionation (Figs. 4.13b, c).

Two granodiorites (69-72 wt. % SiO_2) from the SCZ-MS have some of the highest εNd(t) values in the batholith of +0.2 and -0.4. The granodiorites were collected from a granodiorite-monzogranite lense, located along the southern margin of the batholith. Seven samples from the SCZ-KMGS, ranging in composition from quartz diorite through monzogranite, have εNd(t) values between -2.3 and -5.4. Five samples have a very restricted range between -2.3 and -3.0, over the entire range of rock types, and silica contents between 53 and 72 wt. %. The two samples with the lower εNd(t) values of -5.1 and -5.4 are both granodiorites that are petrologically and otherwise geochemically indistinguishable from others of the series. The SCZ-KMGS samples were collected from the southern, northern and central portions of this zone and over a > 600 Km^2 area.

Eight samples from the NEZ-KMMS, ranging in composition from diorite to monzogranite have εNd(t) values between -1.4 to -6.9. Excluding a syn-plutonic diorite dyke (εNd(t) = -1.4), five of the seven samples with > 60 wt. % SiO_2 ranged between -1.6 to -3.5. Although somewhat wider, this range is similar to, and encompasses the -2.3 to -3.0 range exhibited by the majority of the SCZ KMS samples. Two monzogranite samples have significantly lower εNd(t) values of -6.3 and -6.9. These later 2 samples are otherwise indistinguishable petrologically and geochemically from other monzogranites in the series. The NEZ-KMMS samples were collected throughout the entire NEZ.

Three samples from the NEZ-MS, including a monzodiorite and two quartz monzodiorites, have εNd(t) values of -0.3, -2.7 and -4.0. These values are within the range exhibited by other granitoid series. These samples were all collected from the larger northeast-trending monzodiorite-quartz monzodiorite body located in the NEZ. The sample with the lowest εNd(t) value of -4.0, is a "primitive" monzodiorite with a silica content of 51 wt. %.

Throughout the ~ 3000 km^2 area occupied by the Wathaman Batholith on Reindeer Lake, it

is apparent that εNd values are not associated with specific rock types or silica contents. Somewhat more surprisingly, there are not marked differences between the SCZ and NEZ; whereas, in previous chapters and sections major differences in modal and chemical composition have been documented.

4.3 GEOCHEMISTRY OF THE LA RONGE DOMAIN PLUTONS

4.3.1 Introduction

Field mapping and classification of the major plutons of the LRD has revealed two compositionally distinctive groups of plutons: a more mafic group dominantly comprised of hbl-bio-bearing quartz dioritic and tonalitic plutons; and a more felsic group of bio±hbl-bearing tonalitic and granodioritic plutons. The QAP mesonorms of these two groups indicate that the samples from the more mafic group are almost exclusively tonalitic, and the more felsic group mainly granodioritic (see Figure 3.6). To simplify the nomenclature, in the following discussion, the two groups will be simply be referred to as tonalitic (Bulter and Milton Island Plutons, Cowie Bay Pluton) and granodioritic (McMillan Lake Pluton, Jack Pine Bay Pluton, Foliated Diorite-Granodiorite Pluton), respectively. Compositional overlap occurs between the series, reflecting that there is a range of differentiation in each.

4.3.2 Major Elements

Representative whole rock major, trace and REE analyses of selected samples from the major plutons of the LRD are listed in Table 4.5. Major element (Harker) variation diagrams for the plutons of the LRD are given in Figure 4.14 and 4.15. Comparison data for the Wathaman Batholith is given as fields that encompass the majority of the data. The LRD plutons span a wide compositional range with silica contents from 51 to 71 wt. % SiO_2. The data from the LRD plutons often do not define the linear to curvilinear trends observed in the Wathaman Batholith.

TiO_2, Fe_2O_3 and, to some extent, P_2O_5 show smooth linear decreases in concentration with increasing SiO_2 and overlap well with the Wathaman data. CaO and MgO in the LRD plutons decrease with increasing silica, but many of the data points lie outside the Wathaman comparison field. Considerable scatter, and non-overlap with the Wathaman data is observed for Al_2O_3, Na_2O and K_2O. The more mafic tonalitic plutons seem to have distinctively lower K_2O and Al_2O_3, and higher CaO and MgO than the majority of similarly fractionated granitoids of the Wathaman Batholith (Figure 4.12 and 4.15). The more felsic granodioritic plutons overlap with the Wathaman Batholith granitoids on all major element versus SiO_2 plots, but exhibit significant differences, especially in Al_2O_3, and Na_2O contents, higher and lower respectively (Figure 4.12 and 4.15).

The LRD plutons are all sub-alkaline and calc-alkaline based on the classification scheme of Irvine and Baragar (1971) (Figure 4.16a and b). They are calc-alkalic (~ 58 wt. %) according to the alkali-lime index of Peacock (1931). They have a similar range of total alkalies ($Na_2O + K_2O$) to the SCZ series of the Wathaman Batholith, all below 8 wt. %. On a plot of K_2O versus SiO_2 the plutons are mainly calc-alkaline, but a significant portion also fall in the high-K calc-alkaline series (Figure 4.17a). On the A/NK versus A/CNK plot (Maniar and Piccoli, 1989) the LRD plutons are dominantly metaluminous, and extend to only weakly peraluminous compositions (Figure 4.17b). The tonalitic plutons are distinct from the more granodioritic plutons in that they are strictly metaluminous (Figure 4.17b), and define a calc-alkaline magma series (Figure 4.17a).

4.3.3 Trace Elements

Selected trace element versus SiO_2 (Harker variation) diagrams for the LRD plutons are plotted with comparison fields for the Wathaman Batholith in Figure 4.18 and 4.19. Trace elements contents of the LRD plutons are highly variable. Compared to similarly fractionated

quartz diorites and quartz monzodiorites of the SCZ-KMS, the more mafic tonalitic plutons have similar Ni, Cr, Y, Th and Sr, generally lower Nb, and distinctly lower Zr, Rb, Ba and Pb contents (Figure 4.18 and 4.19). However, the small quartz dioritic and tonalitic pods and dykes within the SCZ of the batholith do have some similarities with the LRD tonalitic plutons. The more felsic granodioritic plutons have similar trace element contents to similarly fractionated granodiorites of the Wathaman Batholith (Figure 4.18 and 4.19). Only one sample, however, contains the very high Ba typical of the K-feldspar megacrystic granodiorites of the batholith.

4.3.4 Rare Earth Elements (REE)

REE data for LRD samples have been normalized to primitive mantle values from Sun and McDonough (1989) and are plotted in Figure 4.20. The more mafic tonalites having silica contents between 58 and 61 wt. %, from the Butler Island, Milton Island, and Cowie Bay plutons, along with a field for similarly fractionated quartz diorites and quartz monzodiorites from the SCZ-KMGS are plotted in Figure 4.20a. The REE patterns of the three LRD plutons are virtually indistinguishable, and characterized by moderately fractionated REE [$(La/Yb)_N$ = 11-14], and small negative, to no Eu-anomalies (Eu/Eu* = 0.8-1.0). Compared to similarly fractionated rocks of the Wathaman Batholith, the LRD rocks have similar MREE and HREE contents and patterns. However, the Wathaman Batholith samples do contain noticeably higher LREE contents [$(Ce)_N$ = 39-43], and a greater degree of LREE fractionation [$(La/Sm)_N$ = 3-4] compared to the tonalites and granodiorite of the LRD [$(Ce)_N$ = 29-31; $(La/Sm)_N$ ~ 2].

The more felsic granodiorites having silica contents between 62-68 wt. % from the foliated diorite-granodiorite, Jack Pine Bay, and McMillian Lake plutons, along with a field for similarly fractionated granodiorites from the SCZ-KMGS are plotted in Figure 4.20B. The REE abundances of the tonalites and granodiorites are highly variable [$(Ce)_N$ = 21-81; $(Yb)_N$ = 1-3], but

characterized by highly fractionated REE [$(La/Yb)_N$ = 24-52], and both small negative, and positive Eu-anomalies (Eu/Eu* = 0.8-1.1). With the exception of the very low REE contents of the most felsic McMillian Lake tonalite (98-D093), the REE patterns, and abundances of the LRD granodiorites are broadly similar, and overlap with a field for similarly fractionated granodiorites of the SCZ-KMGS. The more felsic granodiorites of the LRD also have much steeper (LREE enriched) REE patterns than the more mafic tonalites (Figure 4.20a).

4.3.5 Extended Element Diagrams

Extended element diagrams, including selected REE, LFSE (Rb, Ba, K and Sr), and HFSE (Th, Nb, Zr, P, Ti and Y) for selected LRD plutons are plotted in Figure 4.21. Elements are normalized to primitive mantle values obtained from Sun and McDonough (1989), and fields for similarly fractionated granitoids from the SCZ-KMGS are provided.

Extended element patterns for the more mafic tonalite group are plotted in Figure 4.21a. They have moderate positive Ba anomalies; weakly positive to no Th anomalies; strong positive to no Sr anomalies; and strongly negative Nb, P, and Ti anomalies. Compared to the field for similarly fractionated SCZ quartz diorites and quartz monzodiorites, the LRD tonalites contain distinctly lower Rb, Ba, K, Sr, Th, Nb, Zr, P and LREE. The extended element patterns are similar from P to Lu.

Extended element patterns for the more felsic granodiorite group are plotted in Figure 4.2b. They have: strong positive Ba anomalies; weak to moderate positive Th anomalies; variable Sr anomalies; and strongly negative Nb, P and Ti anomalies. Compared to similarly fractionated SCZ-KMGS granodiorites of the Wathaman Batholith, the LRD granodiorites, with one exception, contain lower Ba contents and slightly lower K.

4.3.6 Sm and Nd Isotopes

Sm and Nd isotopic measurements obtained from LRD pluton samples are listed in Table 4.6. Initial $^{143}Nd/^{144}Nd$ and εNd(t) values for the plutons have been calculated using an age of ca. 1858 Ma, the age of the Butler Island pluton (Corrigan et al., 1998b). Present day CHUR values of $^{143}Nd/^{144}Nd = 0.512638$, and $^{147}Sm/^{144}Nd = 0.1967$ were used in the calculations. Errors on the calculated εNd values are generally not larger than ±0.5, and 2 sigma errors on the measured isotopic ratios are listed (Table 4.6). Sample 97-A001 was analysed at the Geological Survey of Canada, and 2 sigma errors on the measured isotopic ratios are not available for that sample, however errors of $< \pm 0.5$ epsilon units are reported from the GSC radiogenic isotope laboratory (Theriault and Ermanovics, 1997). Also included at the bottom of Table 4.6 are two samples where $^{143}Nd/^{144}Nd$ was measured by TIMS, but the isotope dilution fractions (Sm-Nd) failed during measurement on the mass spectrometer. For these samples the Sm and Nd concentrations obtained from the ICP-MS have been used to calculate the $^{147}Sm/^{144}Nd$. This Sm-Nd ratio is not as precise as values produced by isotope dilution, but good agreement between the ICP-MS and isotope dilution procedure was found in other samples.

Of the samples collected from five plutons within the LRD, and analysed using standard isotope dilution procedures, εNd(t) values range between +4.8 to -0.4. These results are higher than those found in the majority of samples from the Wathaman Batholith. As was found in the Wathaman Batholith, εNd(t) values do not correlate with rock type, silica content or degree of REE fractionation.

The highest εNd(t) value of +4.8 was from a hbl-bio-bearing tonalite of the Butler Island pluton, and is by far the most juvenile value obtained in this study. This Nd isotopic composition is close to estimates of the contemporaneous depleted mantle value of +5 (DePaolo, 1991; Chauvel et al., 1986), and some volcanic rocks of the LRD (εNd(1858) = +4.4 and +4.8 - Thom et al.,

1990). Another fairly juvenile εNd(t) value of +1.6 was obtained from a bio±hbl-bearing tonalite of the McMillian Lake Pluton. The remaining εNd(t) values are more tightly constrained between +0.2 and -0.4, including samples from the Cowie Bay, Milton Island, and Jack Pine Bay plutons. εNd(t) values of the samples calculated using the ICP-MS data were +0.8 and -0.6, from a mafic granodioritic phase associated with the McMillian Lake Pluton, and a granodiorite from the foliated diorite-granodiorite pluton, respectively. These results indicate that εNd(t) values are not related to the type of pluton, or how "primitive" its geochemical signature may be. These data suggest a relatively homogeneous and widespread source region having a Nd isotopic composition close to CHUR, with lesser amounts of more juvenile material isotopically equivalent to the depleted mantle. The two granodiorites of the SCZ-MS, collected at the margin of the Wathaman Batholith have εNd(t) values of +0.2 and -0.4, suggesting that they have tapped a similar source region to that appropriate for the majority of the LRD plutons.

4.4 CHAPTER SUMMARY

Geochemical data obtained from granitoid rocks in the Reindeer Lake support the existence of three distinctive magmatic zones as well as distinctive magma series within each. Table 4.7 summarizes some of the more relevant geochemical parameters that characterize or serve to identify the various granitoid series including: rock type, range in silica content, alkalinity, A/CNK ratio, K_2O-series, $(La/Yb)_N$, εNd(t), and Sr and Ba contents.

Between the LRD and the NEZ of the Wathaman batholith (south-north), the most conspicuous difference, the overall increase in alkalinity in both mafic and felsic compositions is mainly due to increasing K_2O. The batholith also contains generally higher Rb, Sr, Ba and Zr, and distinctly lower $\varepsilon Nd_{(T)}$ values (excluding the SCZ-MS) compared to the satellite intrusions within the LRD. Common to all granitoids are characteristic enrichments in Rb, Ba, K_2O, Sr, ±Th and

LREE and low Nb, P, Ti, Y and HREE compared to primitive mantle compositions. Elevated LFSE to HFSE ratios are considered the geochemical signature of subduction (Saunders et al., 1991).

Within the Wathaman Batholith, despite the great diversity in rocks types and wide range in major/trace element compositions, absolutely no correlation between Nd isotopic composition and any geochemical parameters has been recognized. The entire batholith is, however, characterized by high Sr, Ba and K_2O and uniformly low εNd(t) values. The low εNd values, coupled with elevated Sr, Ba and K2O in some of the most mafic compositions (monzodiorites/quartz diorites), are highly unusual. Table 4.8 displays the average monzodiorite and quartz diorite from the Wathaman Batholith as well as similarly fractionated Phanerozoic andesites from the Central Volcanic Zone (CVZ) of the Andes (Ewart, 1982; Davidson et al., 1990) and Archean high-Mg monzodiorites ("sanukitoids") of the southwestern Superior Province (Stern et al., 1989). Compared to the average andesite from the CVZ, equivalently fractionated monzodiorites and quartz diorites of the batholith contain significantly higher Sr, Ba, LREE, LREE/HREE and lower Rb/Sr (Table 4.8). However, Davidson et al. (1990) have documented andesites with remarkably similar chemical compositions to monzodiorites and quartz diorites, notably elevated Sr, Ba, LREE/HREE and low Rb/Sr (Table 4.8). These characteristics are interpreted to be due to crustal contamination of mantle-derived magmas. Alternatively, Archean LILE-enriched monzodiorites and trachyandesites known as sanukitoids also possess high Sr, Ba, LREE, LREE/HREE and low Rb/Sr. Sanukitoids are interpreted as melts of metasomatized mantle peridotite and crustal contamination is insignificant, within mafic end-members (Stern et al., 1989).

Determining if the "enriched" character of mafic magmas from the Wathaman Batholith

are due to contamination by continental crust or are a feature of the mantle source is evaluated within the next chapter. Also evaluated are the processes responsible for differentiation of the various series, especially the SCZ-KMGS containing the widest and most continuous compositional range amenable to testing.

Table 4.1 Representative major, trace and REE analyses for granitoids of the Southern-Central Zone of the Wathaman Batholith.

Zone	Southern-Central Zone (SCZ)							
Series	K-feldspar megacrystic granodiorite series						Monzogranite series	
Sample No.	99-T062a	98-J176	98-D313	98-T223	98-D349	99-T157	98-D286	98-D301
Rock Type	QD	QD	QMd	Gdr	Gdr	Mgn	Gdr	Mgn
SiO_2	53.08	56.44	61.15	64.29	68.41	71.66	68.83	71.65
TiO_2	0.85	0.80	0.64	0.46	0.35	0.37	0.28	0.26
Al_2O_3	16.91	18.40	16.78	15.98	15.30	13.64	15.74	14.42
FeO	5.40	3.74	3.34	2.44	1.60	1.44	1.14	1.05
Fe_2O_3	2.94	2.39	2.36	1.76	1.26	1.14	0.86	0.78
MnO	0.14	0.07	0.09	0.05	0.04	0.04	0.03	0.02
MgO	5.03	3.73	2.59	1.50	0.90	0.68	0.74	0.60
CaO	7.22	5.53	4.72	3.17	2.19	1.69	2.30	2.00
Na_2O	3.56	4.53	4.50	3.55	3.79	3.31	4.28	3.45
K_2O	1.91	2.12	2.76	3.74	4.02	4.39	3.15	3.67
P_2O_5	0.40	0.34	0.30	0.21	0.15	0.11	0.10	0.09
Total	97.62	98.26	99.41	97.46	98.23	98.60	97.62	98.16
Sc	21	16	17	dl	dl	dl	dl	dl
V	145	95	87	54	32	dl	23	16
Cr	147	161	56	20	23	2	16	dl
Ni	64	36	dl	dl	dl	dl	dl	dl
Cu	71	25	4	9	21	dl	dl	dl
Zn	51	49	42	18	8	4	9	dl
Ga	23	25	20	16	17	15	18	16
Rb	51	66	59	58	57	75	61	55
Sr	942	1084	794	819	803	262	818	495
Ba	1088	1230	1528	2790	2018	1084	1769	1417
Pb	10	11	12	12	16	13	18	14
Ce	187	84	60	102	dl	117	dl	dl
Y	20.70	12.46	19.62	7.37	7.59	8.15	3.46	2.51
Zr	136	282	150	171	149	164	117	88
Nb	12.5	10.9	9.9	4.7	6.2	6.4	4.7	3.3
Th	9.00	4.56	2.49	2.27	1.33	8.05	3.36	0.85
La	81.62	34.46	35.85	42.41	20.43	61.42	22.00	12.31
Ce	164.08	69.34	75.98	73.11	43.67	112.19	41.14	21.85
Pr	19.09	8.06	9.63	7.70	5.71	11.63	4.43	2.44
Nd	70.45	30.96	40.16	27.06	22.95	38.53	14.99	9.26
Sm	10.42	5.18	7.78	4.02	4.01	5.20	2.15	1.57
Eu	2.51	1.32	1.65	1.23	1.18	1.09	0.67	0.87
Gd	8.14	3.77	5.90	2.67	2.62	3.13	1.30	1.08
Tb	0.93	0.47	0.75	0.31	0.30	0.35	0.15	0.12
Dy	5.00	2.47	4.11	1.54	1.55	1.82	0.71	0.57
Ho	0.96	0.47	0.78	0.29	0.28	0.34	0.13	0.10
Er	2.78	1.29	2.07	0.73	0.73	0.93	0.34	0.27
Tm	0.37	0.19	0.28	0.10	0.10	0.11	0.05	0.04
Yb	2.33	1.20	1.76	0.62	0.68	0.65	0.29	0.21
Lu	0.32	0.19	0.25	0.10	0.10	0.10	0.05	0.04

FeO/Fe_2O_3 calculated using the method of LeMaitre (1976), dl=detection limit. Y, Th and REE determined by ICP-MS, major and other trace elements determined by XRF.

Table 4.2 Representative major, trace and REE analyses for granitoids of the Northeast Zone of the Watharnan Batholith.

Zone	Northeast-Zone (NEZ)							
Series	K-feldspar megacrystic monzogranite series							
Sample No.	99-D096	99-T144a	99-D191	99-T139a	99-T141	99-D255	99-D099	99-T139b
Rock Type	D	D	QMd	Gdr	Gdr	Mgn	Mgn	Mgn
SiO_2	51.07	51.23	61.29	65.10	65.13	66.81	69.65	70.65
TiO_2	0.84	0.81	0.59	0.43	0.48	0.43	0.34	0.20
Al_2O_3	17.73	16.80	17.60	15.86	15.85	15.41	14.67	14.83
FeO	5.85	5.83	2.62	1.72	2.08	1.64	1.50	0.82
Fe_2O_3	3.03	3.16	2.07	1.36	1.60	1.35	1.30	0.76
MnO	0.16	0.19	0.08	0.06	0.09	0.05	0.04	0.02
MgO	6.57	6.76	1.74	1.11	1.55	0.85	0.59	0.29
CaO	8.57	7.90	3.65	2.44	3.04	2.19	1.57	1.17
Na_2O	3.56	3.79	4.19	4.15	3.67	3.85	3.18	3.03
K_2O	1.59	1.75	4.10	3.88	4.09	4.44	5.44	6.12
P_2O_5	0.14	0.27	0.26	0.15	0.21	0.19	0.11	0.04
Total	99.22	98.63	98.43	96.41	97.99	97.48	98.58	98.19
Sc	20	27	dl	dl	dl	dl	dl	dl
V	158	152	54	34	50	dl	29	18
Cr	165	247	22	10	23	7	2	dl
Ni	66	85	dl	dl	dl	dl	dl	dl
Cu	60	49	23	dl	11	12	dl	7
Zn	58	65	31	18	43	12	6	dl
Ga	26	22	22	21	23	18	16	15
Rb	47	46	117	125	130	113	126	146
Sr	988	721	741	511	602	1090	261	505
Ba	399	488	2124	1416	1743	2573	1545	2361
Pb	8	9	24	25	36	18	22	40
Ce	142	85	158	163	85	219	188	118
Y	*40	29.09	16.64	25.84	16.91	15.1	12.56	*12
Zr	57	141	266	214	231	203	269	287
Nb	26.1	20.6	17.9	23	17.5	15.6	11.4	15.2
Th	*dl	0.80	13.31	18.38	10.54	12.49	14.54	*22
La		33.22	63.67	61.97	37.62	95.82	81.77	
Ce		94.77	123.57	135.79	80.68	182.16	144.38	
Pr		13.52	13.26	16.20	9.59	19.87	14.33	
Nd		55.92	45.67	58.97	34.91	68.71	46.47	
Sm		10.49	7.17	9.46	5.79	9.63	5.67	
Eu		2.18	1.45	1.43	1.21	1.96	1.13	
Gd		7.49	4.43	6.37	3.87	5.24	3.47	
Tb		0.98	0.57	0.85	0.53	0.60	0.43	
Dy		5.58	3.19	4.80	3.05	3.04	2.37	
Ho		1.09	0.61	0.98	0.61	0.56	0.50	
Er		3.41	1.92	2.95	1.96	1.69	1.50	
Tm		0.47	0.27	0.39	0.28	0.23	0.20	
Yb		3.07	1.79	2.35	1.90	1.47	1.26	
Lu		0.46	0.29	0.31	0.32	0.22	0.19	

FeO/Fe_2O_3 calculated using the method of LeMaitre (1976), dl=detection limit. Th, Y and REE determined by ICP-MS (unless indicated *determined by XRF), major and other trace elements determined by XRF.

Table 4.3 Representative major, trace and REE analyses for the Northeast Zone Monzonitic series.

Zone	Northeast Zone (NEZ)							
Series	Monzonitic series							
Sample No.	99-T077b	99-T191	99-T153a	99-D103	98-T311	99-T077a	99-T188a	99-J061
Rock Type	Md	Md	Mz	Mz	QMd	QMd	QMd	QMd
SiO_2	51.21	53.51	49.21	52.82	55.24	56.95	58.78	59.42
TiO_2	0.94	1.11	1.01	0.76	0.47	0.68	0.81	0.69
Al_2O_3	17.12	16.46	16.10	16.22	20.84	18.50	17.74	18.42
FeO	6.46	5.49	7.84	6.24	3.40	3.27	3.35	2.41
Fe_2O_3	3.30	3.17	4.61	4.16	2.41	2.39	2.60	1.93
MnO	0.14	0.11	0.30	0.26	0.14	0.09	0.09	0.06
MgO	5.33	4.51	4.24	3.06	1.62	2.27	2.24	1.66
CaO	8.26	6.94	7.67	6.83	6.21	4.90	4.33	4.06
Na_2O	3.47	3.80	3.26	3.54	4.20	4.44	4.03	4.17
K_2O	1.59	2.12	3.09	3.69	3.45	3.37	4.23	4.30
P_2O_5	0.35	0.55	0.71	0.56	0.33	0.29	0.29	0.23
Total	98.37	97.96	98.22	98.28	98.54	97.46	98.8	97.67
Sc	23	21	20	11	7	dl	dl	13
V	190	155	202	174	61	83	88	62
Cr	99	113	10	20	dl	32	32	24
Ni	53	41	dl	dl	dl	dl	dl	dl
Cu	52	33	64	59	48	35	40	25
Zn	57	56	94	79	50	34	36	17
Ga	22	22	21	20	19	21	22	21
Rb	40	75	109	114	88	56	95	91
Sr	1036	1057	1075	923	1692	1014	828	920
Ba	1473	1264	1390	1042	2352	2919	2767	2860
Pb	10	18	11	19	10	16	18	16
Ce	53	186	138	133	55	106	124	75
Y	16.2	37.72	*27	26	12.28	14.76	*15	*10
Zr	78	146	17	51	dl	277	330	328
Nb	9	24.5	12.9	11.9	7.2	9.7	14.5	12
Th	1.64	7.1	*5	7	4.62	1.5	*4	*dl
La	36.47	83.66		60.82	32.85	52.40		
Ce	77.57	180.60		129.63	63.83	100.08		
Pr	9.62	22.16		15.64	7.52	11.67		
Nd	38.13	83.06		61.42	29.71	44.50		
Sm	6.86	13.08		10.81	5.22	6.53		
Eu	1.76	1.99		1.98	2.37	2.08		
Gd	4.85	8.88		8.07	3.74	5.05		
Tb	0.62	1.16		1.02	0.47	0.57		
Dy	3.39	6.67		5.57	2.52	3.03		
Ho	0.66	1.41		1.11	0.47	0.58		
Er	1.96	4.44		3.25	1.25	1.65		
Tm	0.26	0.59		0.42	0.17	0.21		
Yb	1.59	3.58		2.64	1.02	1.29		
Lu	0.24	0.50		0.38	0.15	0.19		

FeO/Fe_2O_3 calculated using the method of LeMaitre (1976), dl=detection limit. Th, Y and REE determined by ICP-MS (unless indicated *determined by XRF), major and other trace elements determined by XRF.

Table 4.4 Sm and Nd isotopic analyses from the Wathaman Batholith.

Sample No.	Rock Type	SiO_2	Sm	Nd	Sm/Nd	$^{143}Nd/^{144}Nd$	2σ	$^{147}Sm/^{144}Nd$	2σ	$^{143}Nd/^{144}Nd(t)$	εNd(t)
Southern-Central Zone (SCZ) - Monzogranite series											
98-D286	Gdr	69	2.16	14.93	0.1447	0.511306	28	0.08924	3	0.510217	-0.4
98-D265	Gdr	71	1.42	10.10	0.1406	0.511312	46	0.08704	10	0.510250	0.2
Southern-Central Zone (SCZ) - K-feldspar megacrystic granodiorite series											
99-T062	QD	53	10.67	70.03	0.1524	0.511234	23	0.09405	3	0.510086	-3.0
98-D313	QMd	61	8.94	44.52	0.2008	0.511633	11	0.12398	3	0.510120	-2.3
98-D292	Gdr	63	8.23	46.60	0.1766	0.511309	24	0.10905	3	0.509978	-5.1
99-T033	Gdr	64	7.19	39.25	0.1832	0.511481	27	0.11311	7	0.510100	-2.7
98-T223	Gdr	64	4.07	28.11	0.1448	0.511189	15	0.08949	8	0.510097	-2.8
98-D349	Gdr	68	4.48	24.13	0.1857	0.511362	23	0.11471	4	0.509962	-5.4
99-T157	Mgn	72	5.40	39.82	0.1356	0.511120	15	0.08376	15	0.510098	-2.7
Northeast Zone (NEZ) - K-feldspar megacrystic monzogranite series											
99-T144b	D	50	7.35	42.30	0.1738	0.511475	97	0.10724	10	0.510166	-1.4
99-D191	QMd	61	7.28	46.08	0.1580	0.511283	30	0.09750	4	0.510093	-2.8
99-T139a	Mgn	65	10.04	55.98	0.1793	0.511471	23	0.11071	4	0.510120	-2.3
99-T171	Mgn	67	8.24	57.26	0.1439	0.511215	25	0.08883	7	0.510131	-2.1
99-D255	Mgn	67	10.34	63.56	0.1627	0.511143	79	0.10048	3	0.509917	-6.3
99-T133	Mgn	69	8.63	56.36	0.1531	0.511308	28	0.09449	26	0.510155	-1.6
99-J029b	Mgn	69	6.53	48.31	0.1352	0.510903	32	0.08347	4	0.509884	-6.9
99-D099	Mgn	70	5.59	45.85	0.1219	0.510979	23	0.07530	7	0.510060	-3.5
Northeast Zone (NEZ) - Monzonitic series											
99-T077b	Md	51	6.83	38.56	0.1771	0.511369	36	0.10930	6	0.510035	-4.0
99-T077a	QMd	57	6.83	46.46	0.1470	0.511328	37	0.09079	2	0.510220	-0.3
99-J061	QMd	59	6.30	40.32	0.1563	0.511275	15	0.09647	5	0.510098	-2.7

Initial Nd isotopic ratios are calculated using and average age for the Wathaman Batholith of 1855 Ma and a present day 143Nd/144Nd of 0.512638 and 147Sm/144Nd of 0.1967 for CHUR.

Table 4.5 Representative major, trace and REE analyses for selected plutons of the La Ronge Domain.

Pluton	*Butler Island*	*Milton Island*	*Cowie Bay*	*Cowie Bay*	*McMillan Lake*	*McMillan Lake*	*Jack Pine Bay*	*Foliated D-Gdr*
Sample No.	97-A001	97-D068	98-T204	98-T199	98-T184	98-D093	98-D129	98-D108b
Rock Type	Tn	Gdr	Tn	Tn	Gdr	Tn	Gdr	Gdr
SiO_2	61.3	61.36	57.53	58.03	62.52	67.61	65.44	64.53
TiO_2	0.63	0.66	0.65	0.62	0.61	0.34	0.46	0.9
Al_2O_3	16.7	15.46	17.69	17.61	15.16	16.25	15.4	16.38
FeO	4.2	4.03	4.24	3.51	3.46	1.57	2.22	2.98
Fe_2O_3	1.5	2.28	2.41	1.96	2.19	1.09	1.53	2.11
MnO	0.08	0.1	0.1	0.07	0.08	0.03	0.06	0.07
MgO	3.44	3.46	3.53	3.84	3.68	1.04	2.12	1.27
CaO	5.87	5.6	6.09	6.36	4.1	3.34	3.29	2.83
Na_2O	4.3	3.32	3.7	3.76	3.24	4.72	3.64	3.98
K_2O	1.19	1.99	1.85	1.63	2.94	1.98	3.12	3.11
P_2O_5	0.26	0.21	0.35	0.33	0.23	0.09	0.19	0.27
Total	100.3	98.9	98.29	97.84	98.39	98.2	97.65	98.67
Sc	14	21	15	14	18	14	10	dl
V	110	127	107	103	94	29	64	42
Cr	410	77	63	101	159	20	70	2
Ni	45	11	22	29	44	dl	9	dl
Cu	33	31	16	8	19	dl	dl	11
Zn	74	30	42	29	35	8	15	45
Ga	20	17	21	19	19	21	19	20
Rb	20	42	63	45	79	38	70	115
Sr	800	593	893	1198	776	1024	761	604
Ba	400	630	972	713	1394	1123	1377	2093
Pb	6	5	10	6	17	5	12	16
Ce	dl	dl	95	dl	114	dl	137	199
Y	*15	15.63	*17	14.81	14.87	5.07	10.06	12.78
Zr	dl	76	124	71	163	104	121	352
Nb	4.1	7.5	9	7.3	8.7	4.9	8.5	16.1
Th	1.4	3.19	*6	2.56	8.32	2.29	7.96	5.39
La	21.00	21.37		24.25	46.47	17.97	39.37	73.11
Ce	51.00	53.25		55.69	92.64	37.28	75.36	143.22
Pr	6.90	7.23		7.52	10.57	4.23	8.45	15.99
Nd	31.00	30.65		32.28	38.72	15.93	30.74	57.67
Sm	5.60	6.26		6.15	6.42	2.69	5.04	8.53
Eu	1.60	1.39		1.53	1.44	0.77	1.20	2.22
Gd	4.30	4.66		4.54	4.42	1.74	3.27	4.94
Tb	0.53	0.59		0.57	0.55	0.21	0.39	0.58
Dy	2.80	3.17		3.04	2.99	1.03	2.04	2.95
Ho	0.50	0.58		0.57	0.57	0.19	0.38	0.51
Er	1.30	1.58		1.53	1.55	0.51	1.00	1.38
Tm	0.18	0.22		0.21	0.22	0.07	0.14	0.17
Yb	1.10	1.39		1.28	1.37	0.44	0.93	1.01
Lu	0.17	0.21		0.19	0.21	0.07	0.14	0.16

FeO/Fe_2O_3 calculated using the method of LeMaitre (1976), dl=detection limit. Th, Y and REE determined by ICP-MS (unless indicated *determined by XRF), major and other trace elements determined by XRF.

Table 4.6 Sm and Nd isotopic analyses for La Ronge Domain plutons.

Sample No.	Pluton	Rock Type	SiO_2	Sm	Nd	Sm/Nd	$^{143}Nd/^{144}Nd$	2σ	$^{147}Sm/^{144}Nd$	2σ	$^{143}Nd/^{144}Nd(t)$	εNd(t)
98-T199	Cowie Bay	Tn	58	6.07	31.56	0.19	0.511666	13	0.11871	13	0.510215	-0.4
*97-A001	Butler Island	Tn	61	5.79	30.53	0.19	0.511877		0.11460		0.510476	4.8
97-D068	Milton Island	Gdr	61	7.04	32.76	0.21	0.511871	24	0.13265	10	0.510249	0.3
98-D129	Jack Pine Bay	Gdr	65	5.07	29.97	0.17	0.511493	17	0.10452	4	0.510215	-0.4
98-D093	McMillian Lake	Tn	68	2.75	15.75	0.17	0.511634	32	0.10790	2	0.510315	1.6
φ98-T184	McMillian Lake	Gdr	63	6.42	38.72	0.17	0.511429	27	0.10022	---	0.510204	-0.6
φ98-D108b	fol. Dio-Gdr	Gdr	65	8.53	57.67	0.15	0.511368	28	0.08943	---	0.510275	0.8

Initial Nd isotopic ratios are calculated using an age of 1858 Ma, the age of the Butler Island Pluton (Corrigan et al., 1998b) and a present day 143Nd/144Nd of 0.512638 and 147Sm/144Nd of 0.1967 for CHUR. *97A-001 was analysed at the GSC in Ottawa (Corrigan et al., unpub. rept.). φ Sm and Nd from ICP-MS, 147Sm/144Nd calculated using the Sm and Nd concentrations and the atomic weight and isotopic abundances of Sm and Nd. The measured 143Nd/144Nd is from the isotope dilution procedure.

Table 4.7 Summary of relevant geochemical parameters that identify the magmatic zones and granitoid series in the Reindeer Lake area.

	La Ronge	Wathaman SCZ		Wathaman NEZ	
		KMGS	MS	KMMS	MS
Rock Type	QD-Tn-Gdr	QD-QMd-Gdr-Mgn	Gdr-Mgn	(D) ; QMd-Gdr-Mgn	Md-Mz-QMd
SiO_2	51-71	53-72	69-75	(49-53) ; 61-74	49-59
Alkalinity	Sub-alk	Sub-alk	Sub-alk	Sub-alk	Alk
A/CNK	0.7-1.1	0.8-1.05	1.1-1.1	(0.6-0.8) ; 1.0-1.1	0.7-1.0
K-series	calc-alkaline ; high-K	high-K	high-K	(high-K) ; shoshonitic	high-K; shoshonitic
Rb	15-115	38-83	55-77	(22-47) ; 93-149	40-121
Sr	259-1198	262-1364	366-818	(719-1029) ; 135-1090	828-1350
Ba	400-2093	1083-3388	1417-2768	(399-1273) ; 412-2613	1042-2919
$(La/Yb)_N$	11-52	15-67	41-54	(8-13) ; 14-47	17-29
$\varepsilon Nd(t)$	+4.8 to -0.4	-2.3 to -5.4	0.2 to -0.4	(-1.4) ; -1.6 to -6.9	-0.3 to -4.0

Table 4.8 Geochemical comparison between NEZ monzodiorites and SCZ quartz diorites of the Wathaman Batholith and andesites from the CVZ of the Andes, and Archean Sanukitoids from the southwest Superior Province.

Reference	Wathaman Batholith		Ewart (1982)	Davidson et al. (1990)	Stern et al. (1989)
Rock Type	NEZ Monzodiorite	SCZ Quartz Diorite	Andean Avg. Baslatic Andesite	Andean CVZ Andesites 52-58 wt %	Avg. Sanukitoid
No.	(n=2)	(n=2)		(n=10)	(n=11)
SiO_2	52.36	54.76	53.90	55.31	56.07
Fe_2O_3	9.21	7.24	8.52	7.99	7.08
MgO	4.92	4.38	5.35	4.24	6.85
Na_2O	3.64	4.05	3.67	3.90	4.04
K_2O	1.86	2.02	1.62	2.33	2.23
Cr	106	154	202	78	352
Ni	47	50	68	58	154
Rb	58	59	45	51	60
Sr	1046	1013	644	1091	1229
Ba	1368	1159	676	1192	1214
Ce	129.09	116.73	51.30	96.47	97
Yb	2.58	1.76	2.32	1.22	1.6
$(Ce/Yb)_N$	14	18	6	22	17
Mg #	0.49	0.52	0.53	0.49	0.63
Rb/Sr	0.055	0.058	0.070	0.046	0.049

Mg # = cation mole fraction $Mg^{2+}/(Mg^{2+} + Fe_T)$

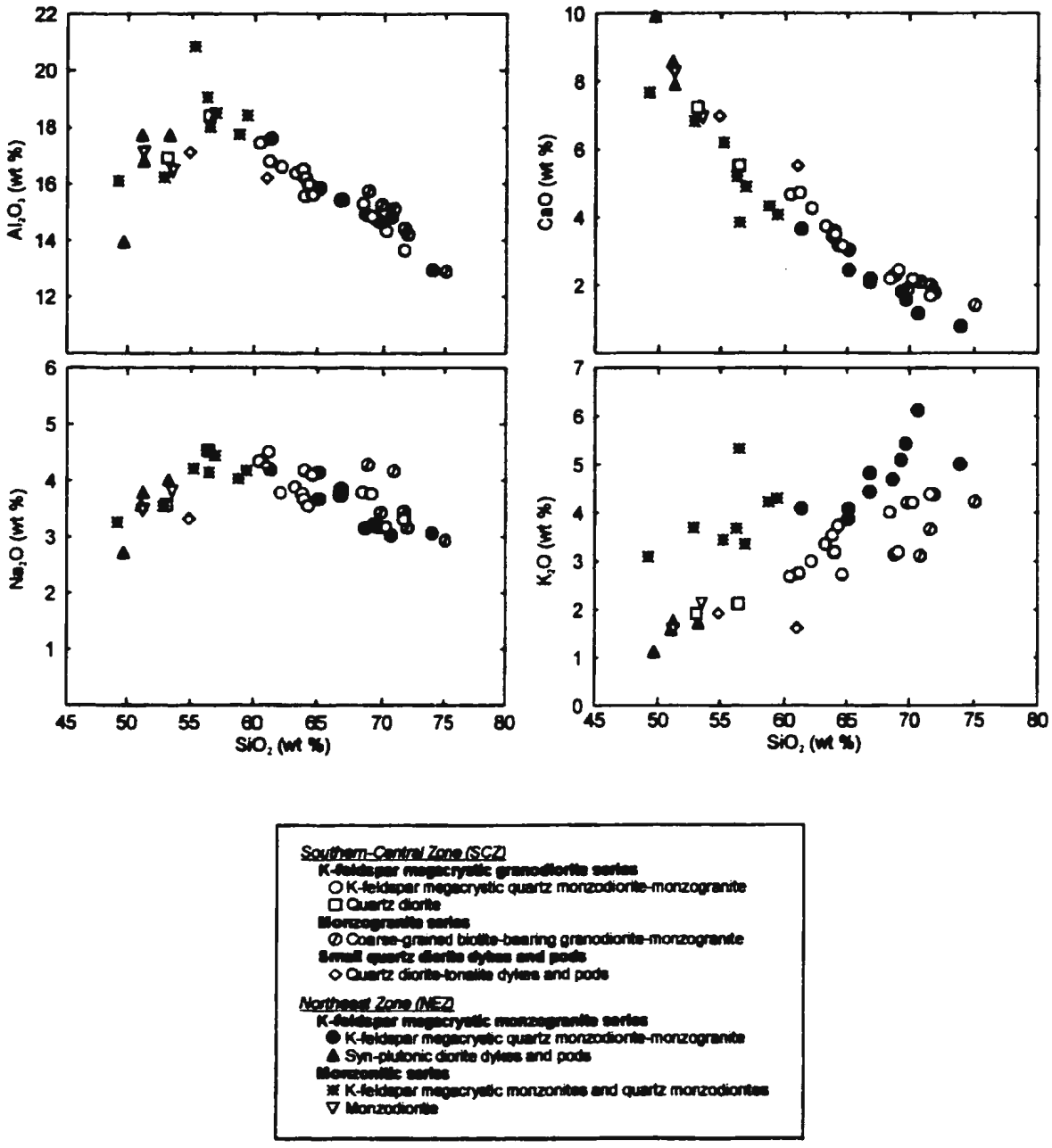

Figure 4.1 Major element Harker variation diagrams for granitoids of the Wathaman Batholith.

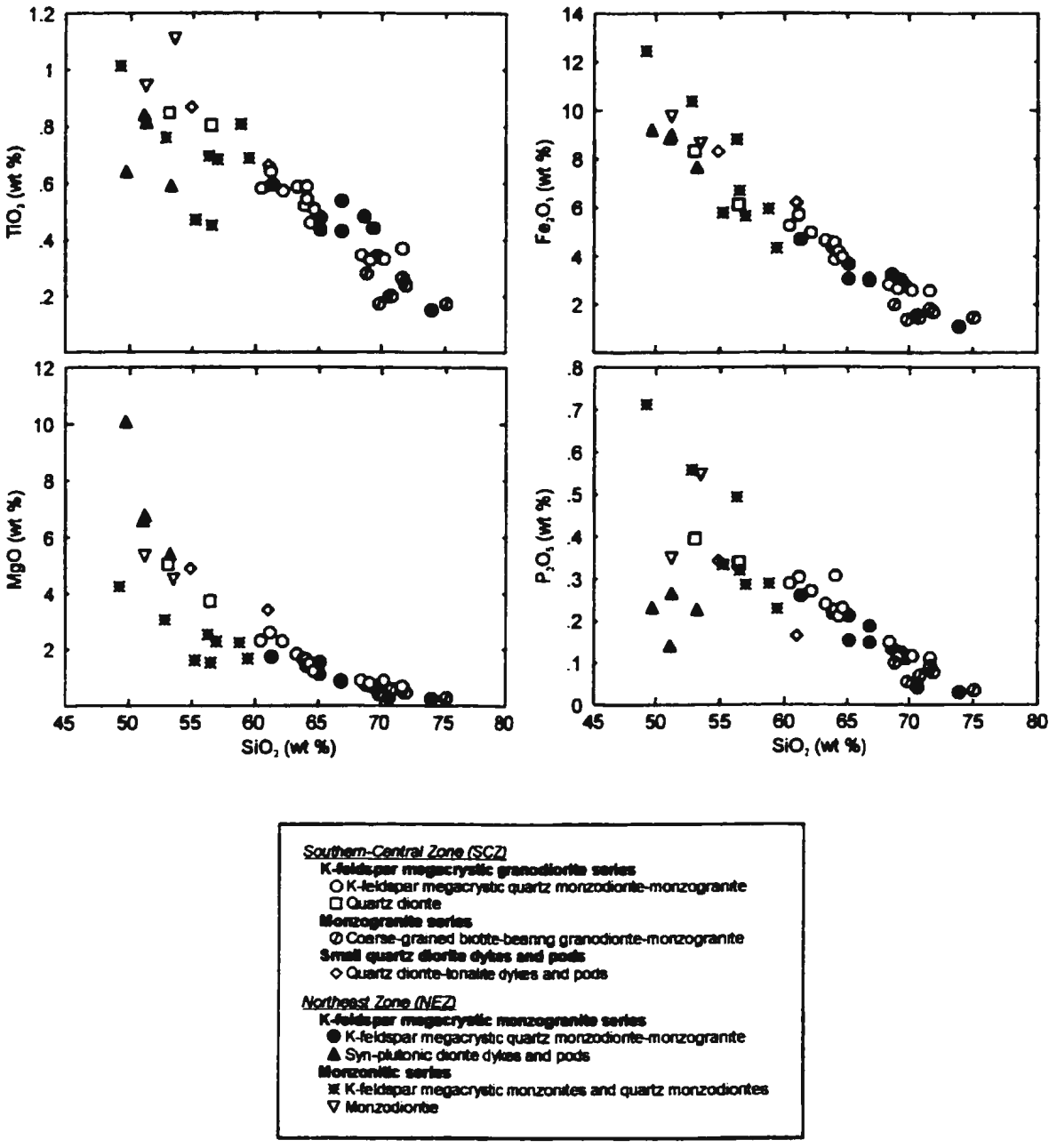

Figure 4.2 Major element Harker variation diagrams for granitoids of the Wathaman Batholith.

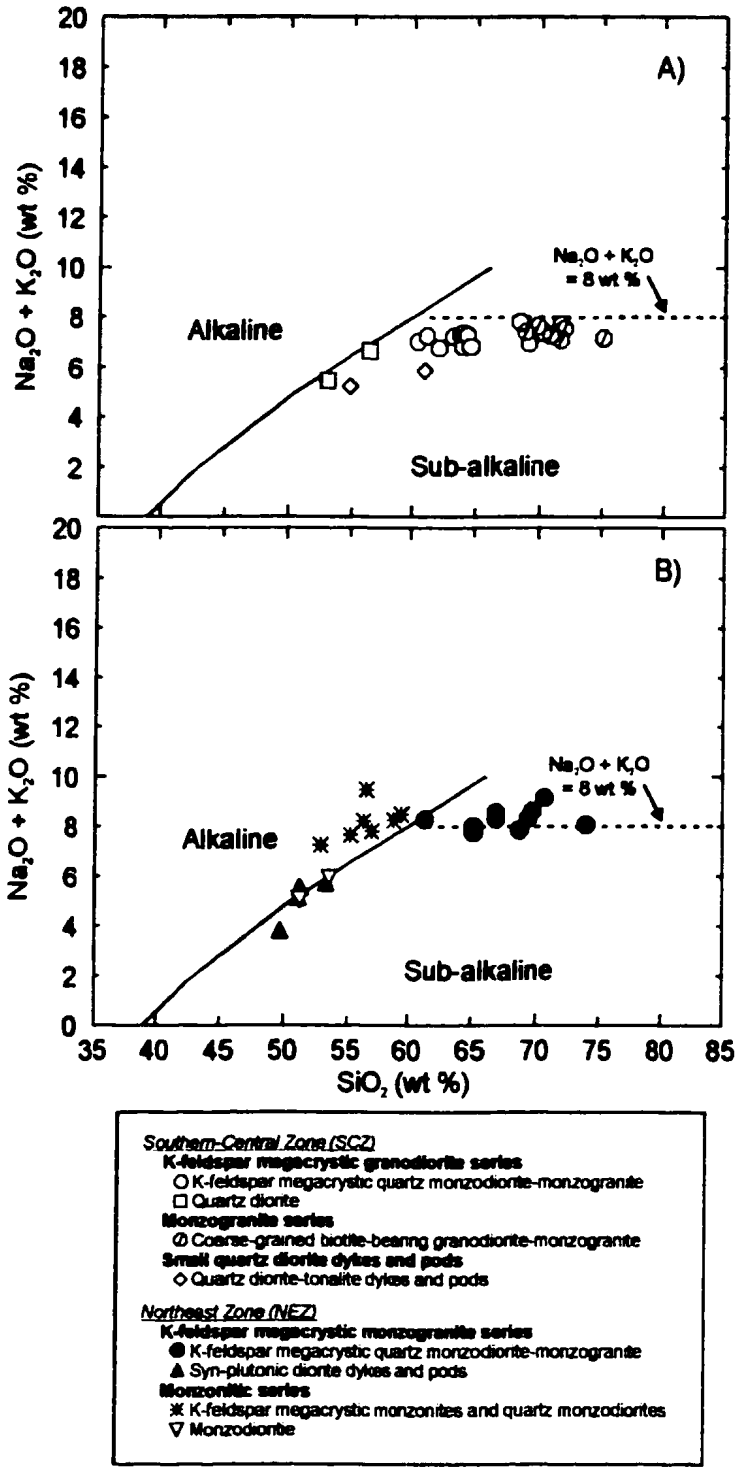

Figure 4.3 Total alkalis versus silica diagram for granitoids of the Wathaman Batholith. A) granitoids of the SCZ. B) granitoids of the NEZ. Alkaline versus sub-alkaline field boundary is from Irvine and Baragar (1971).

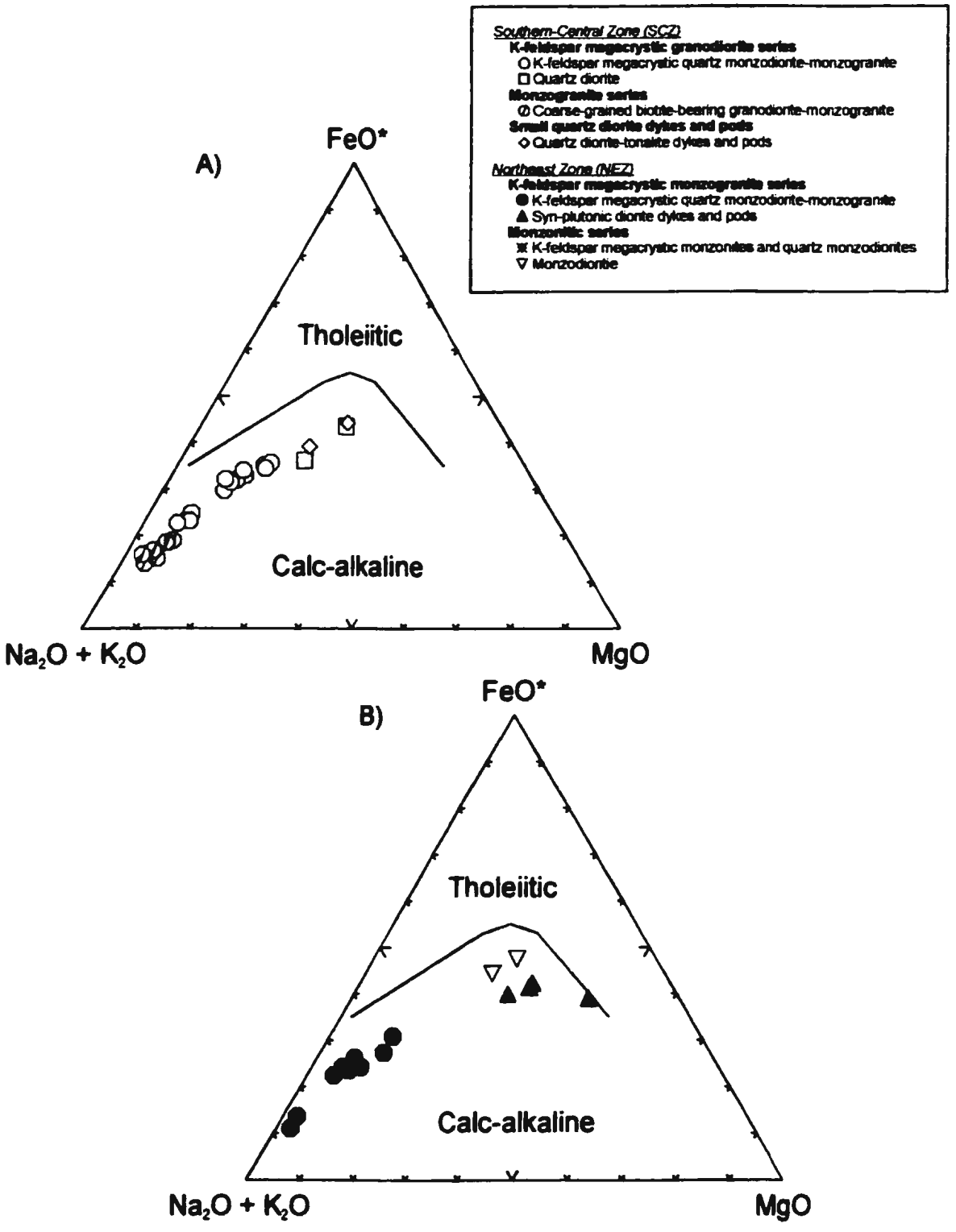

Figure 4.4 Ternary AFM diagram for granitoids of the Wathaman Batholith. A) granitoids of the SCZ. B) granitoids of the NEZ. Field boundary after Irvine and Baragar (1971).

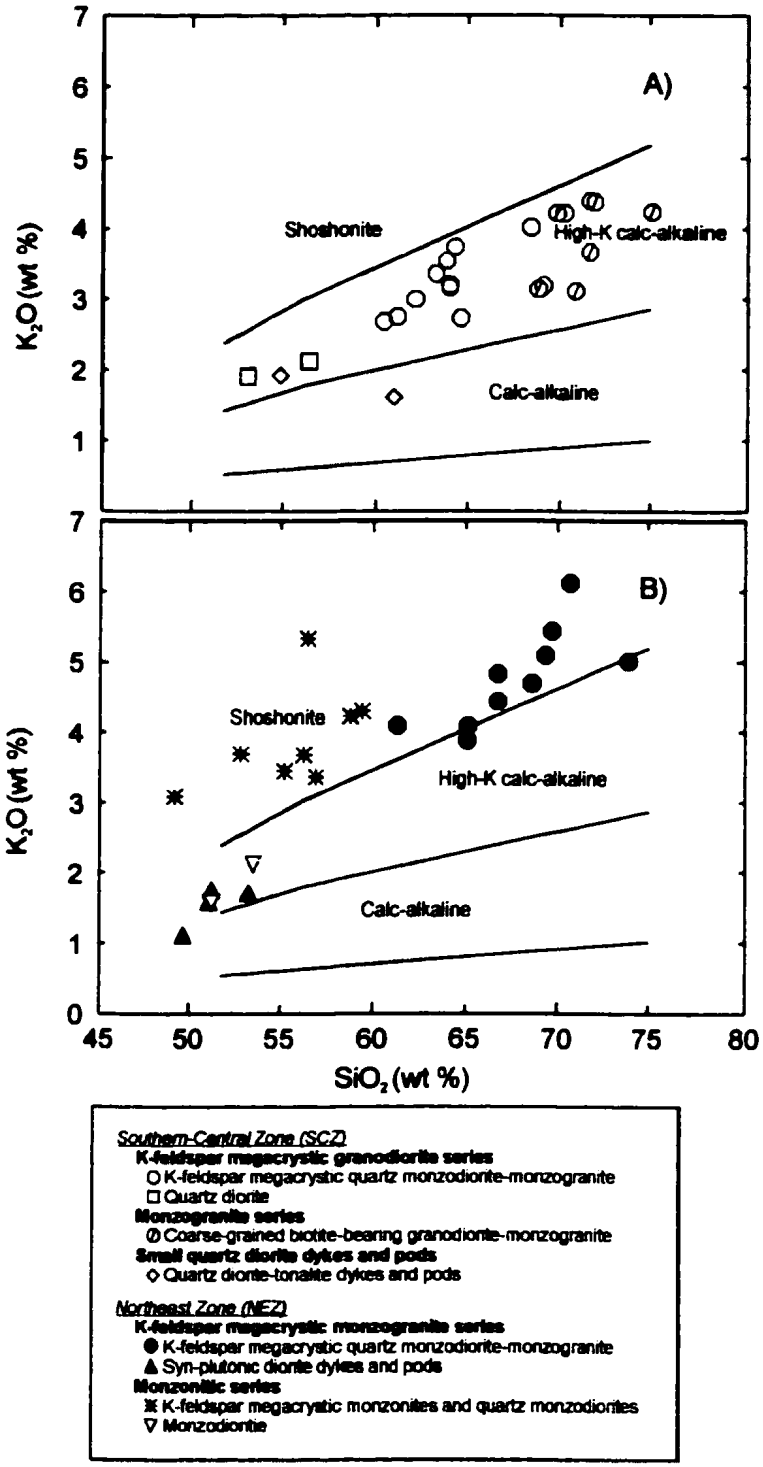

Figure 4.5 K_2O versus SiO_2 diagram for granitoids of the Wathaman Batholith. A) granitoids of the SCZ. B) granitoids of the NEZ. Field boundaries modified from Peccerillo and Taylor (1976).

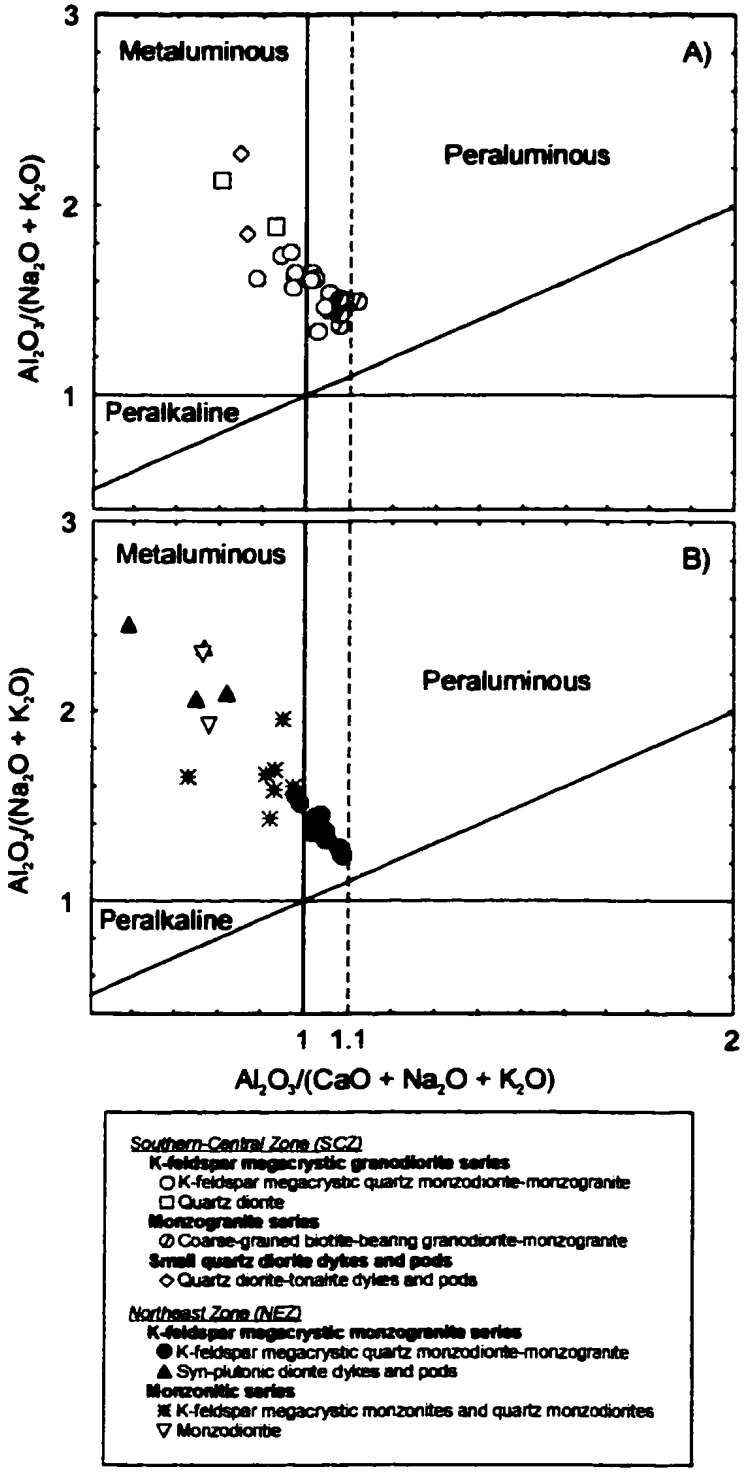

Figure 4.6 Molecular A/NK versus A/CNK plot for granitoids of the Wathaman Batholith. A) granitoids of the SCZ. B) granitoids of the NEZ. Field boundaries after Maniar and Piccoli (1989).

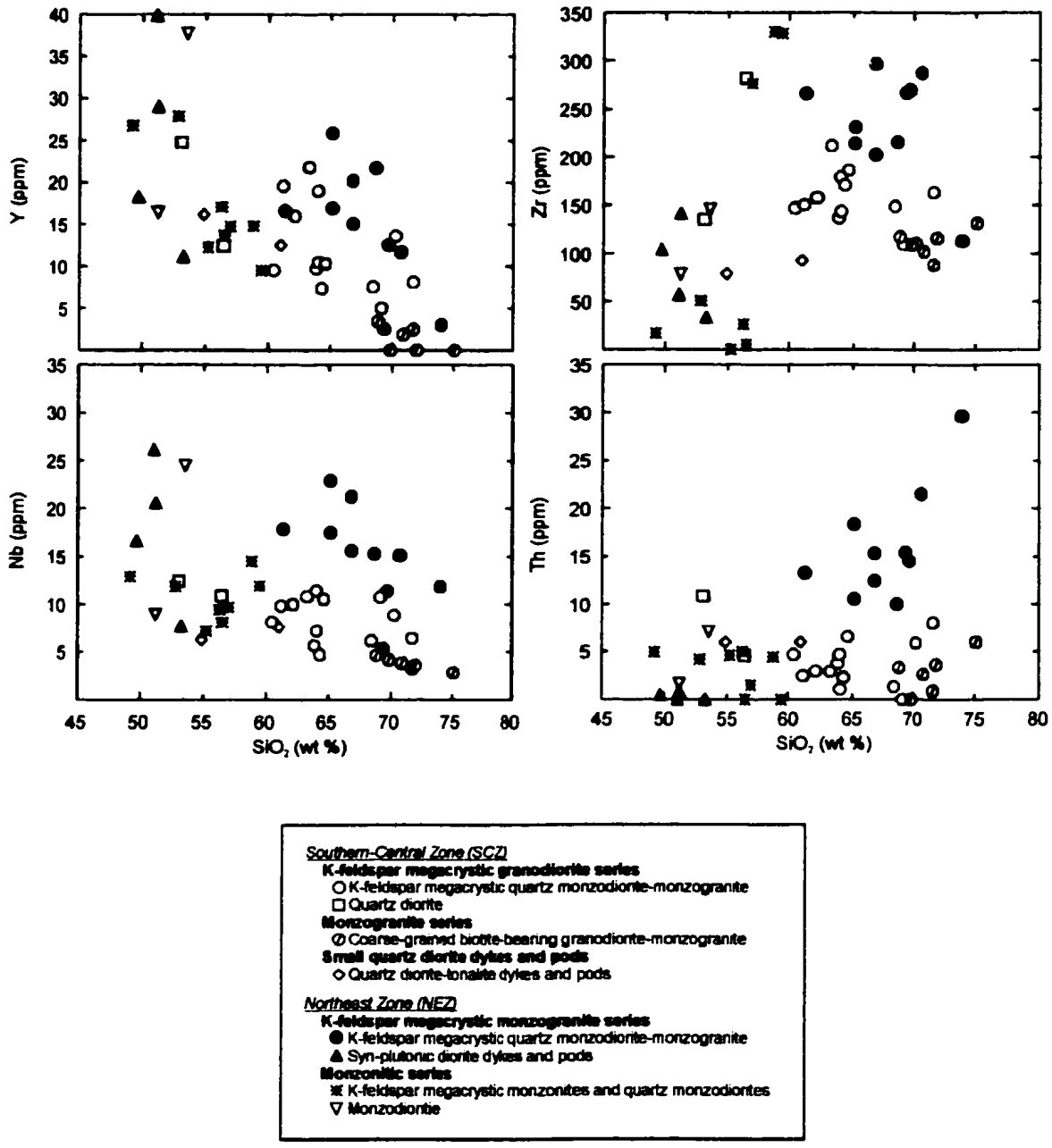

Figure 4.7 Trace element Harker variation diagrams for granitoids of the Wathaman Batholith.

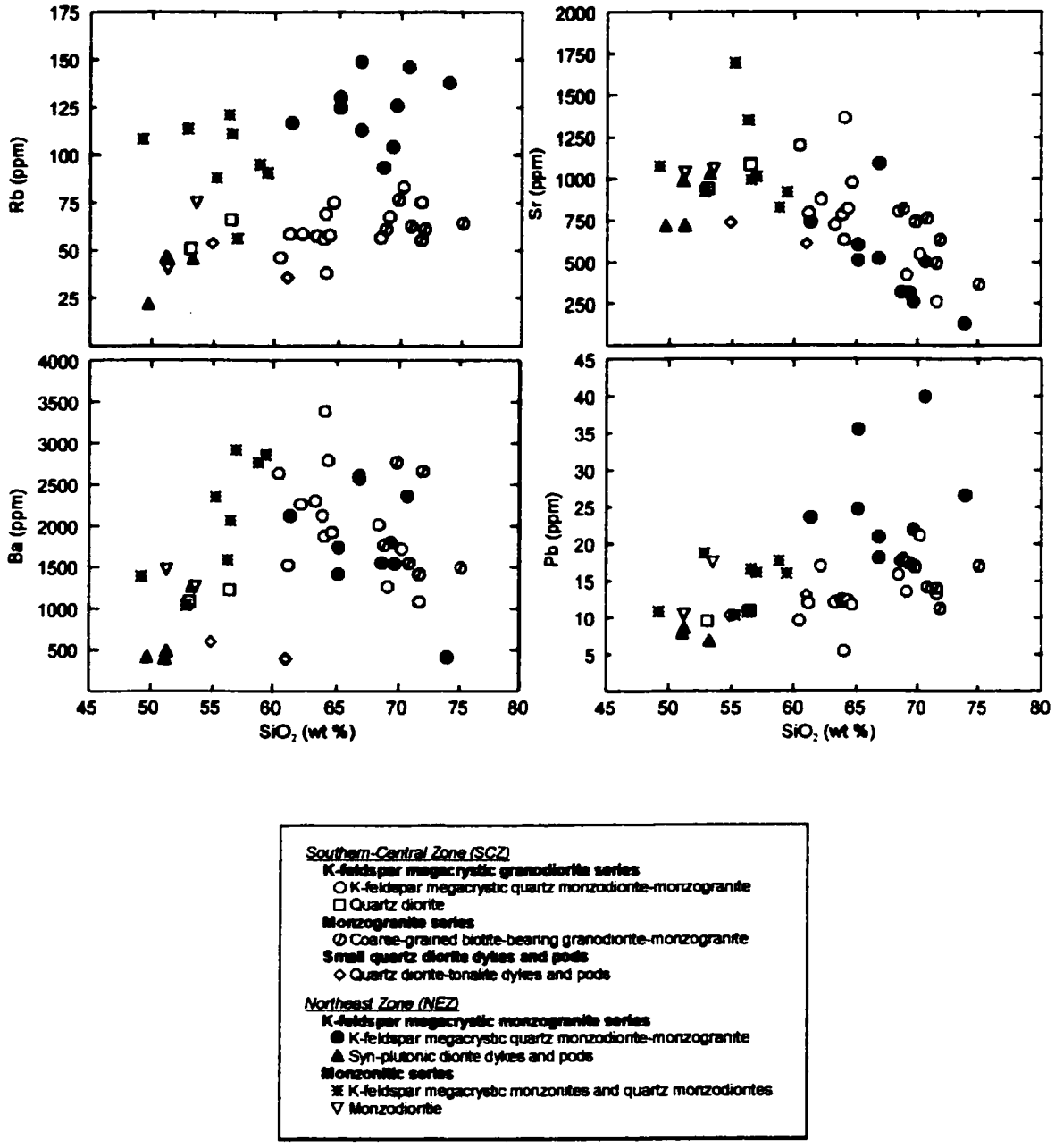

Figure 4.8 Trace element Harker variation diagrams for granitoids of the Wathaman Batholith.

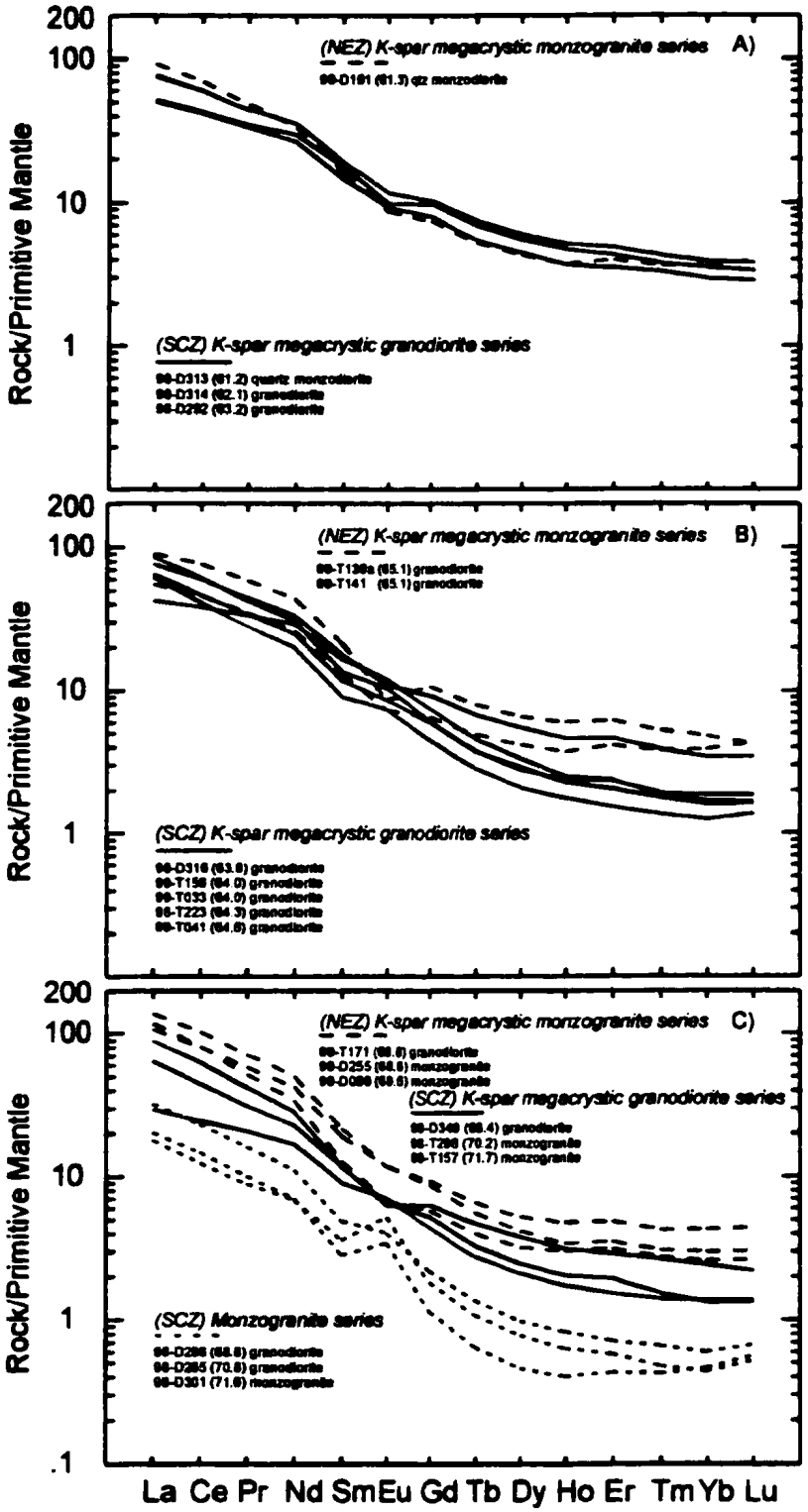

Figure 4.9 Primitive mantle normalized REE plots for granitoids rocks of the Wathaman Batholith containing > 60 wt % SiO_2. A) Granitoids containing 61-63 wt % SiO_2. B) Granitoids containing 64-65 wt % SiO_2. C) Granitoids containing 67-72 wt % SiO_2. Normalizing values from Sun and McDonough (1989).

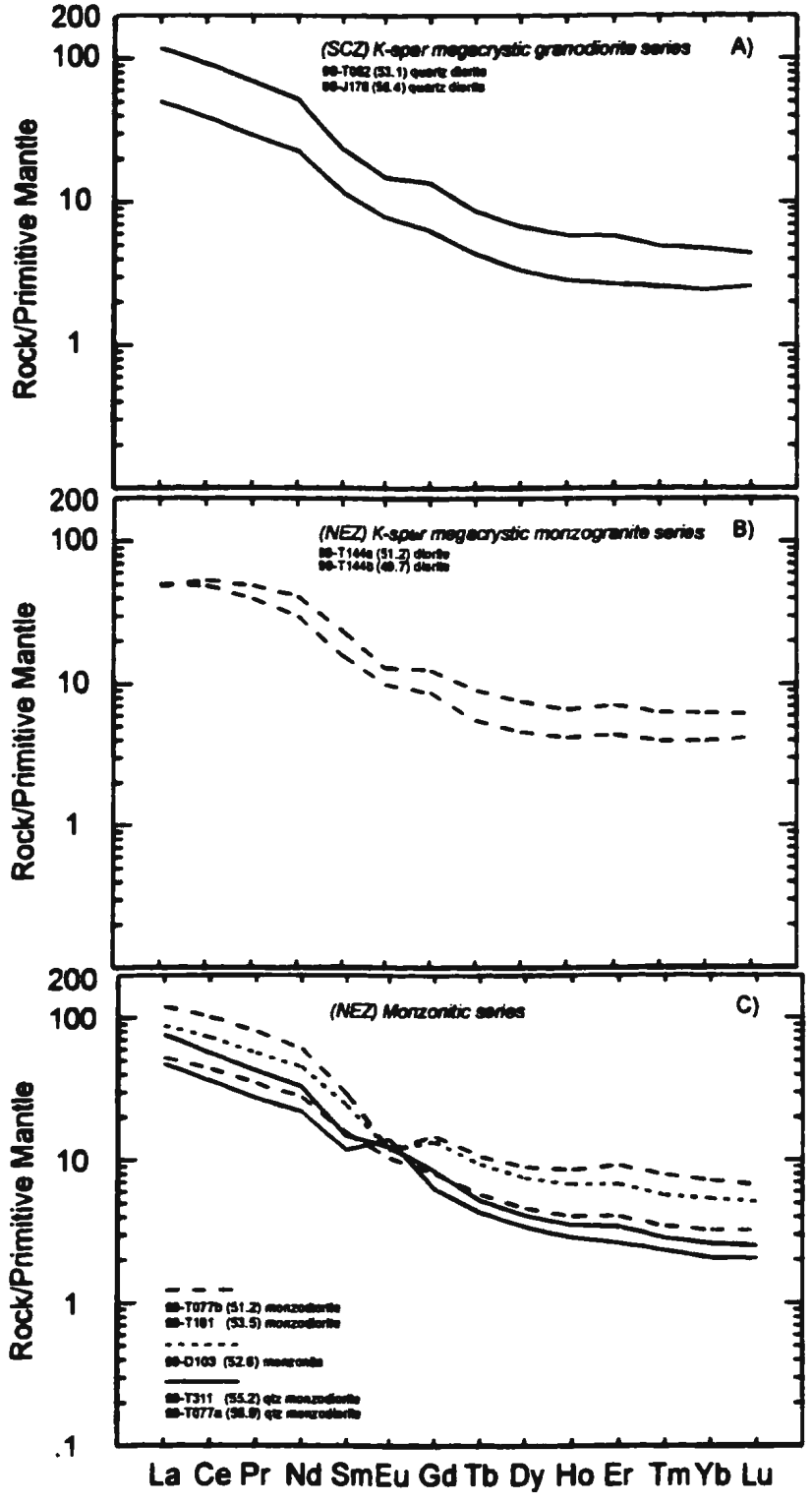

Figure 4.10 Primitive mantle normalized REE plots for granitoid rocks of the Wathaman Batholith containing < 60 wt % SiO_2. A) SCZ quartz diorites. B) NEZ syn-plutonic diorite dykes. C) NEZ monzonitic series rocks. Normalizing values from Sun and McDonough (1989).

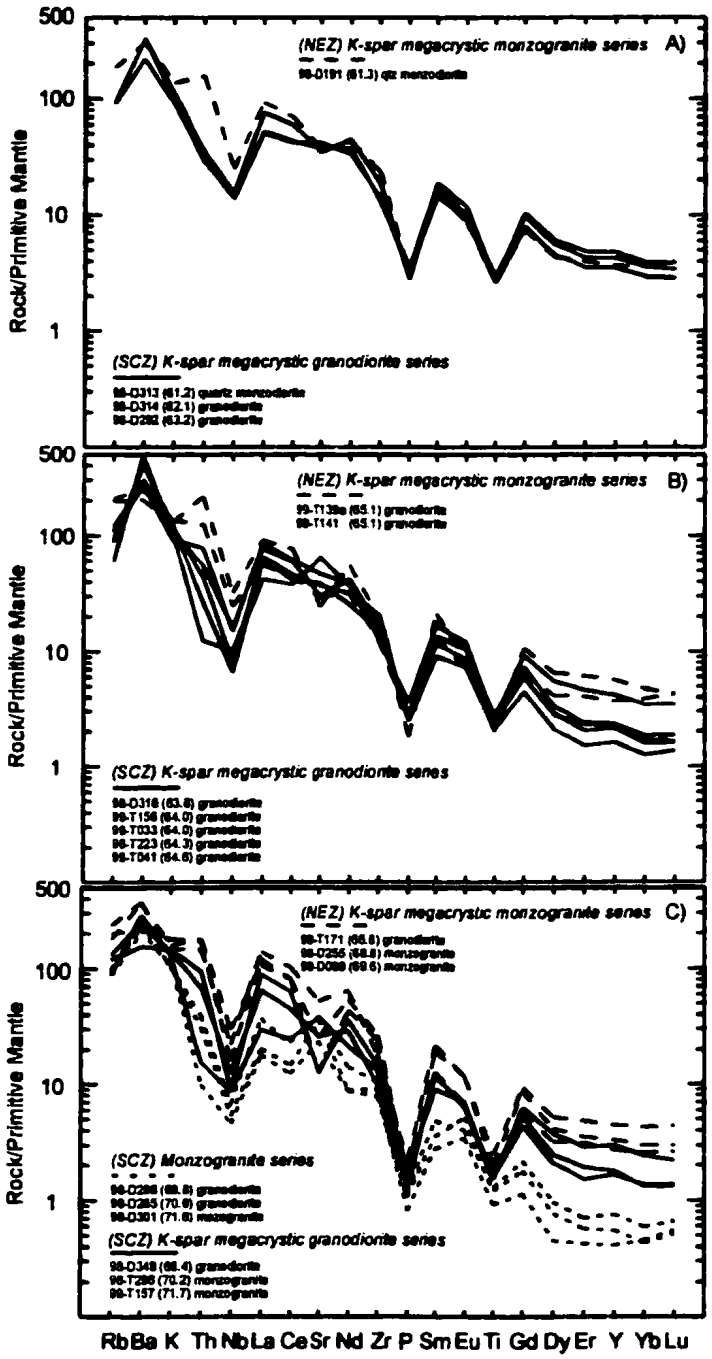

Figure 4.11 Primitive mantle normalized extended element plots for granitoids of the Wathaman Batholith containing > 60 wt % SiO_2. A) granitoids containing 61-63 wt % SiO_2. B) granitoids containing 64-65 wt % SiO_2. C) granitoids containing 67-72 wt % SiO_2. Normalizing values from Sun and McDonough (1989).

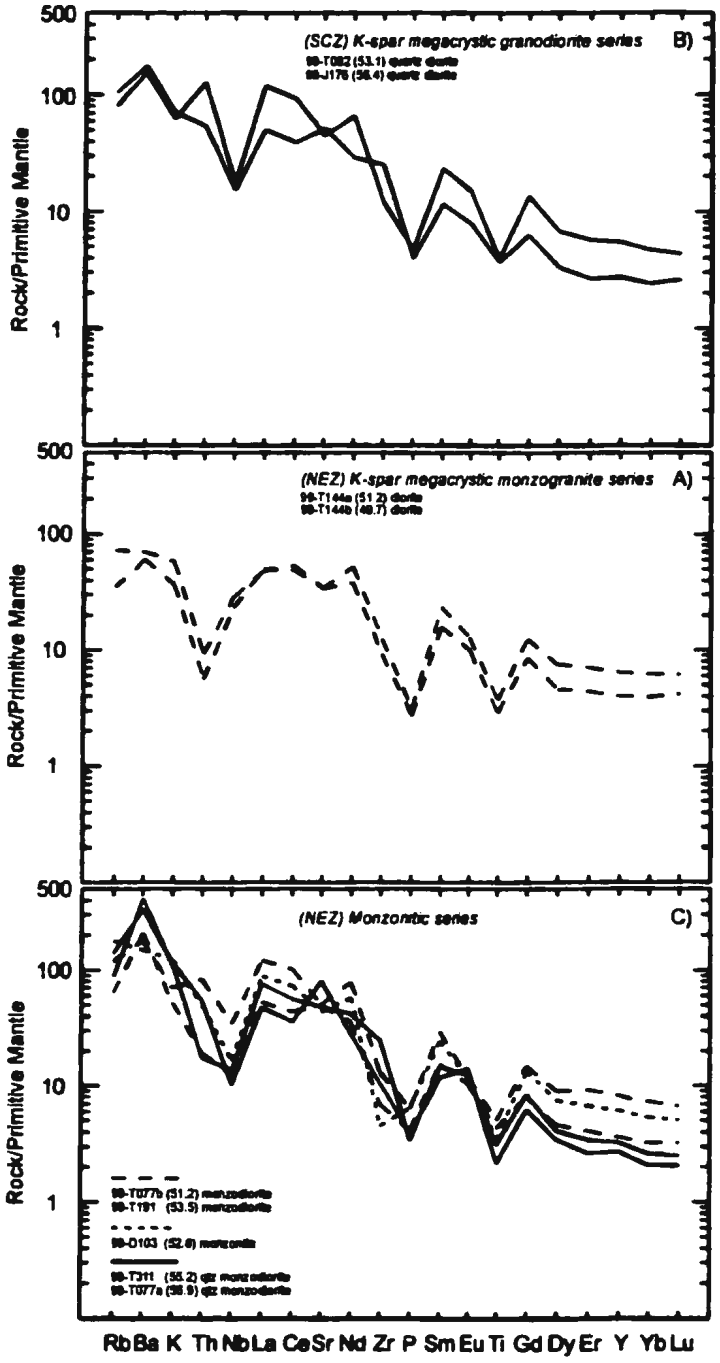

Figure 4.12 Primitive mantle normalized extended element plots for granitoids of the Wathaman Batholith containing < 60 wt % SiO_2. A) SCZ quartz diorites. B) NEZ syn-plutonic diorite dykes. C) NEZ monzonitic series rocks. Normalizing values from Sun and McDonough (1998).

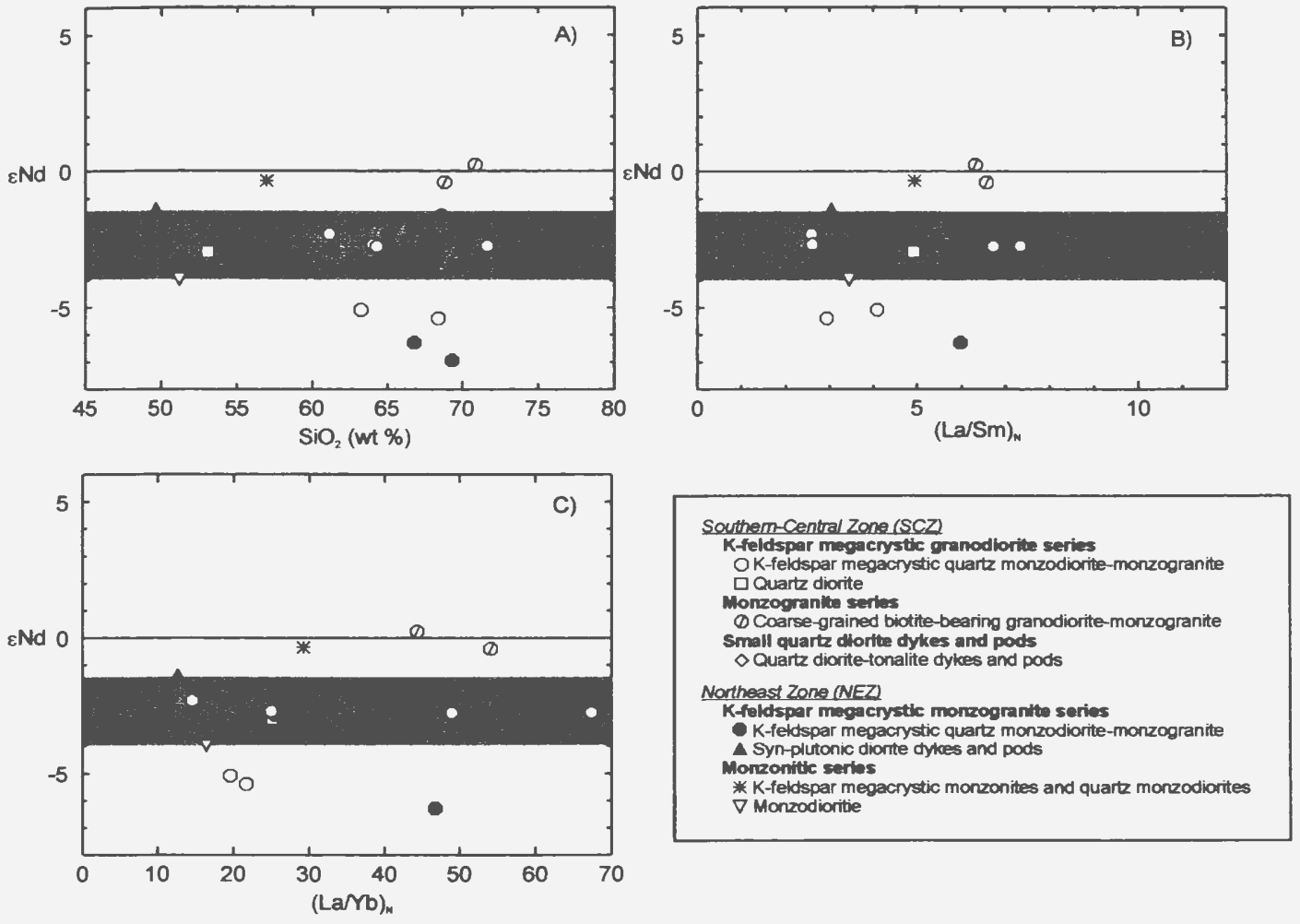

Figure 4.13 A) $\varepsilon Nd_{(T)}$ versus SiO_2. B) $\varepsilon Nd_{(T)}$ versus $(La/Sm)_N$. C) $\varepsilon Nd_{(T)}$ versus $(La/Yb)_N$. Dashed field is εNd = -1.5 to -4.

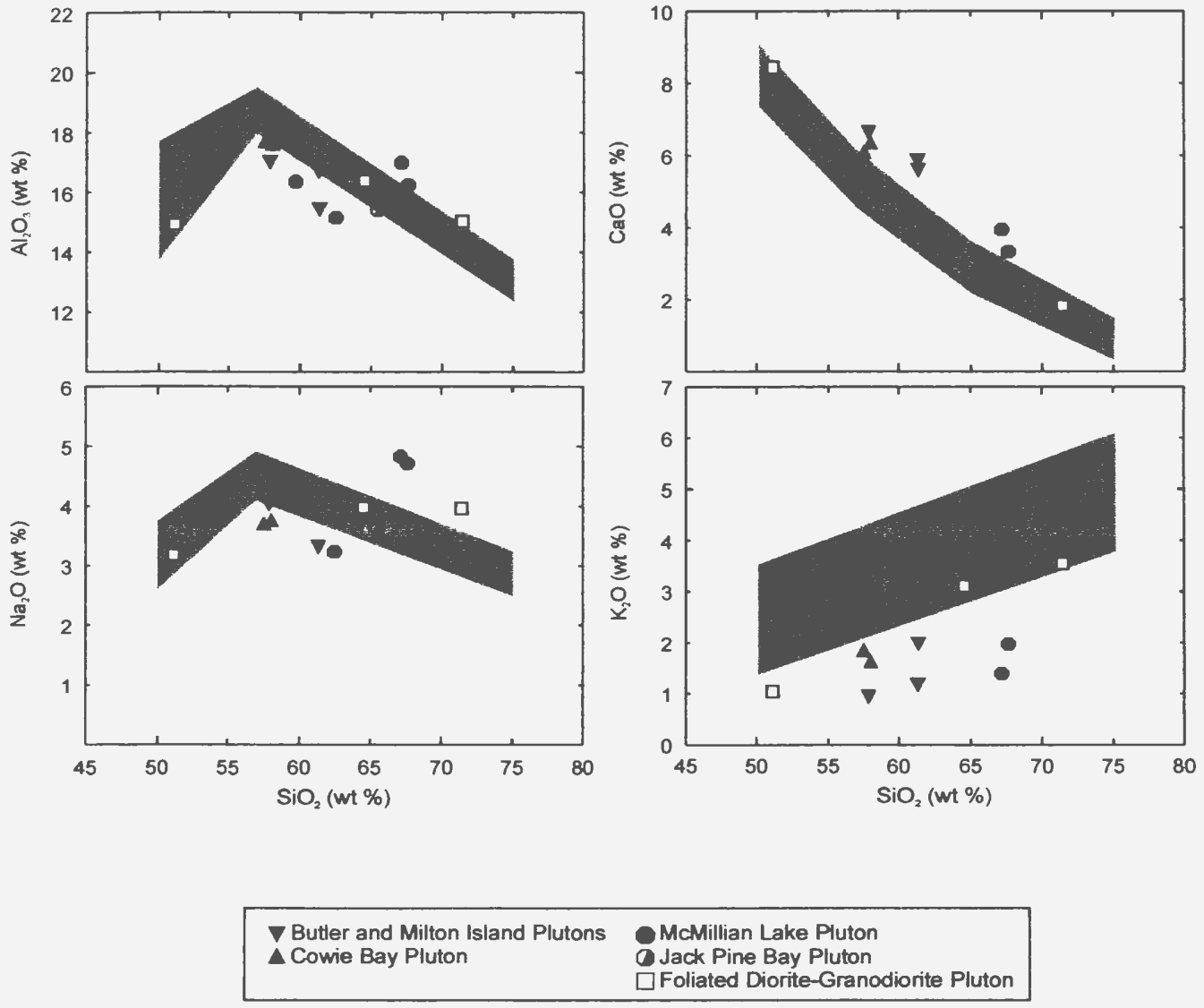

Figure 4.14 Major element Harker variation diagrams for plutons of the La Ronge Domain. For reference fields that enclose the majority of all the Wathaman Batholith granitoids are also plotted.

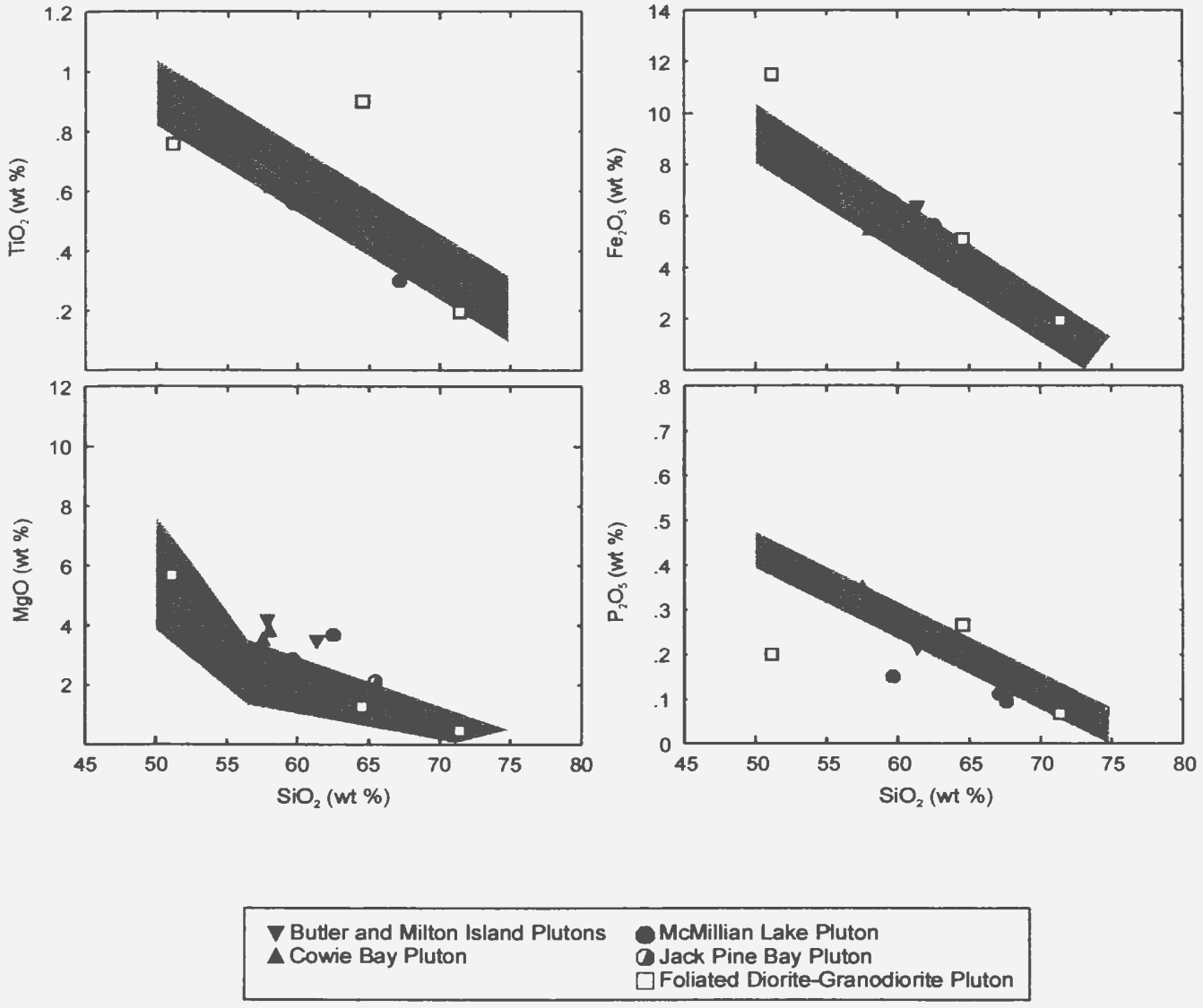

Figure 4.15 Major element Harker variation diagrams for plutons of the La Ronge Domain. For reference fields that enclose the majority of all the Wathaman Batholith granitoids are also plotted.

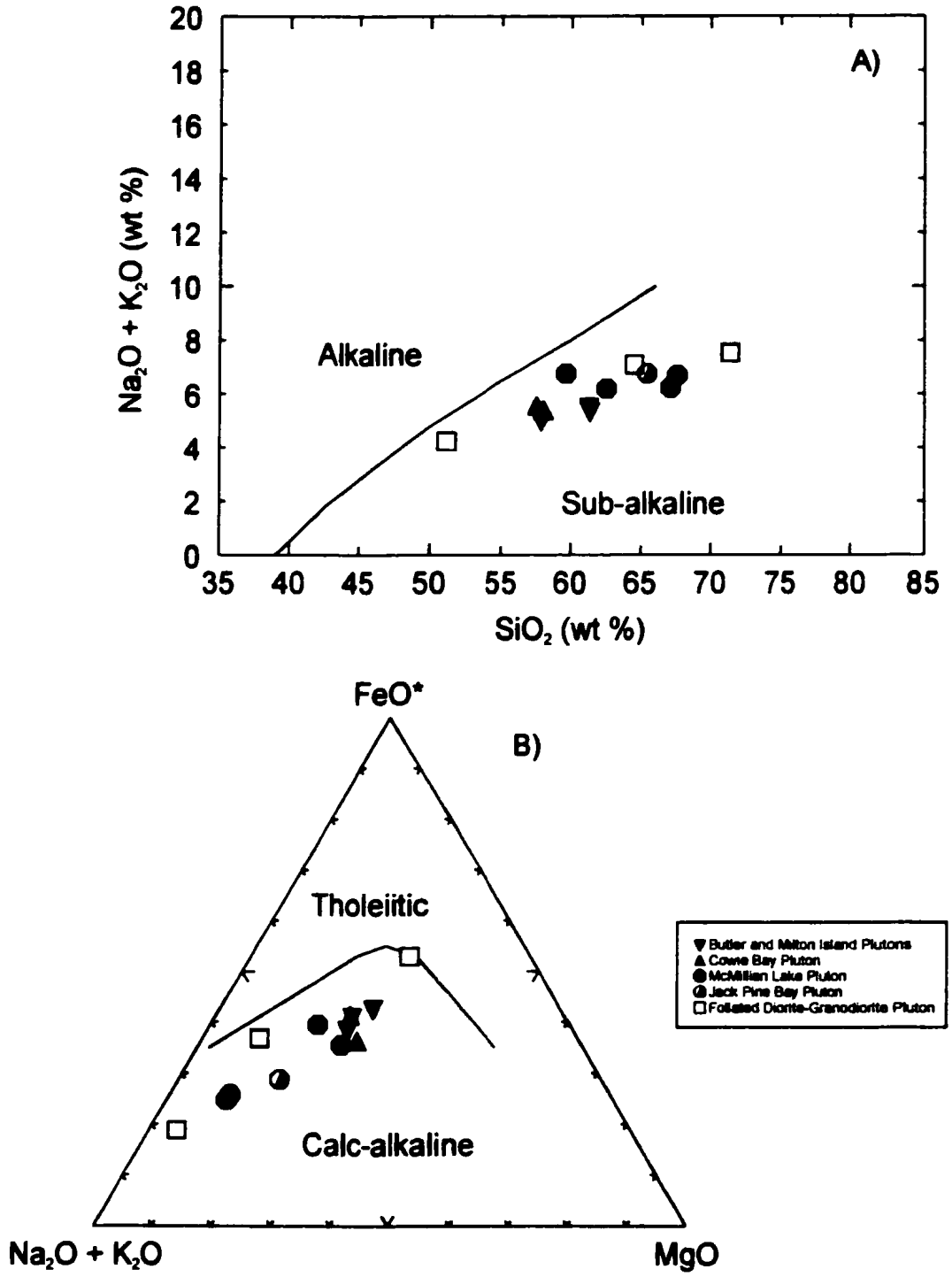

Figure 4.16 A) Total alkalis versus silica diagram for plutons of the La Ronge Domain. Alkaline versus sub-alkaline field boundary after Irvine and Baragar (1971). B) Ternary AFM diagram for plutons of the La Ronge Domain, after Irvine and Baragar (1971).

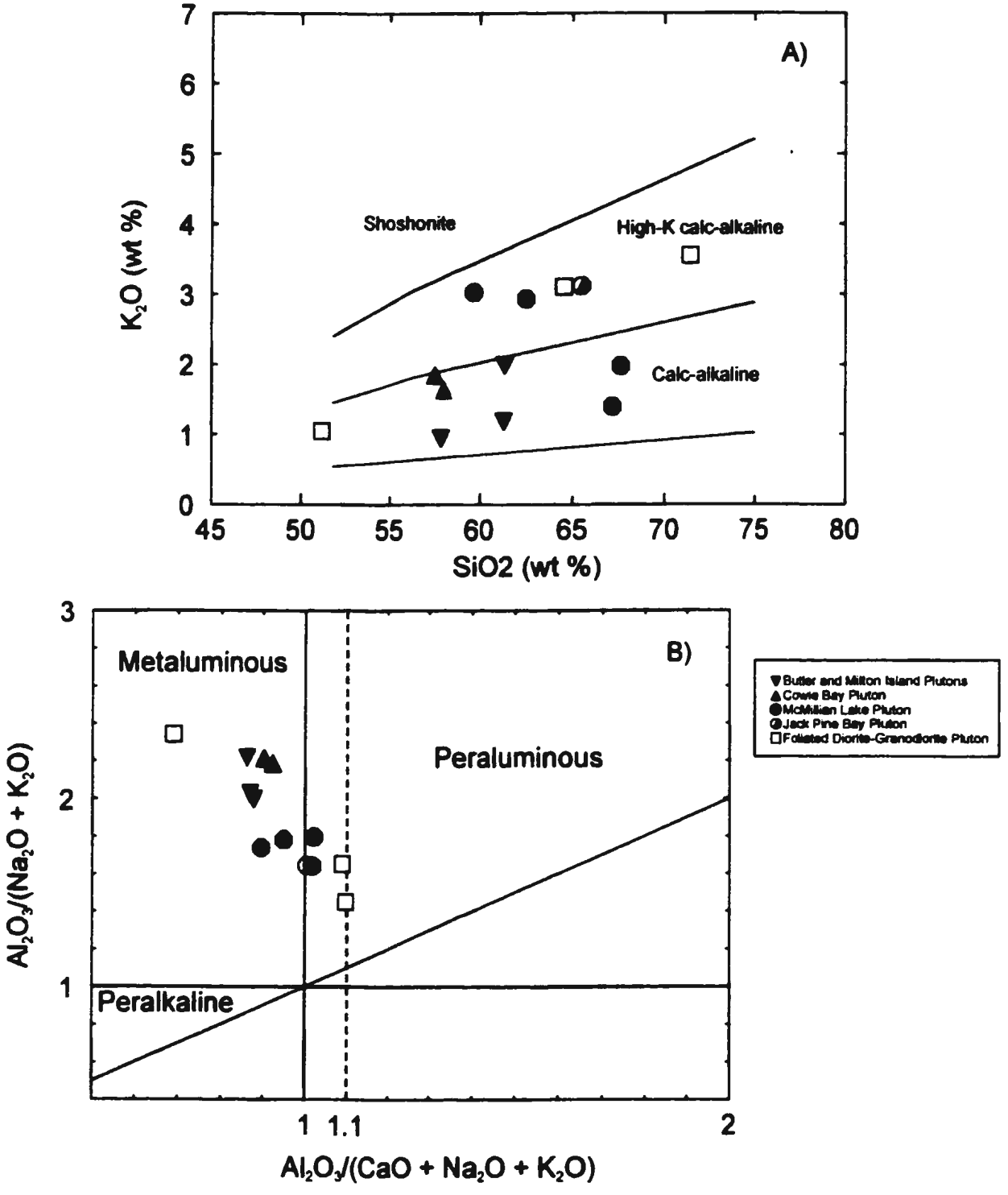

Figure 4.17 A) K_2O versus SiO_2 diagram for plutons of the La Ronge Domain, field boundaries modified after Peccerillo and Taylor (1976). B) Molecular A/NK versus A/CNK plot for plutons of the La Ronge Domain.

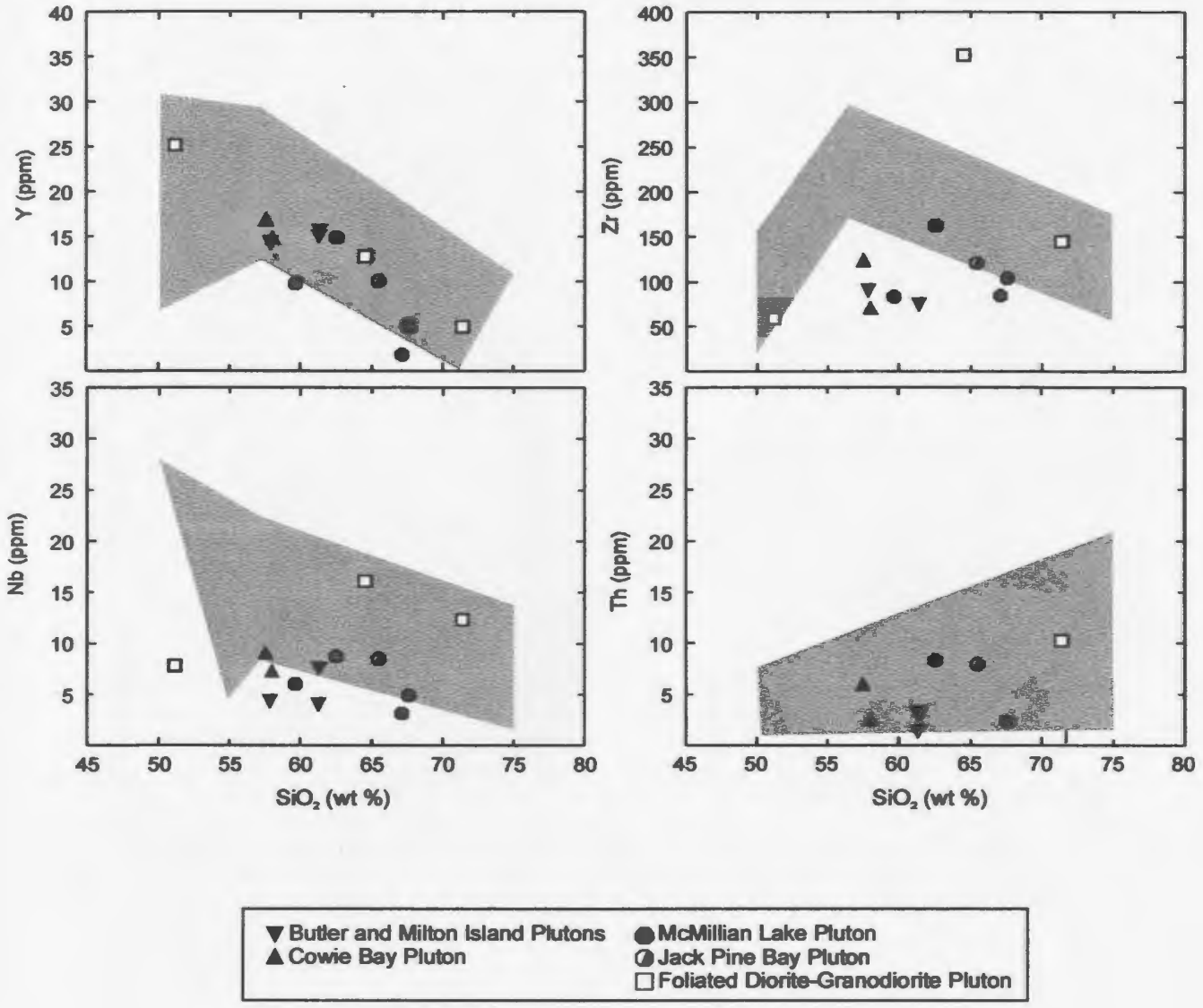

Figure 4.18 Trace element Harker variation diagrams for plutons of the La Ronge Domain. For reference fields that enclose the majority of all the Wathaman Batholith granitoids are also plotted.

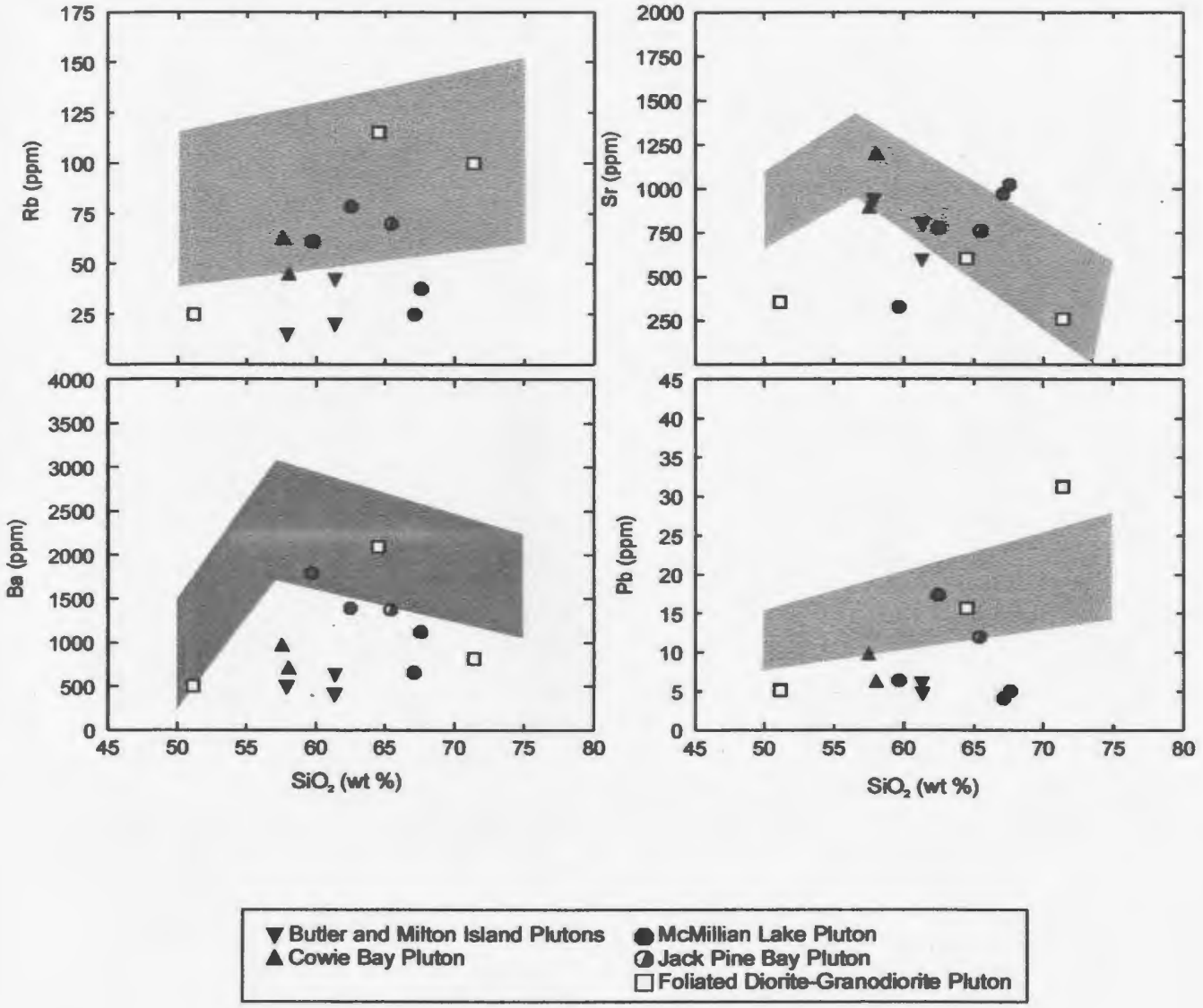

Figure 4.19 Trace element Harker variation diagrams for plutons of the La Ronge Domain. For reference fields that enclose the majority of all the Wathaman Batholith granitoids are also plotted.

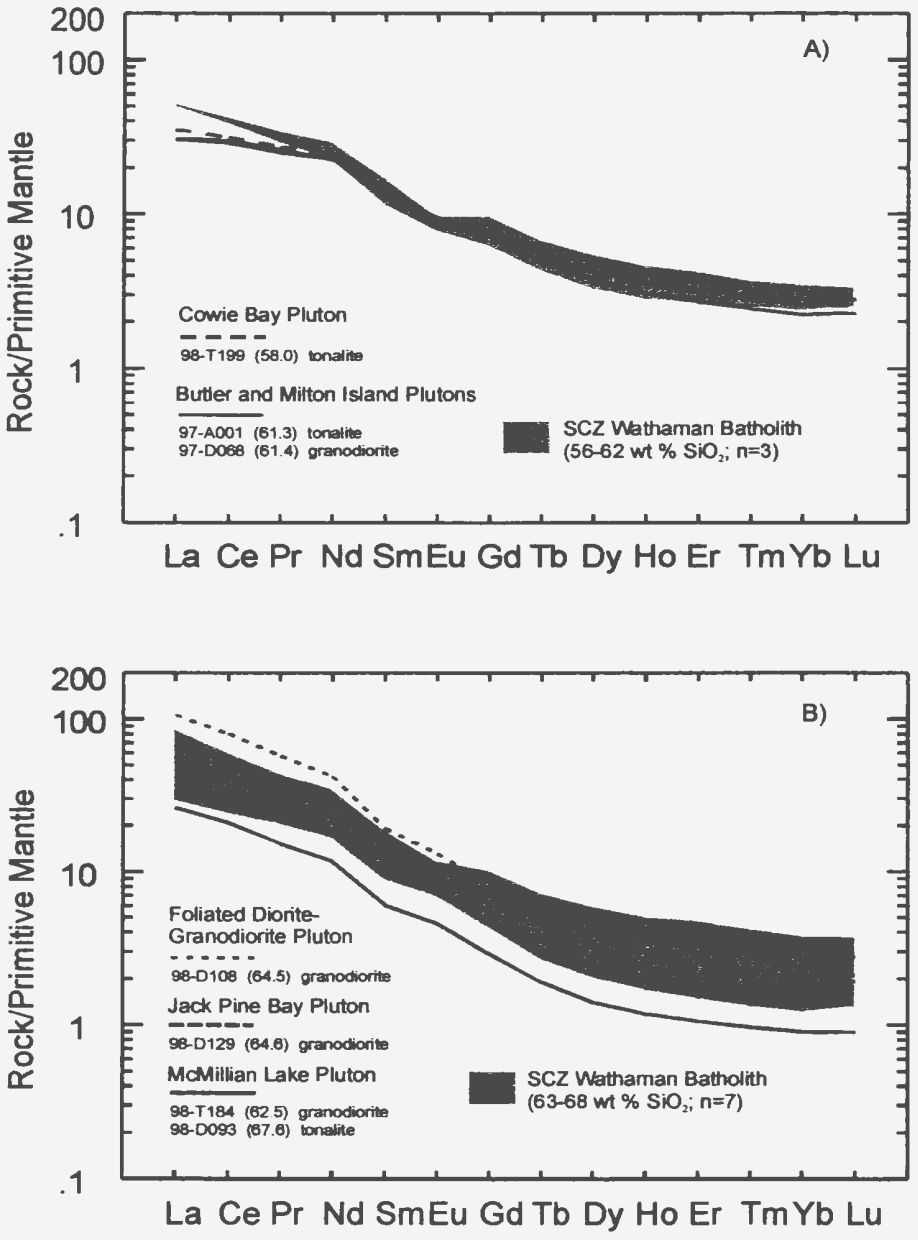

Figure 4.20 Primitive mantle normalized REE plots for plutons of the La Ronge Domain. A) Hbl-bio-bearing tonalites. B) Bio±hbl-bearing granodiorites. Normalizing values from Sun and McDonough (1989).

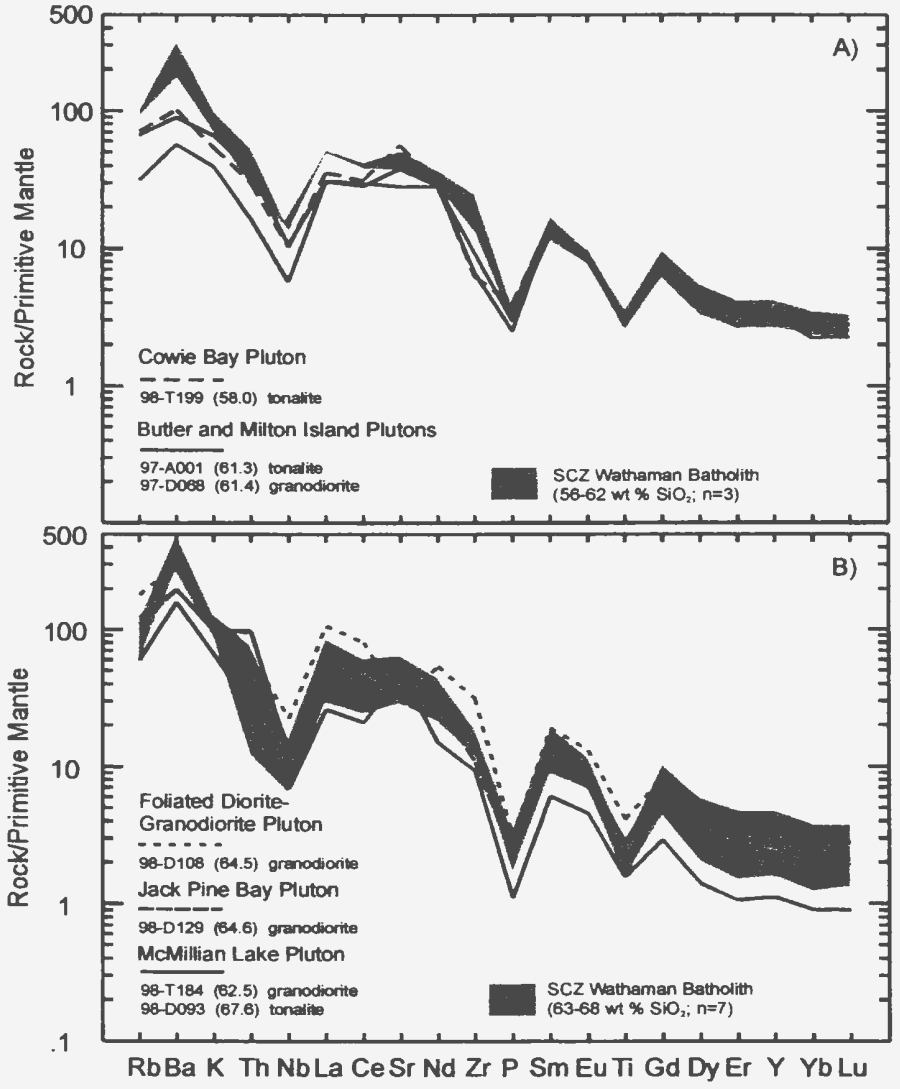

Figure 4.21 Primitive mantle normalized extended element plots for plutons of the La Ronge Domain. A) Hbl-bio-bearing tonalites (58-62 wt % SiO_2). B) Bio"hbl-bearing granodiorites (62-68 wt % SiO_2). Normalizing values from Sun and McDonough (1989).

CHAPTER 5: PETROGENESIS OF THE WATHAMAN BATHOLITH AND THE LA RONGE DOMAIN PLUTONS

5.1 INTRODUCTION

The goal of this chapter is to outline the petrogenetic processes responsible for the formation of the Wathaman Batholith and the La Ronge Domain plutons. Studies of granitoid plutons suggest that a variety of processes may be operative in any given batholith. These include fractional crystallization, assimilation-fractional crystallization (AFC), magma mixing, crust - mantle interaction (*i.e.*, bulk assimilation, mixing-assimilation-storage-homogenization - or MASH). To further complicate matters, we must also acknowledge that there may be various different end-members in any crust-mantle mixing process, for example, the mantle may be a depleted-asthenospheric one, an enriched subcontinental lithospheric one, or depleted mantle affected by a previous, relatively recent subduction zone metasomatic event.

Given the complexity of source-process combinations, it is important to systematically evaluate and identify those that have played a significant (*i.e.*, identifiable) role in the petrogenesis of the granitoids. Since the most volumetrically significant and compositionally diverse rocks are those in the Wathaman Batholith and the SCZ-KMGS in particular, we will first examine their origin. Because of the documented similarities of some series of rocks in the batholith, it will not be necessary to delve into excruciating detail for each and every one.

5.2 PETROGENESIS OF THE WATHAMAN BATHOLITH

5.2.1 The SCZ K-feldspar megacrystic granodiorite series

The SCZ-KMGS is the dominant one in the batholith and has potentially the most to reveal about the source regions and dominant processes involved in the generation and evolution of the batholith. The most notable feature of this series is its wide compositional range, with silica

contents ranging from 53-72 wt. %. Accompanying the wide compositional range is a strong and progressive change in the modal mineralogy throughout the series, ranging from hbl-bio-bearing quartz diorites, monzodiorites and granodiorites to bio-hbl-bearing granodiorites to bio±hbl-bearing monzogranites. K-feldspar megacrysts are found in quite mafic compositions, first appearing in some quartz monzodiorites and increase in abundance along with modal quartz with increasing differentiation. The Nd isotopic data for this series is quite homogeneous, five of seven samples have εNd(t) values between -2.3 and -3.0. The consistency in the Nd isotopic data is quite remarkable considering that the samples were collected over a rather large geographical area and are representing such a wide range in magma compositions (~ 20 wt. % silica).

5.2.1.1 Role of Fractional Crystallization

The progressive changes in the modal mineralogy, whole rock chemistry and rather homogeneous Nd isotopic composition suggest that the mafic and felsic end members of this series are related through some form of crystal-liquid fractionation. Feldspars are a major component of these rocks and must have been important fractionating phases along with hornblende and accessory minerals. Major and trace element variation diagrams for this series showed inflections in Al_2O_3, Na_2O, Sr, and Ba between 55 and 60 wt. % SiO_2. The inflection almost certainly signifies the incoming of feldspars as important fractionating phases, for example, K-feldspar megacrysts are important phases in rocks containing > 60 wt. % SiO_2 but occur as interstitial crystals in rocks with lower silica contents. Figure 5.1a is a plot of Ba versus Sr plot for the series. Plotted with the data are vectors indicating the direction of residual magma for 40 % fractional crystallization of plagioclase, K-feldspar, hornblende and biotite. Note that the correlation between Sr and Ba produces a trajectory intermediate between that expected from plagioclase or K-feldspar fractionation alone. Although Sr remains relatively constant or slightly decreases from quartz

diorites to granodiorites, Ba increases rather abruptly. This trend further suggests that K-feldspar was not an important fractionating phase within compositions containing < 60 wt % SiO_2 and that plagioclase along with an important component of hornblende were dominating the fractionating assemblage (Figure 5.1a).

Average REE patterns in the SCZ-KMGS for the groups defined by silica contents (61-63, 64-65, and 68-72 wt. %) are plotted in Figure 5.1b. With increasing silica the degree of LREE-enrichment increases causing the LREE patterns of more fractionated samples to cross over those of less fractionated samples, and there is a consistent and strong decrease in the MREE and HREE in the more differentiated magmas. This type of REE fractionation is characteristic of hornblende fractionation (*e.g.*, Sawka, 1988). Attempts to semi-qualitatively model hornblende fractionation within the series using the dacitic Kd's of Arth (1976) are plotted in Figure 5.1c. The average REE pattern of the 61-63 wt. % SiO_2 magmas was used as the starting composition and between 10 and 20 % fractionation of hornblende was modelled. The REE modelling of hornblende fractionation did produce similar REE patterns to those observed in the rocks of the SCZ-KMGS. The LREE patterns crossed over and the MREE and HREE showed strong decreases. This result strongly suggests that hornblende was an important fractionating phase, and is potentially a substantial sink for the REE.

Accessory minerals with high Kd's for the REE, for example, titanite, allanite, apatite and zircon are all ubiquitous in the SCZ-KMGS especially in intermediate compositions. This suggests that some of these accessory phases were fractionating from the magmas and in turn may be responsible for the observed REE variations. Titanite, for instance, also has high Kd's for the MREE and its fractionation can produce MREE-depletions in residual liquids similar to those observed for hornblende (*e.g.*, Gromet and Silver, 1993; Stern and Hanson, 1990). The major

elements do however provide important corroborative evidence of hornblende fractionation. The progressive increase in the A/CNK with increasing SiO_2 in the series driving magmas from metaluminous to weakly peraluminous compositions (Figure 5.1d) is certainly produced by hornblende fractionation. Due to the low A/CNK of hornblende, it's fractionation from a melt will produce residual liquids with higher A/CNK. The feldspars have A/CNK near unity and along with the accessory phases cannot significantly shift this ratio.

Evidence that apatite was being removed from the evolving liquids is seen in the strong decrease in P_2O_5 from 0.3-0.4 wt. % in quartz diorites and quartz monzodiorites to about 0.1 wt. % in the most differentiated monzogranites. Apatite has a preference for the LREE and MREE and could certainly be contributing to the decreasing MREE in residual magmas. However, its role is limited by the fact that the LREE increase (on average) with increasing SiO_2 (Figure 5.1b). Allanite, a common accessory phase in the mafic and intermediate compositions has extremely high Kd's for the LREE (Sawka, 1988). Its fractionation should be clearly identifiable by a marked decrease in the LREE and a degree of HREE-enrichment in residual magmas. However, on average, decreasing LREE are not observed in the series, and residual magmas become more LREE-enriched with increasing differentiation (Figure 5.1b). Although allanite does not appear to have been a major REE-bearing phase (on average) evidence that it was locally being removed from or accumulating in magmas comes from a good correlation between $(La/Sm)_N$ and Th (Figure 5.1e), both likely controlled by allanite. Allanite may not have become a major REE-bearing mineral due to the fact it was replaced by epidote fairly early on in the crystallization history of the magmas (*cf.* Chapter 3 - rimming of allanite by epidote in quartz monzodiorite and granodiorite), and is absent or rare in more felsic compositions.

Overall, the major and trace element data support a crystal fractionation model for the SCZ-

KMGS that is satisfied by the mineral assemblages found in the rocks: hbl+plag+K-spar±titanite±apatite±allanite±biotite. The increasing Rb content with increasing differentiation in the series indicates that biotite was not significant fractionating phase as compared to hornblende and the two feldspars.

If the limited abundance of mafic end members (< 58 wt. % SiO_2) is seen as a true reflection of their abundance, rather than a sampling bias, then it is difficult to rationalise crystal fractionation of these magmas to produce the granodiorites and monzogranites. Magmas with ~ 60 wt. % SiO_2 were identified as comprising significant portions of the SCZ-KMGS and, together with quartz diorites of Fumerton et al. (1984), suggests that intermediate rocks are found in sufficient quantity, and possess enough geochemical similarities to the more differentiated granodiorites, to represent the dominant parental magmas in the SCZ-KMGS. The uniformity in Nd isotopic composition across the entire range in compositions argues that crustal contamination did not accompany the fractional crystallization (*cf.* DePaolo, 1981), or was incapable of modifying the Nd isotopic composition in any meaningful way.

5.2.2 Origin of the Isotopic Signature

Quite remarkably the majority of the samples collected from the Wathaman Batholith possess εNd(t) values that lie between -1.5 and -4.0 with a significant number clustering around -2.5 (Figure 5.2a). Notably, Nd isotopic compositions do not correlate with rock type, silica content, rock series or magmatic zone. As indicated earlier, the mafic magmas present throughout the batholith are volumetrically small but possess similar geochemical and Nd isotopic compositions as the more felsic magmas. For instance, the diorites, monzodiorites and quartz diorites also have -εNd values between -1.4 and -4.0, and the monzodiorites and quartz diorites also possess the high to very high Ba, K_2O, Sr and LREE contents that characterize the entire

batholith. The mafic magmas also possess significant amounts of Ni, Cr and MgO indicating derivation from mantle sources. Thus, the primitive magmas not only provide a more accurate glimpse into the source region, but also may hold clues to the source for the unusually high LFSE contents of the batholith. Of great importance is determining if the -εNd values and enriched trace element characteristics observed in the mafic magmas were acquired by crustal contamination of depleted mantle-derived magmas or whether these features were inherited directly from the mantle. In order to evaluate the role of crust - mantle mixing processes we must first discuss the available data that constrain the Nd isotopic composition of the crust and mantle at the time of formation of the batholith. Evaluating the Nd isotopic composition of the crust is particularly relevant since the batholith intrudes mainly juvenile Paleoproterozoic crust in the south and Archean crust in the north, representing a potentially wide range in Nd isotopic compositions.

5.2.2.1 The Nd isotopic composition of Paleoproterozoic and Archean crust

The Nd isotopic compositions of the Paleoproterozoic volcanic assemblages of the LRD southwest of the Reindeer Lake have been well documented from previous studies by Chauvel et al. (1986) and Thom et al. (1990). Nine volcanic rocks ranging in composition from basalt to rhyolite have εNd(1858) values between +2.0 and +4.8. A greywacke also had a similar εNd(1858) value to the volcanic rocks of +2.6. Pre-1865 Ma LRD lithologies collected from Reindeer Lake for Nd isotopic analyses include a tonalite from the Crowe Island Complex with an εNd(1858) value of +3.7, and a dacite from the CMB with an εNd(1858) value of +2.5 (Corrigan et al., unpub. rept.). The consistently positive εNd values indicate the LRD volcanogenic belts were derived from a source region characterised by a long history of LREE depletion, i.e. the depleted mantle. Large portions of the LRD in the Reindeer Lake area are, however, underlain by metasedimentary assemblages and currently no Nd isotopic data are available for them. However,

the Park Island assemblage has been subject to a preliminary U-Pb zircon study. Preliminary results indicate that the majority of the zircons have ages similar to those reported for felsic volcanic rocks in the La Ronge and Lynn Lake domains (Corrigan et al., pers. comm.). In contrast, the Milton Island assemblage is known to contain some Archean zircons (Ansdell, 1999) suggesting it probably has a lower εNd(1858) signature than the volcanogenic belts in the domain.

The Nd isotopic composition of the Archean Peter Lake Domain is less well constrained, with only limited data from this and previous studies available. A leuco-granite from the southwestern portion of the Peter Lake Domain and a tonalitic gneiss collected on Reindeer Lake have εNd(1855) values of -8.1 (Chauvel et al., 1986) and -7.6, respectively (Bickford et al., 1992). These results are similar to the average εNd value calculated for the western Churchill upper crust at ca. 1850 Ma of -8 (Theriault and Tella, 1997). A foliated medium grained granodiorite collected from the northwestern shoreline of Reindeer Lake (this study) had an εNd(1855) value of -10.0, and a gabbro had an εNd(1855) value of -5.4. The Nd concentrations of these samples ranges from as high as 38 ppm for the leuco-granite, 14 ppm for the foliated granodiorite, to 5 ppm for the gabbro.

5.2.2.2 The Nd isotopic composition of ca. 1800-1900 Ma depleted mantle

Previous Nd isotopic studies of Paleoproterozoic volcanic rocks throughout Saskatchewan and other portions of the Trans-Hudson Orogen have documented the presence of a depleted mantle having a maximum εNd value of approximately +5 between ca. 1800-1900 Ma (Chauvel et al., 1986). The maximum value of +5 during this period of Earth history is also supported from similarly aged volcanic rocks found in Colorado (Nelson and DePaolo, 1984) and Greenland (Patchett and Bridgwater, 1984). The depleted mantle evolution curve used in this study (DePaolo, 1991) predicts εNd values between +5.0 and +5.2 between ca. 1800-1900 Ma. Evidence for

depleted mantle at ca. 1865-1850 Ma during peak plutonic activity within the LRD comes from several granodioritic plutons located southwest of Reindeer Lake. One of the granodiorites has been dated at ca. 1849 ±10 Ma (Van Schmus et al., 1987) and possess εNd(1858) values between +4.1 to +4.9 (n=4) (Chauvel et al., 1986). An εNd(1858) value of +4.8 has also been obtained from the Butler Island pluton (Corrigan et al., unpub. rept.) located on Reindeer Lake and dated at ca. 1858 +3/-2 Ma (Corrigan et al., 1998b). Thus, not only was a depleted mantle source region available during the earlier stages of volcanism within the domain, but it was still available between ca. 1865-1850 Ma.

5.2.2.3 Crust - mantle mixing models and the generation of parental magmas

With the crustal and mantle Nd isotopic compositions constrained, it is possible to attempt to quantify the importance of crust-mantle mixing processes in the generation of mafic and intermediate magmas. Figure 5.2b summarizes the Nd isotopic data presented in the previous sections in an εNd(t) versus age (Ga) plot. The Nd isotopic data of the batholith lie between the depleted mantle - juvenile crust of the LRD and the Archean crust of the PLD, potentially due to simple mixing processes. Without using major and trace elements in conjunction with the Nd isotopic data in mixing models it would be impossible to determine if this is indeed the case.

A simple two component crust-mantle mixing model will be used in an attempt to reproduce the -εNd values, SiO_2 and Ba contents of the primitive magmas of the batholith. The end members used will be a basaltic magma derived from the depleted mantle and various Archean crustal end members. The mixing equation used was developed by Langmuir et al. (1978), and adapted for the εNd notation by DePaolo and Wasserburg (1979) and can be found in Faure (1986).

The basaltic magma composition derived from melting of the depleted mantle has 50 wt.

% SiO_2, 10 ppm Nd and an εNd(1855) value of +5. These are the same values used by Chauvel et al. (1986) in their calculations. The Archean crustal end member is felsic, with 70 wt. % SiO_2 (avg. of PLD granitoids sampled), between 30 and 60 ppm Nd and εNd(1855) values between -8 and -10. The 30 ppm Nd concentration was used as it approximates the average concentration of Nd in the upper continental crust (Taylor and McLennan, 1985) and because the Nd concentrations of the granitoids in the PLD ranged between 14 and 38 ppm, respectively. A value of 60 ppm was also used as a maximum value, considering the crustal material may be added as felsic partial melts, in which REE concentrations of the source may be double depending on the degree of incompatibility and melting. The gabbroic rocks of the Swan River Complex are not considered in the models because of their extremely low Nd concentrations.

Figure 5.3a is a plot of εNd(t) versus SiO_2 including a syn-plutonic diorite dyke, monzodiorite and quartz diorite and the two mixing curves that enclose all mixing lines between the depleted mantle and crustal end members used. The results of the modeling indicate that it is extremely difficult to generate the low εNd values of the mafic magmas by crustal contamination because of their very low silica contents. Only the crustal end member having an εNd(1855) value of -10 and very high Nd concentration of 60 ppm came close to being capable of producing the monzodiorite in the mixing model. The more typical crustal end member with an εNd(1855) value of –8 (equal to the average western Churchill upper crust) and 30 ppm Nd does not even come close to being able to reproduce the low εNd values and SiO_2 contents of the primitive magmas.

Crust-mantle mixing models involving εNd and Ba are plotted in Figure 5.3b. In this case the depleted mantle was assigned a Ba content of 350 ppm Ba, typical of calc-alkaline basalts from the CVZ of the Andes and basalts from SW Pacific island arcs (Ewart, 1982). Three crustal end members all having εNd(1855) values of -10 and a Nd concentration of 60 ppm were used. The

three crustal end members are: 1) the average upper continental crust containing ~ 550 ppm Ba (Taylor and McLennan, 1985); 2) The average Ba content of Peter Lake Domain granitoids of ~ 1500 ppm; and 3) a hypothetical Ba-rich crustal end member with 3000 ppm Ba. The modeling results clearly indicate that it is impossible to generate the elevated Ba contents of the monzodiorites and quartz diorites by crust-mantle mixing, and only the syn-plutonic diorite could potentially be produced in this way. An Archean crustal end member with >> 3000 ppm Ba would be needed to be added to depleted mantle-derived magmas to generate compositions similar to the monzodiorite and quartz diorite.

These mixing models indicate that the low εNd values of the most primitive magmas cannot be solely produced by crustal contamination of depleted mantle-derived magmas. The magmas also possess elevated Ni, Cr and MgO contents, suggesting the -εNd(t) values and elevated Ba contents are most likely a characteristic of the mantle source region. Thus, similar to the source for members of the Archean Sanukitoid suite (Stern et al., 1989, *c.f.*, Chapter 4) where "LILE-enriched" peridotite is though to be the source which produced mafic magmas enriched in the LFSE (Sr, Ba, K_2O) and LREE. The major difference between the monzodiorites and quartz diorites of the batholith and members of the Sanukitoid suite are the crustal-like εNd(t) signatures observed in the batholith, whereas the Sanukitoids have depleted mantle like initial Nd isotopic signatures (Stern et al., 1989). Using the measured $^{147}Sm/^{144}Nd$ of the monzodiorite and quartz diorite, depleted mantle model ages can be calculated, i.e., the time in the past when the rocks would have had the same Nd isotopic composition as the depleted mantle. The results are variable but clearly indicate the LREE enrichment of the mantle is an ancient feature and occurred sometime between ca. 2400-2700 Ma. Thus, a Sanukitoid-like mantle source could have formed sometime during the Late Archean and lay dormant until tapped during the Paleoproterozoic. This

would allow sufficient time for the lower Sm/Nd of the metasomatised mantle to develop lower and negative εNd values. The involvement of an enriched lithospheric mantle as a potential source has profound implications for the petrogenesis of the more felsic magmas of the batholith in that they are all high-K calc-alkaline to shoshonitic series (*i.e.*, rich in K_2O), show extreme enrichments in Ba, and the majority of samples have a similar range in εNd(t) values as the more primitive magmas.

Does the homogeneous Nd isotopic signature and similar trace element geochemistry indicate that the entire batholith has been sourced from a heterogeneously enriched lithospheric mantle (εNd(t) = -1.5 to -4.0) and the compositional variation due simply to closed system crystal fractionation processes? The under representation of mafic magmas clearly does not support this thesis and it is probable that crustal materials may be involved. The low volume of the more mafic magmas may be due to deep crustal mixing between enriched mantle-derived magmas and lower crustal melts. For example, a MASH zone (Hildreth and Moorbath, 1989) located within the lower crust or at the crust-mantle boundary could have permitted very thorough mixing and continued crystal fractionation and not allowed large volumes of the more primitive magmas to escape. Thus, the intermediate magmas could be products of mixing of enriched mantle-derived magmas and lower crustal melts. Crustal contamination of primitive magmas with both juvenile Paleoproterozoic LRD or the older PLD Archean crust has almost certainly occurred on some scale, but the enriched characteristics of the primitive magmas are also features expressed by the crust, making it difficult to impossible to determine the extent of crustal interaction. The high LREE contents of these magmas may actually buffer the Nd isotopic composition. For instance, all mafic magmas sampled from the batholith that have silica contents ~ 53 wt. % (n=6) possess an average Nd concentration of 57 ppm, very high considering their mafic compositions. Figure 5.4

reconsiders the εNd versus SiO_2 mixing relationship but now in terms of an enriched primitive magma and a felsic Archean crustal end member. The mafic magma has a Nd concentration of 57 ppm, 52 wt. % SiO_2, and an εNd(t) value of -2.0. The Archean crust is felsic having 70 wt. % SiO_2, 30 ppm Nd and εNd(1855) values between -8.0 and -10.0. The higher Nd concentration of the mantle-derived end member causes the mixing curves to be concave downward, opposite to the previous mixing situation. This plot illustrates two important features: 1) mixing felsic crust into mafic magmas increases the silica content of the resultant magma; and 2) only minimal shifts in the Nd isotopic composition occur when 10's of % crust are added. In fact, to move the εNd(t) value from –2.0 to -3.0 requires between 20-30 % Archean crust to be added to the primitive magmas, also increasing the silica contents from 52 to between 57-58 wt. %. If this type of scenario is operative in the batholith significant quantities of crust may have been added to mafic magmas, thus, leading to the production of more felsic magmas with little evidence recorded in the Nd isotopic composition. In the case of the SCZ-KMGS, the 57-58 wt % magmas produced in the model are close in composition to those demonstrated to be related to more felsic magmas of that series by fractional crystallization. Also, in this type of model the lower εNd(t) values of -5.1 and -5.4 from two samples in the SCK-KMGS are almost impossible to explain in terms of an increased component of older crust in these magmas. Referring back to Figure 5.4, the production of < -5.0 εNd(t) signatures in these two granitoids would require > 50-60 % Archean crust be added to the enriched primitive magmas. This large amount of crust would almost certainly alter the major and trace element geochemistry in some noticeable way, and these samples are indistinguishable geochemically from any other rocks in the SCZ-KMGS. Thus, magmas rising from the mantle or crust mantle boundary may have possessed a range in εNd(t) values, as high as -1.5 and as low as -5. This could be due to heterogeneous enrichment of the lithospheric mantle, mixing between a

more depleted mantle and enriched mantle, or both. The higher εNd(t) value of the syn-plutonic diorite dyke and its lack of enrichment in Ba and K_2O suggest that it may indeed have been generated from a more depleted mantle source region.

Evidence for the existence of an extensive and homogeneously enriched lithospheric mantle that has existed since the Archean has recently been documented beneath the Western Churchill Province within both the Rae and Hearne domains (Cousens et al., in press). These authors presented Nd isotopic data from ultrapotassic minette dykes and flows of the 1830 Ma Christopher Island Formation (CIF) which outcrops over an enormous area of 240 000 km^2. The CIF outcrops between 300-600 km north of the Wathaman Batholith. Good evidence that the enriched mantle reservoir existed well before 1830 Ma comes from very low εNd(t) values between -7 and -10.5. Depleted mantle model ages range between 2671 to 3150 Ma based on the measured $^{147}Sm/^{144}Nd$ of the rocks. Archean and other dykes ranging in age between 2450-2110 Ma also plot within an envelope that encloses the CIF samples that extends back to the depleted mantle. The mantle source for the CIF is also rich in LFSE especially Ba and K_2O, and LREE although to a much greater degree than the Wathaman batholith. The εNd(t) values are also much lower in the batholith considering that it only formed 20-40 Ma before CIF magmatism.

The mixing of enriched lithospheric mantle with a more depleted asthenospheric mantle would be expected to increase the εNd values of resultant primitive magmas. The involvement of the asthenosphere would not only provide mantle material with higher εNd values lacking the extreme Ba, K_2O and Sr enrichment, but also provide a source of heat to facilitate melting of the lithospheric mantle as it remained rigid and cold for several hundred Ma. The fluxing of the lithospheric mantle with hot basaltic magmas from the asthenosphere may essentially be the critical factor needed to trigger magmatism. This will be discussed further in the summary where the

magmatism is discussed in placed in the context of its tectonic setting.

5.2.3 The NEZ K-feldspar megacrystic monzogranite series

The division of the batholith into the SCZ and NEZ was largely due to major and trace element geochemical distinctions between K-feldspar megacrystic granitoids. The major differences between the series and the overall increase in the average silica content from ~ 60-65 wt. % in the SCZ-KMGS to 65-70 wt. % in the NEZ-KMMS and sharp increases in the K_2O and Rb contents of the granitoids over the entire range in silica. Also increasing in concentration in the NEZ are the LREE, Zr, Nb, Th, and Pb. A petrogenetic model for this series must explain the distinctive geochemical features that set it apart from the SCZ-KMGS, but also account for the similarities. For example, the two series have similar ranges in εNd(t) values, and also contain elevated Ba and Sr contents. Six of the of the eight samples analyzed for their Nd isotopic compositions from the NEZ-KMMS series have εNd(t) values between -1.4 and -3.5, similar to the -2.3 to -3.0 range exhibited by the majority of the SCZ-KMGS samples. The low εNd values and high Ba contents of these magmas suggest a component from the enriched lithospheric mantle. From the mixing models between an enriched mafic magma and Archean crust it was clear that substantial amounts of crust could be added to magmas causing increases in the silica content of resultant magmas but producing minimal shifts in the εNd(t) values.

The increased Rb, LREE, Zr, Nb, Th, and Pb of the NEZ magmas compared to those in the SCZ does indeed suggest additions of crustal material. Figure 5.5 includes trace element Harker variation diagrams of SCZ series and the NEZ-KMMS for Rb, Nb, Zr and Th. Also plotted on the diagrams are the average values of these elements (and silica) for some crustal end members. These include: 1) the average upper continental crust (UCC) of Taylor and McLennan (1985); 2) the average composition of megacrystic monzogranites of the PLD (A-Gdr); and 3) the

average composition of the foliated granodiorites and monzogranites of the PLD (F-Mgn). Contamination of 60-63 wt. % magmas of the SCZ with crustal compositions similar to the UCC and A-Gdr end members could potentially produce more felsic magmas with ~ 65 wt. % SiO_2 and elevated Rb, Nb, Zr and Th. The foliated granodiorites and monzogranites are not suitable sources for these elements. The fact that the NEZ-KMMS granitoids actually intrude and contain large rafts of the Archean PLD crust is good evidence of contamination. The dividing line between the SCZ and NEZ outlined by the increased K_2O and Rb concentrations is parallel to and plots as the extension of the contact between the batholith and the PLD further to the southwest. This strongly suggests that the division between the two zones is in fact related to the structure of the Archean crust beneath the batholith. The elevated REE patterns and negative Eu anomalies of the NEZ-KMGS compared to the SCZ-KMGS (Figure 5.6a) suggest that feldspars were important fractionating minerals in this series. A plot of Ba versus Sr with mineral fractionation vectors clearly indicates that feldspars, in particular plagioclase was the dominant fractionating mineral in that series (Figure 5.6b). The high Rb content of the magmas and the importance of plagioclase as a fractionating mineral indicates that differentiation and crustal contamination were probably occurring within the upper crust. The two samples with the very low $\varepsilon Nd(t)$ values of -6.3 and -6.9 are approaching values equal to the Archean crust of –8 and may indicate that they are largely comprised of mobilized portions of the older crust.

5.2.4 The NEZ Monzonitic series

The weakly alkaline magmas of the monzonitic series are an extremely variable series of rocks that possess some unique geochemical characteristics that set them apart from the typical "calc-alkaline" series types of the batholith. The monzodiorites and monzonites of this series have very low modal quartz contents and have compositions more typical of a monzonitic differentiation

trend. However, the bulk of this series is comprised of quartz monzodiorite plotting somewhat intermediate between a true monzonitic and calc-alkaline differentiation trend on a QAP normative plot (*c.f.*, Pitcher, 1999). The highly variable range of rock types and geochemical and isotopic signatures indicate that at least two and possibly three distinctive magma batches have been sampled.

The most unique features of these magmas are their high to very high Na_2O, K_2O, Rb, Sr, Ba, and LREE considering their mafic-intermediate silica contents between 49-59 wt. %. The very high Sr, Ba and LREE contents of these magmas are also found in the calc-alkaline magma series and are attributed largely to the involvement of an enriched lithospheric mantle, may indicate that the monzonitic series magmas was largely derived from this mantle source due to their low silica contents and extreme enrichments in these elements. The most primitive monzodiorites of this series do indeed have the geochemical and isotopic characteristics of magmas derived from the enriched lithospheric mantle and were used along with the quartz diorites of the SCZ-KMGS to identify it. Their elevated MgO, Ni and Cr suggest a mantle derivation, however, the much lower MgO, Ni and Cr contents of the monzonites and quartz monzodiorites are not indicative of a mantle origin. Examination of the major element Harker variation diagrams for this series indicate an extreme variability for FeO, TiO_2 and P_2O_5. These elements are concentrated mainly in Fe-Ti-oxides and apatite that are ubiquitous in this series. The accumulation of these minerals, especially the Fe-Ti-oxides, could explain some of the elevated Fe_2O_3 contents of the magmas relative to MgO. Also the early fractionation of olivine and pyroxenes could rapidly deplete the MgO, Ni and Cr contents of the magmas, explaining their lack of a "mantle-signature". The potential for mixing of these alkaline magmas with crustal materials and with other magmas of the batholith is also a strong possibility. The quartz monzodiorites are in fact in-between the more monzonitic series

trend defined by the monzodiorites and monzonites and are more similar to the calc-alkaline series of the batholith.

The extremely high Ba, K_2O, Sr and LREE contents of these magmas, their low silica and εNd(t) values suggest that they were largely sourced from enriched lithospheric mantle. However, earlier fractionation of olivine and pyroxenes, crustal contamination and magma mixing were all probably important processes in this series.

5.2.5 The SCZ Monzogranite series

The highly differentiated magmas of the SCZ-MS plot largely as continuations of SCZ-KMGS trends on several major and trace element variation diagrams. Along with the close spatial relationship between the two series, this suggests a possible co-genetic relationship. However, rocks of this series possess some unique geochemical and isotopic signatures, distinct from the SCZ-KMGS.

The unusual REE patterns of this series are characteristic of hornblende removal, either as a fractionating mineral during magmatic crystallization or as a residual mineral during partial melting processes. To test if the SCZ-MS samples are indeed differentiates of SCZ-KMGS magmas an attempt was made to reproduce the REE-patterns of SCZ-MS samples by crystal fractionation from a SCZ-KMGS parental magma. The starting REE composition used is the 61-63 wt. % SiO_2 average from the SCZ-KMGS and the Kd's used are for dacitic compositions (Arth, 1976).

Results from REE-modeling are plotted in Figure 5.7a and b. Figure 5.7a plots the results of 10-40 % hornblende fractionation. The results indicate that at least 40 % crystal fractionation of hornblende would be required to reproduce the MREE-HREE abundances and patterns of SCZ-MS samples. This is quite a substantial amount of fractionation considering that only between 10-

15 % hornblende fractionation was required to produce similarly fractionated magmas (67-72 wt. %) of the SCZ-KMGS and that no hornblende is found in any of the SCZ-MS samples. Also, the low LREE contents and highly fractionated LREE of the SCZ-MS samples is also not reproduced by hornblende fractionation, as the Kd's for LREE in hornblende are close to unity in these compositions. These results indicate that hornblende cannot be solely responsible for the observed REE-patterns, a phase that can remove the LREE-MREE is required to bring the REE-patterns down to the concentrations observed in the granitoids. Apatite is a good candidate as it possesses high Kd's for the LREE-MREE and the SCZ-MS samples all contain very low P_2O_5 contents (0.03-0.10 wt. %) suggesting that apatite was fractionated during some point in the history of these magmas. Figure 5.7b models fractionation of 1-2 % apatite from the same starting composition. The modeling results indicate that apatite is efficient in removing the LREE and MREE; however, significantly more than 2 % fractionation would be required even when combined with the ~ 40 % hornblende fractionation to reproduce the REE-patterns of SCZ-MS samples.

From the data, we must conclude that the SCZ-MS granitoids cannot be produced by simple crystal fractionation processes from SCZ-KMGS primitive magmas. This is supported by the Nd isotopic data from the granitoids of this series. Their $\varepsilon Nd(t)$ values of +0.2 and -0.4 are significantly more juvenile than any samples collected from the SCZ-KMGS which are all < -2.3.

The $\varepsilon Nd(t)$ values of the SCZ-MS are indistinguishable from the majority of the La Ronge Domain plutons suggesting a common source region. So an alternative model involving partial melting of a LRD-like source, leaving residual amphibole is worth considering. Potential sources may be hydrated and metamorphosed low- to medium-K basalts-basaltic andesites that are found in that domain. The fact that the SCZ-MS granitoids are found mainly along the southern margin of the batholith where it transgresses into the LRD supports this interpretation. Modeling

(not shown) suggests that the REE-patterns could be produced by small degrees of partial melting of a source rich in amphibole and containing a relatively flat REE pattern ~ 2-5 times primitive mantle REE abundances.

The U-Pb age determined on a sample from this series (98-D301) is one of the youngest ages obtained from the batholith (1850 +6/-2 Ma) and suggests, along with supporting field relationships, that this series was largely emplaced after the majority of the SCZ-KMGS. The intrusion of large volumes of quartz monzodiorite and granodiorite in the SCZ may have mobilized crustal rocks located along the margin of the batholith and generated the SCZ-MS. The fact that these magmas also contain elevated Ba and Sr contents, similar to other series in the batholith, suggests that they also contain a component derived from the SCZ-KMGS.

5.3 PETROGENESIS OF THE LA RONGE DOMAIN PLUTONS

The limited geochemical and Nd isotopic data obtained on the LRD during this study limits the interpretation of their petrogenesis. The origin of the LRD plutons certainly involves sources that are distinctly more juvenile (depleted) than those of the Wathaman Batholith, as no samples have $\varepsilon Nd(t)$ values lower than -0.4 and range as high as +4.7. The extremely juvenile $\varepsilon Nd(t)$ value obtained from the Butler Island pluton and other granodiorite plutons located to the southwest (Chauvel et al., 1987) indicate derivation from depleted mantle source regions. However, the majority of the LRD plutons have $\varepsilon Nd(t)$ values that are significantly lower, grouping around $\varepsilon Nd(t) = 0 \pm 0.5$. These lower values indicate input from an older LREE-enriched source. The lower $\varepsilon Nd(t)$ values may be due to contamination by older crustal material, either added to the mantle source via subduction of sediments or through direct contamination with continental crust during differentiation and emplacement of the plutons within the crust. The latter can be accomplished by direct contact with older crust, i.e., Archean crust underlying the

supracrustal sequences in the LRD or by an older crustal component within the Proterozoic sedimentary rocks in the domain. Certainly all three options are possible and distinguishing between them is difficult considering the limited amount of data. However, some evidence suggests that the isotopic signature of the plutons is related to the distribution of crust within the domain. For instance, the Butler Island pluton intrudes the mafic-ultramafic volcanogenic belts of the LRD that have some of the most juvenile isotopic signatures recorded in the domain of +4.7 and +4.8 (Thom et al., 1990). Thus, a mantle derived magma at ca. 1865-1850 Ma intruding this portion of the crust would not have its Nd isotopic signature changed at all. The lower $\varepsilon Nd(t)$ values are from plutons that largely intrude the portions of the domain dominated by metasedimentary assemblages for which the isotopic compositions are unknown. The Archean zircons documented in the Milton Island metasedimentary assemblage by Ansdell (1999) means that this assemblage must be considered as a possible source component for some of the plutons of the domain.

Major and trace element geochemistry can also distinguish between the more juvenile plutons of the LRD and the SCZ of the WB and places constraints on the sources involved in the petrogenesis of LRD plutons. The mafic rocks sampled from the LRD are metaluminous calc-alkaline quartz diorites and tonalites and possess distinctly lower Rb, Ba, K_2O, LREE and Zr than the equivalently fractionated quartz diorites and quartz monzodiorites of the SCZ-KMGS. This combined with the more juvenile Nd isotopic compositions of the LRD plutons negates the presence of the LREE- and Ba-enriched lithospheric mantle source, as called on for the SCZ-KMGS.

Several of the more differentiated granodiorites of the LRD do possess some similar major and trace element geochemical characteristics to granodiorites of the SCZ-KMGS. They define a

high-K calc-alkaline magma series, and possess similar Rb, and REE abundances. However, the granodiorites of the LRD lack the low εNd(t) and consistently elevated Ba contents that characterize the entire batholith. This suggests that they also do not contain a component from the enriched lithospheric mantle. Their elevated LREE, K_2O and Rb contents, compared to the less enriched quartz diorites and tonalites of the domain, are most likely simply due to the more differentiated character of these magmas.

Thus, the mantle source for the LRD was certainly more depleted than that of the WB and the interaction of these mantle-derived magmas with a mainly juvenile crust with some input from older crustal sources best explains their petrogenesis. The SCZ-MS granitoids located along the southern margin of the batholith possess identical εNd(t) values to the majority of the plutons of the LRD providing the magmatic link between the LRD and the batholith.

5.4 TECTONOMAGMATIC SUMMARY OF GRANITOID MAGMATISM ALONG THE REINDEER LAKE TRANSECT

On Reindeer Lake, the Wathaman batholith and satellite plutons of the La Ronge Domain are considered as part of a larger co-genetic batholithic suite formed largely between ca. 1865-1850 Ma. The progressive changes in modal, chemical and isotopic compositions of granitoids along the ~ 125 km transect can be explained by variable inputs from depleted mantle, enriched lithospheric mantle and older crust. The increasing involvement of enriched lithospheric mantle and older continental crust northward, and the progressive increase in K_2O-series from calc-alkaline to high-K calc-alkaline and both alkaline and sub-alkaline shoshonitic series strongly suggests a continental arc setting formed above a northward dipping oceanic plate. The recognition of mafic magmas as important constituents of the batholith and the presence of syn-plutonic diorite dykes and enclaves indicates the mantle was actively involved in the genesis of the batholith, an

important feature of magmatism associated with subduction. All mafic and felsic magmas within the LRD, SCZ and NEZ contain elevated Rb, Ba, K_2O, Sr and LREE relative to HFSE Nb, Ti, P, Zr and Y and these are considered the geochemical signature of subduction.

Figure 5.8 is a schematic north-south tectonic section of the northwest Reindeer Zone and the southeastern Hearne province between ca. 1865-1850 Ma. In the south, the LRD plutons were generated through mixing between a subduction modified depleted mantle and crust. The domain is comprised mainly of juvenile Paleoproterozoic oceanic arc crust, although an older Archean material is present in the domain as components of the metasedimentary rocks or old crust underlying the juvenile assemblages. Large volumes of metaluminous calc-alkaline quartz diorite, tonalite and granodiorite were produced throughout the domain with $\varepsilon Nd(t)$ values equivalent to the depleted mantle of +4.8 (no older crust) to as low as 0±0.5 indicating input of older crust to mantle-derived magmas.

As magmatism transgressed and intensified northward into the Wathaman Batholith it involved the older Archean crust where it is thicker and its lithospheric mantle root became an important component of the mantle wedge (Figure 5.8), profoundly influencing the character of magmatic activity. The lithospheric mantle had been previously enriched in LREE, Ba, K_2O and Sr several hundred Ma prior to ca. 1865-1850 Ma magmatism. The primitive magmas entering the crust from the mantle in the SCZ of the batholith were most likely hybrid mixtures of magmas derived from subduction zone-modified depleted asthenosphere and melts of the older enriched lithospheric mantle. The influx of hot asthenosphere into the older and relatively cold lithospheric mantle was probably a critical factor in inducing it to melt. These hybrid mantle-derived magmas entered the crust already enriched in LREE, Ba, Sr and K_2O and possessing very low $\varepsilon Nd(t)$ values. The invasion of the lower crust by these hybrid magmas probably induced melting of

lower crustal materials; however, the enriched nature of the primary magmas makes them relatively insensitive to moderate additions of older crustal material making the amount of crustal recycling very difficult to quantify. Within the SCZ-KMGS crystal fractionation of quartz dioritic and quartz monzodioritic magmas led to the production of larger volumes of granodiorite and monzogranite. As magmatism transgressed even further northward into the NEZ of the batholith, the production of alkaline and sub-alkaline shoshonitic magmas was due to increases in both the contribution from the enriched lithospheric mantle and the crust. The mafic-intermediate alkaline magmas of the NEZ-MS have very high Sr, Ba, and K_2O and similarly low although variable $\varepsilon Nd(t)$ values. These features suggest larger contributions from the enriched lithospheric mantle; however, the elevated FeO/MgO and low Ni and Cr in quartz monzodiorites suggest significant fractionation of ferromagnesian minerals and possibly the accumulation of Fe-Ti-oxides. The mixing of primitive alkaline magmas with crustal material or with other calc-alkaline magmas within the batholith were also probably important processes. The sub-alkaline NEZ-KMMS is interpreted to be derived by mixing of magmas similar to the 60-63 wt. % SiO_2 magmas of the SCZ-KMGS series with crustal melts producing large volumes of ~ 65 wt. % granodiorite with elevated K_2O, Rb, Y, Zr, Nb, Th and Pb. The similar Sr, Ba and range in $\varepsilon Nd(t)$ values to magmas in the SCZ-KMGS were also acquired from the enriched lithospheric mantle and the addition of crustal materials did not significantly effect these features. The youngest magmatism in the batholith was focussed along its southern margin. The granodiorites and monzogranites of the SCZ-MS have REE patterns and Nd isotopic signatures that are consistent with partial melting of La Ronge Domain crustal rocks. The melting was probably induced by the influx of large volumes of granodiorite along this zone.

In summary, the ca. 1865-1850 Ma plutonism in the Reindeer Lake area preserves remnants of an extensive and complex Proterozoic continental margin arc. The involvement of

depleted asthenosphere and enriched lithospheric mantle along with contributions from both old and juvenile crust were important in its petrogenesis.

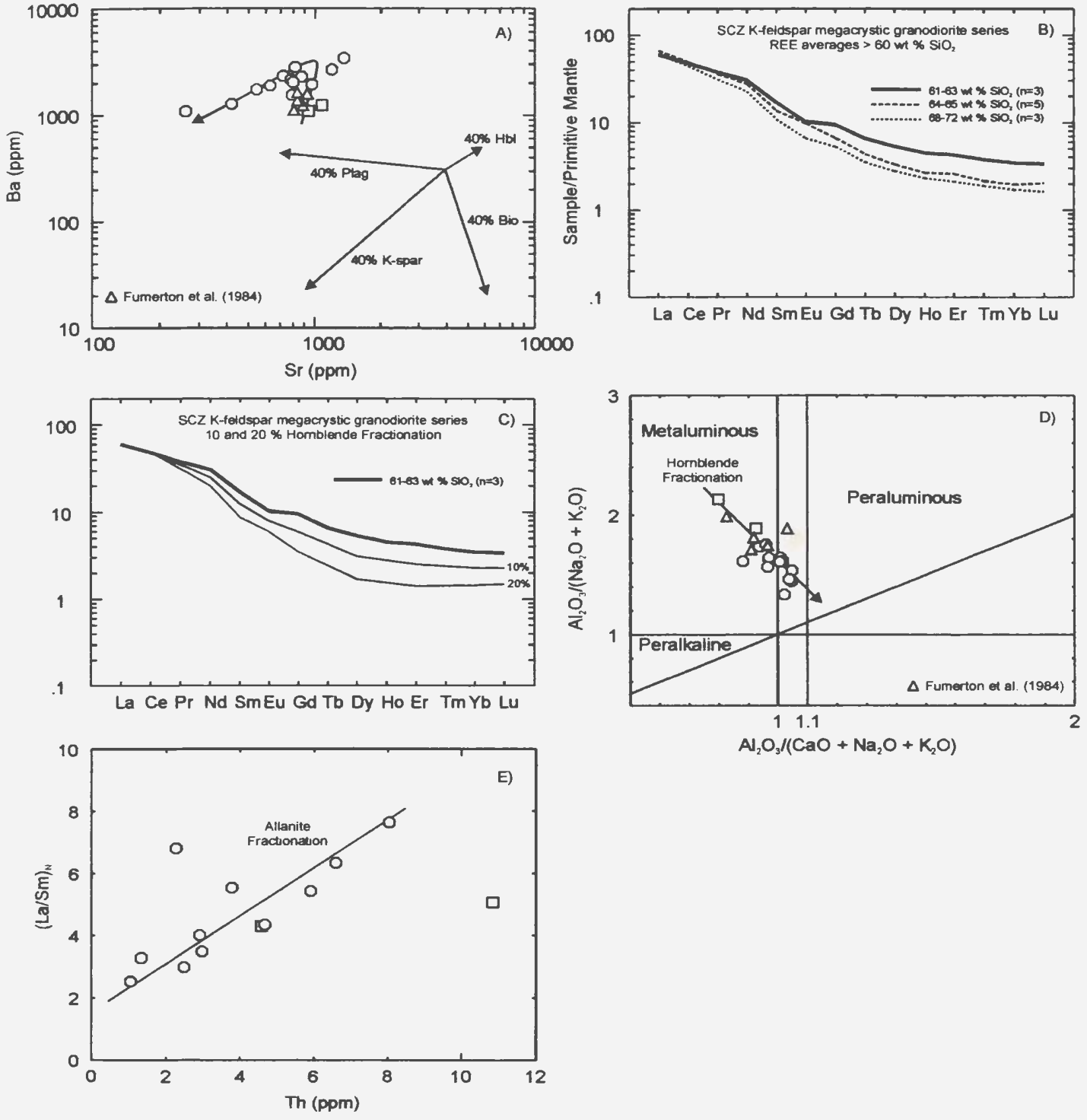

Figure 5.1 Major, trace and REE petrogenetic diagrams for the SCZ-KMGS. A) Ba versus Sr diagram with 40% fractional crystallization vectors for plag, K-spar, bio, and hbl, the vectors indicate the direction taken by residual magmas. B) 61-63; 64-65; and 68-72 wt % SiO_2 REE averages. C) 10 and 20% hornblende fractionation using the 61-63 wt % SiO_2 average as starting material. D) A/CNK versus A/NK plot. E) $(La/Sm)_N$ versus Th (ppm) plot.

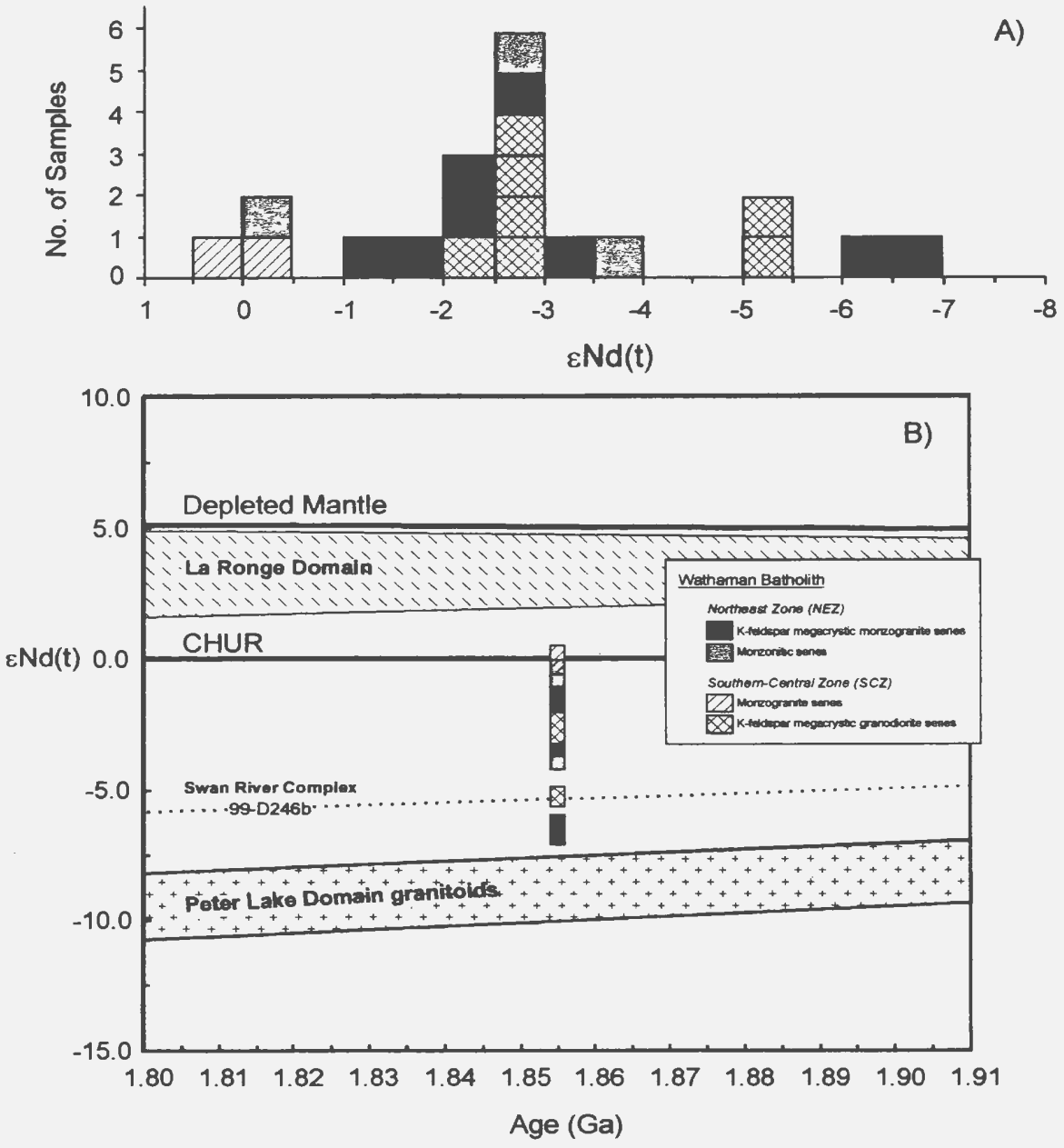

Figure 5.2 A) Frequency of εNd(t) values for granitoids of the Wathaman Batholith. The εNd values of most samples including all series except the SCZ monzogranite series are between -1 and -4. A significant number of values cluster between -2 and -3. B) εNd(t) versus Age (Ga) diagram for granitoids of the Wathaman Batholith (1855 Ma) and the La Ronge Domain (1858 Ma) from Reindeer Lake. The field for the La Ronge Domain includes: volcanics (n=3), and a greywacke (n=1) from Chauvel et al. (1986); volcanics (n=6) from Thom et al. (1990); a tonalite from the Crowe Island Complex (97-D373); and a dacite from the Central Metavolcanic Belt (97-D433) collected from Reindeer Lake (Corrigan et al., unpub. rept.). The field for Archean granitoids of the Peter Lake Domain includes: a tonalite from Chauvel et al. (1986); a tonalite from Bickford et al. (1990); and a foliated and recrystallized granodiorite from this study (99-D171). A gabbro from the Swan River Complex collected during this study is represented by the dotted line (99-D246b). The Depleted Mantle evolution curve is calculated using the equation $\varepsilon Nd_{(t)} = 8.6 - 1.91(t)$, where (t) is age (DePaolo et al., 1991)

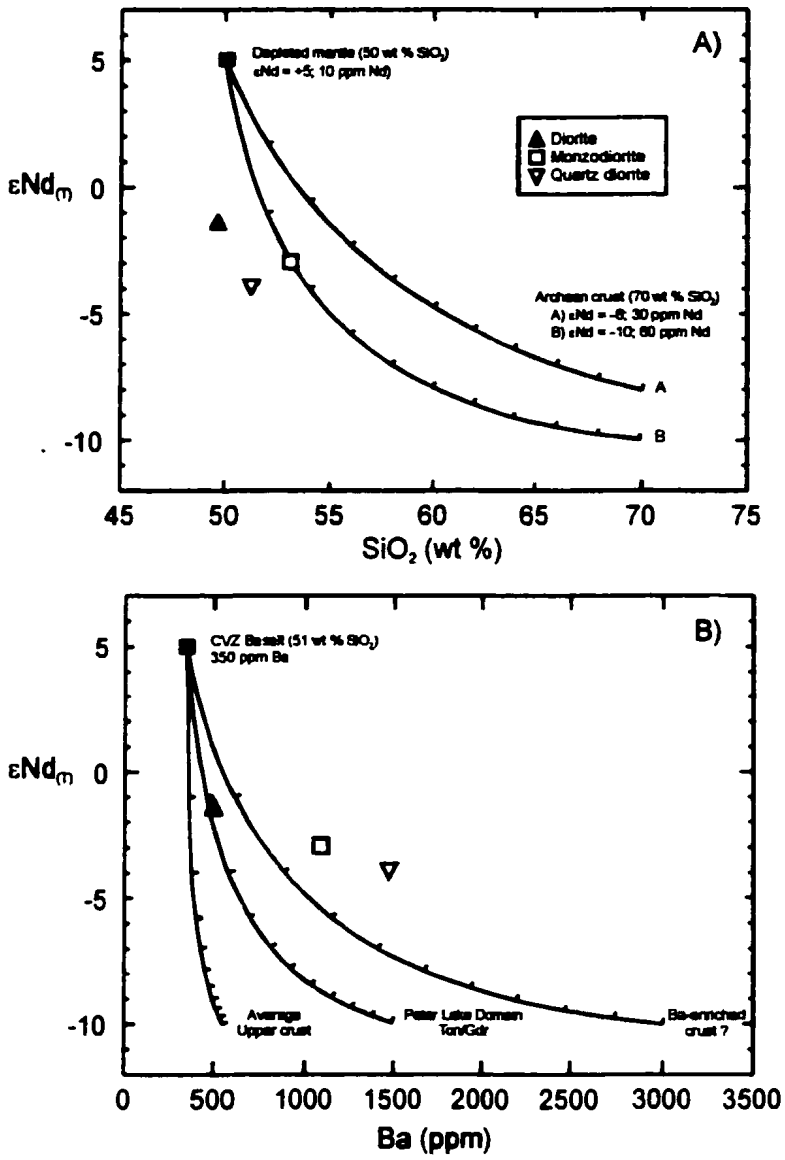

Figure 5.3 A) $\varepsilon Nd_{(t)}$ versus SiO_2 plot of primitive Wathaman Batholith magmas with two generated mixing curves between a depleted mantle end member and Archean continental crust with a variable Nd isotopic composition and Nd concentration. B) $\varepsilon Nd_{(t)}$ versus Ba plot of primitive Wathaman Batholith magmas with two generated mixing curves between a depleted mantle end member with Ba and SiO_2 contents equal to an average Andean basalt (Ewart, 1982) with: 1) average upper crust (Taylor and McLennan, 1985); 2) Peter Lake Domain granitoids; and 3) a hypothetical Archean Ba-rich crustal end member. Tick marks represent 10 % divisions.

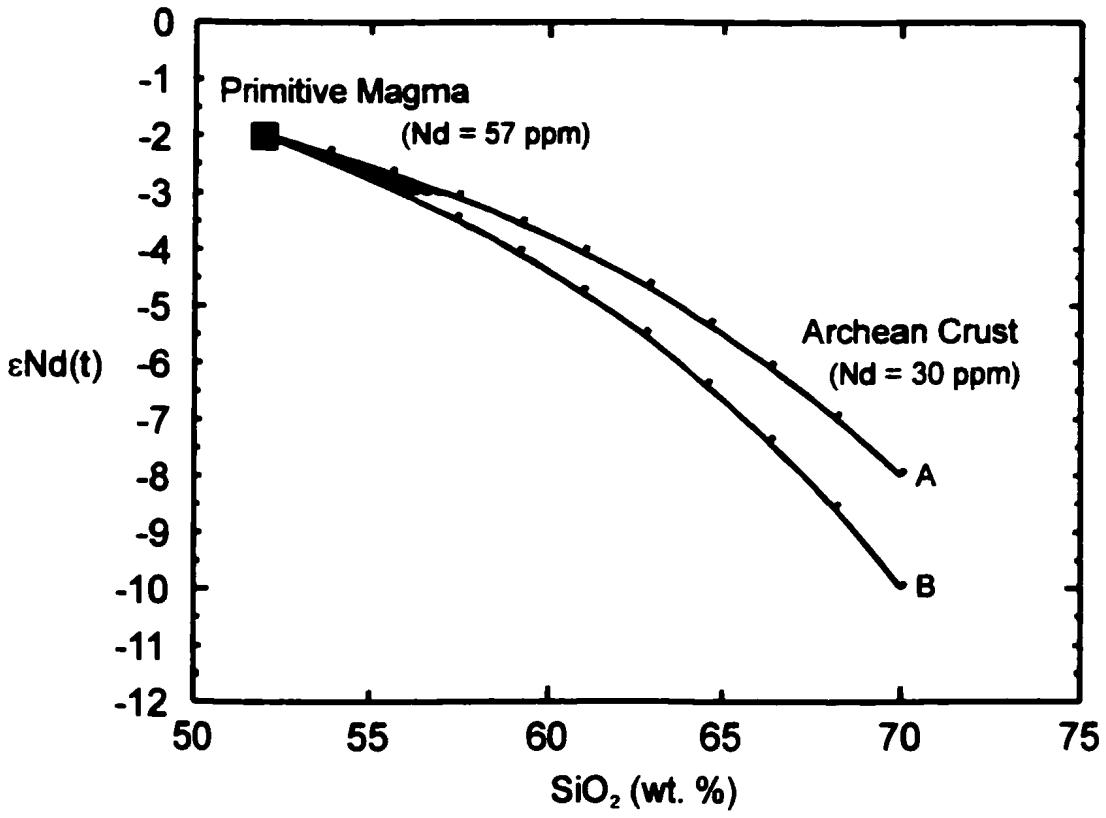

Figure 5.4 εNd(t) versus silica diagram showing mixing relationships between a primitive magma derived from an enriched lithospheric mantle source having an εNd(t) = -2.0 mixing with: A) Archean crust with εNd(1855) = -8.0; and B) gNd(1855) = -10.0. The primitive magma contains 57 ppm Nd and 52 wt. % silica, the Archean crust contains 30 ppm Nd and 70 wt. % silica. The shaded field indicates that between 20-30 % Archean crust can be added to the primitive magmas shifting the Nd isotopic composition 1 epsilon unit.

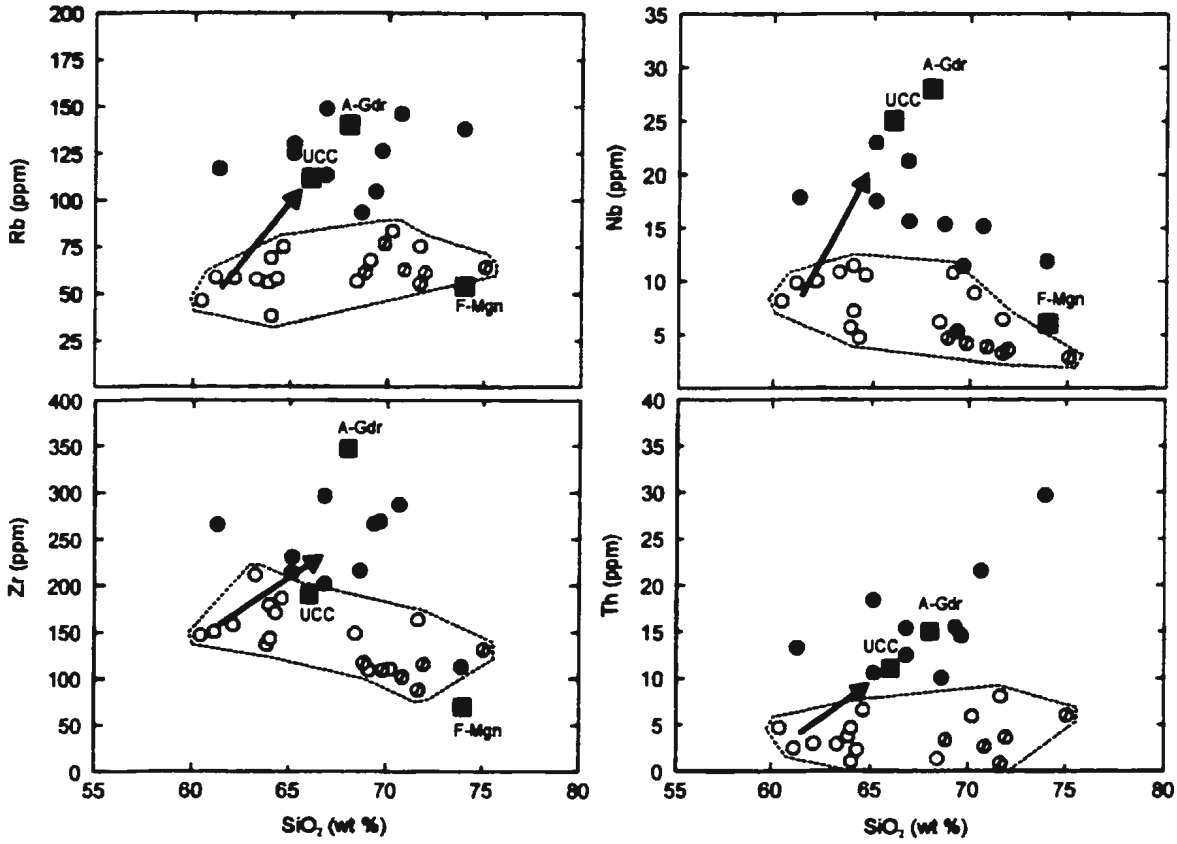

Figure 5.5 Selected trace element Harker variation diagrams for NEZ K-feldspar megacrystic monzogranite series. Also plotted are the SCZ granitoids (field) and possible crustal contaminants to SCZ magmas. UCC is the average upper crust from Taylor and McLennan (1985), A-Gdr is the average composition of the Within-plate type granitoids of the Peter Lake Domain, and F-Mgn is the average composition of the foliated and recrystallized tonalites and granodiorites of the Peter Lake Domain. Vectors indicate possible paths taken by crustally contaminated SCZ magmas.

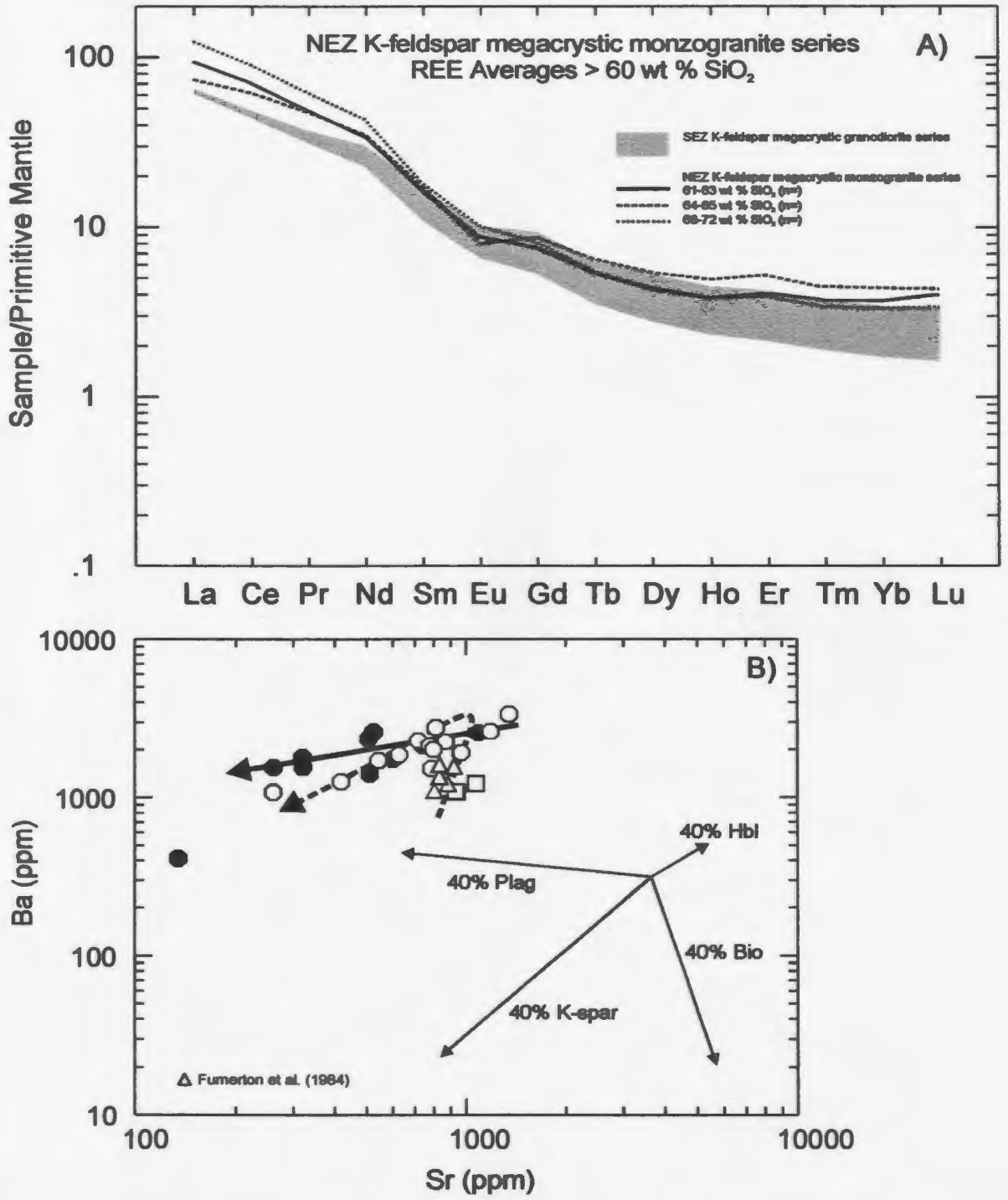

Figure 5.6 Primitive mantle normalized REE patterns for K-feldspar megacrystic granitoids from the NEZ and SCZ. The comparison field for the SCZ incloses the average REE patterns of the 61-63, 64-65 and 68-72 wt % SiO_2 groups. The average REE patterns of the same SiO_2 groups for the NEZ K-feldspar megacrystic granitoids are plotted. B) Ba versus Sr diagram for the NEZ and SCZ K-feldspar megacrystic granitoids. Fractional crystallization vectors (40 %) for plag, K-spar, bio and hbl are plotted and indicate the direction taken by the residual liquid after removal of the respective phase.

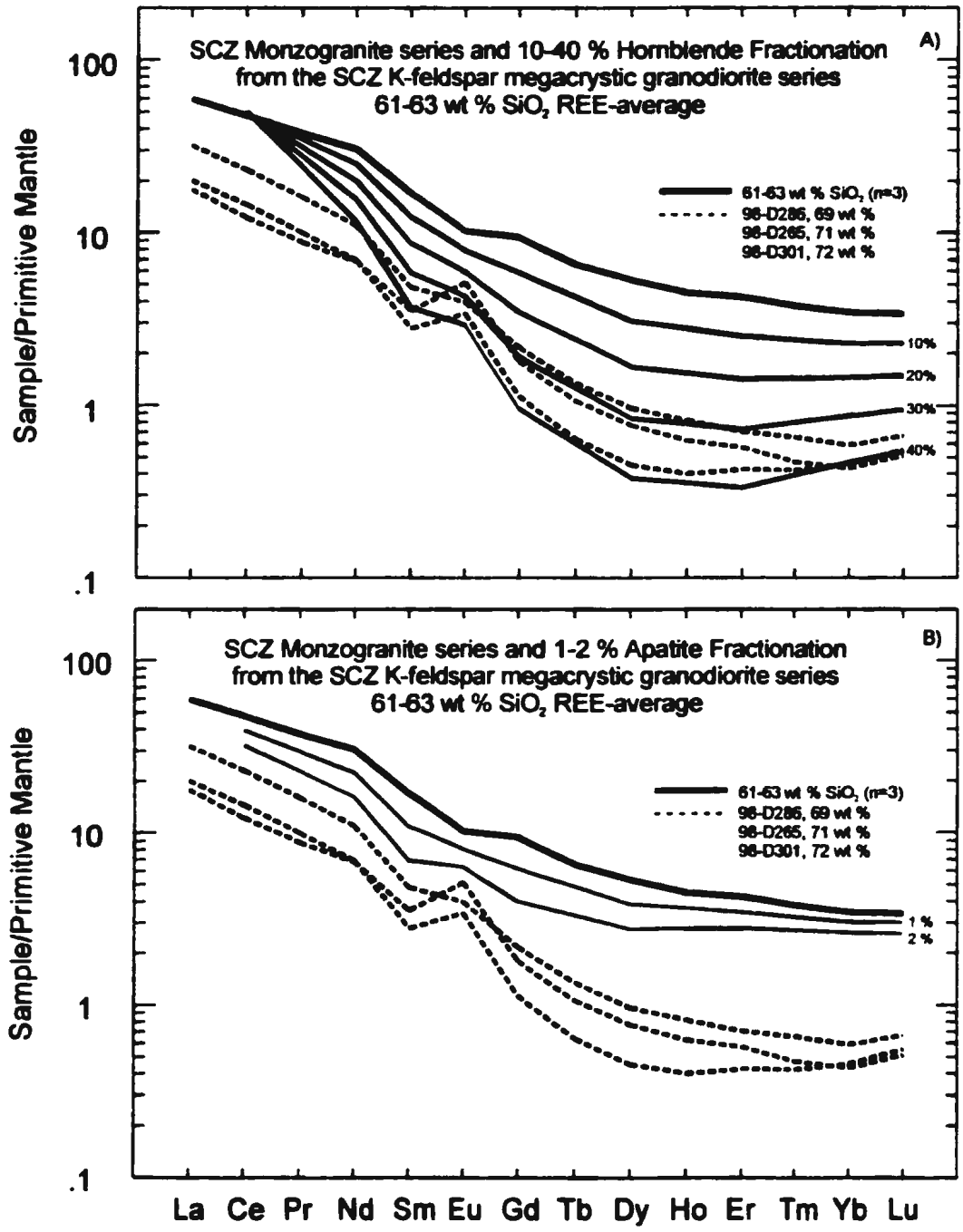

Figure 5.7 Primitive mantle normalized REE plots for the SCZ monzogranite series samples. A) Results of 10-40% fractional crystallization of hornblende from the SCZ K-feldspar megacrystic granodiorite series 61-63 wt % SiO_2 average. B) Results of 1 and 2 % fractional crystallization of apatite from the SCZ K-feldspar megacrystic granodiorite series 61-63 wt % SiO_2 average.

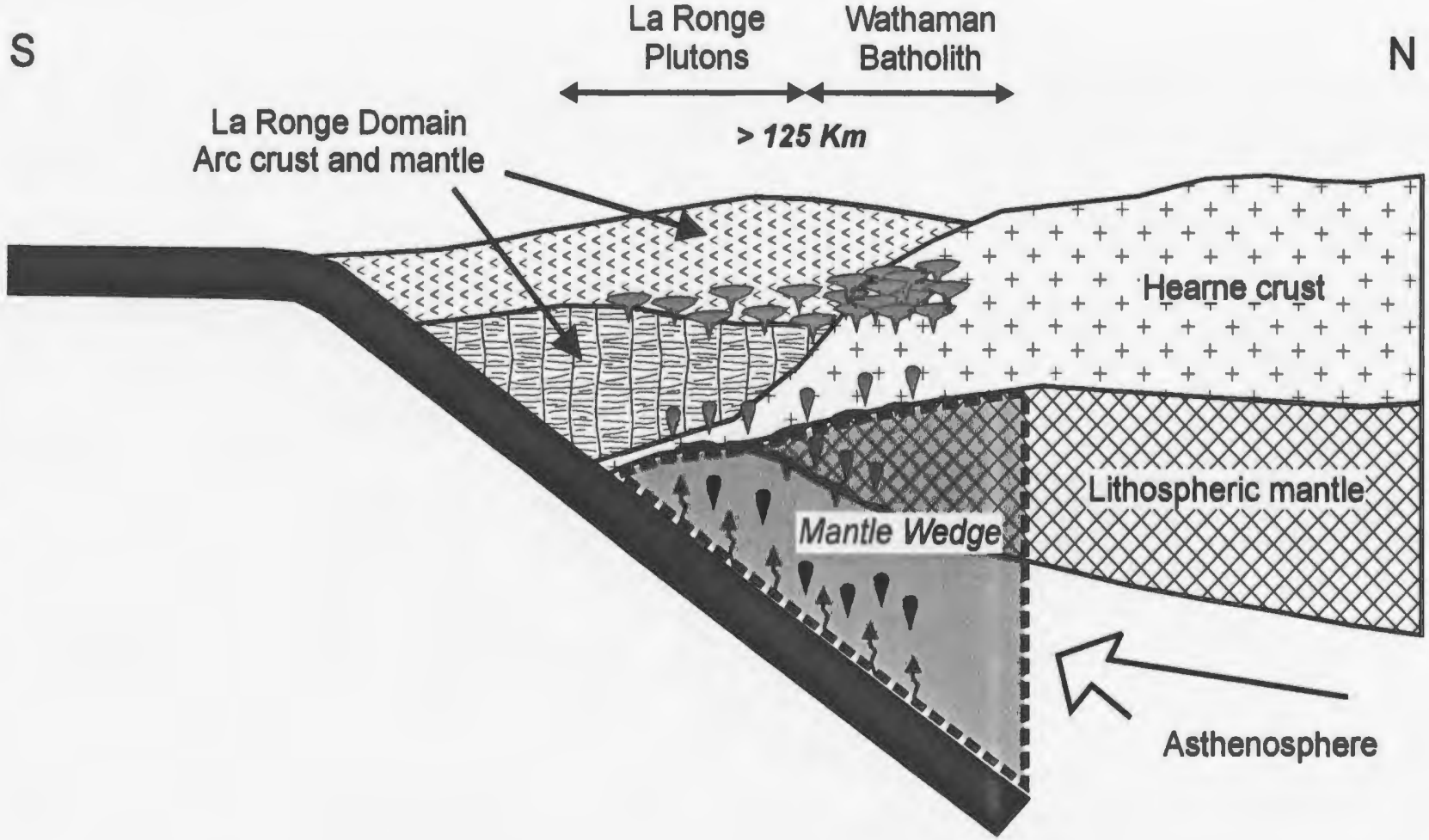

Figure 5.8 Schematic and vertically exaggerated tectonic diagram of the northwest Reindeer Zone and the southeastern Hearne Province during ca. 1865-1850 Ma subduction. The mantle wedge beneath the La Ronge Domain is composed of depleted asthenosphere and northward late Archean lithospheric mantle becomes an important component of the mantle wedge. The composition and thickness of the crust also changes from thin, mainly juvenile arc crust and mantle in the south to thicker Archean basement to the north. Some thinned under-thrust Archean crust may underlie the La Ronge Domain based on Nd isotopic arguments.

REFERENCES:

Alcock, F.J. 1938. Reindeer Lake south map area, Saskatchewan. Geological Survey of Canada, Paper 38-15, 17p.

Annesley, L.R., Madore, C. and Krogh, T.E. 1992. U-Pb Geochronology of Some Granitoids from the Peter Lake Domain: A Summary. *In* Summary of Investigations 1992. Saskatchewan Geological Survey, Saskatchewan Energy and Mines, Miscellaneous Report 92-4, pp. 168-171.

Ansdell, K.M., Lucas, S.B., Connors, K. and Stern, R.A. 1995. Kisseynew metasedimentary gneiss belt, Trans-Hudson orogen (Canada): Back-arc origin and collisional inversion. Geology, **23**: 1039-1043.

Ansdell, K., Corrigan, D., Stern R. and Maxeiner, R. 1999. Shrimp U-Pb geochronology from zircons from Reindeer Lake, Saskatchewan: Implications for timing of sedimentation and metamorphism in the northwestern Trans-Hudson Orogen (abstract), Geol. Assoc. Ca./Mineral. Assoc. Can., Joint Annual Meeting, May 26-28, Sudbury, Canada, p3.

Arth, J.G. 1976. Behaviour of trace elements during magmatic processes - a summary of theoretical models and their applications. J. Res. U.S. Geol. Surv., **4**: 41-47.

Ashton, K.E. 1999. A proposed lithotechtonic domainal re-classification of the southeastern Reindeer Zone in Saskatchewan. *In* Summary of Investigations 1999, Volume 1, Saskatchewan Geological Survey, Saskatchewan Energy and Mines, Miscellaneous Report 99-4, pp.92-100.

Atherton, M.P. 1993. Granite magmatism. Journal of the Geological Society, London, **150**: 1009-1023.

Baldwin, D.A., Syme, E.C., Zwanzig, H.V., Gordon, T.M., Hunt, P.A., and Stevens, R.D. 1987. U-Pb zircon ages from the Lynn Lake and Rusty Lake metavolcanic belts, Manitoba: two ages of Proterozoic magmatism. Canadian Journal Earth Sciences, **24**: 1053-1063.

Bennett, V.C., and DePaolo, D.J. 1987. Proterozoic crustal history of the western United States as determined by neodymium isotopic mapping. Geological Society of America Bulletin, **99**: 674-685.

Bickford, M.E., Van Shmus, W.R., Macdonald, R., Lewry, J.F., and Pearson, J.G. 1986. U-Pb zircon geochronolgy project for the Trans-Hudson Orogen: Current sampling and recent results. *In* Summary of Investigations 1986, Saskatchewan Geological Survey, Saskatchewan Energy and Mines, Miscellaneous Report 86-4, pp. 101-107.

Bickford, M.E., Van Schmus, W.R., Collerson, K.D., and Macdonald, R. 1987. U-Pb zircon geochronology project: New results and interpretations. *In* Summary of Investigations

1987, Saskatchewan Geological Survey, Saskatchewan Energy and Mines, Miscellaneous Report 87-4, pp. 76-79.

Bickford, M.E., Collerson, K.D., Lewry, J.F., and Orrell, S.E. 1992. Pegmatites and Leucogranites as Probes of Crust Beneath Allochthonous Orogenic Rocks in the Glennie and La Ronge Domains. *In* Summary of Investigations 1992, Saskatchewan Geological Survey, Saskatchewan Energy and Mines, Miscellaneous Report 92-4, pp. 124-129.

Bickford, M.E., Collerson, K.D., Lewry, J.F., Van Schmus, W.R., and Chiarenzelli, J.R. 1990. Proterozoic collisional tectonism in the Trans-Hudson orogen, Saskatchewan. Geology, **18**: 14-18.

Boily, M., Brooks, B., and Ludden, J.N. 1989. Chemical and Isotopic Evolution of the Coastal Batholith of Southern Peru. Journal of Geophysical Research, **94**: 12,483-12,498.

Carmichael, I.S.E., Turner, F.J., and Verhoogen, J. 1974. Igneous Petrology. McGraw-Hill, Inc. United States of America.

Chauvel, C., Arndt, N.T., Kielinzcuk, S., and Thom, A. 1987. Formation of Canadian 1.9 Ga old continental crust. I: Nd isotopic data. Canadian Journal of Earth Sciences, **24**: 396-406.

Cheesman, R.L. 1959. The Geology of the Wapus Bay Area (west half), Saskatchewan. Saskatchewan Department of Mineral Resources, Report 35, 22p.

Chiarenzelli, J.R. 1989. The Nistowiak and Guncoat gneisses: implications for the tectonics of the Glennie and La Ronge domains, northern Saskatchewan, Canada. Ph.D. thesis, University of Kansas, Lawrence.

Clarke, D.B. 1992. Granitoid Rocks. Chapman and Hall, London.

Corrigan, D., Bashforth, A., and Lucas, S. 1997. Geology and Structural Evolution of the La Ronge-Lynn Lake Belt in the Butler Island Area (parts of 64D-9 and -10), Reindeer Lake, Saskatchewan. *In* Summary of Investigations 1997, Saskatchewan Geological Survey, Saskatchewan Energy and Mines, Miscellaneous Report 97-4, pp. 18-30.

Corrigan, D., Maxeiner, R.O., Bashforth, A., and Lucas, S.B. 1998a. Preliminary report on the geology and tectonic history of the Trans-Hudson Orogen in the northwestern Reindeer Zone, Saskatchewan. *In* Current Research, Part C; Geological Survey of Canada, Paper 98-1C, pp. 95-106.

Corrigan, D., MacHattie, T.G., Piper, L., Wright, D., Pehrsson, S., Lassen, B., and Chakungal, J. 1998b. La Ronge-Lynn Lake Bridge Project: New Mapping Results from Deep Bay (parts 64D-6 and -7) to North Porcupine Points of 64E-7 and -8), Reindeer Lake. *In* Summary of Investigations 1998, Saskatchewan Energy and Mines, Miscellaneous Report 98-4, pp.111-122.

Corrigan, D., MacHattie, T.G., and Chakungal, J. 1999b. The Wathaman Batholith and its relation to the Peter Lake Domain: Insights from recent mapping along the Reindeer Lake Transect, Trans-Hudson Orogen. *In* Summary of Investigations 1999, Volume 2, Saskatchewan Geological Survey, Saskatchewan Energy and Mines, Miscellaneous Report 99-4.2, pp.132-142.

Corrigan, D., Pehrsson, S.J., MacHattie, T.G., Piper, L., Wright, D., Lassen, B., and Chakungal, J. 1999a. Lithotectonic framework of the Trans-Hudson Orogen in the northwestern Reindeer Zone, Saskatchewan: an update from recent mapping along the Reindeer Lake transect. *In* Current Research 1999-C; Geological Survey of Canada, pp. 169-178.

Cousens, B.L., Aspler, L.B., Chiarenzelli, J.R., Donaldson, J.A., Sandeman, H., Peterson, T.D. and LeCheminant, A.N. 2001. Enriched Archean lithosperic mantle beneath Western Churchill Province tapped during Paleoproterozoic orogeesis. *In press*.

Davidson, J.P., Harmon, R.S., Worner, G. 1991. The source of central Andean magmas; Some considerations. Geological Society of America, Special Paper **265**.

Davidson, J.P., McMillan, N.J., Moorbath, S., Worner, G., Harmon, R.S., and Lopez-Escobar, L. 1990. The Nevados de Payachata volcanic region (18° S/69° W, N. Chile) II. Evidence for widespread crustal involvement in Andean magmatism. Contributions to Minerology and Petrology 1990, pp.412-432.

DePaolo, D.J., and Wasserburg, G.J., 1979. Petrogenetic mixing models and Nd-Sr isotopic paterns. Geochim. Cosmochim. Acta, **43**: 615-627.

DePaolo, D.J. 1981b. Trace Element and Isotopic Effects of Combined Wallrock Assimilation and Fractional Crystallization. Earth and Planetary Science Letters, **53**: 189-202.

DePaolo, D.J. 1981a. A Neodymium and Strontium Isotopic Study of the Mesozoic Calc-Alkaline Granitic Batholiths of the Sierra Nevada and Peninsular Ranges, California. Journal of Geophysical Reasearch, **86**: 10470-10488.

DePaolo, D.J. 1991. The Continental Crustal Age Distribution: Methods of Determining Mantle Separation Ages From Sm-Nd Isotopic Data and Application to the Southwestern United States. Journal of Geophysical Research, **96**: 2071-2088.

Ewart, A. 1982. The mineralogy petrology of Tertiary-Recent orogenic volcanic rocks: with special reference to the andesitic-basaltic compositional range. *Edited by* Thorpe, R.S. *In* Andesites: orogenic andesites and related rocks, 26-27. Chichester: Wiley.

Farmer, G.L., and DePaolo, D.J. 1983. Origin of Mesozoic and Tertiary Granite in the Western United States and Implications for Pre-Mesozoic Crustal Structure 1. Nd and Sr Isotopic Studies in the Geocline of the Northern Great Basin. Journal of Geophysical Research, **88**: 3379-3401.

Faure, G. 1986. Principles of Isotope Geology (second edition). John Wiley and Sons, New York.

Fossenier, K., Delaney, G.D., and Watters, B.R. 1994. Lithogeochemical Investigation of Volcanic Rocks and Age of Their Host Sediments, Lower Proterozoic Courtenay Lake-Cairns Lake Fold Belt, Courtenay Lake, Saskatchewan. *In* Summary of Investigations 1994, Saskatchewan Geological Survey, Saskatchewan Energy and Mines, Miscellaneous Report 94-4. pp. 63-69.

Fujimaki, H. 1986. Partition coefficients of Hf, Zr, and REE between zircon, apatite, and liquid. Contributions to Mineralogy and Petrology, **94**: 42-45.

Fumerton, S.L., Stauffer, M.R., and Lewry, J.F. 1984. The Wathaman batholith: largest known Precambrian pluton. Canadian Journal of Earth Sciences, **21**: 1082-1097.

Gilboy, C.F. 1975. Project 8: Foster Lake area. *In* Summary of Investigations 1975. *Edited by* J.E. Christopher and R.M. Macdonald. Saskatchewan Department of Mineral Resources.

Gilboy, C.F. 1980. Geology of the Reindeer Lake South (southeast) Area (NTS area 64D-SE). Saskatchewan Department of Mineral Resources, Report 198, 62p.

Govindaraju, K. 1989. Geostand. News. **13**, p.11.

Gromet, L.P., and Silver, L.T. 1983. Rare earth element distributions among minerals in a granodiorite and their petrogenetic implications. Geochimica et Cosmochimica Acta, **47**: 925-939.

Gromet, L.P., and Silver, L.T. 1987. REE Variations Across the Peninsular Ranges Batholith: Implications for Batholith Petrogenesis and Crustal Growth in Magmatic Arcs. Journal of Petrology, **28**: 75-125.

Hanson, G.N. 1978. The application of Trace Elements to the Petrogenesis of Igneous Rocks of Granitic Composition. Earth and Planetary Science Letters, **38**: 26-43.

Harper, C.T. 1996. La Ronge-Lynn Lake Bridge Project: Sucker Lake-Fleming Lake Area. *In* Summary of Investigations 1996, Saskatchewan Geological Survey, Saskatchewan Energy and Mines, Miscellaneous Report 96-4, pp. 66-78.

Harper, C.T. 1997. Sucker Lake-Fleming Lake update. *In* Summary of Investigations 1997, Saskatchewan Geological Survey, Saskatchewan Energy and Mines, Miscellaneous Report 97-4, pp. 42-50.

Harper, C.T. 1998. The La Ronge Domain-Glennie Domain transition: Street Lake area (parts of NTS 64D-3 and -6). *In* Summary of Investigations 1998, Saskatchewan Geological Survey, Saskatchewan Energy and Mines, Miscellaneous Report 98-4, pp.66-80.

Harper, C.T. 1999. Geology and mineral potential of the northwest margin of the Central Metavolcanic Belt, May Lake area (part of 64D-5). *In* Summary of Investigations 1999, Volume 2, Saskatchewan Geological Survey, Saskatchewan Energy Mines, Miscellaneous Report 99-4.2, pp.181-195.

Heaman, L.M., Kamo, S.L., Delaney, G.D., Harper, C.T., Reilly, B.A., Slimmon, W.L., and Thomas, D.J. 1991. U-Pb geochronological investigations in the Trans-Hudson Orogen, Saskatchewan: Preliminary results by the ROM Laboratory in 1990-91. *In* Summary of Investigations 1991, Saskatchewan Geological Survey, Saskatchewan Energy and Mines, Miscellaneous Report 91-4, pp.74-75.

Heaman, L.M., Kamo, S.L., Ashton, K.E., Reilly, B.A., Slimmon, W.L., and Thomas, D.J. 1992. U-Pb Geochronological Investigations in the Trans-Hudson Orogen, Saskatchewan. *In* Summary of Investigations 1992, Saskatchewan Geological Survey, Saskatchewan Energy and Mines, Miscellaneous Report 92-4, pp. 120-123.

Hildreth, W., and Moorbath, S. 1988. Crustal contributions to arc magmatism in the Andes of Central Chile. Contrib Mineral Petrol, **98**: 455-489.

Horan, P. 1998. Rb/Sr and Sm/Nd isotopic analyses procedure. Internal report, Atlantic Universities Radiogenic Isotope Facility (AURIF), Memorial University of Newfoundland, St. John's.

Hoffman, P.F. 1988. United plates of America, the birth of a craton: Early Proterozoic assembly and growth of Laurentia. Annual Reviews of Earth and Planetary Science, **16**: 543-603.

Irvine, T.N., and Baragar, W.R.A. 1971. A guide to the chemical classification of the common volcanic rocks. Canadian Journal of Earth Sciences, **8**: 523-548.

Janser, B.W. 1994. The Star Lake Pluton, LaRonge Domain, northern Saskatchewan: petrogenesis of a Proterozoic island-arc pluton. Precambrain Research, **70**: 145-164.

Jenner, G.A., Longerich, H.P., Jackson, S.E., Fryer, B.J. 1990. ICP-MS - A powerful tool for high-precision trace-element analysis in Earth Sciences: evidence from analysis of selected U.S.G.S. reference samples. Chemical Geology, **83**: 133-148.

Johnston, W.G.O. 1983. Geology of the Southend area. Saskatchewan Energy and Mines, Open Files Report 82-4, 151p.

Johnston, W.G.O., and Thomas, M.W. 1984. Compilation Bedrock Geology Series, Reindeer Lake South, NTS area 64D. Saskatchewan Energy and Mines, Report 230, 1:250 000 scale map with marginal notes.

Krogh, T.E., and Clark, L.A. 1987. Zircon dating of sub-Athabasca granitoid rocks, Saskatchewan. Geological Association of Canada - Mineralogical Association of Canada., Annual Meeting Abstract, p. 64.

Lafrance, B., and Varga, M. 1996. Structural studies of the Parker Lake shear zone and the Reilly Lake shear zone, Reindeer Lake. *In* Summary of Investigations 1996, Saskatchewan Geological Survey, Saskatchewan Energy and Mines, Miscellaneous Report 96-4, pp.119-124.

Langmuir, C.H., Vocke, R.D., Hanson, G.N., and Hart, S.R. 1978. A general mixing equation with applications of Icelandic basalts. Earth Planet. Sci. Letters, **37**: 380-392.

Leake, B.E. 1990. Granite magmas: their sources, initiation and consequences of emplacement. Journal of Geological Society, London, **147**: 579-589.

LeMaitre, R.W. 1976. Some Problems of the Projection of Chemical Data into Mineralogical Classifications. Contribution to Mineralogy and Petrology, **56**: 181-189.

Lewry, J.F. 1976. Reconnaissance geological mapping of the Reindeer Lake North (SW quarter) area. *In* Summary of Investigations 1976. *Edited by* J.E. Christopher and R. Macdonald. Saskatchewan Department of Mineral Resources.

Lewry, J.F., and Sibbald, T.I.I. 1980. Thermotectonic Evolution of the Churchill Province in Northern Saskatchewan. Technophysics, **68**: 45-82.

Lewry, J.F., and Stauffer, M.R. 1990. The Early Proterozoic Trans-Hudson Orogen of North America. The Geological Association of Canada, Special Paper 37.

Lewry, J.F., Thomas, D.J., Macdonald, R., and Chiarenzelli, J. 1990. Structural relations in accreted terranes of the Trans-Hudson Orogen, Saskatchewan: Telescoping in a collisional regime? *In* The Early Proterozoic Trans-Hudson Orogen of North America. *Edited by* J.F. Lewry and M.R. Stauffer, Geological Association of Canada, Special Paper 37, pp. 75-94.

Lewry, J.F., Stauffer, M.R., and Fumerton, S. 1981. A Cordilleran-Type Batholithic Belt in the Churchill Province in Northern Saskatchewan. Precambrian Research, **14**: 277-313.

Liew, T.C., and McCulloch, M.T. 1985. Genesis of granitoid batholiths of Peninsular Malaysia and implications for models of crustal evolution: Evidence from a Nd-Sr isotopic and U-Pb zircon study. Geochimica et Cosmochimica Acta, **49**: 587-600.

Longerich, H.P. 1995. Analysis of Pressed Pellets of Geological Samples Using Wavelength-Dispersive X-Ray Fluorescence Spectrometry. X-Ray Spectrometry, **24**: 000-000.

Longerich, H.P., Jenner, G.A., Fryer, B.J., and Jackson, S.E. 1990. Inductively coupled plasma-mass spectrometric analysis of geological samples: A critical evaluation base on case studies. Chemical Geology, **83**: 105-118.

Macdonald, R., and Thomas, M.W. 1983. Compilation Bedrock Geology, Reindeer Lake North, NTS Area 64E. Saskatchewan Energy and Mines, Report 232 (1:250 000 scale map with marginal notes)

MacDougall, D.G. 1988. Bedrock geological mapping, Patterson Island area, Reindeer Lake (part of NTS 64E-10). *In* Summary of Investigations 1988, Saskatchewan Geological Survey, Saskatchewan Energy and Mines, Miscellaneous Report 88-4, pp.61-66.

MacLachlan, K., and Dunning, G.R. 1998. U-Pb ages and technomagmatic relationships of early Ordovician low-Ti tholeiites, boninites and related plutonic rocks in central Newfoundland, Canada. Contributions to Mineralogy and Petrology, **133**: 235-258.

MacNeil, A. 1998. The Courtenay Lake Formation in the Cook Lake Area-Wollaston Domain, Saskatchewan, Unpublished B.Sc. thesis, University of Saskatchewan, 55p.

Maniar, P.D., and Piccoli, P.M. 1989. Tectonic discrimination of granitoids. Geological Society of America Bulletin, **101**: 635-643.

Maxeiner, R.O. 1996. Bedrock Geology of the Henry Lake Area (parts of NTS 64D-6 and -11), Northern La Ronge Domain. *In* Summary of Investigations 1996, Saskatchewan Geological Survey, Saskatchewan Energy and Mines, Miscellaneous Report 96-4, pp. 51-65.

Maxeiner, R.O. 1997. Geology of the Lawrence Bay (Reindeer Lake) Area, Northeastern La Ronge Domain. *In* Summary of Investigations 1997, Saskatchewan Geological Survey, Saskatchewan Energy and Mines, Miscellaneous Report 97-4, pp. 3-17.

Maxeiner, R.O. 1998. Geology of the Birch Point (Reindeer Lake) area, northeastern La Ronge Domain. *In* Summary of Investigations 1998, Saskatchewan Geological Survey, Saskatchewan Energy and Mines, Miscellaneous Report 98-4, pp.81-99.

Maxeiner, R.O. 1999. La Ronge-Lynn Lake Bridge: Geology of the Wapus Bay-Lowdermilk Bay (Reindeer Lake) area. *In* Summary of Investigations 1999, Volume 2, Saskatchewan Geological Survey, Saskatchewan Energy and Mines, Miscellaneous Report 99-4.2, pp.143-158.

Meyer, M.T., Bickford, M.E., and Lewry, J.F. 1992. The Wathaman batholith: An Early Proterozoic continental arc in the Trans-Hudson orogenic belt, Canada. Geological Society of America Bulletin, **104**: 1073-1085.

Morris, G.A., Larson, P.B., and Hooper, P.R. 2000. 'Subduction Style' Magmatism in a Non-subduction Setting: the Colville Igneous Complex, NE Washington State, USA. Journal of Petrology, **41**: 43-67.

Nelson, B.K., and DePaolo, D.J. 1984. 1,700-Myr greenstone volcanic successions in southwestern North America and isotopic evolution of Proterozoic mantle. Nature, **312**

Peacock, M.A. 1931. Classification of igneous rocks. Journal of Geology, **39**: 54-67.

Patchett, P.J., and Bridgwater, D. 1984. Origin of continental crust of 1.9-1.7 Ga age defined by Nd isotopes in the Ketilidian terrain of South Greenland. Contrib Mineral Petrol, **87**: 311-318.

Peccerillo, A., and Taylor, S.R. 1976. Geochemistry of Ecocene calc-alkaline volcanic rocks in the Kastamonu area, Northern Turkey. Contributions to Mineralogy and Petrology, **58**: 63-81.

Pitcher, W.S. 1997. The Nature and Origin of Granite (second edition). Chapman & Hall, London.

Potter, D. 1979. Investigations of basic igneous rocks, Peter Lake Domain. *In* Summary of Investigations 1979, Saskatchewan Geological Survey, Saskatchewan Department of Mineral Resources, Miscellaneous Report 79-10, pp.56-60.

Pyke, M.W. 1960. The Geology of the Wapus Bay Area (east half), Saskatchewan. Saskatchewan Department of Mineral Resources, Report 40, 32p.

Ray, G.E., and Wanless, R.K. 1979. The age and geological history of the Wollaston, Peter Lake, and Rottenstone domains in northern Saskatchewan. Canadian Journal of Earth Sciences, **17**: 333-347.

Rollinson, H, R. 1993. Using Geochemical data: Evaluation, Presentation, Interpretation. Longman, England.

Samson, S.D., Patchett, P.J., and McClelland, W.C. 1991. Nd and Sr isotopic constraints on the petrogenesis of the west side of the northern Coast Mountain batholith, Alaskan and Canadian Cordillera. Canadian Journal Earth Science, **28**: 939-946.

Saunders, A.D., Norry, M.J., and Tarney, J. 1991. Fluid influence on the trace element compositions of subduction zone magmas. Phil. Trans. R. Soc. Lond., **A335**: 377-392.

Sawka, W.N. 1988. REE and trace element variations in accessory minerals and hornblende from the strongly zoned McMurry Meadows Pluton, California. Transactions of the Royal Society of Edinburgh: Earth Sciences, **79**: 157-168.

Shklanka, R. 1962. The Geology of the MacLean Bay Area, Saskatchewan. Saskatchewan Department of Mineral Resources, Report 74 (map with marginal notes).

Sibbald, T.I.I. 1977. The geology of the Milton Island area (west half). Saskatchewan Department of Mineral Resources, Report 153, 38p.

Stauffer, M.R. 1984. Manikewan: An Early Proterozoic ocean in Central Canada, Its Igneous History and Orogenic Closure. Precambrian Research, **25**: 257-281.

Stauffer, M.R., Fumerton, S.L., Coleman, L.C., Mossman, D.J., and Langford, F.F. 1981. Geology of the Ballentin Island vicinity, Reindeer Lake (parts of NTS area 64 E-NE).

Saskatchewan Geological Survey, Report 206.

Stauffer, M.R., Langford, F.F., Coleman, L.C., and Mossman, D.J. 1979. Geology of the area around Amiskit Island, Reindeer Lake (part of NTS area 64D-NE). Saskatchewan Department of Mineral Resources, Report 191, 21p.

Stauffer, M.R., Langford, F.F., Coleman, L.C., and Mossman, D. 1980. Geology of the Reindeer Lake north (southeast) area. Saskatchewan Geological Survey, Report 200.

Stauffer, M.R., and Lewry, J.F. 1993. Regional setting and kinematic features of the Needle Falls Shear Zone, Trans-Hudson Orogen. Canadian Journal of Earth Science, **30**: 1338-1354.

Stern, R.A., Gilbert, N.H., and Shirey, S.T. 1989. Petrogenesis of mantle-derived, LILE-enriched Archean monzodiorites and trachyandesites (sanukitoids) in southwestern Superior Province. Canadian Journal of Earth Science, **26**: 1688-1712.

Stern, R.A., and Hanson, G.N. 1991. Archean High-Mg Granodiorite: A Derivative of Light Rare Earth Element-enriched Monzodiorite of Mantle Origin. Journal of Petrology, **32**: 201-238.

Stockwell, C.H. 1929. Reindeer Lake area, Saskatchewan and Manitoba. Geological Survey of Canada, Summary Report, pp.46-72.

Streckeisen, A.L. 1976. To each plutonic rock its proper name. Earth Science Reviews, **12**: 1-33.

Sun, S., and McDonough, W.F. 1989. Chemical and isotopic systtematics of oceanic basalts: implications for mantle composition and processes. *In* Magmatism in the Ocean Basins. *Edited by* Saunders, A.D., and Norry, M.J., Geological Society Special Publication 42, pp. 313-345.

Syme, E.C. 1990. Stratigraphy and Geochemistry of the Lynn Lake and Flin Flon Metavolcanic Belts, Manitoba. *In* The Early Proterozoic Trans-Hudson Orogen of North America: Geological Association of Canada. *Edited by* Lewry, J.F. and Stauffer, M.R., Special Paper 37, pp. 143-161.

Taylor, S.R., and McLennan S.M. 1985. The Continental Crust: its Composition and Evolution. Blackwell, Oxford.

Thom, A., Arndt, N.T., Chauvel, C., and Stauffer, M. 1990. Flin Flon and Western La Ronge Belts, Saskatchewan: Products of Proterozoic Subduction-related Volcanism. *In* The Early Proterozoic Trans-Hudson Orogen of North America: Geological Association of Canada. *Edited by* Lewry, J.F., and Stauffer, M.R., Special Paper 37, pp. 163-175.

Theriault, R.J. and Tella, S. 1997. Sm-Nd isotopic study on mafic volcanic rocks from the Rainken Inlet and Tavani regions, District of Keewatin, Northwest Territories. Geological Survey of Canada, Current Research Paper 1997-F, P. 61-66.

Theriault, R.J., and Ermanovics, I. 1997. Sm-Nd isotopic and geochemical characterisation of the Paleoproterozoic Torngat orogen, Labrador, Canada. Precambrian Research, **81**: 15-35.

Thomas, D.J. 1985. Geological Mapping Roundish-Bervin Lakes Area (part of NTS 73P-15 and -16). *In* Summary of Investigations 1985, Saskatchewan Geological Survey; Saskatchewan Energy and Mines, Miscellaneous Report 85-4, pp. 18-27.

Thomas, D.J. 1993. Geology of the Star Lake-Otter Lake Portion of the Central Metavolcanic Belt, La Ronge Domain. Saskatchewan Energy and Mines, Report 236, 132p.

Van Schmus, W.R., and Bickford, M.E. 1984. Preliminary U-Pb Age Data for the Trans-Hudson Orogen in Northern Saskatchewan. *In* Summary of Investigations 1984, Saskatchewan Geological Survey, Saskatchewan Energy and Mines, Miscellaneous Report 84-4, pp. 81-85.

Van Schmus, W.R., Bickford, M.E., Lewry, J.F., and MacDonald, R. 1987. U-Pb geochronology in the Trans-Hudson Orogen, northern Saskatchewan, Canada. Canadian Journal of Earth Sciences, **24**: 407-424.

Vernon, R.H. 1983. K-feldspar Megacrysts in Granites - Phenocrysts, not Porphyroblasts. Earth Science Reviews, **23**: 1-63.

Watters, B.R. 1984. Geochemical Patterns for Metavolcanic Rocks of the La Ronge Domain. *In* Summary of Investigations 1984, Saskatchewan Geological Survey, Saskatchewan Energy and Mines, Miscellaneous Report 84-4, pp. 88-91.

Watters, B.R. 1985. Geochemistry of Metavolcanic and Plutonic Rocks, Star Lake and Waddy Lake Areas. *In* Summary of Investigations 1985, Saskatchewan Geological Survey, Saskatchewan Energy and Mines, Miscellaneous Report 85-4, pp. 28-34.

Watters, B.R. 1986. Geochemistry and Geochronology of Metavolcanic and Plutonic Rocks in the Central Metavolcanic Belt. *In* Summary of Investigations 1986, Saskatchewan Geological Survey, Saskatchewan Energy and Mines, Miscellaneous Report 86-4, pp. 76-83.

Watters, B.R., and Pearce, J.A. 1987. Metavolcanic rocks of the La Ronge Domain in the Churchill Province, Saskatchewan: geochemical evidence for a volcanic arc origin. *In* , Geochemistry and Mineralization Of Proterozoic Volcanic Suites. *Edited by* Pharoah, T.C., Beckinsale, T.C., and Rickard, D., Geological Society Special Publications 33, pp. 167-182.

Whalen, J.B., Syme, E.C., and Stern, R.A. 1999. Geochemical and Nd isotopic evolution of Paleoproterozoic arc-type granitoid magmatism in the Flin Flon Belt, Trans-Hudson orogen, Canada. Canadian Journal of Earth Science, **36**: 227-250.

APPENDIX A: ANALYTICAL METHODS

A.1 GEOCHEMICAL SAMPLING, PREPARATION AND METHODOLOGY

All geochemical data reported in this work are from samples collected by the author during two summers mapping in conjunction with the Geological Survey of Canada on Reindeer Lake in northern Saskatchewan. Field preparation of all samples included: (1) cleaning samples of all noticeable weathering and alteration and; (2) reducing the samples into fragments no more than 4 to 5 cm across. Several of the collected samples are coarse grained and contain large K-feldspar megacrysts sometimes on the order of several cm in size. Steps were taken in the field as well as during crushing to avoid biassing the whole rock geochemistry toward the composition of the K-feldspar megacrysts. Two steps were undertaken in the field to ensure that this was not the case; (1) samples containing very large megacrysts as well as those containing excessive amounts of modal K-feldspar (obvious accumulation of megacrysts) were avoided; and (2) large samples were collected, generally on the order of several (5-10) kg's for the coarsest grained rocks.

All samples were subsequently crushed in a steel-jaw crusher, this reduced the samples to several 0.5-1 cm sized chips. The rock chips were then reduced to a fine powder in a tungsten-carbide bowl and puck assembly. The powders produced were approximately 200 mesh size. In order to reduce contamination of the sample with Nb from the tungsten-carbide assembly, small sample sizes were loaded, allowing the actual pulverizing time to be kept below 60 seconds. In order to collect a representative sample this procedure was repeated several times for all samples, with the coarser grained samples composed of approximately 6-8 separate batches. The powders were then mixed in a 10 kg plastic bag in order to homogenize the sample. Approximately 50 g of the sample was then transferred to a clean plastic vial for use in all subsequent chemical

analysis. To test the possibility of sample contamination with Nb by interaction with the tungsten carbide assembly a quartz diorite sample was pulverized in a silica-agate assembly as well as within the tungsten-carbide assembly. XRF results of 7.3 ppm and 6.9 ppm were found for samples crushed in the tungsten carbide and agate respectively. These results indicate that Nb contamination is not occurring, or is negligible.

A.2 X-RAY FLUORESCENCE (XRF)

Major element as well as selected trace element analyses were preformed at Memorial University of Newfoundland, Department of Earth Sciences, X-Ray Fluorescence (XRF) Laboratory. Analyses were collected from a Fisons/ARL model 8420+ sequential wavelength-dispersive X-ray spectrometer. The major elements oxides, SiO_2, TiO_2, Al_2O_3, Fe_2O_3, MnO, MgO, CaO, Na_2O, K_2O, and P_2O_5 were determined from silicate glass beads. The trace elements Sc, V, Cr, Ni, Cu, Zn, Ga, As, Rb, Sr, Y, Zr, Nb, Ba, Ce, Pb, Th, and U were determined on pressed powder pellets.

A.2.1 Silica glass bead method for major element analysis

Approximately 2 g of sample was accurately weighed into a dried porcelain crucible and heated in an oven to 1050°C. The high temperature oxidizes the sample and coverts all iron in the sample to Fe^{3+}, and is thus measured as Fe_2O_3. Loss-on-ignition (LOI) values are also obtained from the % difference between the pre-ignited and dried sample weights.

Into a clean plastic vial 1.5000 ± 0.0005 g of the dried sample powder was combined with 6.0000 ± 0.0005 g of Lithium Metaborate and 1.5000 ± 0.0005 g of Lithium Tetraborate. This mixture was then poured into a clean platinum crucible and three drops of Lithium Bromide were added. The crucibles were then loaded into an automatic fluxer along with platinum moulds (~35 mm diameter). The samples were heated in stages up to approximately 1200°C causing

them to melt. Once molten, the samples were poured into the platinum moulds and allowed to cool to room temperature. This procedure forms a smooth, homogeneous glass disk ready for analysis in the XRF.

An automated computer system connected to the XRF was used in the data collection. Four quality control reference materials (JP-1-G, W-2-G, JG-2-G, JG-1A-G) and six internal standards (JB-1A-G, MRG-1-G, SY-2-G, SY-3-G, SiO_2-G, BIR-1-G) were analysed with the fused beads. The data reduction was performed using an in-house written program and was carried out using a personal computer on spreadsheet software.

A.2.2 Pressed powder pellet method for Trace Elements

A 5.00 ± 0.05 g rock powder sample was combined with 0.70 g of phenolic resin into a 100 ml glass jar. Two 0.5 inch diameter stainless steel ball bearings were added to the mixture and a plastic lid attached. The jar was then placed on a small mixer for 10 minutes in order to homogenize the sample-resin mixture. The mixture was then inserted into a pellet press (29 mm diameter) and pressed for 10 seconds at a pressure of 20 tonnes. These pellets were then placed in an oven for 15 minutes at 200°C in order fuse the material into a hard disk ready for analysis on the XRF.

An automated computer system connected to the XRF was used in the data collection. Four quality control reference materials (AGV-1, DNC-1, JG-2, BCR-2) and six internal standards (DTS-1, BHVO-1, SY-2, SY-3, SiO_2, PACS-1) were analysed with the pressed powder pellets. The data reduction was performed using an in-house written program and was carried out using a personal computer on spreadsheet software.

A.2.3 Test for X-ray Fluorescence (XRF) precision and accuracy

The quality of the major and trace element determinations (precision and accuracy)

obtained by the X-ray fluorescence method can be monitored by considering analyses of standard materials collected during the runs containing rock samples. Considered here are two measures of quality control: (1) relative standard deviations (RSD's), which are a measure of the precision of the instrument; and (2) relative differences (RD's), which are a measure of accuracy as compared to accepted values for a particular standard. Excellent precision and accuracy is obtained when RSD's and RD's are between 0 and 3 %, and good precision and accuracy is defined as being between 3 and 7 % (Jenner et al., 1990).

The precision and accuracy of the major element oxides was monitored by considering results obtained on the standard JG-1A-G during the period between March 1999 and December 1999 for 8 separate runs. Standard JG-1A-G is a calc-alkaline granite and is very similar in composition to many of the samples analysed during this study. The precision was excellent for all the major element oxides with all having RSD's < 3%. The best precision was found for the oxides of Si, Al, Fe, Ca, and K with all having RSD's of less than 1 % (Table A.1). The accuracy was evaluated by comparing the mean of the 8 runs with accepted values for JG-1A-G from Govindaraju (1989). All samples show good to excellent accuracy (RD's 0-7 %) with the exception of P_2O_5 which has an RD of 12.34 %. This large number is misleading in that the mean for P_2O_5 was 0.09 wt. %, and when compared to the quoted value from Govindaraju (1989) of 0.08 wt. % the two are very close and the accuracy of the method is limited by the precision of the instrument (0.00 wt. %).

The precision and accuracy of the trace elements measured by the XRF was evaluated considering the standard AGV-1. This standard is an andesite and has similar abundances for the trace elements of interest in this study, i.e. the high field-strength elements (HFSE) and the low field-strength elements (LFSE). Low abundances of some transition metals in this standard cause

severe underestimations of the precision and accuracy of the instrument as detection limits are approached (discussed below). The HFSE Y, Zr, Nb show excellent precision with all having RSD's < 2%, Th is the exception with an RSD of 17.22 %. This result for Th is due to AGV-1 having a Th abundance close to the detection limit of the XRF (3 ppm). Longerich (1995) quotes an RSD for Th of 0.24 % with samples having Th concentrations greater than three times the detection limit. RSD's for the LFSE Rb, Sr, Ba and Pb are good to excellent, with exceptional results for Rb and Sr having RSD's of 0.49 and 0.34 % respectively. The LFSE Ce has a high RSD similar to that of Th, and is also the result of concentrations approaching the detection limit of the XRF. An RSD of 0.40 % is quoted by Longerich (1995) for samples containing abundant Ce. High RSD's for most of the transition metals (mentioned above) is a artifact of the low abundances in the standard (Table A.1). The absence of Cr and As from the table is due to abundances for these elements being below detection limits for the XRF in all 8 runs, as was also the case for U. Relative differences (RD's) as compared to the accepted values of Govindaraju (1989) are similar to the RSD values discussed above. High RD's correspond to those elements with high RSD's and elemental abundances less than 2 or 3 times the quoted detection limit. All elements without detection limit problems show good accuracy, with the exception of Y and Nb. These elements are considered accurate even though they have high RD's when compared to Govindaraju's (1989) compilation.

A.3 INDUCTIVELY COUPLED PLASMA MASS SPECTROMETRY (ICP-MS)

Selected trace elements (Y, Th, La, Ce, Nd, Sm, Eu, Gd, Tb, Dy, Ho, Er, Tm, Yb, Lu) were analysed on a HP 4500 inductively coupled plasma mass-spectrometer (ICP-MS) and prepared by the sodium peroxide (Na_2O_2) sinter method. The Na_2O_2 sinter dissolution method was chosen because of its ability to decompose the more refractory minor phases (eg. zircon)

common in geological samples. These minor phases commonly contain the majority of the HFSE and rare earth elements (REE), which are difficult to decompose using HF-based dissolution procedures. A 0.2 g rock powder sample is accurately weighed and combined with 0.8 g of Na_2O_2 into a clean nickel crucible. The crucibles are then placed in a muffle furnace at 500°C and sintered for 1.5 hours. The samples are then removed from the furnace and cooled for about 20 minutes. Once cool, 10 ml of distilled water is added. The cover is rinsed into the crucible and the mixture poured into a centrifuge tube, being careful to rinse the crucible well. Distilled water is then added to a final volume of 30 ml and centrifuged for 15 minutes. The liquid is poured off and the residue rinsed with 25 ml of distilled water and centrifuged again, the rinse and centrifuge procedure is then repeated. The residue is then dissolved in 2.5 ml of 8N HNO_3 and 4 ml of oxalic acid. The crucible is then rinsed with 0.2N HNO_3 and added to the centrifuge tube and left overnight. In the morning 4 mls of 0.113M HF/0.453M boric acid solution is added and the solution is left to dry in the drying oven for 2 hours. The solution is then transferred to a clean jar and made up to 50 g with distilled water. Before the solutions can be run on the ICP-MS they must be diluted. This is done by accurately weighing approximately 2 g of the sample solution and 8 g of 0.2N HNO_3 into a labelled test tube.

During each run by ICP-MS the samples are also run with: (1) pure quartz reagent blanks; (2) two geological reference standards (MRG-1, BR-688) and; (3) duplicates of one, or more of the samples. A method of internal standardization is used to correct for matrix and drift effects (Longerich et al., 1990).

A.3.1. Inductively Coupled Plasma-Mass Spectrometry (ICP-MS) test for precision and accuracy

As discussed previously in section A.2.3 on XRF precision and accuracy, RSD's and

RD's are used to evaluate the precision and accuracy of the instrument. The quality control standard MRG-1 is run with dissolved rock samples during analysis by ICP-MS. Precision and accuracy are based on 26 analyses of MRG-1, between April 1999 and December 1999 (Table A.2). RSD's for Y and the REE La, Ce, Pr, Nd, Sm, Eu, Gd, Tb, Dy, Ho, Er, Tm, Yb and Lu are all good i.e. < 7 %, and almost all fall between 4 and 5 %. RSD's for Th are higher and were found to be 12.55 % for the 26 analyses considered. Quoted long term averages of over 160 analyses of MRG-1 yield RSD's for Th of less than 10 % (Longerich, pers. com.). The accuracy of the instrument as compared to the quoted values of MRG-1 from Govindaraju (1989) are generally less than 10 % for most of the REE, however deviations of > than 10 % do occur and are especially evident in the heavy REE Tm and Yb, with > than 30 % relative differences. Although these differences are large, they do not reflect problems with ICP-MS accuracy, but rather the poorer quality of measurements compiled in Govidaraju (1989). This is evident when chondrite normalized plots are generated for the REE for the MRG-1 mean of 26 determinations and the Govindaraju (1989) compilation. The MRG-1 mean has a more realistic REE profile with smooth variations in the heavy rare earth elements (HREE), as opposed to that of the accepted values from Govindaraju (1989) which show an abnormally low REE abundances at Tm an Yb. The RSD's for Y are also high (17.98 %) as compared to the Govindaraju's (1989) compilation. A method of internal standardisation between the XRF and ICP-MS at Memorial is used to ensure the quality of analyses obtained by ICP-MS. A good agreement between Y values determined on the XRF and ICP-MS ensures that values obtained are as close as possible to the correct value.

A.4 ISOTOPE DILUTION PROCEDURE FOR THE ANALYSIS OF SAMARIUM AND NEODYMIUM ISOTOPES

Samarium and Neodymium isotopic measurements were conducted on 27 selected granitoid samples during this study. Sm and Nd isotopic compositions were analysed by thermal ionization mass spectrometry (TI-MS) using the isotope-dilution preparation technique outlined by MacLachlan and Dunning (1998) and Horan (1998). A powdered sample is accurately weighed to the fifth decimal place and then attacked with 1 ml each of 2X 8N nitric and 2X hydrofluoric acids. The sample is then allowed to reflux for a period of 2 to 7 days. Following redissolution, the sample is then split into isotopic concentration (IC) and isotopic dilution (ID) fractions. The ID fraction is spiked with ORNL ^{150}Nd-^{147}Sm mixed spike based on the whole rock Nd concentration. Initial separation of the REE was completed by loading the samples onto EICHROM TRU-Spec resin. This resin is an elementally specific ion exchange resin which retains the REE while removing the major and trace elements. The REE are collected after using 2B (double teflon bottle distilled) water. The collected fractions are then evaporated to dryness. The separation of Sm and Nd from the IC and ID fractions is then conducted by pipetting samples onto EICHROM Ln resin using 2X 1.5N nitric acid. This resin is similar to older teflon resins and behaves in a similar fashion. The first of the Light Rare Earth Elements (LREE) are stripped off using 2X 0.25N hydrochloric acid. The isotopic concentration and isotopic dilution Nd fractions are then collected with 2X 0.25N hydrochloric acid. The isotopic dilution Sm fraction is collected using 2X 0.75N hydrochloric acid. Two drops of 1N phosphoric acid are added to each of the three collected fractions. All three fractions are then evaporated down to a single drop, ready for analysis on the mass spectrometer. The IC and ID Nd and Sm fractions are loaded on outgassed Re double filaments and measured in a Finnigan MAT 262V TI-MS. Samples are then analysed using static faraday multicollector routines. The static faraday multicollector routine collects 5 blocks of 20 scans for a total of 100 scans with online drift and

mass fractionation correction and statistical analysis. The $^{143}Nd/^{144}Nd$ errors are reported at the 95 % confidence level (2 sigma) and are based solely on mass spectrometry measurements. The $^{147}Sm/^{144}Nd$ ratios are calculated with data reduction software created at Memorial University using Lotus 123 97. The calculations are based on measured $^{147}Sm/^{149}Sm$ and $^{150}Nd/^{144}Nd$ spiked ratios. The $^{147}Sm/^{144}Nd$ reported errors are absolute 2 sigma and are quadratically added using the 2 sigma errors for $^{147}Sm/^{149}Sm$ and $^{150}Nd/^{144}Nd$ measured isotopic ratios. Average of (n=62) analyses of AMES Nd standard was 0.512149 (2σ = 18); accepted is 0.512150 (15). Average of (n=25) analyses of AMES Sm standard was 1.084950 (2σ = 90); accepted is 1.084955 (150). Values of εNd are calculated using present day Chondritic Uniform Reservoir (CHUR) values of 0.512638 for $^{143}Nd/^{144}Nd$ and 0.1967 for $^{147}Sm/^{144}Nd$ and a decay constant of $\lambda = 6.54 \times 10^{-12}$ a^{-1}. The results of two duplicate analyses were found to be in good agreement with each other (Table A.3). Three samples reported in this thesis were analysed at the GSC in Ottawa (Corrigan et al., unpub. rept.) following the method of Theriault and Ermanovics (1997).

Table A.1 X-ray fluorescence (XRF) precision and accuracy for standards JG-1A-G (major element oxides) and AGV-1 (trace elements) for (n=8) determinations during the period of March 1999 to December 1999.

Oxide (wt.%) Element (ppm)	Min.	Max.	Mean (n=8)	Limit of Detection	Std. Deviation	RSD (%)	Govindaraju (1989)	RD (%)
SiO_2	70.93	71.56	71.40	0.020	0.199	0.28	72.68	-1.76
TiO_2	0.23	0.25	0.24	0.005	0.006	2.60	0.25	-4.32
Al_2O_3	13.82	14.05	13.98	0.055	0.067	0.48	14.32	-2.39
Fe_2O_3T	2.05	2.07	2.06	0.006	0.009	0.45	2.06	0.04
MnO	0.06	0.06	0.06	0.004	0.002	2.85	0.06	0.35
MgO	0.70	0.75	0.73	0.021	0.014	1.91	0.69	5.10
CaO	2.12	2.18	2.15	0.006	0.021	0.99	2.14	0.43
Na_2O	3.46	3.60	3.56	0.034	0.044	1.25	3.43	3.77
K_2O	3.94	4.03	4.00	0.006	0.032	0.79	4.04	-1.10
P_2O_5	0.09	0.09	0.09	0.010	0.003	3.08	0.08	12.34
Sc	9	20	16	7	3.29	20.88	12	31.33
V	108	122	114	6	5.18	4.53	121	-5.50
Ni (n=6)	6	9	7	5	1.34	19.48	16	-57.00
Cu	54	59	56	4	1.66	2.97	60	-6.80
Zn	67	69	68	3	1.06	1.57	88	-23.14
Ga	18	22	20	3	1.27	6.33	20	0.30
Rb	69.5	70.5	69.9	0.7	0.35	0.49	67.3	3.90
Sr	681.7	689.5	685.6	1.2	2.30	0.34	662.0	3.57
Y	16.7	17.6	17.1	0.7	0.33	1.93	20.0	-14.38
Zr	237.3	245.7	242.7	1.1	3.60	1.48	227.0	6.90
Nb	16.4	17.1	16.7	0.7	0.24	1.44	15.0	11.51
Ba	1200	1337	1272	23	38.15	3.00	1226	3.78
Ce	58	109	79	41	14.94	18.92	67	17.84
Pb	32	37	35	4	1.60	4.63	36	-4.11
Th	4	7	6	3	1.03	17.22	7	-14.57

RSD (%) = relative standard deviation = (standard deviation / mean) x 100
RD (%) = relative difference = [(mean determination - standard) / standard] x 100

Table A.2 ICP-MS (Na_2O_2 dissolution) precision and accuracy for standard MRG-1 for (n=26) determinations during the period of April 1999 to December 1999.

Element (ppm)	Min.	Max.	Limit of Detection	Mean (n=26)	Std. Deviation	RSD (%)	Govindaraj u (1989)	RD (%)
Y	9.958	12.489	0.001	11.483	0.532	4.63	14	-17.98
Th	0.692	1.194	0.001	0.820	0.103	12.55	0.93	-11.84
La	7.761	9.537	0.001	8.755	0.403	4.61	9.8	-10.66
Ce	22.677	27.258	0.001	24.999	1.163	4.65	26	-3.85
Pr	3.210	4.007	0.002	3.618	0.170	4.70	3.4	6.42
Nd	15.475	19.197	0.006	17.502	0.854	4.88	19.2	-8.84
Sm	4.123	4.796	0.002	4.415	0.186	4.21	4.5	-1.90
Eu	1.318	1.554	0.001	1.407	0.060	4.26	1.39	1.25
Gg	3.763	4.535	0.002	4.097	0.195	4.75	4	2.43
Tb	0.502	0.607	0.001	0.549	0.025	4.61	0.51	7.57
Dy	2.701	3.300	0.004	2.957	0.143	4.84	2.9	1.98
Ho	0.450	0.549	0.001	0.504	0.023	4.55	0.49	2.96
Er	1.111	1.396	0.002	1.246	0.080	6.43	1.12	11.26
Tm	0.130	0.163	0.001	0.146	0.007	4.90	0.11	32.99
Yb	0.723	0.865	0.003	0.807	0.032	3.95	0.6	34.49
Lu	0.099	0.119	0.001	0.110	0.005	4.41	0.12	-8.49

Table A.3 Duplicate Sm and Nd isotopic analyses of two granitoid samples.

Sample	Sm	Nd	$^{143}Nd/^{144}Nd$	2σ	$^{147}Sm/^{144}Nd$	2σ
98-D313	8.93	44.47	0.511633	0.000011	0.12394	0.00006
	8.94	44.52	0.511607	0.000086	0.12398	0.00003
98-D349	4.61	24.81	0.511396	0.000036	0.11468	0.00006
	4.48	24.13	0.511362	0.000023	0.11471	0.00004

APPENDIX B: GEOCHEMICAL AND ISOTOPIC ANALYSES DATABASE

B.1 MAJOR AND TRACE ELEMENT XRF ANALYSES

Wathaman Batholith
Southern-Central Zone (SCZ) - K-feldspar megacrystic granodiorite series

Sample	99-T062a	98-J176	99-T193b	98-D313	98-D314
Rock Type	QD	QD	QMd	QMd	Gdr
Northing	6386882	6363548	6407995	6358578	6358891
Easting	640680	672159	662473	641305	642239
SiO_2	53.08	56.44	60.42	61.15	62.11
TiO_2	0.85	0.80	0.58	0.64	0.57
Al_2O_3	16.91	18.40	17.44	16.78	16.60
FeO	5.40	3.74	3.12	3.34	2.97
Fe_2O_3	2.94	2.39	2.14	2.36	2.00
MnO	0.14	0.07	0.08	0.09	0.07
MgO	5.03	3.73	2.30	2.59	2.29
CaO	7.22	5.53	4.66	4.72	4.27
Na_2O	3.56	4.53	4.34	4.50	3.78
K_2O	1.91	2.12	2.68	2.76	3.00
P_2O_5	0.40	0.34	0.29	0.30	0.27
Total	97.62	98.26	98.36	99.41	98.20
Sc	21	16	11	17	13
V	145	95	72	87	73
Cr	147	161	28	56	45
Ni	64	36	dl	dl	7
Cu	71	25	17	4	3
Zn	51	49	30	42	31
Ga	23	25	20	20	19
Rb	50.9	66.1	46.4	58.7	58.6
Sr	941.6	1083.7	1201.2	794.1	876.3
Ba	1088	1230	2639	1528	2264
Pb	10	11	10	12	17
Ce	187	84	131	60	115
Y	20.7	11.4	9.6	17.5	15.3
Zr	135.5	281.9	146.9	150.4	158.2
Nb	12.5	10.9	8.2	9.9	10.0
Th	9	4	5	3	dl

Wathaman Batholith

Southern-Central Zone (SCZ) - K-feldspar megacrystic granodiorite series

Sample	98-D292	98-D316	99-T156	99-T033	98-T223
Rock Type	Gdr	Gdr	Gdr	Gdr	Gdr
Northing	6349938	6361608	6399633	6381171	6364014
Easting	645006	639924	654248	656508	645300
SiO_2	63.25	63.84	63.99	64.01	64.29
TiO_2	0.59	0.52	0.59	0.54	0.46
Al_2O_3	16.38	16.50	15.56	16.20	15.98
FeO	2.71	2.55	2.70	2.24	2.44
Fe_2O_3	1.94	1.84	1.85	1.64	1.76
MnO	0.08	0.06	0.07	0.05	0.05
MgO	1.83	1.66	1.63	1.42	1.50
CaO	3.74	3.43	3.58	3.50	3.17
Na_2O	3.89	3.77	3.66	4.18	3.55
K_2O	3.36	3.55	3.17	3.20	3.74
P_2O_5	0.24	0.22	0.22	0.31	0.21
Total	98.27	98.16	97.25	97.64	97.46
Sc	14	dl	dl	dl	dl
V	62	49	60	51	54
Cr	31	dl	6	11	20
Ni	dl	dl	dl	dl	dl
Cu	dl	21	7	dl	9
Zn	30	18	19	22	18
Ga	18	19	16	17	16
Rb	57.7	55.9	69.2	38.1	58.1
Sr	724.2	783.5	631.5	1364.2	819.1
Ba	2303	2127	1876	3388	2790
Pb	12	12	12	5	12
Ce	94	106	100	49	102
Y	20.2	8.5	17.0	9.1	5.6
Zr	211.8	137.0	179.3	143.4	171.1
Nb	10.9	5.7	11.5	7.2	4.7
Th	dl	4	5	dl	dl

Wathaman Batholith

Southern-Central Zone (SCZ) - K-feldspar megacrystic granodiorite series

Sample	99-T041	98-D349	99-T193a	98-T296	99-T157
Rock Type	Gdr	Gdr	Gdr	Mgn	Mgn
Northing	6386820	6366503	6407995	6352639	6399088
Easting	657522	629737	662473	662511	653453
SiO_2	64.61	68.41	69.10	70.22	71.66
TiO_2	0.51	0.35	0.33	0.33	0.37
Al_2O_3	15.61	15.30	14.85	14.33	13.64
FeO	2.36	1.60	1.56	1.48	1.44
Fe_2O_3	1.62	1.26	1.12	1.13	1.14
MnO	0.05	0.04	0.06	0.04	0.04
MgO	1.23	0.90	0.80	0.88	0.68
CaO	3.15	2.19	2.44	2.17	1.69
Na_2O	4.10	3.79	3.77	3.18	3.31
K_2O	2.73	4.02	3.20	4.22	4.39
P_2O_5	0.23	0.15	0.11	0.12	0.11
Total	96.41	98.23	97.46	98.30	98.60
Sc	dl	dl	dl	dl	dl
V	46	32	27	28	dl
Cr	3	23	dl	11	2
Ni	dl	dl	dl	dl	dl
Cu	13	21	23	7	dl
Zn	19	8	6	dl	4
Ga	20	17	19	14	15
Rb	75.2	56.6	67.7	83.5	75.4
Sr	977.6	803.2	421.6	547.6	262.2
Ba	1924	2018	1268	1725	1084
Pb	12	16	14	21	13
Ce	121	dl	76	119	117
Y	6.8	5.5	5.0	11.8	6.6
Zr	186.4	148.9	109.7	110.5	163.6
Nb	10.6	6.2	10.8	8.9	6.4
Th	4	dl	dl	5	6

Wathaman Batholith

Southern-Central Zone (SCZ) - Monzogranite series

Sample	98-D286	98-D262	98-D265	98-D301	98-D300
Rock Type	Gdr	Mgn	Gdr	Mgn	Mgn
Northing	6344675	6345584	6343702	6355632	6354624
Easting	646718	648264	648804	642735	642542
SiO_2	68.83	69.82	70.85	71.65	71.93
TiO_2	0.28	0.17	0.20	0.26	0.24
Al_2O_3	15.74	15.24	15.12	14.42	14.21
FeO	1.14	0.78	0.84	1.05	0.95
Fe_2O_3	0.86	0.61	0.63	0.78	0.74
MnO	0.03	0.02	0.02	0.02	0.02
MgO	0.74	0.42	0.58	0.60	0.46
CaO	2.30	1.89	2.09	2.00	1.78
Na_2O	4.28	3.43	4.17	3.45	3.17
K_2O	3.15	4.22	3.12	3.67	4.38
P_2O_5	0.10	0.05	0.07	0.09	0.08
Total	97.62	96.93	97.86	98.16	98.24
Sc	dl	dl	dl	dl	dl
V	23	9	17	16	18
Cr	16	dl	12	dl	dl
Ni	dl	dl	dl	dl	dl
Cu	dl	dl	dl	dl	dl
Zn	9	dl	dl	dl	dl
Ga	18	15	19	16	12
Rb	61.3	76.7	62.9	55.4	61.3
Sr	817.7	742.3	762.9	495.0	633.6
Ba	1769	2768	1553	1417	2661
Pb	18	17	14	14	11
Ce	dl	dl	dl	dl	52
Y	2.3	dl	dl	1.6	dl
Zr	117.1	109.4	101.9	88.1	115.6
Nb	4.7	4.2	3.8	3.3	3.6
Th	3	dl	3	dl	4

Wathaman Batholith
Southern-Central Zone (SCZ) - Monzogranite series

Sample	98-J162a
Rock Type	Mgn
Northing	6355654
Easting	656235
SiO_2	75.07
TiO_2	0.17
Al_2O_3	12.90
FeO	0.83
Fe_2O_3	0.64
MnO	0.01
MgO	0.28
CaO	1.41
Na_2O	2.94
K_2O	4.24
P_2O_5	0.03
Total	98.70
Sc	dl
V	17
Cr	dl
Ni	dl
Cu	dl
Zn	dl
Ga	11
Rb	64.3
Sr	365.7
Ba	1496
Pb	17
Ce	86
Y	dl
Zr	131.7
Nb	2.8
Th	6

Wathaman Batholith

Southern-Central Zone (SCZ) - Quartz diorite dykes and pods

Sample	98-J180	98-J162b
Rock Type	Qd	Qd
Northing	6360307	6355654
Easting	670707	656235
SiO_2	54.87	60.97
TiO_2	0.87	0.66
Al_2O_3	17.10	16.19
FeO	5.42	3.87
Fe_2O_3	2.91	2.34
MnO	0.12	0.07
MgO	4.89	3.42
CaO	6.98	5.51
Na_2O	3.31	4.26
K_2O	1.92	1.61
P_2O_5	0.34	0.16
Total	98.85	99.16
Sc	25	19
V	145	119
Cr	177	111
Ni	41	30
Cu	38	34
Zn	55	38
Ga	21	20
Rb	53.8	35.8
Sr	737.5	610.7
Ba	602	397
Pb	10	13
Ce	94	54
Y	16.2	12.6
Zr	79.1	92.7
Nb	6.3	7.6
Th	6	6

Wathaman Batholith

Northeast Zone (NEZ) - K-feldspar megacrystic monzogranite series

Sample No.	99-T144b	99-D096	99-T144a	99-J029a	99-D191
Rock Type	D	D	D	D	QMd
Northing	6410318	6415991	6410318	6409173	6394112
Easting	663185	661351	663185	662585	663702
SiO_2	49.68	51.07	51.23	53.24	61.29
TiO_2	0.64	0.84	0.81	0.59	0.59
Al_2O_3	13.94	17.73	16.80	17.72	17.60
FeO	6.42	5.85	5.83	4.92	2.62
Fe_2O_3	2.79	3.03	3.16	2.76	2.07
MnO	0.16	0.16	0.19	0.12	0.08
MgO	10.09	6.57	6.76	5.39	1.74
CaO	9.90	8.57	7.90	7.26	3.65
Na_2O	2.71	3.56	3.79	4.00	4.19
K_2O	1.12	1.59	1.75	1.73	4.10
P_2O_5	0.23	0.14	0.27	0.23	0.26
Total	97.84	99.22	98.63	98.12	98.43
Sc	37	20	27	15	dl
V	170	158	152	102	54
Cr	624	165	247	16	22
Ni	134	66	85	55	dl
Cu	58	60	49	41	23
Zn	45	58	65	47	31
Ga	17	26	22	22	22
Rb	21.9	46.7	45.6	45.7	117.1
Sr	719.0	988.2	721.1	1028.9	740.8
Ba	419	399	488	1273	2124
Pb	dl	8	9	7	24
Ce	77	142	85	59	158
Y	21.0	39.9	32.5	11.2	15.0
Zr	104.2	56.5	141.3	33.4	265.9
Nb	16.7	26.1	20.6	7.7	17.9
Th	dl	dl	dl	dl	13

Wathaman Batholith

Northeast Zone (NEZ) - K-feldspar megacrystic monzogranite series

Sample	99-T139a	99-T141	99-T171	99-D255	99-T133
Rock Type	Gdr	Gdr	Mgn	Mgn	Mgn
Northing	6402990	6397476	6415944	6408217	6405000
Easting	666575	667606	671418	673304	651750
SiO_2	65.10	65.13	66.79	66.81	68.63
TiO_2	0.43	0.48	0.54	0.43	0.48
Al_2O_3	15.86	15.85	15.45	15.41	14.91
FeO	1.72	2.08	1.66	1.64	1.81
Fe_2O_3	1.36	1.60	1.40	1.35	1.43
MnO	0.06	0.09	0.06	0.05	0.04
MgO	1.11	1.55	0.89	0.85	0.83
CaO	2.44	3.04	2.09	2.19	2.26
Na_2O	4.15	3.67	3.73	3.85	3.16
K_2O	3.88	4.09	4.82	4.44	4.70
P_2O_5	0.15	0.21	0.15	0.19	0.13
Total	96.41	97.99	97.85	97.48	98.56
Sc	dl	dl	dl	dl	dl
V	34	50	26	dl	30
Cr	10	23	dl	7	dl
Ni	dl	dl	dl	dl	dl
Cu	dl	11	15	12	dl
Zn	18	43	17	12	10
Ga	21	23	17	18	18
Rb	125.1	130.3	148.9	113.4	93.5
Sr	510.9	601.9	524.1	1090.3	319.8
Ba	1416	1743	2613	2573	1555
Pb	25	36	21	18	18
Ce	163	85	162	219	167
Y	22.8	13.6	15.1	9.8	21.7
Zr	214.2	231.0	296.5	202.5	216.0
Nb	23.0	17.5	21.2	15.6	15.4
Th	19	11	16	12	10

Wathaman Batholith

Northeast Zone (NEZ) - K-feldspar megacrystic monzogranite series

Sample	99-D099	99-J029b	99-T139b	99-T187
Rock Type	Mgn	Mgn	Mgn	Mgn
Northing	6418810	6409173	6402990	6415204
Easting	662246	662585	666575	671998
SiO_2	69.65	69.34	70.65	73.93
TiO_2	0.34	0.44	0.20	0.15
Al_2O_3	14.67	14.79	14.83	12.94
FeO	1.50	1.65	0.82	0.59
Fe_2O_3	1.30	1.38	0.76	0.50
MnO	0.04	0.04	0.02	0.02
MgO	0.59	0.69	0.29	0.25
CaO	1.57	1.81	1.17	0.79
Na_2O	3.18	3.23	3.03	3.07
K_2O	5.44	5.10	6.12	5.01
P_2O_5	0.11	0.12	0.04	0.03
Total	98.58	98.78	98.19	97.33
Sc	dl	dl	dl	dl
V	29	dl	18	dl
Cr	2	2	dl	dl
Ni	dl	dl	dl	dl
Cu	dl	dl	7	dl
Zn	6	dl	dl	dl
Ga	16	16	15	17
Rb	126.1	104.4	146.3	138.1
Sr	261.2	318.4	505.4	134.6
Ba	1545	1797	2361	412
Pb	22	17	40	27
Ce	188	196	118	77
Y	8.5	2.5	11.7	3.1
Zr	269.4	266.6	287.3	113.1
Nb	11.4	5.3	15.2	11.9
Th	14	15	22	30

Wathaman Batholith

Northeast Zone (NEZ) - K-feldspar megacrystic monzonitic series

Sample	99-T077b	99-T191	99-T153a	99-D103	98-T311
Rock Type	Md	Md	Mz	Mz	QMd
Northing	6412185	6407013	6386694	6389408	6391500
Easting	664912	662402	637997	641422	637750
SiO_2	51.21	53.51	49.21	52.82	55.24
TiO_2	0.94	1.11	1.01	0.76	0.47
Al_2O_3	17.12	16.46	16.10	16.22	20.84
FeO	6.46	5.49	7.84	6.24	3.40
Fe_2O_3	3.30	3.17	4.61	4.16	2.41
MnO	0.14	0.11	0.30	0.26	0.14
MgO	5.33	4.51	4.24	3.06	1.62
CaO	8.26	6.94	7.67	6.83	6.21
Na_2O	3.47	3.80	3.26	3.54	4.20
K_2O	1.59	2.12	3.09	3.69	3.45
P_2O_5	0.35	0.55	0.71	0.56	0.33
Total	98.37	97.96	98.22	98.28	98.54
Sc	23	21	20	11	7
V	190	155	202	174	61
Cr	99	113	10	20	dl
Ni	53	41	dl	dl	dl
Cu	52	33	64	59	48
Zn	57	56	94	79	50
Ga	22	22	21	20	19
Rb	40.3	75.2	108.6	113.8	88.1
Sr	1036.0	1057.0	1074.7	923.3	1692.0
Ba	1473	1264	1390	1042	2352
Pb	10	18	11	19	10
Ce	53	186	138	133	55
Y	16.2	35.2	26.8	26.0	10.2
Zr	78.3	146.1	16.7	50.6	dl
Nb	9.0	24.5	12.9	11.9	7.2
Th	dl	5	5	7	3

Wathaman Batholith

Northeast Zone (NEZ) - K-feldspar megacrystic monzonitic series

Sample	98-T310	99-T153b	99-T077a	99-T188a	99-J061
Rock Type	QMd	QMd	QMd	QMd	QMd
Northing	6390000	6386694	6412185	6414599	6401755
Easting	637750	637997	664912	666281	659533
SiO_2	56.26	56.49	56.95	58.78	59.42
TiO_2	0.70	0.45	0.68	0.81	0.69
Al_2O_3	19.05	18.02	18.50	17.74	18.42
FeO	5.02	3.58	3.27	3.35	2.41
Fe_2O_3	3.81	3.13	2.39	2.60	1.93
MnO	0.23	0.20	0.09	0.09	0.06
MgO	2.52	1.53	2.27	2.24	1.66
CaO	5.20	3.84	4.90	4.33	4.06
Na_2O	4.53	4.14	4.44	4.03	4.17
K_2O	3.68	5.33	3.37	4.23	4.30
P_2O_5	0.49	0.32	0.29	0.29	0.23
Total	101.68	97.27	97.46	98.80	97.67
Sc	19	dl	dl	dl	13
V	132	52	83	88	62
Cr	dl	dl	32	32	24
Ni	dl	dl	dl	dl	dl
Cu	24	15	35	40	25
Zn	50	43	34	36	17
Ga	20	17	21	22	21
Rb	121.2	111.2	56.4	95.1	90.9
Sr	1350.4	993.7	1013.6	827.6	919.5
Ba	1595	2066	2919	2767	2860
Pb	11	17	16	18	16
Ce	202	93	106	124	75
Y	17.1	13.7	12.7	14.9	9.6
Zr	26.5	5.3	276.5	330.1	328.3
Nb	9.5	8.1	9.7	14.5	12.0
Th	5	dl	dl	4	dl

La Ronge Domain Plutons

Pluton	*Fol Dio-Grn*	*Cowie Bay*	*Butler Island*	*Cowie Bay*	*McMillian*
Sample	98-D108a	98-T204	98-BIP	98-T199	98-B015
Rock Type	D	Tn	QD	Tn	QMd
Northing	6344374	6336793	6281750	6337821	6311891
Easting	680313	637811	638750	637448	676808
SiO_2	51.14	57.53	57.87	58.03	59.66
TiO_2	0.76	0.65	0.70	0.62	0.56
Al_2O_3	14.94	17.69	17.02	17.61	16.37
FeO	7.86	4.24	4.57	3.51	3.96
Fe_2O_3	3.64	2.41	2.43	1.96	2.62
MnO	0.20	0.10	0.10	0.07	0.10
MgO	5.68	3.53	4.15	3.84	2.90
CaO	8.43	6.09	6.66	6.36	4.87
Na_2O	3.19	3.70	4.04	3.76	3.73
K_2O	1.05	1.85	0.95	1.63	3.03
P_2O_5	0.20	0.35	0.30	0.33	0.15
Total	97.20	98.29	98.90	97.84	98.15
Sc	41	15	17	14	17
V	229	107	134	103	118
Cr	189	63	109	101	64
Ni	15	22	32	29	27
Cu	17	16	10	8	4
Zn	67	42	44	29	42
Ga	18	21	21	19	16
Rb	24.8	62.7	14.8	45.1	61.2
Sr	355.5	892.8	934.9	1197.8	327.9
Ba	503	972	498	713	1792
Pb	5	10	dl	6	6
Ce	0	95	78	dl	dl
Y	25.1	16.8	14.3	13.3	9.7
Zr	59.2	124.0	90.8	70.8	83.4
Nb	7.8	9.0	4.4	7.3	6.0
Th	dl	6	dl	dl	dl

La Ronge Domain Plutons

Pluton	*Butler Island*	*Milton Island*	*McMillian*	*Fol Dio-Grn*	*Jack Pine*
Sample	97-A001	97-D068	98-T184	98-D108b	98-D129
Rock Type	Tn	Gdr	Gdr	Gdr	Gdr
Northing	6282737	6286219	6308308	6344374	6327017
Easting	641005	643668	673770	680313	676494
SiO_2	61.30	61.36	62.52	64.53	65.44
TiO_2	0.63	0.66	0.61	0.90	0.46
Al_2O_3	16.70	15.46	15.16	16.38	15.40
FeO	4.20	4.03	3.46	2.98	2.22
Fe_2O_3	1.50	2.28	2.19	2.11	1.53
MnO	0.08	0.10	0.08	0.07	0.06
MgO	3.44	3.46	3.68	1.27	2.12
CaO	5.87	5.60	4.10	2.83	3.29
Na_2O	4.30	3.32	3.24	3.98	3.64
K_2O	1.19	1.99	2.94	3.11	3.12
P_2O_5	0.26	0.21	0.23	0.27	0.19
Total	100.30	98.57	98.39	98.67	97.65
Sc	14	21	18	dl	10
V	110	127	94	42	64
Cr	410	77	159	2	70
Ni	45	11	44	dl	9
Cu	33	31	19	11	dl
Zn	74	30	35	45	15
Ga	20	17	19	20	19
Rb	20.0	42.1	78.5	115.2	69.9
Sr	800.0	592.7	776.0	604.0	761.1
Ba	400	630	1394	2093	1377
Pb	6	5	17	16	12
Ce	dl	dl	114	199	137
Y	15.0	14.7	14.1	11.4	8.9
Zr	dl	75.7	162.7	352.1	120.9
Nb	4.1	7.5	8.7	16.1	8.5
Th	dl	dl	9	6	8

La Ronge Domain Plutons

Pluton	*McMillian*	*McMillian*	*Fol Dio-Grn*
Sample	98-T150	98-D093	99-D108c
Rock Type	Tn	Gdr	Gdr
Northing	6312911	6306203	6344374
Easting	671971	667191	680313
SiO_2	67.14	67.61	71.40
TiO_2	0.30	0.34	0.20
Al_2O_3	17.00	16.25	15.02
FeO	1.59	1.57	1.09
Fe_2O_3	1.04	1.09	0.85
MnO	0.03	0.03	0.03
MgO	1.00	1.04	0.47
CaO	3.94	3.34	1.83
Na_2O	4.83	4.72	3.96
K_2O	1.40	1.98	3.55
P_2O_5	0.11	0.09	0.07
Total	98.46	98.20	98.57
Sc	7	14	dl
V	34	29	9
Cr	8	20	12
Ni	dl	dl	dl
Cu	7	dl	dl
Zn	dl	8	8
Ga	20	21	18
Rb	25.0	37.8	100.0
Sr	971.0	1023.6	259.1
Ba	660	1123	819
Pb	4	5	31
Ce	dl	dl	dl
Y	1.8	3.9	4.9
Zr	84.8	104.2	144.9
Nb	3.1	4.9	12.3
Th	dl	dl	10

Peter Lake Domain
Swan River Gabbro Complex

Sample	99-D087b	99-D246b	99-D246a	99-D087a	99-D087c
Rock Type	Gb	Gb	Gb	Gb	Gb
Northing	6412632	6412902	6412902	6412632	6412632
Easting	658970	659594	659594	658970	658970
SiO_2	42.59	47.87	50.05	50.79	51.49
TiO_2	0.12	0.17	0.21	0.24	0.21
Al_2O_3	9.57	14.65	15.90	15.79	17.03
FeO	11.99	5.91	4.93	6.06	5.18
Fe_2O_3	3.35	1.74	1.66	2.19	2.00
MnO	0.22	0.14	0.13	0.15	0.14
MgO	21.04	13.50	10.29	9.17	8.64
CaO	7.04	13.57	13.05	11.07	10.95
Na_2O	0.96	0.92	1.29	2.18	2.53
K_2O	0.16	0.24	0.63	0.19	0.28
P_2O_5	0.02	0.03	0.04	0.01	0.01
Total	97.10	98.85	98.31	97.89	98.51
Sc	22	42	45	37	38
V	56	122	142	132	126
Cr	181	607	690	110	134
Ni	408	173	110	69	68
Cu	211	69	32	98	107
Zn	60	16	16	17	14
Ga	9	10	10	14	12
Rb	2.5	5.7	14.9	1.7	4.8
Sr	315.3	372.5	414.7	533.2	533.0
Ba	91	141	176	148	124
Pb	dl	dl	dl	dl	dl
Ce	dl	dl	dl	dl	dl
Y	2.5	5.0	6.4	4.9	4.3
Zr	dl	dl	6.8	dl	dl
Nb	dl	0.8	dl	0.8	dl
Th	dl	dl	dl	dl	dl

Peter Lake Domain
Fine grained foliated granitoids

Sample	99-D171	99-D172
Rock Type	Gdr	Gdr
Northing	6409500	6408813
Easting	652414	652275
SiO_2	73.63	73.63
TiO_2	0.09	0.11
Al_2O_3	13.63	14.06
FeO	0.50	0.67
Fe_2O_3	0.39	0.47
MnO	0.03	0.02
MgO	0.14	0.28
CaO	1.28	1.94
Na_2O	4.12	4.21
K_2O	3.39	2.21
P_2O_5	0.02	0.03
Total	97.37	97.82
Sc	dl	dl
V	dl	7
Cr	dl	dl
Ni	dl	dl
Cu	dl	dl
Zn	dl	dl
Ga	18	17
Rb	79.0	29.5
Sr	427.5	649.8
Ba	1509	1937
Pb	7	5
Ce	dl	65
Y	2.2	1.3
Zr	71.8	68.5
Nb	7.6	4.7
Th	dl	dl

Peter Lake Domain

Foliated to Augen K-feldspar megacrystic granitoids

Sample	99-D221	98-T312
Rock Type	Mgn	Mgn
Northing	6395808	6394000
Easting	636407	638250
SiO_2	67.28	68.93
TiO_2	0.65	0.48
Al_2O_3	13.08	13.57
FeO	3.38	2.45
Fe_2O_3	2.56	2.07
MnO	0.11	0.09
MgO	0.67	0.46
CaO	2.24	1.65
Na_2O	3.17	3.58
K_2O	4.34	4.87
P_2O_5	0.20	0.13
Total	97.87	98.42
Sc	13	12
V	32	13
Cr	2	8
Ni	dl	dl
Cu	dl	4
Zn	59	42
Ga	21	22
Rb	128.6	151.2
Sr	193.0	145.4
Ba	1612	1081
Pb	18	26
Ce	263	201
Y	43.3	43.9
Zr	344.0	349.8
Nb	26.4	28.8
Th	15	15

B.2 ICP-MS TRACE ELEMENT ANALYSES

Wathaman Batholith
Southern-Central Zone (SCZ) - K-feldspar megacrystic granodiorite series

sample	99-T062a	98-J176	98-D313	98-D314	98-D292	98-D316
Rock Type	QD	QD	QMd	Gdr	Gdr	Gdr
Northing	6386882	6363548	6358578	6358891	6349938	6361608
Easting	640680	672159	641305	642239	645006	639924
Th	10.853	4.577	2.485	2.97	2.906	3.77
Y	24.790	12.458	19.624	16.00	21.831	10.00
La	81.616	34.462	35.847	34.85	52.160	44.71
Ce	164.076	69.377	75.978	74.21	105.467	82.53
Pr	19.094	8.063	9.626	9.17	12.332	9.38
Nd	70.447	30.956	40.163	35.92	47.928	33.77
Sm	10.417	5.179	7.780	6.45	8.403	5.21
Eu	2.513	1.322	1.651	1.55	1.956	1.43
Gd	8.135	3.765	5.900	4.77	6.202	3.58
Tb	0.934	0.470	0.749	0.59	0.805	0.40
Dy	4.997	2.472	4.105	3.31	4.438	2.13
Ho	0.960	0.472	0.778	0.61	0.847	0.37
Er	2.783	1.292	2.070	1.70	2.342	0.99
Tm	0.366	0.191	0.280	0.24	0.318	0.13
Yb	2.329	1.196	1.760	1.46	1.912	0.79
Lu	0.323	0.192	0.252	0.21	0.283	0.12

Wathaman Batholith

Southern-Central Zone (SCZ) - K-feldspar megacrystic granitoids

Sample	99-T156	99-T033	98-T223	99-T041	98-D349	98-T296
Rock Type	Gdr	Gdr	Gdr	Gdr	Gdr	Mgn
Northing	6399633	6381171	6364014	6386820	6366503	6352639
Easting	654248	656508	645300	657522	629737	662511
Th	4.674	1.054	2.267	6.594	1.332	5.910
Y	18.998	10.520	7.373	10.353	7.587	13.635
La	52.896	29.033	42.411	58.609	20.431	44.397
Ce	105.963	67.649	73.108	108.939	43.674	79.179
Pr	12.165	9.230	7.698	11.680	5.709	8.586
Nd	45.233	39.580	27.058	41.704	22.949	30.948
Sm	7.869	7.404	4.023	5.983	4.013	5.279
Eu	1.828	2.003	1.226	1.751	1.183	1.050
Gd	5.548	4.427	2.672	3.630	2.622	3.743
Tb	0.727	0.496	0.306	0.407	0.296	0.505
Dy	4.067	2.443	1.535	2.050	1.547	2.778
Ho	0.759	0.411	0.288	0.392	0.284	0.516
Er	2.230	1.135	0.729	1.117	0.731	1.390
Tm	0.286	0.138	0.101	0.142	0.104	0.195
Yb	1.694	0.832	0.621	0.914	0.675	1.193
Lu	0.257	0.123	0.102	0.138	0.101	0.162

Wathaman Batholith

Southern-Central Zone (SCZ) - K-feldspar megacrystic granodiorite series

Sample	99-T157
Rock Type	Mgn
Northing	6399088
Easting	653453
Th	8.045
Y	8.154
La	61.419
Ce	112.186
Pr	11.626
Nd	38.530
Sm	5.197
Eu	1.093
Gd	3.130
Tb	0.354
Dy	1.817
Ho	0.335
Er	0.934
Tm	0.112
Yb	0.654
Lu	0.099

Wathaman Batholith

Southern-Central Zone (SCZ) - Monzogranite series

Sample	98-D286	98-D265	98-D301
Rock Type	Gdr	Gdr	Mgn
Northing	6344675	6343702	6355632
Easting	646718	648804	642735
Th	3.355	2.644	0.851
Y	3.463	1.884	2.505
La	22.004	13.899	12.314
Ce	41.143	25.927	21.846
Pr	4.430	2.766	2.437
Nd	14.994	9.404	9.257
Sm	2.151	1.247	1.574
Eu	0.669	0.575	0.869
Gd	1.298	0.678	1.079
Tb	0.146	0.069	0.115
Dy	0.712	0.334	0.566
Ho	0.134	0.066	0.103
Er	0.339	0.204	0.274
Tm	0.049	0.031	0.035
Yb	0.291	0.225	0.214
Lu	0.049	0.041	0.038

Wathaman Batholith

Northeast Zone (NEZ) - K-feldspar megacrystic monzogranite series

Sample	99-T144b	99-T144a	99-D191	99-T139a	99-T141	99-T171
Rock Type	D	D	QMd	Gdr	Gdr	Mgn
Northing	6410318	6410318	6394112	6402990	6397476	6415944
Easting	663185	663185	663702	666575	667606	671418
Th	0.479	0.795	13.312	18.380	10.539	15.374
Y	18.258	29.090	16.640	25.843	16.909	20.204
La	34.600	33.218	63.667	61.972	37.618	73.691
Ce	87.102	94.767	123.573	135.785	80.683	143.984
Pr	10.905	13.515	13.259	16.204	9.593	16.092
Nd	40.856	55.915	45.669	58.965	34.908	57.565
Sm	7.040	10.489	7.172	9.456	5.790	8.543
Eu	1.683	2.184	1.452	1.430	1.214	1.963
Gd	5.133	7.493	4.432	6.366	3.869	5.584
Tb	0.604	0.982	0.568	0.854	0.527	0.705
Dy	3.410	5.576	3.186	4.797	3.051	3.845
Ho	0.693	1.091	0.612	0.984	0.607	0.784
Er	2.123	3.413	1.917	2.951	1.962	2.321
Tm	0.295	0.468	0.271	0.389	0.280	0.312
Yb	1.948	3.067	1.786	2.353	1.901	2.098
Lu	0.310	0.456	0.291	0.310	0.320	0.324

Wathaman Batholith

Northeast Zone (NEZ) - K-feldspar megacrystic monzogranite series

Sample	99-D255	99-D099
Rock Type	Mgn	Mgn
Northing	6408217	6418810
Easting	673304	662246
Th	12.487	14.537
Y	15.101	12.560
La	95.818	81.766
Ce	182.155	144.381
Pr	19.866	14.334
Nd	68.710	46.469
Sm	9.630	5.671
Eu	1.963	1.133
Gd	5.238	3.466
Tb	0.603	0.430
Dy	3.039	2.365
Ho	0.558	0.499
Er	1.688	1.500
Tm	0.226	0.202
Yb	1.469	1.263
Lu	0.222	0.194

Wathaman Batholith

Northeast Zone (NEZ) - K-feldspar megacrystic monzonitic series

Sample	99-T077b	99-T191	99-D103	98-T311	99-T077a
Rock Type	Md	QMd	Mz	QMd	QMd
Northing	6412185	6407013	6389408	6391500	6412185
Easting	664912	662402	641422	637750	664912
Th	1.638	7.103	4.180	4.622	1.496
Y	16.437	37.724	27.877	12.283	14.764
La	36.472	83.662	60.816	32.852	52.402
Ce	77.574	180.600	129.630	63.828	100.078
Pr	9.622	22.162	15.643	7.519	11.670
Nd	38.133	83.064	61.419	29.711	44.495
Sm	6.860	13.077	10.814	5.223	6.525
Eu	1.758	1.988	1.983	2.369	2.080
Gd	4.852	8.882	8.072	3.743	5.049
Tb	0.620	1.157	1.020	0.465	0.566
Dy	3.394	6.673	5.569	2.516	3.031
Ho	0.664	1.409	1.108	0.471	0.575
Er	1.956	4.436	3.252	1.254	1.649
Tm	0.255	0.585	0.419	0.172	0.210
Yb	1.588	3.580	2.642	1.021	1.285
Lu	0.238	0.496	0.377	0.151	0.185

La Ronge Domain Plutons

Pluton	*Cowie Bay*	*Butler Island*	*Milton Island*	*McMillian*	*Fol Dio-Grn*	*Jack Pine*
Sample	98-T199	97-A001	97-D068	98-T184	98-D108b	98-D129
Rock Type	Tn	Tn	Gdr	Gdr	Gdr	Gdr
Northing	6337821	6282737	6286219	6308308	6344374	6327017
Easting	637448	641005	643668	673770	680313	676494
Th	2.562	1.400	3.186	8.322	5.386	7.961
Y	14.806	---	15.626	14.873	12.780	10.064
La	24.254	21.000	21.368	46.465	73.107	39.374
Ce	55.686	51.000	53.254	92.637	143.216	75.360
Pr	7.516	6.900	7.232	10.565	15.992	8.454
Nd	32.277	31.000	30.653	38.720	57.670	30.736
Sm	6.148	5.600	6.263	6.415	8.526	5.035
Eu	1.529	1.600	1.387	1.442	2.215	1.200
Gd	4.540	4.300	4.658	4.418	4.937	3.267
Tb	0.566	0.530	0.585	0.550	0.581	0.393
Dy	3.036	2.800	3.167	2.991	2.952	2.036
Ho	0.567	0.500	0.582	0.569	0.505	0.380
Er	1.530	1.300	1.575	1.545	1.379	1.004
Tm	0.211	0.180	0.217	0.217	0.169	0.144
Yb	1.280	1.100	1.390	1.370	1.005	0.928
Lu	0.186	0.170	0.206	0.208	0.157	0.141

La Ronge Domain Plutons

Pluton	*McMillian*
Sample	98-D093
Rock Type	Tn
Northing	6306203
Easting	667191
Th	2.293
Y	5.070
La	17.969
Ce	37.279
Pr	4.230
Nd	15.927
Sm	2.690
Eu	0.767
Gd	1.740
Tb	0.206
Dy	1.033
Ho	0.193
Er	0.507
Tm	0.072
Yb	0.444
Lu	0.066

Peter Lake Domain

Swan River Gabbro Complex (D246b), fine grained foliated granitoid (D171) and foliated to augen K-feldspar megacrystic granitoid (D221).

Sample	99-D246b	99-D171	99-D221
Rock Type	Gb	Gdr	Mgn
Northing	6412902	6409500	6395808
Easting	659594	652414	636407
Th	0.273	5.385	13.642
Y	4.200	6.309	42.205
La	3.430	18.099	81.647
Ce	7.919	35.055	174.675
Pr	1.050	3.894	20.911
Nd	4.613	13.888	79.223
Sm	1.062	2.435	13.962
Eu	0.428	0.583	2.390
Gd	0.937	1.615	10.541
Tb	0.135	0.205	1.464
Dy	0.845	1.114	8.527
Ho	0.180	0.218	1.720
Er	0.557	0.680	5.289
Tm	0.073	0.092	0.722
Yb	0.455	0.593	4.695
Lu	0.070	0.099	0.738

B.3 SM AND ND ISOTOPIC MEASUREMENTS

Wathaman Batholith granitoids. Initial isotopic ratios are corrected to 1855 Ma.

Sample No.	Rock Type	Sm	Nd	Sm/Nd	$^{143}Nd/^{144}Nd$	2σ	$^{147}Sm/^{144}Nd$	2σ	$^{143}Nd/^{144}Nd(t)$	εNd(t)
Southern-Central Zone (SCZ) - Monzogranite series										
98-D286	Gdr	2.16	14.93	0.1447	0.511306	28	0.08924	3	0.510217	-0.4
98-D265	Gdr	1.42	10.10	0.1406	0.511312	46	0.08704	10	0.510250	0.2
Southern-Central Zone (SCZ) - K-feldspar megacrystic granodiorite series										
99-T062	QD	10.67	70.03	0.1524	0.511234	23	0.09405	3	0.510086	-3.0
98-D313	QMd	8.94	44.52	0.2008	0.511633	11	0.12398	3	0.510120	-2.3
98-D292	Gdr	8.23	46.60	0.1766	0.511309	24	0.10905	3	0.509978	-5.1
99-T033	Gdr	7.19	39.25	0.1832	0.511481	27	0.11311	7	0.510100	-2.7
98-T223	Gdr	4.07	28.11	0.1448	0.511189	15	0.08949	8	0.510097	-2.8
98-D349	Gdr	4.48	24.13	0.1857	0.511362	23	0.11471	4	0.509962	-5.4
99-T157	Mgn	5.40	39.82	0.1356	0.511120	15	0.08376	15	0.510098	-2.7
Northeast Zone (NEZ) - K-feldspar megacrystic monzogranite series										
99-T144b	D	7.35	42.30	0.1738	0.511475	97	0.10724	10	0.510166	-1.4
99-D191	QMd	7.28	46.08	0.1580	0.511283	30	0.09750	4	0.510093	-2.8
99-T139a	Gdr	10.04	55.98	0.1793	0.511471	23	0.11071	4	0.510120	-2.3
99-T171	Mgn	8.24	57.26	0.1439	0.511215	25	0.08883	7	0.510131	-2.1
99-D255	Mgn	10.34	63.56	0.1627	0.511143	79	0.10048	3	0.509917	-6.3
99-T133	Mgn	8.63	56.36	0.1531	0.511308	28	0.09449	26	0.510155	-1.6
99-J029b	Mgn	6.53	48.31	0.1352	0.510903	32	0.08347	4	0.509884	-6.9
99-D099	Mgn	5.59	45.85	0.1219	0.510979	23	0.07530	7	0.510060	-3.5
Northeast Zone (NEZ) - K-feldspar megacrystic monzonitic series										
99-T077b	Md	6.83	38.56	0.1771	0.511369	36	0.10930	6	0.510035	-4.0
99-T077a	QMd	6.83	46.46	0.1470	0.511328	37	0.09079	2	0.510220	-0.3
99-J061	QMd	6.30	40.32	0.1563	0.511275	15	0.09647	5	0.510098	-2.7

Initial Nd isotopic ratios are calculated using and average age for the Wathaman Batholith of 1855 Ma. CHUR values used: present day $^{143}Nd/^{144}Nd = 0.512638$; $^{147}Sm/^{144}Nd = 0.1967$.

La Ronge Domain plutons. Initial isotopic ratios are corrected to 1858 Ma.

Sample No.	Rock Type	Sm	Nd	Sm/Nd	$^{143}Nd/^{144}Nd$	2σ	$^{147}Sm/^{144}Nd$	2σ	$^{143}Nd/^{144}Nd(t)$	εNd(t)
98-T199	Tn	6.07	31.56	0.1923	0.511666	13	0.11871	13	0.510215	-0.4
97-D068	Gdr	7.04	32.76	0.2149	0.511871	24	0.13265	10	0.510249	0.3
98-D129	Gdr	5.07	29.97	0.1692	0.511493	17	0.10452	4	0.510215	-0.4
98-D093	Tn	2.75	15.75	0.1746	0.511634	32	0.10790	2	0.510315	1.6
*97-A001	Tn	5.79	30.53	0.1896	0.511877	---	0.11460	---	0.510476	4.8

Initial Nd isotopic ratios are calculated using an age of 1858 Ma, the age of the Butler Island pluton (Corrigan et al. unpub. rept.). CHUR values used: present day $^{143}Nd/^{144}Nd = 0.512638$; $^{147}Sm/^{144}Nd = 0.1967$.*97-A001 was analysed at the GSC in Ottawa (Corrigan et al., unpub. rept.).

Pre-1858 Ma rocks of the La Ronge and Peter Lake domains. Initial isotopic ratios are corrected to 1858 Ma.

Sample No.	Rock Type	Sm	Nd	Sm/Nd	$^{143}Nd/^{144}Nd$	2σ	$^{147}Sm/^{144}Nd$	2σ	$^{143}Nd/^{144}Nd(t)$	εNd(t)
La Ronge Domain. Initial isotopic ratios are corrected to 1855 Ma.										
Crowe Island Complex (1892 ±2 Ma)										
*97-D373	Tn	3.14	14.99	0.2095	0.511971	---	0.12660	---	0.510426	3.7
Central Metavolcanic Belt (~1880 Ma)										
*97-D433	Dacite	1.91	7.93	0.2409	0.512143	---	0.14580	---	0.510363	2.5
Peter Lake Domain. Initial isotopic ratios are corrected to 1855 Ma.										
Swan River Gabbro Complex										
99-D246b	Gb	1.11	5.35	0.2075	0.511521	22	0.12766	5	0.509963	-5.4
Fine grained foliated granitoid										
99-D171	Gdr	2.21	13.97	0.1582	0.510919	37	0.09784	3	0.509725	-10.0

Initial Nd isotopic ratios are calculated using an age of 1858 Ma, the age of the Butler Island pluton (Corrigan et al. unpub. rept.). CHUR values used: present day $^{143}Nd/^{144}Nd = 0.512638$; $^{147}Sm/^{144}Nd = 0.1967$. *97-D373 and *97-D433 were analysed at the GSC in Ottawa (Corrigan et al., unpub. rept.).

APPENDIX C: PRIMITIVE MANTLE TRACE ELEMENT NORMALIZING VALUES

Element	Primitive Mantle
Rb	0.635
Ba	6.989
K	250
Th	0.085
Nb	0.713
La	0.687
Ce	1.775
Sr	21.1
Nd	1.354
Zr	11.2
P	95
Sm	0.444
Eu	0.168
Ti	1300
Gd	0.596
Dy	0.737
Er	0.480
Y	4.55
Yb	0.493
Lu	0.074

Reference: Normalizing values are from Sun and McDonough (1989).

APPENDIX D: PARTITION COEFFICIENTS USED

Element	Hornblende	Biotite	Plagioclase	K-feldspar	Apatite
Rb	0.014	3.26	0.041	0.659	
Sr	0.22	0.12	4.4	3.87	
Ba	0.044	6.36	0.31	6.12	
Ce	0.899				21.1
Nd	2.890				32.8
Sm	3.990				46
Eu	3.440				25.5
Gd	5.480				43.9
Dy	6.200				34.8
Er	5.940				22.7
Yb	4.890				15.4
Lu	4.530				13.8

References: Partition coefficients for Rb, Sr and Ba are from Hanson (1978). Rare Earth Element (REE) partition coefficients for hornblende in dacitic melts are from Arth (1976), and apatite in dacitic melts from Fujimaki (1986). All partition coefficients can be found in Rollinson (1993).

Legend

Peter Lake Domain

- Foliated medium grained granitoids
- Migmatitic ortho- and paragneiss
- Swan River Complex
  mainly fine to medium grained gabbro and diorite
- Foliated K-feldspar augen monzogranite

Wathaman Batholith

- K-feldspar megacrystic
  hornblende-biotite granodiorite and monzogranite
  with lesser quartz diorite and quartz monzodiorite
- K-feldspar megacrystic to coarse grained
  biotite +/- hornblende granodiorite and monzogranite,
  with lesser quartz monzodiorite and diorite
- Medium to coarse grained
  biotite granodiorite and monzogranite
- K-feldspar megacrystic to coarse grained
  quartz monzodiorites and monzonites with lesser diorite
- Medium grained
  hornblende-biotite tonalite and granodiorite

La Ronge Domain

Plutonic Rocks

- Medium to coarse grained
  granodiorite and monzogranite
- Medium to coarse grained
  tonalite and granodiorite
- Medium to coarse grained
  diorite, quartz diorite and tonalite
- Crowe Island Compex
  (dioritic to granitic banded orthogneiss)

Supracrustal assemblages

- Park Island metasedimentary assemblage
  (arkose, polymictic conglomerate, calcareous arkose, psammite)
- Milton Island metasedimentary assemblage
  (psammite, pelite)
- Volcano-sedimentary assemblages

Kisseynew Domain

- McLennan Group
  (arkose, polymictic conglomerate, calcareous arkose)

Kilometers
0 5 10 15 20 25

Scale 1:250 000

Symbols

- Geological Contact
- Shear Zone